**Universidade do Minho**
Escola de Engenharia

Ana Rita Machado Ferreira

# New processing technologies for improved compression piston ring performance

New processing technologies for improved compression piston ring performmance
Ana Rita Machado Ferreira
Uminho | 2022

outubro de 2022

REPÚBLICA PORTUGUESA FCT Fundação para a Ciência e a Tecnologia NORTE2020 POCH PORTUGAL 2020

**Universidade do Minho**
Escola de Engenharia

Ana Rita Machado Ferreira

# New processing technologies for improved compression piston ring performance

Tese de Doutoramento
Programa Doutoral em Líderes para Indústrias Tecnológicas

Trabalho efetuado sob a orientação de

**Professor Doutor Filipe Samuel Pereira Correia da Silva**

**Professor Doutor Sandra Maria Fernandes Carvalho**

**Engenheiro Luís Diogo Ramos de Azevedo Sobral**

outubro de 2022

# Acknowledgments

First of all, I would like to thank Professor Filipe, my supervisor, for the encouragement and confidence, and most of all, for the guidance during this journey. The knowledge and enthusiasm shared through these years were of a real leader. I would be eternally grateful for this opportunity! To my co-supervisors, Professor Sandra Carvalho and Engineer Luís Sobral, thank you for all the support and insights, and for being available to help me and to clarify my doubts.

To all members of the Microfabrication and Integrated Systems Laboratory, and in particular, those close to me, which were available to list me during the harder times, thank you for your support and willingness to help. A special thanks to Sara, Pinto and Óscar. You were an outstanding team! I would also like to acknowledge to Marco, João Pinto and Filipe Marques for the valuable insights for this work. Thank you to the master students that I had supervised, but especially to Ângela for her precious help, it was a pleasure to work with you. I am truly grateful to Helena, Francisca, Cristina, Caroline, Telma and Mafalda, for your friendship and for our happy moments!

To all people from other laboratories and institutions, that in one way or another helped me during these years. To my family and all my friends for always being present. Thank you for putting up with my concerns and for cheering me up.

To my mother, my sister, and my grandparents, for their unconditional love and encouragement! To my husband Bruno, I would like to express my deep gratitude for the unconditional support and patience! Without you all, nothing of this would have been possible!

To my daughter Clara, for had changed my perspective of life, you were an outstanding source of motivation, encouragement and love.

I gratefully acknowledge Fundação para a Ciência e a Tecnologia (FCT) and MAHLE – Componentes de Motores, S.A. for the financial support throughout the BD - Bolsa de Doutoramento em Empresa (FCT PhD Grant) with the reference SFRH/BDE/110654/2015. I gratefully acknowledge the opportunity given to me to work at the Centre for Micro-Electro Mechanical Systems (CMEMS) and to the reference project PTDC/EME-EME/7860/2020.

## STATEMENT OF INTEGRITY

I hereby declare having conducted this academic work with integrity. I confirm that I have not used plagiarism or any form of undue use of information or falsification of results along the process leading to its elaboration.

I further declare that I have fully acknowledged the Code of Ethical Conduct of the University of Minho.

University of Minho, _____/___/_____

Assinatura: _____

Ana Rita Machado Ferreira

# Resumo

*Novas tecnologias de processamento utilizadas para melhorar o desempenho de segmentos de compressão*

Nos motores de combustão interna um dos pares tribológicos mais estudados é representado pelo contacto entre o segmento e o cylindro do motor. O seu funcionamento sob altas temepaturas e exposto a cargas elevadas torna a superfície do segmento mais susceptível a apresentar um elevado desgaste, podendo afectar a sua principal função que é a vedação da câmara de combustão. Uma vedação pouco eficaz pode estar associada ao aumento de emissão de gases, ao aumento do consumo de combustível e ainda a um acréscimo dos custos de manutenção. Como tal, e tendo em conta a elevada competitiividade desta indústria, o seu desempenho deverá ser otimizado.

A solução mais convencional é a aplicação de revestimentos na superfície radial dos segmentos de compressão. Esta camada é habitualmente depositada através de uma técnica de deposição física de em fase de vapor, o arco catódico. No presente trabalho de doutoramento será desenvolvida, produzida e testada uma nova solução para a superfície do segmento utilizando novas tecnologias de processamento que permitam uma melhoria do seu desempenho. De forma a utilizar o mesmo equipamento de avaliação tribológica ao longo de todo o projecto for desenvolvido um novo tribómetro adaptado para o contacto entre as amostras do segmento e do cilindro e capaz de reproduzir condições de teste semelhantes às do motor.

Numa abordagem inicial foi estudada a influência dos parâmetros de deposição (utilizando a técnica de deposição convencional) no desempenho tribológico do contacto entre o segmento e o cilindro. Posteriormente foi ainda investigada a influência de técnicas de acabamento de superfíce na resistência ao desgaste dos dois componentes. A introdução de novas tecnologias passaram pela utilização da ténica de texturização a laser para produzir cavidades ao longo da superfície radial do segmento, eficazes na redução do atrito e do desgaste. A tecnologia laser associada à tecnica de metalurgia dos pós *hot pressing* foram duas das novas tecnologias de manufactura utilizadas no desenvolvimento de um segmento com superficie multifunctional.

Palavras-chave (5): *segmento; desgaste; atrito; texturiação de superfícies; metalurgia dos pós.*

## Abstract

*New processing technologies for improved compression piston rings performance*

In the internal combustion engine (ICE), the piston ring-cylinder liner contact is one of the most studied tribological pairs. Operating under elevated temperatures and heavy-loaded conditions, the compression piston ring surface is more prone to wear, which affects the efficacy of the main top ring role, the combustion chamber sealing. The principal consequences of an ineffective combustion chamber sealing are the increase in exhaust emissions, the increase in fuel consumption and an increment of maintenance costs. In an increasingly competitive global market, the ICE performance must continue under improvement.

The conventional compression piston ring possesses a bulk coating layer over its radial surface, the one in contact with the cylinder liner bore. The coating layer is usually deposited through a physical vapor deposition technique, the cathodic vacuum arc. In this PhD thesis is concerned the development, production and testing of a new piston ring surface solution using new processing technologies to obtain an improved compression piston ring performance. In order to use the same testing equipment during the PhD thesis it was developed a new tribometer, adapted for the ring-liner samples assembly and able to reproduce similar engine operation conditions.

In a preliminary approach it was studied the influence of different deposition parameters, using the conventional PVD technique, on the final ring-liner tribological performance. In a subsequent study, it was investigated the influence of the post-deposition processing. Different surface finishing techniques were applied and it was assessed the piston ring and cylinder liner wear resistance. The introduction of new processing technologies encompassed the use of the laser surface texturing (LST) to produce dimples over the ring radial surface. Those revealed to be effective for friction reduction and consequent improvement of the ring wear resistance. This latter manufacturing technology, LST, combined with a powder metallurgy technique, hot pressing, were used on the development of a multifunctional piston ring surface.


Keywords (5): *piston ring; wear; friction; surface texturing; powder metallurgy.*

# Contents

# List of symbols, abbreviations and notations

| | |
|---|---|
| $Al_2O_3$ | Aluminum oxide (alumina) |
| FCC | Face centered cubic |
| COF | Coefficient of friction |
| CVD | Chemical vapor deposition |
| E | Young's modulus |
| EDS | Energy dispersive spectrometer |
| H | Hardness of material |
| HP | Hot pressing |
| P | Laser power (W) |
| PM | Powder metallurgy |
| PVD | Physical vapor deposition |
| SEM | Scanning electron microcopy |
| XRD | X-ray diffraction |
| DLC | Diamond-like carbon |
| IC | Internal combustion |
| ICE | Internal combustion engine |
| TDC | Top dead center |
| BDC | Bottom dead center |
| TS | Thermal spray |
| CrN | Chromium nitride |
| NbN | Niobium nitride |
| HiPIMS | High power impulse magnetron sputtering |
| OCA | Oil contact angle |
| FWHM | Full width half maximum |
| DSC | Differential scanning calorimetry |
| MMC | Metal matrix composite |
| SS | Stainless steel |
| ICDD | International Centre for Diffraction Data |

# List of figures

## Chapter 2

## Chapter 3



## Chapter 4

**Chapter 5**



**Chapter 6**

**Chapter 7**

# List of tables

# CHAPTER 1.

## Introduction

## 1.1 Motivation

The automotive industry has been revolutionized by stricter emission regulations and zero-emissions policies. Passenger cars, motorsports, light, medium, and heavy-duty trucks, and vehicles for construction and agricultural industries shared a similar powertrain, but regulators are tightening emissions rules. The internal combustion engine (ICE) is facing this challenge against the battery electric vehicles. However, in heavy trucks, electric technologies still presenting several constrains. Batteries require more time to recharge than any fuel, are heavy and constrained on space. In some business areas with around-the-clock operations, such as mining, construction and agriculture, large batteries are associated to high capex requirements. Conversely, the combustion engines represent a consolidated technology, with large potential to compete with zero-emission vehicles using alternative fuels. Besides diesel and gasoline, reduced emissions can be achieved using hybrid and gas engines, and the zero-emission solutions comprise hydrogen internal combustion engines (H2-ICEs), biofuel or synfuel. Regardless of the fuel source, the increase of the ICE's efficiency is a primary goal to raise its competitiveness.

The final performance of the internal combustion engine is dependent on the efficacy of its mechanical systems. In respect to energy consumption within the engine, the engine friction loss represents 48% [1]. From the diverse energy losses resulting from friction and wear of the engine's contact surfaces, the sliding movement of the piston rings and piston skirt against the cylinder liner wall represents the largest contribution to friction in the engine. In the piston assembly, the primary role of the top piston ring, also known as compression piston ring, is to maintain an effective gas seal between the combustion chamber and the crankcase. The top ring is subjected to high loads and temperatures along its radial surface in contact with the cylinder liner inner wall. The continuous reciprocating movement cause severe wear in the ring radial surface. The conventional solution to avoid the compression ring failure is a wear resistant coating, such as a bulk chromium layer, deposited using a physical vapor deposition (PVD) technique. Recent advancements with improved wear resistant solutions for compression piston rings faced multilayered coatings and diamond-like carbon (DLC) films, with similar deposition techniques. But it is still feasible and necessary to make progress and optimize the surface's contact.

Disruptive solutions can lead to an additional enhancement of the tribological performance. In the present work are introduced new processing technologies, such as laser surface texturing

(LST) and powder metallurgy (PM) to study, develop and characterize new ring surface solutions. The developed solutions aimed to increase the wear resistance of the compression piston ring and reduce the coefficient of friction of the piston ring- cylinder liner tribological pair. A further improvement in the performance of the ring-liner contact will contribute for a decrease in the engine friction loss.

The present work was developed in the context of the Engineering Design and Advanced Manufacturing focus areas from the MIT Portugal. The study and investigation of new processing technologies to improve the piston ring tribological performance intended to contribute for a product development with social and economic interest. In a near future and with the environmental regulation the target of the automotive market will be the business of cars built for e-hailing services. Combustion engines with zero-emission fuels must be designed for high utilization and robustness. The more efficient the piston ring sealing, the more efficient the combustion process, and the lower is the energy consumption and the emission of atmospheric pollutants.

According to the guidance of the Leaders for Technical Industries (LTI) doctoral program, in this PhD was implemented a straight and permanent relationship between academia and industry. This cooperation was established with an industrial partner, MAHLE Componentes de Motores, SA, which is one of the main piston rings manufacturers in the automotive industry. This partnership endorsed the motivation on developing an innovative solution from the current commercial products and without disregard the existent production requirements.

## 1.2 Objectives

The performance of a tribological pair is dependent on the surface's characteristics and properties. Those embrace the coating material, the deposition technique and the surface finishing process of both surfaces. The piston ring surface will be the focus of the present PhD work and as counterpart surface was maintained the cylinder liner commercial solution.

As previously mentioned, the conventional piston ring possesses a coating layer along its radial surface for wear resistance purposes. This coating is typically deposited using vacuum deposition methods using a single layer or a multilayer design. The main goal of this project is to improve the compression piston ring tribological performance, namely its wear resistance and the coefficient of friction against the cylinder liner surface, exploring different manufacturing technologies. To achieve such purpose, it is necessary to fulfill the following main objectives:

- To explore different surface engineering solutions for compression piston rings of heavy-duty engines, improving its wear resistance and the coefficient of friction against the cylinder liner surface;
- To validate the new surface solutions using the same tribological characterization method.

Some specific objectives were therefore established to ensure that these two general objectives are accomplished:

- To develop a tribometer adapted to reproduce the combustion engine operating conditions;
- To evaluate the influence of the conventional coating deposition process, namely cathodic arc, on the compression piston ring wear resistance;
- To study the influence of the surface characteristics, particularly the surface finishing, on the piston ring tribological performance;
- To explore different surface engineering solutions and validate the influence of the radial surface topography on the piston ring tribological performance with reference to the commercial vacuum deposited coatings;
- To explore disruptive manufacturing technologies with potential to produce a multifunctional surface, with an enhanced tribological performance.

## 1.3 Structure of the thesis

This PhD thesis is organized as a compilation of research papers that are already published, accepted or submitted in international ISI journals. Apart from the review paper and research papers, this thesis is also composed by two other chapters: chapter 1 and chapter 8.

Chapter 1 corresponds to the Introduction. In this chapter it is possible to find the motivation and objectives of this research work, as well as the structure of the thesis.

Chapter 2 – "Tribological solutions for engine piston ring surfaces: an overview on the materials and manufacturing" – corresponds to a review article on the tribological solutions for the compression piston rings. This review comprehends the state-of-the-art of compression piston rings, regarding the piston ring operational conditions into the combustion engine, the surface

materials and the manufacturing technologies. This review article also addresses some solutions under development and innovative solutions for future implementation, already explored in the research papers of the present PhD work. This review paper is published in *Materials and Manufacturing Processes*, 2020; 35: 498-520. (a Taylor and Francis journal with an impact factor of 4.306, Quartile 1).

Chapter 3 – "A New Tribometer for the Automotive Industry: Development and Experimental Validation" – presents the methodology followed for the development of a new tribometer and its functional validation. This device was used to assess the tribological performance of the conventional and new piston ring solutions, and represented a fundamental tool of this PhD work. Conversely to the evaluation of simplified contact geometries (such as ball-on-plate or pin-on-disk), the development of a customized test rig allowed to assess samples of final engine parts. Using the real contact geometry, and broader ranges for the testing parameters, the developed tool raised the scientific relevance of the developed work. This research paper is published in *Experimental Mechanics*, 2022; 62:483-492 (a Springer journal with an impact factor of 2.872, Quartile 1).

Chapter 4 – "Influence of morphology and microstructure on the tribological behavior of arc deposited CrN coatings for the automotive industry" – investigates the influence of the PVD coating deposition process on the tribological properties of the compression ring. Conventional CrN-coated piston rings with distinct deposition parameters were physically, chemically and mechanically characterized. Their tribological response was evaluated through the developed tribometer. In this work it was analyzed the influence of the coating deposition on coating properties, and consequently on its wear resistance and friction coefficient results against the cylinder liner surface. This research paper is published in *Surface and Coatings Technology*, 2020; 397: 126047 (an Elsevier journal with an impact factor of 4.865, Quartile 1).

Chapter 5 – "Influence of a DLC coating topography in the piston ring/cylinder liner tribological performance" – aimed to study the influence of the surface finishing processes and surface finishing parameters on the tribological response. The experimental procedure comprehended several surface finishing techniques. The post-processing stage of the deposition process influenced the interfacial contact between the ring and the liner surfaces. The topographical characterization was followed by wear tests and coefficient of friction measurements. This research paper is published in *Journal of Manufacturing Processes*, 2021; 66: 483-493 (an Elsevier journal with an impact factor of 5.684, Quartile 1).

Chapter 6 – "Surface engineering for optimized compression piston ring tribological performance" – studies and validates a different surface engineering approach in the piston ring surface. Along the radial ring surface over the NbN/CrN coating deposited by PVD were produced dimples by laser surface texturing. Varying the dimensions and area densities of the textured dimples was modified the topography of the radial surface. Textured and non-textured samples followed the same protocol to evaluate their wear resistance and their friction coefficient against the cylinder liner. This article is submitted in *Friction* (an Springer journal with an impact factor of 5.662, Quartile 1).

Chapter 7 – "Design, manufacturing, and testing of a laser textured piston ring surface reinforced with a CuCoBe-diamond composite by hot-pressing" – aimed to develop a multifunctional piston ring surface using different materials and alternative manufacturing technologies. The experimental procedure encompassed laser surface texturing of the stainless steel ring according to different designs followed by the production of functionalized surfaces and their validation using the home-developed tribometer. This article is submitted in *Journal of Powder Technology* (an Elsevier journal with an impact factor of 5.640, Quartile 1).

The last chapter of the thesis – Chapter 8 – presents a general discussion and conclusions of the developed work (a functionalized piston ring surface with improved tribological performance) and some suggestions for future work.

## References

[1] B. Bhushan, Modern Tribology Handbook, CRC Press LLC, 2001.

# CHAPTER 2.

## Tribological solutions for engine piston ring surfaces: an overview on the materials and manufacturing

Published in Materials and Manufacturing Processes, 2019, 35: 498-520
R. Ferreira [a,c,d,*], J. Martins [b], Ó. Carvalho [a], L. Sobral [c], S. Carvalho [d], F. Silva [a]

[a] Centre for Micro-Electro Mechanical Systems (MEMS) University of Minho, Campus de Azurém, 4800-058 Guimarães, Portugal
[b] Mechanical Engineering Department, Universidade do Minho, 4800-058 Guimarães, Portugal
[c] MAHLE - Componentes de Motores S.A., Núcleo Industrial Murtede, 3060-372 Cantanhede, Portugal
[d] GRF-CFUM, Department of Physics, University of Minho, Campus de Azurém, 4800-058 Guimarães, Portugal

## Abstract

This paper exhibits an outline of the piston rings operational characteristics and consequently, of their main functional challenges. The basic geometrical shapes, materials and manufacturing technologies used to produce compression rings for up to date diesel engines are summarized. Based on this description, each technological solution to enhance the behaviour of the piston rings is fully described and explained. The state-of-the-art solutions such as a DLC (diamond-like carbon) layer, multi-layered coatings and compound coatings are tersely presented and discussed. New approaches suggest surface textures, which are expected to be a major improvement on the development of optimized surface coatings of the piston rings, and the latest progress in that area are examined and debated. Also, a novel solution for the enhancement of the behaviour of ring coatings is presented, using a proposed and previously tested solution for a different application. This solution attempts to optimise most of the properties in relation to friction, wear, mechanical stresses, heat dissipation and self-lubrication. The overall idea is to use specific materials in specified positions over the surface to individually enhance the referred properties, creating a multifunctional surface.

Keywords: *engine; piston ring; tribology; wear; friction; coatings; multilayer; surface; textures; cavities; powder; reinforcement*.

## 2.1 Introduction

During the last decades, internal combustion engines (ICEs) have becoming an unwelcome topic in the automotive industry. Environmental issues are the main reason presented to the society to replace ICEs by electric and hybrid propulsion systems, as fossil fuel consumption minimization has becoming an ever more important issue. In fact, to survive in the market, ICE need to implement disruptive improvements [1].

A quick look over the internal combustion engine performance is enough to realize that most of the internal sub-systems associated to fuel and oil consumption, and consequently, to the emission of pollutant gases, are dependent on specific parts of the ICE [2,3]. One of those parts with a major impact on the referred critical issues are the piston rings, which were invented in 1854 by John Ramsbottom. Despite their association with the engine piston, piston rings were designed as an additional part with a supporting role in the sealing or prevention of gas leakages from the combustion chamber. The contact area between the cylinder liner and the piston ring is significantly reduced when compared with the contact area between the entire piston body and the liner.

The sealing effect, which is one of their main roles, will prevent the flow of the combustion mixture (fuel and/or gases) to the crankcase before, during and after the combustion process [4,5].

In the opposite direction, it will prevent the oil getting to the combustion chamber. In this way, the piston rings also control the fuel and oil consumptions [6]. However, the sealing effect also produces undesired friction and surfaces wear [7].

Moreover, to ensure a proper sealing, the compression piston ring has a larger diameter than the cylinder bore, when free-standing, but a slightly shorter perimeter. The free end gap existing on its perimeter comes with an inherent elasticity enabling the piston ring to press onto the cylinder bore surface. Its spring effect creates a continuous outward contact pressure between the external surface of the piston ring and the inner surface of the cylinder liner, raising the undesired contact friction and surfaces wear [8].

Regarding its functional demands, the top compression ring requires a superior mechanical, thermal and, most of all, tribological resistance in respect to wear and friction [9,10]. Figure 2.1 shows some of the most relevant characteristics to be implemented in the compression ring performance, highlighting its tribological performance.


Figure 2.1 Characteristics to be improved in the compression ring performance.

Regarding such different characteristics that a compression ring would ideally bring together, its performance must follow a multifunctional profile. The present paper aims at presenting an overview of recent solutions proposed for the compression ring surface, including different materials and manufacturing processes, in order to present improved solutions for the ring-liner pair. Some of the discussed solutions in this work have already been introduced in the automotive industry and others are still in the development and evaluation phases. The main properties and characteristics of compression ring, as well as the interacting conditions with the tribological counter-body, are presented in third section. The fourth section reports solutions against wear and

friction and their application and the possible impact on compression ring performance regarding the entire system (ring-liner contact).

Besides hard coatings and the further developments in the surface engineering field [11], textured surfaces represent the focal point, with a more detailed analysis of the work already published in this field. The paper finishes with the presentation of an innovative proposal using multifunctional surfaces which introduces a discussion related to possible future trends in the piston rings development and their impact in engine operation and in the materials engineering evolution.

## 2.2 Top compression ring – cylinder liner assembly

The design of the piston includes a smaller outer diameter than the internal cylinder wall, to allow for thermal expansion and lubrication. However, during engine operation, combustion chamber must be sealed to achieve the required thermodynamic conditions for the combustion process. Thus, to eliminate the existent clearances between piston and cylinder liner, piston rings seal the possible contact between the combustion chamber and the engine crankcase. Those clearances have minimum and maximum values when the internal combustion engine is running hot or cold. To use an accurate control of those measures, compression ring dimensions and design vary according to the engine application (light or heavy engines), type of engine (Diesel or Otto) and also according to its specific manufacturer requirements.

Piston rings are placed into the piston grooves and, generally, there are three different types (Figure 2.2):

a) Top compression ring;
b) Second compression or wiper ring;
c) Oil control ring.

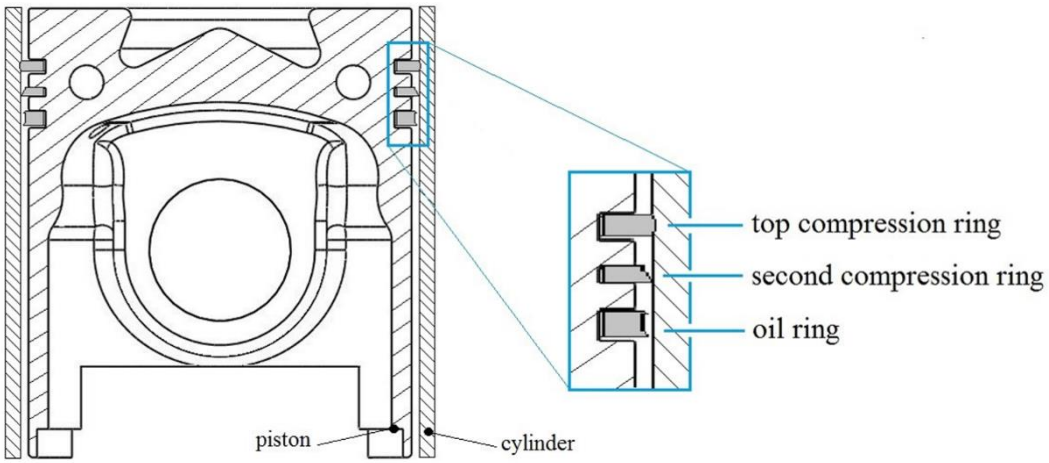


Figure 2.2 Scheme using a section view of an assembly of the cylinder, the piston and the piston rings, with particular focus on the respective cross-sectional geometry of each piston ring.

Each one of these rings has a specific role during engine operation and has different geometries and characteristics. Figure 2.2 shows the position of each ring on the piston. The top compression ring represents the first sealing element between the combustion chamber (sealing the passage of high pressure combustion gases) and the crankcase (sealing the passage of oil) and is one of the most relevant element of the assembled piston. The second compression ring increases the effectiveness of the top ring and the lower ring is intended to regulate the oil supply to the top compression ring - cylinder liner contact.

According to their function, fuel type and engine size, each piston ring has a specific cross-section geometry, which has a direct influence in the piston ring tribology performance [12–14]. In the periphery, where they contact with the cylinder bore, they may either have a barrel profile or a taper shape, as shown in the Figure 2.3. While the former geometry is conventionally used in the top groove [15] and ensures an effective sealing under normal operating conditions, the taper shape is usually found in the second compression ring. During the downward movement that tapered ring, being pushed against the cylinder liner, scrapes the excess oil.

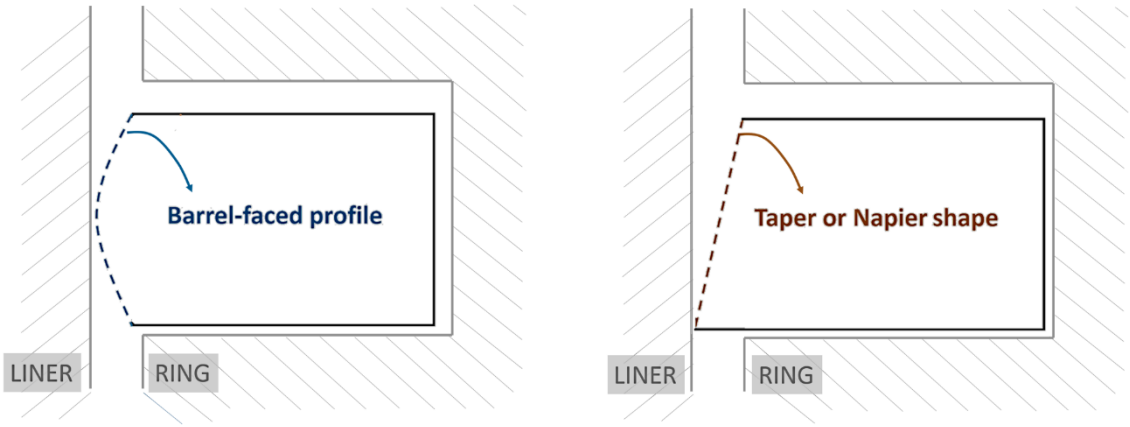


Figure 2.3 Cross-view of two possible shapes of the external/functional face of the piston ring that can have direct influence in the piston ring functioning.

In addition to the peripheral form, the top ring surface the bottom ring surface in contact with the piston groove may also have tapered faces or an edge relief (bevel) in the upper or in the lower inside (piston side) corner (Figure 2.4).

Top and bottom tapered faces enable a minimum contact of the top and bottom ring surfaces against the groove. This geometry is commonly used to prevent sticking resulting from the combustion residues of the diesel engines. The presence of a bevel, either in the upper or in the lower inner corner, has the benefit of providing a twist effect during engine operation. In particular during the compression stroke, when the inertia force prevails in the piston ring dynamics and a positive moment is created by the force generated at the top outside edge of the ring, it causes a positive twist effect (in the clockwise direction, following the representation of the Figure 2.4). With the increase of the cylinder pressure, the force at the bottom inside edge generates a negative moment, causing a twist in the negative direction (counterclockwise direction according to the representation of the Figure 2.4).

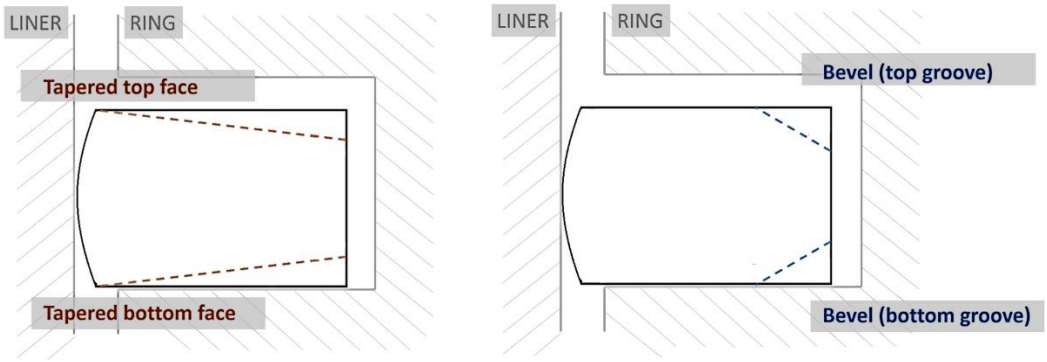


Figure 2.4 Cross-view of two possible geometries of the top and bottom piston ring faces in contact with the piston ring groove that can influence the piston ring motion during the engine operation.

During each four-stroke cycle presented in the Figure 2.5 the piston travels twice from the Top Dead Centre (TDC) to the Bottom Dead Centre (BDC) and comes back also twice. During this sliding movement, the radial pressure applied by the compression ring onto the cylinder bore produces a continuous compressive stress applied onto the ring outer surface. Radial and axial contact between the top ring and the piston groove is generated by the gas pressure from the combustion chamber, by the acceleration forces and by the ring-liner friction. Those effects result in an enhanced sealing of the compression and combustion processes. While the radial contact with the cylinder surface is continuously active, axial contact surfaces are swapping between the top and bottom internal piston groove surfaces.

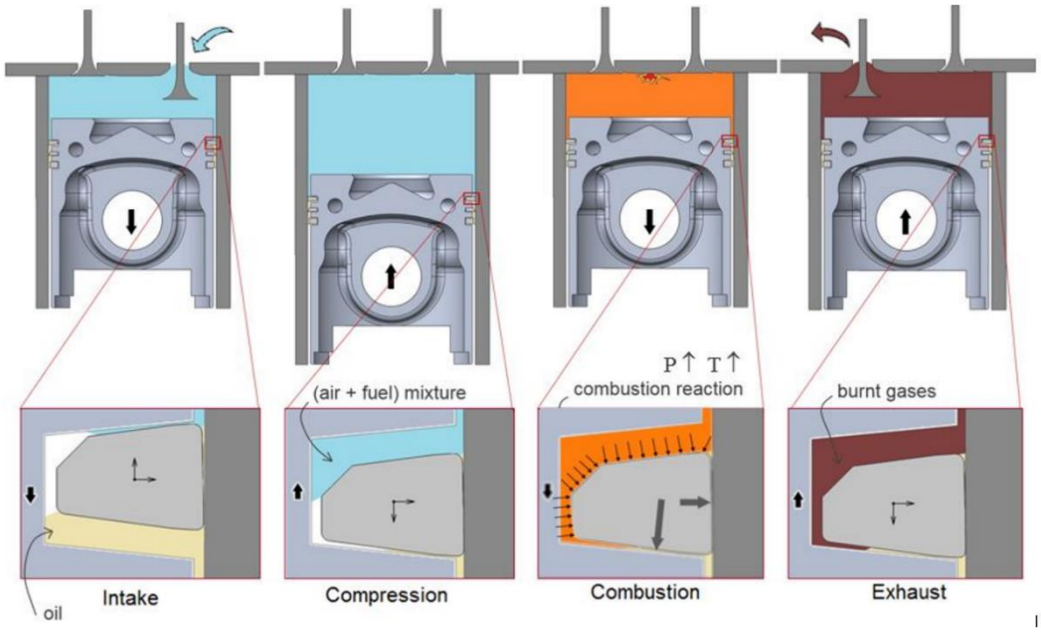


Figure 2.5 Schematic representation of the four stages of a four-stroke internal combustion engine with a particular focus on the behavior of the top compression ring.

In the Figure 2.5 it is also shown how these variations occur due to the inertia forces from alternating movements of the piston, friction forces from radial contact and gas pressure from the combustion process. In fact, the pressure from the combustion gases acts onto the sides of the ring, as it can be seen in the "combustion" stage of the Figure 2.5. The resulting forces compel the ring to move down (counteracting the ring-liner friction) and outwards. This latter effect increases the pressure of the ring-liner contact and therefore, improves the sealing effect.

## 2.3 Challenges of the top compression ring

### 2.3.1 Sealing of the combustion chamber – the main role

Most of the studies consider a constant ring-liner circular contact but that is not the real operating condition. The small gap (or local pressure) between ring and bore is not uniform over the circumferential length, leaving a non-uniform gap between them as shown in the Figure 2.6. So, the radial deformation of the compression ring has a variable influence on the film profile along the contact area, promoting an excessive oil consumption where the film thickness has the maximum value. However, despite that variability during the engine cycle, the existence of some radial contact with the cylinder liner is continuous due to the inherent compression ring spring

force. The overall contact pressure has a high value, typically in the order of $10^5$ Pa [16], to prevent the generation of a thicker film, and this effect has a large impact on engine friction losses.

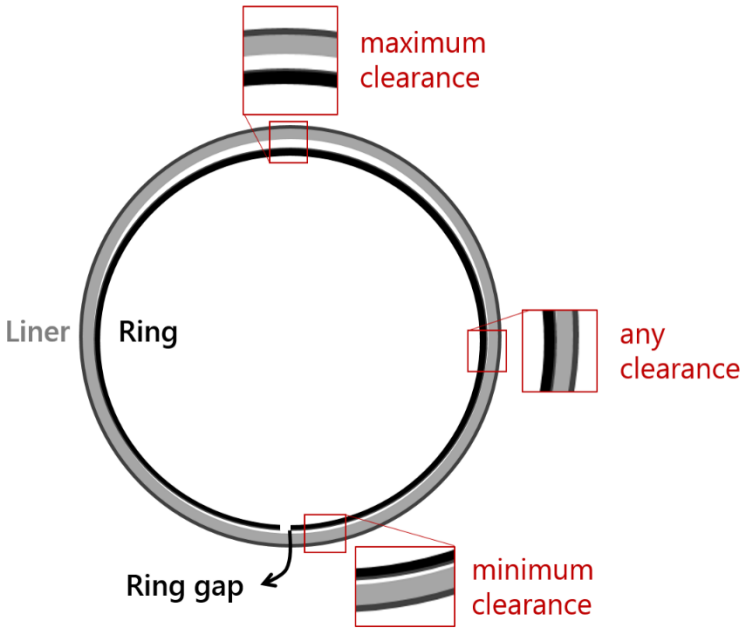


Figure 2.6 Non-constant circular gap in the ring-liner assembly.

Besides its dimensions and its semi-circumferential geometry, the cross section geometry is also determinant to the engine operation and it has a direct impact on several performance factors, such as, for instance, the engine oil consumption [17] and the blow-by effect. Although each manufacturer uses their own cross section geometries, the most common shapes are rectangular rings (with a barrel face in the running surface) and taper faced rings. The use of a tapered side or both tapered sides influences gas flow trajectory around the ring into the groove. As said before, the gas pressure acts on the ring surface furthest from the ring-liner contact, pressing it against the liner [18]. This improves the sealing during the engine power stroke using geometrical conformability of the compression ring to adapt it to the existing stresses. Passenger car and truck diesel engines commonly use a compression ring with taper faced geometry, with a top internal bevel and tapered upper and down sides, as considered in the present work.

The design and development of piston rings must follow a list of geometrical and dimensional tolerances particularly defined for a specific compression piston ring - cylinder liner pair. The purpose of the present study lies on the development of top piston rings for heavy-duty diesel

application. Therefore, characteristics for other piston ring - cylinder liner pair will not be specified or detailed here.

### 2.3.2 Friction and wear – the major threats

The piston (including the rings) friction is one of the major issues contributing to the mechanical losses of IC engines. Although the oil control ring is the one with the highest contribution, the ring pack (in general) contributes for a significant part of the engine friction losses [19]. The quantification of this impact varies among authors, but those particularly focused in this field referred that 20% of the engine frictional losses occur due to the piston ring pack [20,21].

Briefly, friction can be described as the existing resistance between two contact surfaces during their relative movement. During engine operation, the combustion gas pressure acting onto the piston (together with the connecting rod slope) increases the friction force on the ring-liner contact, and consequently, the frictional resistance to the sliding movement. The maximum pressure values are achieved slightly after TDC and, consequently, it is in the period in the vicinity of TDC that occurs the maximum power loss due to friction [22]. To overcome this problem (and others, such as surface oxidation and heat transfer) lubricating oil is universally used between the piston/piston rings and the cylinder liner [23–26].

In a complete engine cycle the piston operates under different lubrication regimes comprising the boundary, mixed and hydrodynamic lubrication [27,28]. When the piston reaches the dead centres (TDC and BDC) its velocity drops to zero, so the existent hydrodynamic regime that occurs during most of the piston movement, drops to mixed or even boundary regime, where the layer of oil is significantly reduced and there is the chance of the surfaces becoming in contact [29]. This is particularly critical at TDC during combustion and is the reason that most of the liner wear occurs at the top of the liner [30]. Even though, the amount of lubrication oil left in the top walls of the liner must be kept to a minimum without jeopardizing the tribological performance. An excess of oil may foster oil consumption which increases the pollutant emissions resulting from the oil vaporization and/or burning when exposed to the combustion temperatures [31].

The presence of this third element in liquid state (oil) between the interacting solid surfaces will require an upgraded sealing between the upper and lower spaces (combustion chamber and crankcase) during the relative motion. As previously referred, the sealing effectiveness has several consequences as, for instance, the control of the lubricant leakage. In this context, dynamic sealing represents one of the most important challenges for compressing rings [32]. During the piston

reciprocating movement the dynamic sealing will perform another relevant task: the cleaning of the contact surfaces. This prevents the presence of contaminants or solid particles in the interface of the sliding piston ring and the inner liner surface. Those particles, even in a micro-scale, may trigger a fast increasing of the surface wear of the metallic surfaces as a consequence of the three-body abrasion wear mechanism [33].

The solid particles do not only represent an issue for the piston ring surface but also for its counterbody, the cylinder liner. For this reason, the cylinder liner is textured using honed textures on its surface (Figure 2.7) to lodge some small abrasive particles, to control oil consumption and to allow the oil to adhere to the walls. Although polished surfaces may seem to create less friction, they may not hold the oil layer as efficiently as a honed surface. However, some of the manufacturers manufacture cylinder liner solutions using hard and polished surfaces produced by hard metal deposition.

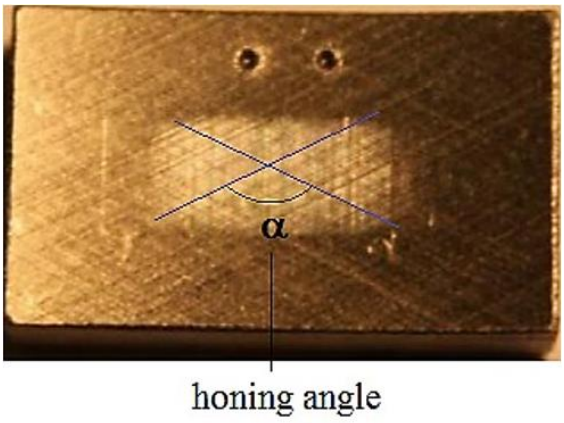


Figure 2.7 Honed cylinder liner surface texture (adapted from [13]).

In general, roughness and surface texture represent relevant parameters with higher contribution to the existing frictional forces due to the potential for varying the contact area [34–38]. Some authors studied the impact of the surface finishing process on both surfaces of the piston ring - cylinder liner assembly on the frictional losses and on the wear of the ring and liner surfaces [39–48]. For example, the honing angle has an important impact on the tribological results of this pair. Mezghani et al. [49] specified two ranges of honing angles (40-55 degrees and 115-130 degrees) in which the hydrodynamic contact achieves the minimum coefficient of friction. Grabon et al. [50] took a step forward and stated that with honing angles of liners smaller than 55

degrees (the lowest range) it is possible to reach a lower coefficient of friction (COF). A broad assessment to surface texturing solutions for friction and wear reduction is presented by Gachot et al. [51]. The authors sum up the most relevant findings on texture geometry and lubrication conditions, presenting the geometries which had the best results and suggesting the surface texturing techniques for each condition. Despite those solutions are effectively applied in the cylinder bore, they do not overcome the consequences on the top ring surface caused by abrasive wear.

The wear of the compression ring running surface, illustrated in Figure 2.8, represents one of the main failures of the compression ring [52]. As soon as the ring running surface begins to wear, the hot gases from the combustion accelerates the rings' surface degradation. When the compression ring peripheral surface begins to wear, some wear tracks appear on its running surface corresponding to the axial movement direction [53] and the surface quality begins to deteriorate. This changes the initial preconditions created for the dynamic sealing [54]. Aside from subsequent performance factors in the tribological point of view, the presence of wear tracks will promote the increasing of wear. A worn external surface will directly affect the geometrical, dimensional and functional properties of the compression ring. The wear of the compression ring surface or of the ring groove surface, or even of the cylinder liner, will limit the life of the internal combustion engine.

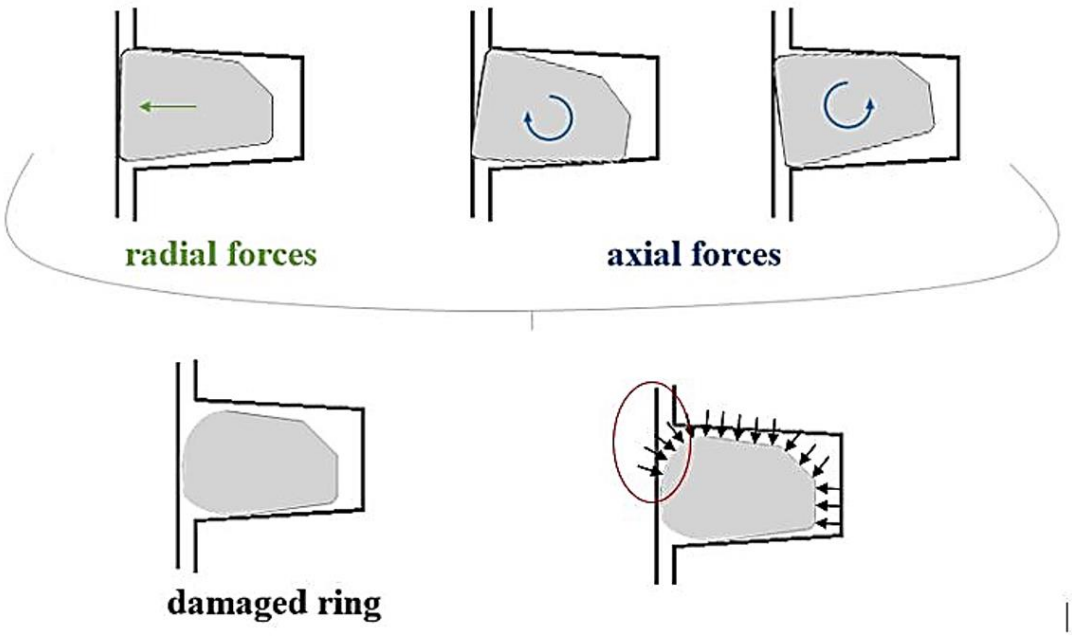


Figure 2.8 Changes in the cross-section geometry due to the presence of radial and axial forces during engine operation.

Figure 2.8 points out the possible failure consequences of compression piston rings, which are the critical changes identified in the ring cross sectional shape. Thus, wear resistance enhancement and COF reduction represents the leading goals and ongoing research topics of this engine tribological system. Figure 2.8 also shows an effect on the performance of the worn ring: the gas pressure resultant from the combustion process is also applied on the outer surface of the ring, reducing the improved sealing. During the combustion/expansion stroke (with the piston downward movement), the gas will act on the periphery of the ring, above the contact between the ring and the liner (see Figure 2.8, lower, right figure), reducing the ring force onto the liner, decreasing the effectiveness of the sealing.

The consequences of the piston ring wear are not only observed in its running surface. When the surface begins to wear the consequent local erosion, which represents a surface discontinuity, will affect the lubrication oil circulation and its local hydrodynamic pressure [55]. Associated to a poorly lubricated zones due to the presence of high operating temperatures, high pressures and low speeds, local micro weldings or material adhesion, known as scuffing, are common in the top ring face [56,57]. The most usual problem of compression ring top and bottom faces is sticking on the contact with the piston material, causing a micro-welding contact through the presence of the carbon deposits (generated from an inefficient combustion process), which are almost melted due to the high temperature conditions.

The strategy used by piston rings manufacturers has been the deposition a layer of a material with high wear resistance onto the piston ring sliding surface. Current hard coating materials on the functional surface of the ring act as a protection body against surface wear but have a limited performance against abrasion by dirt particles. Differentiated materials have provided solutions to this problem in the last decades. The next section presents specific contextualization on some well-known concepts in this field.

### 2.3.3 Top ring coatings – surface protecting solutions

The most effective conventional solution to increase the wear resistance of the structural material and, consequently, enhance combustion chamber sealing, have been dependent on the surface engineering development [58]. Surface coating materials and their deposition processes have been deeply studied over the years. The implemented strategies are usually based on

mechanical and tribological solutions which associate low cost materials in the base structure with a superior performance material covering the functional surface [59].

To be applied to the piston ring surface, the selected materials must be able to endure a complex stressing system composed by mechanical, thermal and tribological loads in a dynamic context [60]. Materials' strength (mainly in the elastic range), one of the main properties of almost every mechanical part, is a key property for material selection [61]. In addition to sealing, the prevention of oil access to the combustion chamber and the dissipation of heat to the liner are also important roles of the piston rings. Thus, thermal conductivity and thermal expansion are also important properties to take into account.

Thermal and tribological optimisation have push forward the state-of-the-art science material development for the last half a century. The application of a protective layer over the component material is the basis of the most recent commercial solutions.

Until a decade ago most of the piston rings used a heat-treated low-alloyed nodular cast iron as the structural material [62]. Other coatings [63] or composite materials using an aluminium alloy matrix [64] have been proposed, but without success for commercial implementation. The high modulus of elasticity and high bending strength of nodular cast iron fulfilled the mechanical requirements for the ring. The requirements for reduced ring friction led to slimmer widths and the subsequent increase in combustion pressure imposed a radical change in the structural materials, with high chromium alloyed steels being the norm (of 300 and 400 series groups of stainless steel). Its improved fatigue strength, greater durability and superior wear resistance supported that change. To further increase their mechanical strength and their wear resistance, different surface treatments were applied to the structural material. Surface treatments such as nitriding are commonly used to increase surface hardness through a phase transformation of the near-surface region, creating a diffusion layer. This process is still being used by some manufacturers [65–67].

The use of additional treatments to improve the resistance to wear of the existing material was not effective to get a superior wear resistance. This boosted the use of different materials added to/deposited onto the piston ring functional surface with far superior wear resistance, the surface hard coating. The selection of the surface coating material has two main specifications: high wear resistance and high adhesion to the substrate.

Hard chromium was one of the first solutions to coat compression rings. Hard chrome electroplating surfaces were introduced as a solution for the reduction of the oil film thickness associated to high mechanical loads [10,68,69]. Thick coatings (up to 100 μm) can be produced

using the electroplating technique, which provides good corrosion and wear resistance. It can be implemented as a large scale production technology which makes it the material/technique adopted on most automotive manufacturing production. However, due to its low heat stability and high internal stress associated to the production of significant quantity of aqueous waste (incorporating highly toxic Cr), the industry has discontinued this process [70].

With the implementation of hard materials on the functional surface, the strategy to optimize the component performance was not focused on the material hardness but on their interaction, trying to match the performance of a single part. The adhesion between the two different materials and the coating thickness had shown to have influence on the coating or/and substrate stresses. As reported by Lima et al. [71] in their numerical study, compressive stresses are associated to thinner coatings, while thicker coatings presented mostly tensile stresses. The compressive axial stresses in the ring-liner contact, in comparison with the tensile stresses in the central regions of the ring, resulted on a system less prone to crack propagation. As the hard materials are more prone to a higher brittleness (crack formation), the prevention of crack propagation is a fundamental characteristic of the functional coating.

Table 2.1 lists some works with reference to possible solutions for piston rings coating materials through different processes of two distinct technologies, Thermal Spraying (TS) and Physical Vapour Deposition (PVD). They show a connection between the developed and/or characterized coatings and the requirement of high wear resistance of the piston rings.

Looking at Table 2.1, part of the presented works uses thermal spraying as the deposition technology. Most of the techniques of the TS technology result in inflight surfaces oxidation and porosity due to the presence of oxides in the coating and due to vacant spaces between splats, respectively [72]. In top of these unwanted characteristics, TS coatings present other two limitations with high relevance to their use in the piston rings surface: the mechanisms of adhesion of TS coatings are mainly produced by mechanical anchorage rather than by metallurgical bonding; and the coatings usually contain residual stresses, mainly tensile stresses, which can occur based on the difference of the coefficient of thermal expansion between the coating and the substrate material [73–76]. These limitations restrict the coating service life and expose the coatings to adhesion problems with cracking and/or delamination phenomena.

Beside the listed works, more recently Deepak [77] proposed a new Ni-Mo-Al coating mixed with 20% $Cr_2AlC$ deposited by arc plasma spraying. This study demonstrated a decreasing of the erosion rate caused by the addition of the $Cr_2AlC$ compound. This result is achieved due to the

presence of a protective oxide layer and a carbide layer. Even though those results are relevant for the piston ring operation, there are no evidences on their improved tribological performance, comparing with the state-of-the-art solutions.

Although thermal spray limitations are detrimental on its usage to coat the piston ring surface, this technology is widely used to coat the cylinder bores [78–81]. In the last developments, the internal plasma spray coatings have iron oxide particles embedded in the deposited material to act as solid lubricants [78]. After deposition, the surface roughness is rectified by the honing process.

Conversely, physical vapour deposition technology was introduced as an enabler of thinner coatings. Also, it enabled the phasing-out of electroplating environmental problems [82–85]. With the spread of different PVD techniques, the use of a thinner surface coating with far superior mechanical property than the base material became prominent among the piston ring manufacturers. Different techniques using PVD technology, such as the cathodic arc deposition process, were common solutions for coating compression rings (Table 2.1). With a broad spectrum of available materials to be applied as protective coatings, the transition metal nitrides offered the demanded resistance [85–90]. TiN coatings were studied by some authors [82,86,91], but the CrN coatings were the preferred choice due to its superior corrosion and oxidation resistance and higher fracture toughness and ductility, ideal to high stress applications [85,87,88,90,92].

Table 2.1 List of scientific papers ordered according the respective year of publication, in which the development and/or characterization of different coating materials is presented (and have some reference to the application of the coating under research in piston rings).

| **Year** | **Ref.** | **Coating** | **Technique** | **Thickness (μm)** | **Substrate** |
|---|---|---|---|---|---|
| 1992 | [82] | Ti, TiN (multilayer)) | (PVD) - Cathodic arc evaporation | 9 | Cast iron |
| 1996 | [202] | Mo coating | (TS) – By flame | 100, 500, 900 | Mild steel ASTMC633 |
| 1997<br>1999 | [83]<br>[84] | CrxN | (PVD) - Radio frequency magnetron sputtering | 6-8 | - |
| 2000 | [91] | Ti/TiN (multilayer) | (PVD) - Multi-arc and magnetron sputtering ion compound plating | 4 | Cast iron |
| 2003 | [203] | CrN<br>DLC | (TS) – *not defined*<br>(PVD) – *not defined* | ~ 3.5<br>~ 2 | Nitrided SS |
| 2004<br>2005 | [204]<br>[205] | Al-Mo-Ni | (TS) – By plasma | 550-700 | AISI 440C steel |
| 2010 | [206] | Cr3C2-25%NiCr | (TS) – High velocity oxy-fuel coating spraying | 433 | Carbon steel (CSN 11 523) |
| 2010 | [86] | TiN | (PVD) - Cathodic arc evaporation | 6.7 | D2 tool steel |

| | | | | | |
|---|---|---|---|---|---|
| 2012 | [87] | CrN | (PVD) - Cathodic arc evaporation | <50 | Nitrided 17 wt.% Cr stainless steel |
| 2012<br>2013 | [85]<br>[88] | CrN | (PVD) - Plasma enhanced magnetron sputtering | 1, 5, 10 | H-13 steel |
| 2015 | [89] | NbN/CrN (multilayer) | (PVD) - Cathodic arc evaporation | 25-30 | Martensitic SS (AISI440B) |
| 2016 | [123] | TiSiCN | (PVD) - Plasma enhanced magnetron sputtering | 20 | AISI304 SS |
| 2017 | [90] | CrN | (PVD) - Cathodic arc evaporation | 12.3 | Cast iron alloy |
| 2017 | [207] | Diamond-reinforced hard chrome plated (multilayer) | (TS) – *not defined* | 75-78 | Steel 1.4112 (X90CrMoV18) |
| 2017 | [124] | Mo-NiCrBSi | (TS) – By plasma | 100-150 | 304 SS |
| 2017 | [208] | NiCrBSi | (TS) – By plasma | 350 | 304 SS |

*

**PVD** – Physical Vapor Deposition
**TS** – Thermally Sprayed

Figure 2.9 presents a cross section view of a compression ring where the use of a surface coating and the use of a nitride layer can be identified. Using a thin protective coating of a hard material with high wear, oxidation and corrosion resistance, the tribological response of the piston ring is defined by the coating layer. The surface finishing must be rectified before and after the coating deposition. Several grinding steps are applied to the piston ring profile to define the cross-section geometry. The resulted surface roughness improves the adhesion of the coating layer, but on the other side, it will be replicated by the deposited material as illustrated in Figure 2.10. An additional step is needed to decrease surface roughness using a polishing process or even a lapping process, for an enhanced surface finishing.

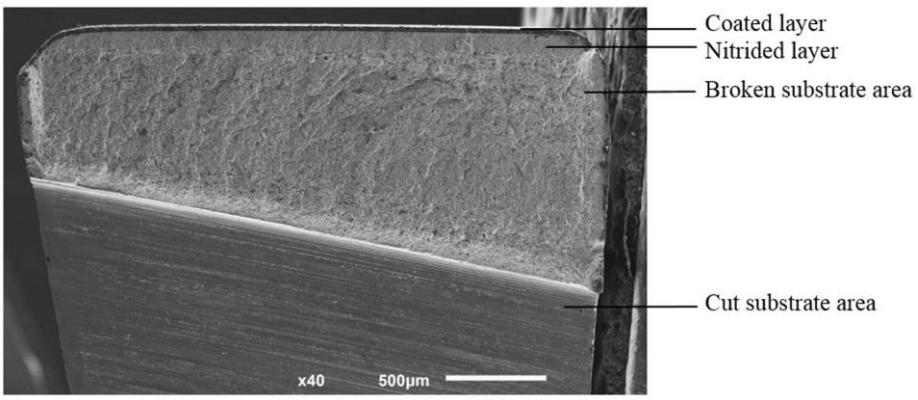


Figure 2.9 SEM image of a cross-section view of a compression ring with the respective coated and nitride layers above the substrate material.

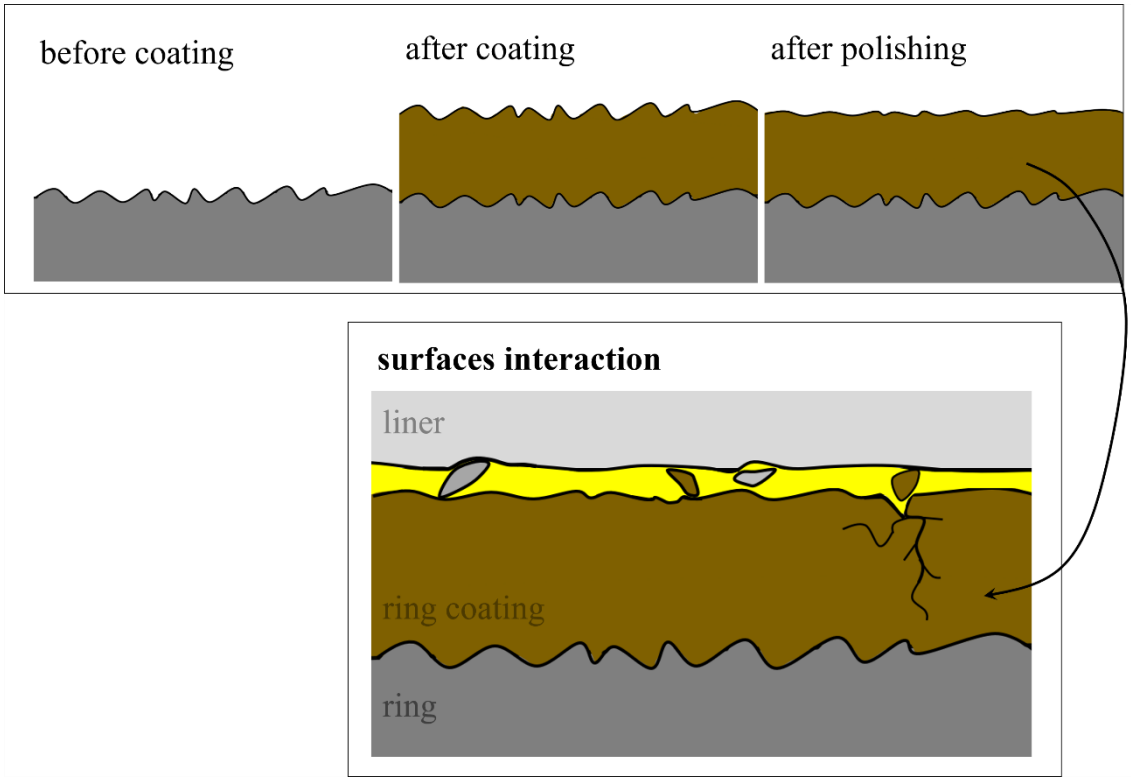


Figure 2.10 Effect of the ring coating layer on the surface roughness and its interaction with the liner surface in the presence of lubricant oil and wear debris.

The classic PVD coatings are deposited as a bulk layer, having a growing columnar structure. During engine functioning, and due to thermal and mechanical fatigue loading, some cracks may initiate in the ring coating layer. Those cracks propagate through columnar boundaries, and consequently a portion of material can be detached from the surface, as exemplified in Figure 2.10. Debris from both surfaces may also be detached due to the contact between asperities from the piston ring and the cylinder liner. Smaller debris flow between surfaces through the lubricant oil, while bigger particles cause three-body abrasive wear.

The need for a superior scuffing resistance and an even greater wear resistance has pushed the advance of new coating materials to be applied in the piston rings. The proposed strategies to find the best tribological performance include changing the coating technology, coating materials or changing both. The following section presents the forthcoming progressions in this field with an outline of the main challenges and the conventional solutions.

## 2.4 Top compression ring surface - research trends

New ground-breaking approaches involving novel material engineering and materials design have been introducing different solutions to solve the existing tribological concerns: low friction for enhancing engine efficiency and low wear to ensure a long engine operation. Figure 2.11 outlines an innovative proposal based on the present trends of evolution in the field of compression rings design and development. Each topic will be thoroughly described in the following subsections.

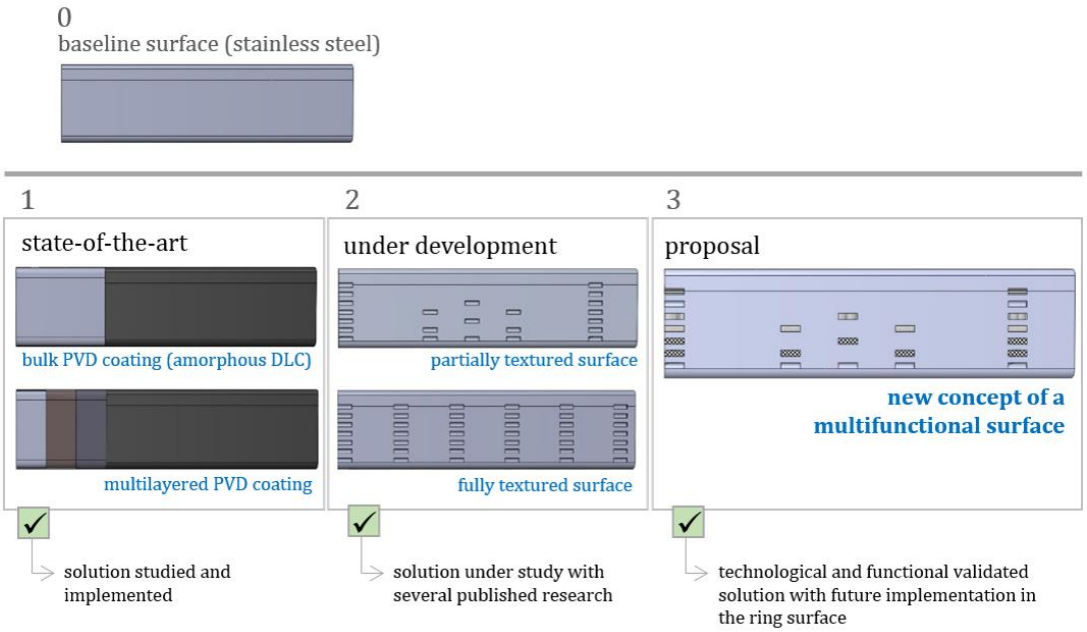


Figure 2.11 Progress of the tribological solutions already proposed and under development to be applied to the compression rings (all solutions were presented using the top view of a section of a compression piston ring).

Multilayered coatings and hard carbon coatings have been widely developed during the last decade and proved to have potential to be quickly implemented in the market. However, its application in piston rings needed further improvements before being established as a viable solution in this industry. The developed coatings have not yet proved their efficiency and still represent a problem during the engine service life due to excessive oil consumption caused by their worn surfaces and geometry change.

While the referred solutions (multilayered and hard carbon) are intended to intensify the surface wear resistance, the used of textured surfaces is suggested to diminish the coefficient of

friction of that surface. Surface texture may represent a potential tool to be used in friction reduction applications with feasible implementation in a large-scale production.

A greater technological breakthrough may be achieved with the development of a surface which comprises different elements intended for distinct purposes. Much more flexible manufacturing technologies are able to be implemented in a series production allowing the development of a more creative and more complex solutions with enhanced functionalities. Some disruptive proposals may alter the way of thinking of the piston ring industry, showing the way to the required leap which may alter the way of thinking of the piston ring industry.

The following sections present a brief scientific review of the intended technologies, with particular focus on the most relevant research in each field. Each topic is initially contextualized, together with its main working principle and the fundamental concepts of each technology.

### 2.4.1 State-of-the-art: Surface coatings

*Diamond-Like Carbon Coatings*

During the last two decades, the performance of the chromium coatings fulfilled the requirements of the standard engines. However, for the last few years, engines operating pressures have been significantly increased both in commercial vehicles and in motor sport.

In the automotive industry, among the premium materials the carbon-based materials appeared as one of the most advantageous solutions of surface engineering [93–101]. Representing an affordable alternative of the harder and one of the most expensive material on earth (diamond), when applied to tribological environments DLC achieves superlubricity conditions and, consequently, significantly reduces the coefficient of friction [102–105], in particular when compared to conventional solutions such as CrN coatings [106]. As a general rule, the harder the surface material is, the higher its mechanical resistance will be [107]. In the same correspondence, the increase of its mechanical resistance will also provide a superior wear resistance [108]. Gathering low friction and low wear characteristics, DLC coatings have already been proposed for powertrain parts with the goal of improving their tribological performance [109].

Currently, DLC material application uses chemical or physical vapour deposition technologies (CVD or PVD), which comprise similar techniques used to apply conventional coatings such as CrN. Those coatings are characteristics of a low temperature (up to 200°C) and a long duration deposition process (may be greater than 8 hours). Its superior duration, compared to

classic coatings (such as CrN), is a consequence of its low deposition rate, to prevent the increase of the temperature of the substrate material. The processing temperature must be well controlled because temperature variations may vary the microstructure of the deposited material, modifying the carbon allotrope.

The DLC material amorphous structure is composed by graphite (the softest) and diamond (the hardest), corresponding respectively $sp^2$ and $sp^3$-bonds, shown in the diagram of the Figure 2.12. The graphitization phenomenon begins above 300°C and the $sp^3/sp^2$ bonds ratio (the quantity of $sp^3$-bonds relatively to the quantity of $sp^2$-bonds) starts to decrease [94,103].

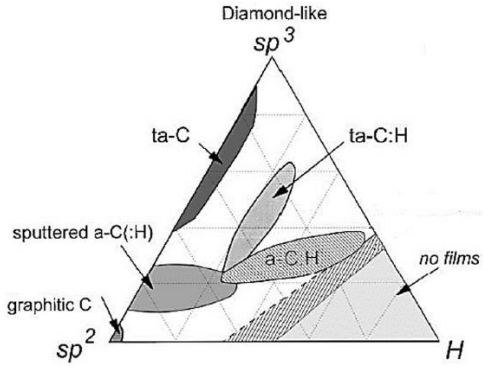


Figure 2.12 Ternary phase diagram adapted according to and using data from.[40].

Recent studies have arisen with the goal of studying, not only wear resistance, but also scuffing resistance of those carbon-based coatings, which is one of the weaknesses of the conventional bulk coatings. Tas et al. [110] studied the influence of surface roughness on piston rings scuffing resistance and Wan et al. [111] presented the evaluation of wear and scuffing resistance of a carbon-based engineered coating for automotive piston rings which is already on the market. Both research groups concluded that the most favourable condition is a DLC coating associated to a ring surface with low surface roughness (named as mirror-polish finish).

Hydrogen-free carbon-based coatings have been recommended for piston rings. Aside from its improved temperature resistance compared to hydrogenated DLC, it provides the lowest coefficient of friction when applied with lubrication oil [112]. Higuchi et al. [113] compared hydrogen-free DLC coating with a chromium coating and reported an improvement of 17% in the coefficient of friction of the compression rings against the cylinder bore using a low viscosity engine oil. Some engine running conditions were also studied using hydrogen-free DLC material as a piston ring coating. Dorner-Reisel et al. [104] analysed the wear resistance of a DLC coating using diesel fuel at different temperatures and discussed the composition and the behaviour of the diesel fuel

up to 450 °C, when the coating pre-oxidation and phase transformation begins and confirmed the coating resistance up to 450 – 600 °C.

Although several works have been published on the subject of DLC coating properties, only a few focused on the DLC coating tribological properties as a function of the technology used to produce them. Mabuchi et al. [114] evaluated the wear resistance of a hydrogen-free DLC layer of a piston ring comparing four different deposition techniques: trigger-type arc ion plating, laser-discharge-induced arc ion plating, filtered cathodic vacuum arc ion plating and magnetron sputtering. They concluded that with the increase of the coating hardness, its wear resistance is also enhanced. Further analysis enabled to assume the less suitable techniques were those with the presence of surface droplets inside the coating, as it tends to increase the wear amount under severe sliding conditions. Through this study it is possible to conclude that DLC coating thickness must be accurately controlled. The final coating should be built up by sequential thin layers, avoiding the use of large particles to ensure a uniform thickness at the end of the deposition process.

Later, Kano [109] took a step forward and presented a review work where he discussed the current implementation of the DLC material in mass production applications. This work gathered three important topics: the DLC material, automotive engine components and tribological issues of DLC coatings, using piston rings (compression ring and oil ring) as case studies. He mentions the use of the arc ion plating PVD method in a mass production scale. After mentioning some works about friction reduction, adhesion strength and wear resistance, Kano committed himself to report the advancements and the new findings related to DLC coatings 10 years after his initial work [109].

Figure 2.13 presents schematically the state-of-the-art solutions on the implementation of the DLC coatings in the piston rings surface, considering the scientific works previously referred.

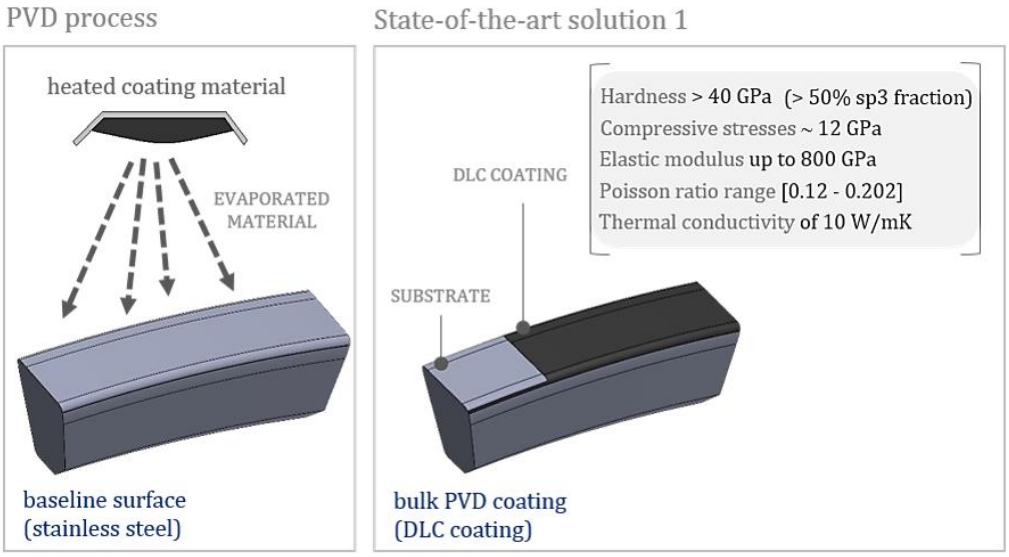


Figure 2.13 Deposition of a carbon-based coating to the compression ring running surface and the expected coating properties according to Vetter.[43].

Among the possible PVD techniques, the cathodic arc deposition process has a major advantage: the atomized evaporated material has an ionization fraction of the close to 100%, even using a graphite target. The control parameters of the deposition process, such as chamber pressure or target voltage, vary with the substrate material onto where the carbon atoms will be deposited, with the desired coating thickness and with the required final surface roughness. The coating layer thickness has a minimum of 5 nm (to ensure the properties presented in Figure 2.13 [97]) and it can reach thicknesses up to 6 μm [110].

If the piston ring DLC coating has high hardness values (around 80 GPa), when in contact with the counter-body material (grey cast iron), an abrasive effect may occur on the softer surface. However, the contact among the piston ring and the cylinder liner must guarantee that the improvement of one part of the tribological pair will not cause the damage of the opponent part.

*Multilayered and Compound Coatings*

Diamond-like carbon coatings, such as other PVD bulk coatings, have a relevant characteristic in common: a high level of intrinsic stress. On the one side, compressive stress helps to relieve mechanical loads on the perpendicular direction, contributing for the surface wear protection. On the other side, the presence of residual tensile stress causes low adhesion strength

to the carbon-based coatings, resulting on a shorter durability and on a poor performance, particularly in tribological applications. To overcome this and other shortcomings the application of a transition layer [115] and different coating arrangements using carbon-based materials have been proposed by several authors [116–122].

Similar approaches may enable a wider application of PVD coatings [123] (even coatings from a different manufacturing process [124,125]) with specific use on the piston ring's surface. According to the latest developments in surface engineering, advancements in the development of more complex and efficient coatings may convert classic bulk coatings into an outdate solution to the premium market.

A practical solution to enhance some DLC coating properties, such as mechanical toughness, is the possibility of being doped with other elements, forming compound coatings. Molybdenum and tungsten elements, which are known by their self-lubricating properties, were already associated with the DLC coatings to form an enhanced solution, showing simultaneously lower coefficients of friction and higher resistance against wear [126,127].

On the other hand, the use of a soft material (providing solid lubrication and a low COF) staggered with a hard material (protecting against wear) have providing multilayered architectures with improved tribological results. Table 2.2 lists four works with application on the piston rings industry, two of them proposing compound coatings and the other two proposing multilayered coatings.

Table 2.2 Enunciated research works with reference to the needed piston rings wear resistance.

| Year | Ref. | Multilayer material | Deposition technique | Type of coating |
|---|---|---|---|---|
| 2000 | [91] | Ti/TiN | Magnetron sputtering ion compound plating | Multilayered |
| 2015 | [89] | CrN/NbN | Cathodic arc deposition | Multilayered |
| 2016 | [123] | TiSiCN | Plasma enhanced magnetron sputtering | Compound |
| 2017 | [124] | Mo-NiCrBSi | Atmospheric plasma-spraying | Compound |

Almost two decades ago Zhuo et al. [91] presented the Ti-TiN multilayer compound coating to be applied on a cast iron piston ring. The target of the authors was to optimize the properties of this multilayer with a total thickness of 4 μm, using two different deposition methods: multi-arc and magnetron sputtering ion compound plating. According with the obtained results, the multilayered coating showed better wear resistance than the Cr-plating coating.

The research group of Ehiasarian and Hovsepian, two relevant authors in this field, developed a nanoscale multilayer CrN/NbN coating [128–131], which became a multilayered coating intensively studied [132,133]. CrN coating is seen as one of the classical solutions applied on several components on the market such as compression rings, and it is easily produced using several PVD techniques. The deposition of NbN coatings using cathodic arc technique was presented by Cansever [134], where he details different deposition conditions and presents the mechanical characterization of the coating, with hardness values up to 39 GPa.

Recently, Araujo et al. [89] proposed a similar nanoscale multilayer coating deposited with the cathodic arc technique. They studied the effect of the coating layer periodicity on its hardness and scratch resistance. In the Figure 2.14 the cross-section of the final coating is presented where is possible differentiate the sequential layers.

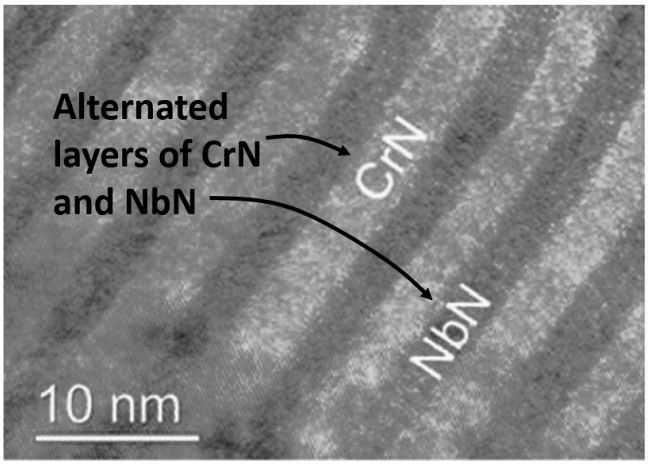


Figure 2.14 TEM micrograph of the cross-section of the NbN/CrN multilayer coating (adapted from[36]).

In their study they determined that the hardness of the nanostructured multilayered coatings increased with the decreasing of the bilayer thickness. The multilayer periodicity, as well as the layers thickness, have impact on different properties of the final coating. This demands for an earlier accurate design of the coating architecture. Using available technologies already installed in the piston rings production lines, such as cathodic arc (the most used large-scale PVD technique), the implementation of these solutions (compound and multilayer) would comprise only the adjustment of the deposition conditions of the different materials.

Figure 2.15 presents a schematic representation of a multilayer state-of-the-art solution in the piston ring surface.

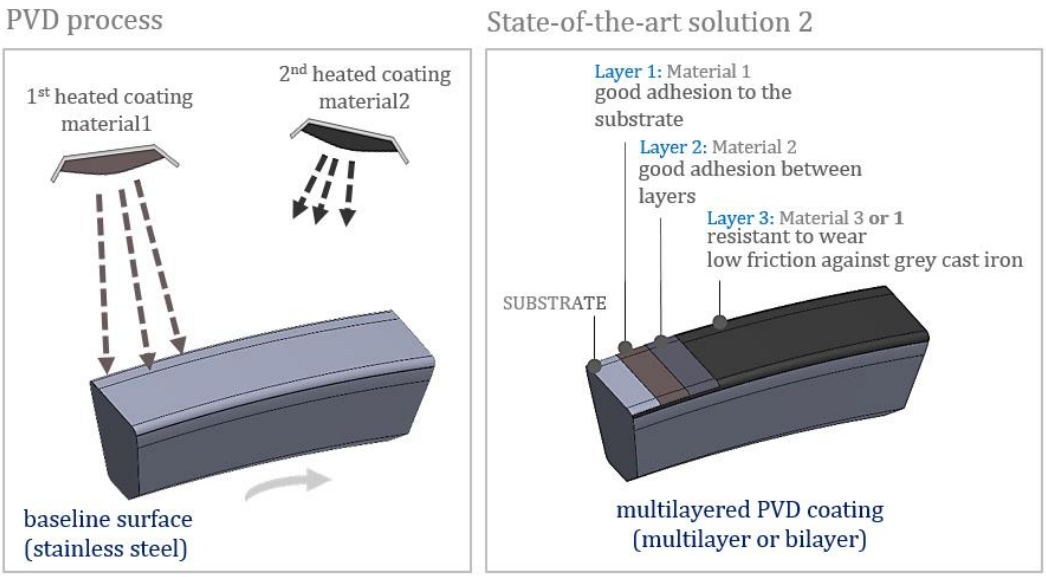


Figure 2.15 Simplified scheme of the PVD deposition of more than one material (using two different targets) on the substrate using a multilayer architecture, or a bilayer solution, repeating material 1 in the third layer and so on.

The presented scheme infers the possibility of different material deposition. The targets of the distinct materials are positioned in opposite sides and the deposition of each material occurs alternately according to the rotation of the substrates holder. The use of a third material may result from the use of a reactive gas, such as nitrogen, which will react with the material to be deposited and form a new compound layer over the substrate.

A gradient of a specific property, such as hardness, may be formed from the layer closer to the substrate to outer surface. A limitation of this solution is that the transition materials have no direct influence on the physical contact of the tribological pair considered in the work. The role of the layers underneath the final layer is to connect the previous layer to the following material and only the final layer has a direct impact on that physical contact.

### 2.4.2 Under development research: Surface textures

The creation of protuberances (outgrowth prominences) [135] or dimples (pockets or cavities) [136] using high precision machining techniques, such as laser technology, has been

extensively explored for tribological applications due to their influence on the dynamic contact between two surfaces. This is called surface texturing and has been seen as one of the most promising solutions to obtain enhanced tribological results in sliding contacts [137,138,147–150,139–146]. Ordered structures were not only proposed to the coating core but also for its external surface in the shape of surface textures.

A decade ago Bruzzone et al. [151] wrote about the advancements of the engineering surfaces and mentioned textured surfaces as a potential solution to improve tribological properties. According to the authors, the texturing of surfaces is used to optimize lubrication and lower friction and wear among engine components with relative sliding movement, with the entrapment of debris into the patterns. As the entrapment of wear debris is regularly claimed by most authors as a functional gain of the presence of surface textures, in Figure 2.16 is illustrated that effect. In this figure the debris formation is represented in the surface coating material of the piston ring, but it should be mentioned that it can also occur because of a worn liner surface.

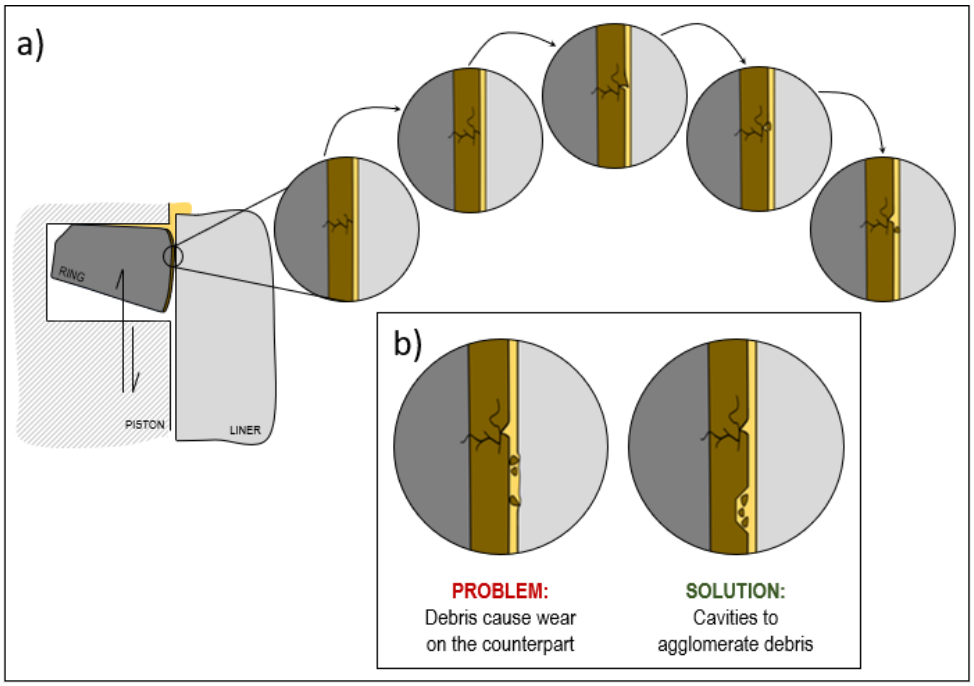


Figure 2.16 (a) Interaction of the piston ring-cylinder liner surfaces occurring crack formation, crack propagation, surface material detachment and debris formation. (b) Illustration of the effect of cavities produced by surface texturing acting as a potential solution for debris agglomeration, preventing the surfaces of three-body abrasive wear.

Gachot et al. [51] published a critical assessment mentioning some parameters of the practical implementation of textured surfaces in tribological applications. They presented a table in

tribological contacts (dry sliding and different lubrication regimes) which are linked to texture characteristics, texturing techniques and the functional effects of surface texturing reported by several works. The textures geometry, size, shape orientation and coverage area are compared according to the lubrication regime. Pockets and groves are the most referred shapes and the coverage area ranges vary from 10 to 70% in dry sliding and 10 to 20% in fully film lubrication. Texture height and width tend to decrease with the raise of the quantity of lubrication oil in the contact. The largest values reported for dry sliding are a height of about 60 μm and a width of 20 μm.

In fact, as previously referred, surface texturing is a process already applied to some engine components. A plateau-honing with crossed-hatched geometries (called "honing") is applied to the cylinder liner bore surfaces since the 1940s with the purpose of preventing seizure under hot engine running conditions [152]. Currently, cylinder liner texturing continues to be comprehensively studied [9, 88–95]. Among several works, Biboulet and Lubrecht [161] developed recently a 1D analysis of the liner-oil ring contact to optimize the pressure distribution and, consequently, the load carrying capacity of an idealized textured liner surface. In the oil control ring, due to its much flatter surface than the compression ring, the application of a cross-hatched texture also increases its the load carrying capacity.

Some of the published studies are based on numerical simulations [147,162–165]. In general, they conclude that surface textures have a good potential to generate an enhanced hydrodynamic support with potential to reduce wear and friction. In this context, Zavos and Nikolakopoulos [162,166] developed a two dimensional numerical model to study the behaviour of a worn compression ring when against a cylinder liner. Usman and Park [163] used a 2D transient model of mixed lubricated contact to study the effect of some geometrical parameters, like depth, length, area density or diameter on the interaction of the piston ring and the cylinder liner during warm-up engine conditions. As highlighted by those authors, the use of numerical tools has certain shortcomings, such as the use of a circular cylinder liner-piston ring contact (which does not consider ring conformability) and a fully flooded inlet condition (without consider oil starvation). Tomanik [164] and by Gu et al. [165] used a simplified one-dimensional model with the particularity of considering a starved lubrication condition.

In his study, Tomanik [164] presented the following key points among the wide range of different geometries and morphologies, as major advantages in a tribological analysis:

**i.** The avoidance of the presence of wear particles in the contact (which could cause abrasive wear): they are entrapped into the textured pockets;

**ii.** The oil-holding capacity to guarantee a lubricated contact will contrast to very smooth lubricated surfaces that usually show an ineffective tribological behaviour.

**iii.** The presence of secondary reservoirs of lubricant could be helpful in conditions involving high plastic deformation;

**iv.** The improvement of a hydrodynamic pressure between the ring and liner surfaces.

Although some experimental studies have been carried out, final results have shown to be more difficult to converge [167,168]. The reliability of the results widely varies either with the reproducibility of the experimental rigs or with the reproducibility of the texture manufacturing. Some authors have examined some technologies to produce surface textures on the piston rings. Etsion and Sher [169] tested a partial laser surface texturing applied by a YAG laser in a compression ring. Ryk and Etsion [167] and Ryk et al. [168] presented a similar proposal using a partial laser surface texture on an experimental procedure. In their study, the partial laser textured surface provides a higher friction reduction than the full laser surface textured. Figure 2.17 illustrates a schematic representation of a piston ring section with partial and full texturing effects. In regard to partial texturing, it may result in a pre-defined organized distribution of the textures over the surface according to its functional purpose.

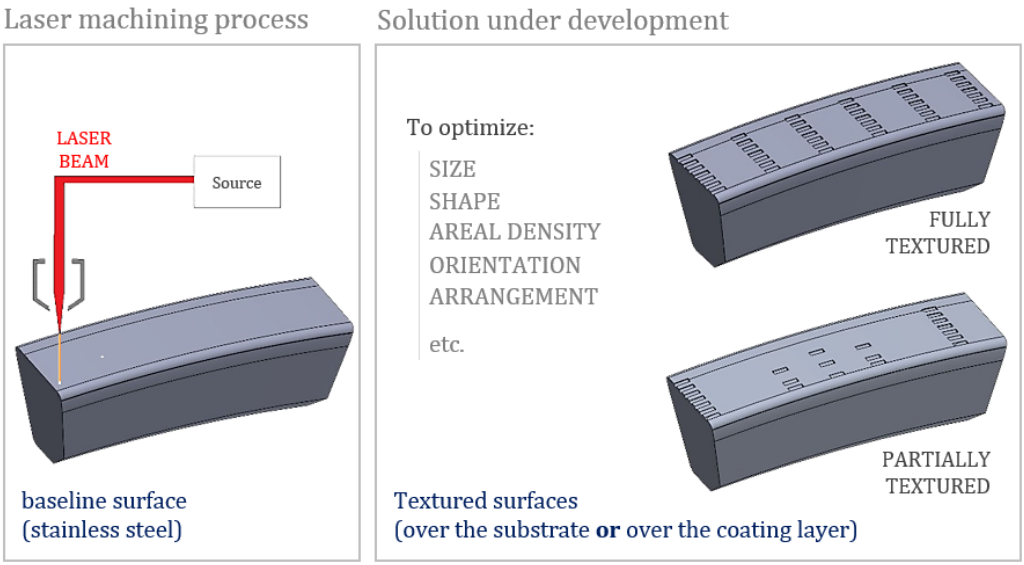


Figure 2.17 Schematic representation of the laser machining process applied to the piston ring surface with reference to some physical characteristics of the textures that should be optimized according to the final purpose.

Using an experimental and a numerical approach, Shen and Khonsari [170] proposed the application of textures to generate the hydrodynamic lift of the piston ring (the textures act as bearings). They used laser ablation (with a Nd: Ytterbium fiber laser) to eliminate the material from the surface. As a main conclusion, they found that compared to the effect of the pocket area ratio and depth, the pocket shape has a limited effect. Those pockets with a large area ratio and depth did not show any friction reduction effect.

The large diversity of available techniques for surface texturing is reflected on the variety of equipment referred by the different authors. Tomanik [164] referred the 'femtosecond' laser technique, the same used by Zavedeev et al. [171] in a diamond-like nanocomposite film, where they associate a hard coating to a surface textured solution. The potential of using a thin coating layer is the association of the wear resistance properties from the hard coatings to the possibility of reducing friction though an improved hydrodynamic support from the surface texturing. Three years earlier, Zavedeev et al.[171] and Al-Azizi et al. [172] had proposed the application of a pre-textured surface with a subsequent diamond-like carbon coating where wear resistance is required . The principal shortcoming of the latter solution is the covering of the texture, masking its predefined effect.

Figure 2.17 shows a schematic representation of fully and partially textured piston rings and some processing parameters to be optimized according to the specific material and purpose for which the texture will be applied.

The arrangement of the textures over the surface cannot interfere with the main role of the top ring, which is the sealing of the engine combustion chamber. Regarding the previous contextualization about the cross-section geometry of a compression piston ring, when a tapered shape is used, the presence of textures in the lowest part of the contact surfaces should be avoided, while on a barrel shape geometry those textures should be avoided at the middle position.

The texturing of the surface may help to improve fuel economy and vehicle performance by the reduction of friction losses [169]. According with Mishra and Ramkumar [173], the use of a lubricant with additives and a textured ring with dimples geometries also improves the lubrication through the hydrodynamic effect of dimples.

Nevertheless, the surface texturing results in additional costs, which compels a prominent enhancement of the component performance. A reliable evaluation of its effectiveness demands more accurate experimental studies, reproducing real engine operating conditions.

### 2.4.3 Future studies: Surface structures

The responsiveness and capacity of the automotive industry to undergo a continuous innovative approach to respond to different challenges have been proved for the last decades. In fact, the concept of land-based transportation systems is extensively and intensively used on a daily routine for transport of people or products. As a consequence of the intensive research for more efficient solutions, the automotive industry is in hand with the transforming industry in term of scientific and technical advances, and this progress is not an exception for the piston ring manufacturers.

The introduction of new techniques, such as the removal or adding/sintering material, increased the potential to use different materials with different properties in the same part. For example, using powder raw materials, it is possible to fill cavities with different materials for distinct purposes:

- To reduce friction (lubricity properties);
- To reduce wear (high fracture toughness);
- To accommodate coating stresses (superior ductility);
- To dissipate the combustion heat (high thermal conductivity);
- To improve oxidation resistance (self-lubrication reaction).

Based on this concept, an optimized compression ring (which includes an effective tribological pair) may benefit from different innovative solutions regarding the state-of-the-art and the most recent research in that field. Figure 2.18 shows the basic concept proposed in this paper.

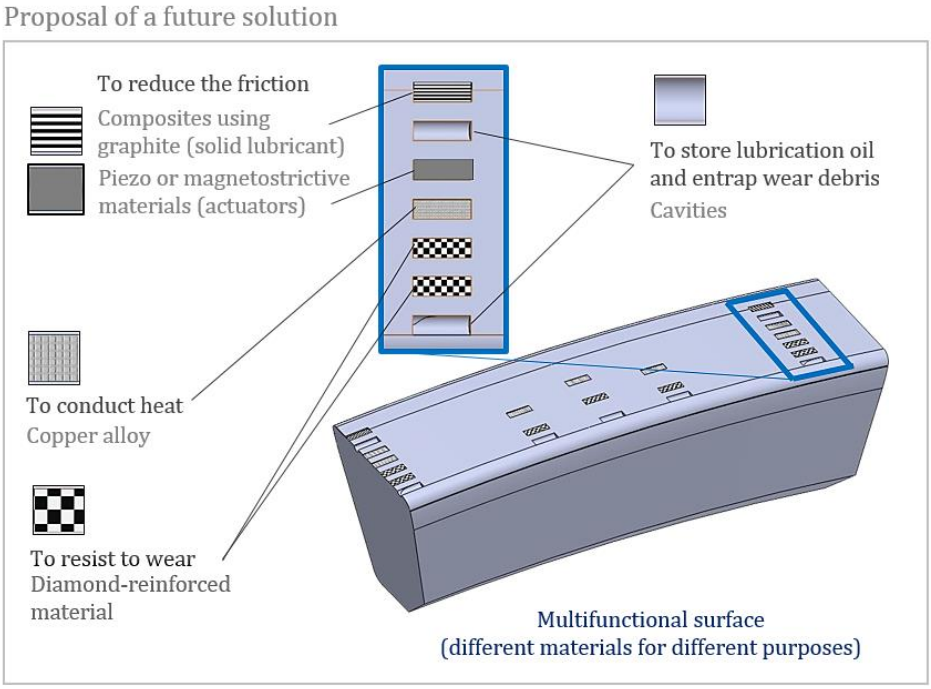


Figure 2.18 Innovative proposal of a conceptual solution to improve the tribological performance of a compression piston ring with an illustration of the presence of different materials along the surface for distinct purposes.

This proposal includes a new concept for the tribological surface and also a new approach for the piston ring manufacturing. Surface texturing is associated to numerous advantages, mainly related to the ability of provide more efficient lubrication conditions when the boundary lubrication regime sets-in. Those textures are cavities with circular, rectangular or other shape and may be used to store lubrication oil and, more importantly, to entrap small particles resulted from the abrasive contact.

Also, these cavities can also be filled with various materials for different purposes, as illustrated in Figure 2.18. Different metal, ceramic or composite materials may be positioned along the surface according to their most effective location to optimize the tribological response. This is achieved by the use of powder metallurgy. The geometric patterns range from linear to semi-random, from circular to rectangular, and the dimensions range from less than ten to a few hundred micrometres. Surface textures with cavities and multi-materials have a huge potential to increase the compression ring service lifetime while simultaneously reducing friction and enabling higher combustion pressures. The major advantage for this solution is the potential for the use of each material with a specific and controlled quantity and location.

Materials with superior thermal conductivity, as the suggested copper alloys [174–177] or aluminium alloys [178], may be placed close to the combustion chamber to improve the heat removal from the combustion process to the cylinder liner. Materials with superior wear resistance would be desired in the areas that are more prone to wear (those illustrated in Figure 2.8). Diamond-reinforced composites are suitable for this application [179–181], as their increased hardness is usually related to a remarkable wear resistance. The third functionality referred in that figure is friction reduction. Graphite compounds are suggested for this purpose, as self-lubricated elements [182].

The first step to introduce this concept for tribological purposes was made by Garcia et al. [183] for a distinct application. Future implementation of this solution in the piston ring surface is under development.

This concept may also introduce a potential function to reduce friction: the use of functionalized surface with incorporated actuators, magnetostrictive or piezoelectric materials. Some authors [184–186] discussed the influence of active vibration control on the friction forces contact of sliding surfaces. Littman et al. [184] supported that the decrease of friction registered in sliding vibrational contacts can be explained with a theoretical explanation based on Coulomb's friction law for sliding (regarding the relative velocity among two bodies in contact). Based on their theoretical models and their experimental validation processes, they have revealed that the lowering of friction is dependent on the ratio of the moving velocity to the vibration velocity. Later, Storck et al. [187] studied the superposition of ultrasonic vibrations. They studied two distinct directions: longitudinal (xx) and transversal (yy), and confirmed the previous theoretical approach by experimental results.

In fact, based on published research, ultrasonic vibrations represent a potential solution to diminish and control the effective friction coefficient among two sliding surfaces, in particular on applications where traditional lubrication methods are impractical or insufficient. By now, the beneficial impact of ultrasonic vibrations on friction reduction has been established and confirmed by several authors using analytical, numeral and some experimental methodologies [188–190]. Although most of the research about magnetostrictive materials is focused on the processing parameters for these materials (such as temperature, pressure, sintering stage), further approaches are exploring this solution to suppress the existing restrains of lubrication systems in several industries, such as the automotive industry.

At the moment those technological advancements have just been proposed to improve machining processes or the operation of equipments [184], however its use on the piston rings surface must be accurately explored. Regarding the material arrangement, the geometry and size of the surface textures must be adapted to the functional demands of those incorporated actuators. In terms of the main role of the top ring, a compromise among the ring transversal vibration and its sealing function must be achieved. If feasible, the incorporation of an active vibration control system either in the piston ring, or in the cylinder liner (or even both), may lead to a significant reduction of the coefficient of friction. This may be the result of bringing together the optimal performance with the proper surface structure and the best functional results, in terms of lubrication.

## 2.5 The manufacturing strategy approach

The technological solutions to implement the proposed overall concept are associated to the powder metallurgy transforming industry [191]. The advancements in materials engineering upheld the development of new materials, particularly in industries with high performance and in which constricted properties are required. Using new composite materials it can be achieved outstanding properties, hard to be obtained from a single material [192].

Figure 2.19 illustrates a proposal for the manufacturing steps involved on a production of surface texturing of a piston ring. A preliminary surface treatment and a protective coating are still considered in this process (as in the conventional solution), but their use will be dependent of their potential advantages they may add to the solution.

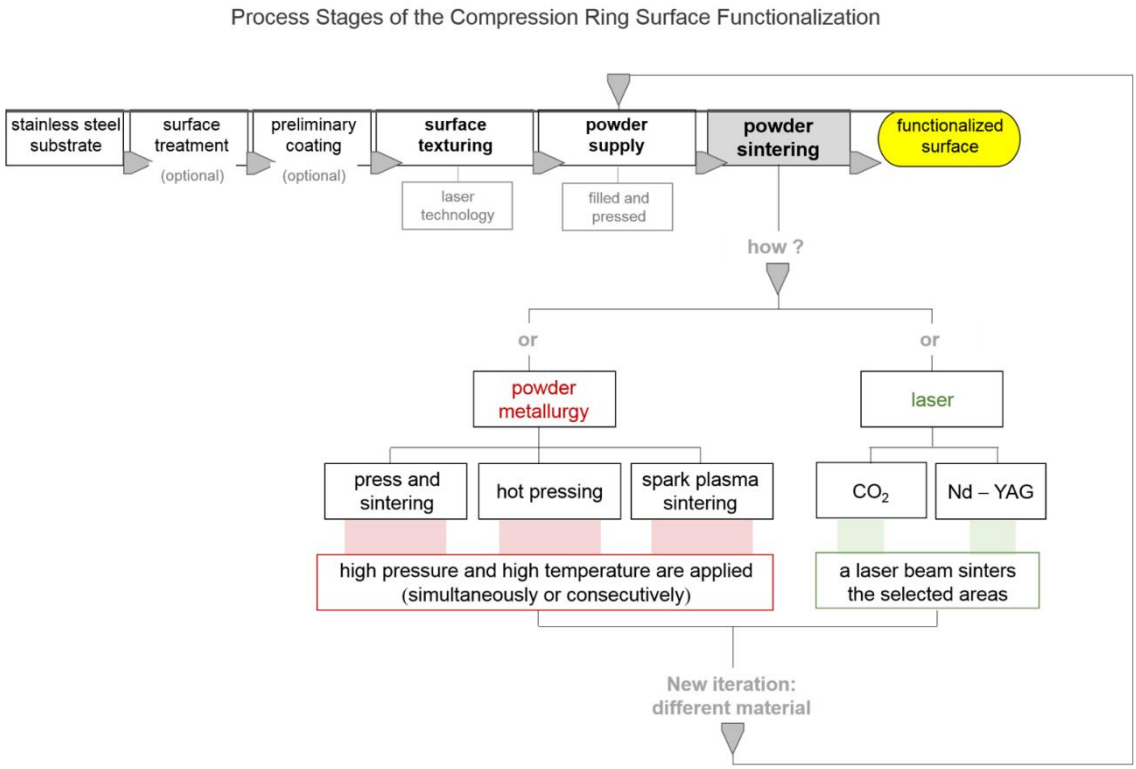


Figure 2.19 Proposal of the process stages of the compressing ring surface functionalization process.

The creation of surface features along the piston ring surface is performed by laser texturing or laser honing. The proposal arose with the purpose of friction reduction, claiming the previously described advantages: increased hydrodynamic load support; entrapments of wear debris and secondary lubricant reservoir. Further advancements on this solution embraces the geometrical [193] and dimensional [194] optimization of the textured cavities and even their spatial distribution [195], to improve the wear and friction reduction effect.

The predefined properties are achieved by controlling by laser operating parameters such as: power, speed, frequency, pulses per point, among others. Each material will have a different response to the laser energy, being required a preliminary study to find the desired processing parameters.

To enable the sintering of the different powder materials it is possible to use two different technological approaches, powder metallurgy or laser technology.

The powder metallurgy technology includes different techniques, such as press and sintering, hot pressing or spark plasma sintering. Using powder metallurgy technology each material is sintered in a single step along the piston ring functional surface, either using

simultaneously high temperature and high-pressure conditions or being cold pressed and then sintered in a furnace. The first conditions are replicated using hot pressing [196] and spark plasma sintering [197] techniques and the second are executed using the press and sintering technique. This process should be repeated for each different material required to functionalize the surface (even those with magnetic properties [198]), since each material has a different sintering temperature and pressure [174,179,199]. The use of this technology must ensure that the sequence of sintering is from the material with a higher sintering temperature to that with a lower sintering temperature, so that the successive steps do not interfere with the previously sintered material. In compensation, the association of high pressure improves the densification of the powder material and, consequently, its mechanical properties.

In the present work the selected manufacturing technique is hot pressing. This technique uses a temperature above the recrystallization temperature but lower than conventional sintering temperature and partially or fully consolidates the green compact through the application of high uniaxial pressure [200].

Using hot pressing, the resultant physical and mechanical properties of the sintered material depend on several powder specifications: shape, agglomeration, size distribution and purity, which have influence on the resultant microstructure. The optimization of the sintering process is associated to the use of powders with a high-purity level, and preferably, with finer-sized particles, resulting in an improved densification and consequently enhanced mechanical properties [201]. When a composite material has matrix and reinforcement powders of different sizes the spaces between coarser particles are filled with the finer powder particles, improving densification.

The alternative technology is to use a $CO_2$ or a Nd-YAG laser to sinter locally each material, going through each filled texture. Using this technology, the flexibility of sintering different shapes and sizes of each material without interfere to the remaining materials is the main advantage. With this methodology, the main challenge is the final density of the added powder material, regarding that the lower powder layer may receive reduced laser energy.

The presented concept allows the design of several solutions according to the purpose (type of engine) in which it will be applied. The layout, the percentage of each material along the surface and even the density of cavities disposed over the surface will vary according to the customer specifications. Therefore, that flexibility in the piston rings development will represent an added-value not only to the manufacturers but also to the final consumer. Later, this concept may be implemented in other tribological pairs using a sliding movement or a similar relation.

## 2.6 Concluding remarks

This work describes the various processes comprehended in the development of novel and enhanced piston rings for high-performance diesel engines.

For the last decades, material engineering has provided interesting solutions for the tribological problems faced by the piston ring/cylinder liner pair. Hard coatings, such as chromium compounds and compounds of other transition metals (as Ti) were intensively studied by the academic community and were successfully industrially implemented, in particular on the compression ring industry. A coating layer of materials such as CrN, which have superior tribological performance, was extensively used on the top rings of heavy duty diesel engines.

Most of those coatings are applied using PVD techniques, such as cathodic arc evaporation, which are currently used and integrated in the automotive industry production lines. Diamond-like carbon coatings has promising solutions without excessive investments and can be applied with conventional manufacturing techniques, leading to improved performance. Even so, the lack of published research about the viability of the implementation of these materials with the conventional industrial technologies has been constraining some manufactures of making the transition to this amorphous carbon material.

The operation of an internal combustion engine is the result of the performance of each part. Although the tribological performance of the compression ring coating material strongly influences the performance of the tribological pair, additional improvements will require the evaluation of some already established concepts. When the engine is started from cold, a residual lube oil film is between the ring and the liner. During this period, the coefficient of friction achieves the highest values and the surface wear intensifies. On these conditions, textured surfaces appeared as an effective solution. The presence of cavities on the compression ring surface will help to store lubrication oil while the engine is off and then supply it directly to the contact area during the first period of engine operation.

Despite the potential of these materials on ring wear enhancement, other properties need further development, such as heat removal and the reduction of the coefficient of friction. Those several functionalities were gathered together in a proposal to use the most effective material for each role. By associating surface texturing with powder material, it is possible to design different

surface arrangements and different material additions. With this purpose, each material would be positioned according to the most effective position for its specific role.

## Acknowledgements

This work was supported by FCT (Fundação para a Ciência e Tecnologia) and MAHLE, Componentes de Motores, S.A under Grant SFRH/BDE/110654/2015; and FCT (Fundação para a Ciência e Tecnologia) under Grant SFRH/BSAB/142994/2018, and by FEDER funds through the COMPETE 2020 – Programa Operacional Competitividade e Internacionalização (POCI) with the project with reference NORTE-01- 0145-FEDER-000018-HAMaBICo, with the reference project UID/EEA/04436/2019 and by the project POCI-01-0145-FEDER-006941.

## References

[1] Tung SC, McMillan ML. Automotive tribology overview of current advances and challenges for the future. Tribol. Int. 2004;37:517–536.
[2] Holmberg K, Andersson P, Nylund NO, et al. Global energy consumption due to friction in trucks and buses. Tribol. Int. 2014;78:94–114.
[3] Abdulqadir LB, Mohd Nor NF, Lewis R, et al. Contemporary challenges of soot build-up in IC engine and their tribological implications. Tribol. - Mater. Surfaces Interfaces [Internet]. 2018;12:115–129. Available from: https://doi.org/10.1080/17515831.2018.1464256.
[4] Comfort A. An Introduction to Heavy-Duty Diesel Engine Frictional Losses And Lubricant Properties Affecting Fuel Economy - Part I. SAE Tech. Pap. 2003-01-3225 [Internet]. 2003; Available from: http://digitallibrary.sae.org/content/2003-01-3225%5Cnhttp://papers.sae.org/2003-01-3225/.
[5] Mishra PC. A review of piston compression ring tribology. Tribol. Ind. 2014;36:269–280.
[6] Tian T. Modeling the performance of the piston ring-pack. 1997. p. 194.
[7] Morris N, Rahmani R, Rahnejat H, et al. The influence of piston ring geometry and topography on friction. Proc. Inst. Mech. Eng. Part J J. Eng. Tribol. 2013;227:141–153.
[8] Andersson P, Tamminen J, Sandstrom C-E. Piston ring tribology - A literature survey. 2002;105.
[9] Salazar F. Internal Combustion Engines. 1998;87.
[10] Shuster M, Mahler F, Crysler D. Metallurgical and metrological examinations of the cylinder liner-piston ring surfaces after heavy duty diesel engine testing©. Tribol. Trans. 1999;42:116–125.
[11] Dearnley PA. Meeting tribological challenges with surface engineered materials. Tribol. - Mater. Surfaces Interfaces. 2007;1:18–27.
[12] Smith EH. Optimising the design of a piston-ring pack using DoE methods. Tribol. Int. [Internet]. 2011;44:29–41. Available from: http://dx.doi.org/10.1016/j.triboint.2010.09.002.

[13] Wu B, Zhang ZN, Wang P. Effect of Design Parameters on the Reduction of Top Piston Ring Friction. Appl. Mech. Mater. [Internet]. 2012;246–247:1268–1272. Available from: https://www.scientific.net/AMM.246-247.1268.
[14] Söderfjäll M, Herbst HM, Larsson R, et al. Influence on friction from piston ring design, cylinder liner roughness and lubricant properties. Tribol. Int. [Internet]. 2017;116:272–284. Available from: http://dx.doi.org/10.1016/j.triboint.2017.07.015.
[15] Zhang Z, Liu J, Tang Y, et al. Optimizing the shape of top piston ring face using inverse method. Ind. Lubr. Tribol. 2016;68:9–15.
[16] Taylor CM. Engine Tribology. Taylor CM, editor. Tribol. Ser. Elsevier B.V.; 1993.
[17] Sonthalia A, Kumar CR. The Effect of Compression Ring Profile on the Friction Force in an Internal Combustion Engine Tribology in Industry. Tribol. Ind. 2013;35:74–83.
[18] Tian T. Dynamic behaviours of piston rings and their practical impact. Part 1: Ring flutter and ring collapse and their effects on gas flow and oil transport. Proc. Inst. Mech. Eng. Part J J. Eng. Tribol. 2002;216:209–228.
[19] Taylor RI. Lubrication , Tribology & Motorsport. Proc. 2002 SAE Mot. Eng. Conf. Exhib. 2002.
[20] Taylor RI, Coy RC. Improved fuel efficiency by lubricant design: A review. Proc. Inst. Mech. Eng. Part J J. Eng. Tribol. 2000;214:1–15.
[21] Smith O, Priest M, Taylor RI, et al. Simulated fuel dilution and friction-modifier effects on piston ring friction. Proc. Inst. Mech. Eng. Part J J. Eng. Tribol. 2006;220:181–189.
[22] Mishra PC. Tribodynamic modeling of piston compression ring and cylinder liner conjunction in high-pressure zone of engine cycle. Int. J. Adv. Manuf. Technol. 2013;66:1075–1085.
[23] Gupta M, Singhal S, Biswas S. Analytical investigation on the effect of multigrade oil in piston ring lubrication. Tribol. Trans. 1994;37:719–726.
[24] Morina A, Lee PM, Priest M, et al. Challenges of simulating 'fired engine' ring-liner oil additive/surface interactions in ring-liner bench tribometer. Tribol. - Mater. Surfaces Interfaces. 2011;5:25–33.
[25] Woydt M, Kelling N. Testing the tribological properties of lubricants and materials for the system "piston ring/cylinder liner" outside of engines. Ind. Lubr. Tribol. 2003;55:213–222.
[26] Zavos A, Nikolakopoulos P. Thermo-mixed lubrication analysis of coated compression rings with worn cylinder profiles. Ind. Lubr. Tribol. 2017;69:15–29.
[27] Delprete C, Razavykia A. Piston ring – liner lubrication and tribological performance evaluation : A review. 2017;0:1–17.
[28] Fatjo GG, Smith EH. Piston-ring film thickness : Theory and experiment compared. 2017;0:1–18.
[29] Tamura K, Kasai M. Impact of Boundary Lubrication Performance of Engine Oils on Friction at Piston Ring-Cylinder Liner Interface Yukinobu Nakamura and Tomoyuki Enomoto. 2014;875–881.
[30] Bulsara MA, Bhatt D V., Mistry KN. Measurement of oil film thickness between piston ring and liner using strain gauge. Ind. Lubr. Tribol. 2013;65:297–304.
[31] Hamatake T, Wakuri Y, Soejima M, et al. Some studies on the tribology of diesel engines. 23rd CIMAC world Congr. Combust. engine Technol. Sh. propulsion, power Gener. Hamburg, Germany; 2001. p. 1426–1440.
[32] Gulwadi SD. Analysis of tribological performance of a piston ring pack. Tribol. Trans. 2000;43:151–162.
[33] Gee AWJ de. Friction and wear as related to the composition, structure, and properties of metals. Int. Met. Rev. 1979;24:57–67.

[34] Ligier J, Ragot P. Mixed Lubrication and Roughness Surface Effects Application to Piston Rings. CI SI Power Cylind. Syst. 2007;01.
[35] Isaksson P, Nilsson D, Larsson R, et al. The influence of surface roughness on friction in a flexible hybrid bearing. 2011;225:975–985.
[36] Ba L, He Z, Guo L, et al. Piston ring-cylinder liner tribology investigation in mixed lubrication regime: part I-correlation with bench experiment. Ind. Lubr. Tribol. 2015;67:520–530.
[37] Cheng J, Meng X, Xie Y, et al. On the running-in behavior of rough surface of piston rings in mixed lubrication regime. Ind. Lubr. Tribol. 2015;67:468–485.
[38] Sahlin F, Larsson R, Almqvist A, et al. A mixed lubrication model incorporating measured surface topography . Part 1 : theory of flow factors. 2009;224:335–351.
[39] Michail SK, Barber GC. The effects of roughness on piston ring lubrication part I: Model development. Tribol. Trans. 1995;38:19–26.
[40] Michail SK, Barber GC. The effects of roughness on piston ring lubrication— part II: The relationship between cylinder wall surface topography and oil film thickness. Tribol. Trans. 1995;38:173–177.
[41] Durga V, Rao N, Boyer BA, et al. Influence of surface characteristics and oil viscosity on friction behaviour of rubbing surfaces in reciprocating engines. Fall Tech. Conf. ASME-ICE. 1998;31:23–35.
[42] Galligan J, Torrance AA, Liraut G. A scuffing test for piston ringrbore combinations Part I. Stearic acid lubrication. Wear. 1999;236:199–209.
[43] Galligan J, Torrance AA, Liraut G. A scuffing test for piston ringrbore combinations: Pt. II. Formulated motor lubrication. Wear. 1999;236:210–220.
[44] Pandazaras CN, Petropoulos GP. Characterization and modelling of piston ring-cylinder tribosystem microtopography in lubricated contact. Ind. Lubr. Tribol. 2000;52:257–267.
[45] Wei HJ. Study on the Tribology of the Cylinder and Piston Ring of the Vehicle Diesel with Surface Roughness and Lubrication Oil. Adv. Mater. Res. [Internet]. 2011;268–270:322–325. Available from: https://www.scientific.net/AMR.268-270.322.
[46] He Z, Zhang J, Ma W, et al. A Concurrent Reynolds BC Algorithm for Piston Ring Cavitation Lubrication Problems with Surface Roughness. Tribol. Trans. 2014;57:353–365.
[47] Wolff A. Influence of sliding surface roughness and oil temperature on piston ring pack operation of an automotive IC engine. IOP Conf. Ser. Mater. Sci. Eng. 2016.
[48] Checo HM, Jaramillo A, Ausas RF, et al. Down to the roughness scale assessment of piston-ring/liner contacts. IOP Conf. Ser. Mater. Sci. Eng. 2017.
[49] Mezghani S, Demirci I, Zahouani H, et al. The effect of groove texture patterns on piston-ring pack friction. Precis. Eng. [Internet]. 2012;36:210–217. Available from: http://dx.doi.org/10.1016/j.precisioneng.2011.09.008.
[50] Grabon W, Pawlus P, Wos S, et al. Effects of honed cylinder liner surface texture on tribological properties of piston ring-liner assembly in short time tests. Tribol. Int. [Internet]. 2017;113:137–148. Available from: http://dx.doi.org/10.1016/j.triboint.2016.11.025.
[51] Gachot C, Rosenkranz A, Hsu SM, et al. A critical assessment of surface texturing for friction and wear improvement. Wear [Internet]. 2017;372–373:21–41. Available from: http://dx.doi.org/10.1016/j.wear.2016.11.020.
[52] Priest M, Taylor CM. Automobile engine tribology—approaching the surface. Wear [Internet]. 2000;241:193–203. Available from: http://linkinghub.elsevier.com/retrieve/pii/S0043164800003756%5Cnpapers3://publication/doi/10.1016/S0043-1648(00)00375-6.

[53] Lacey PI, Stockwell RT. Development of a methodology to predict cylinder liner scuffing in the 6v92ta engine lubricant test©. Tribol. Trans. 1999;42:192–201.
[54] Dellis PS. Piston-ring performance: limitations from cavitation and friction. Int. J. Struct. Integr. 2019;
[55] Thirouard B. Characterization and modeling of the fundamental aspects of oil transport in the piston ring pack of internal combustion engines. 2001;
[56] Shuster M, Mahler F, Macy D, et al. Piston Ring Microwelding Phenomenon and Methods of Prevention. SAE Tech. Pap. Ser. 2010;1.
[57] Zhang W, Becker E, Wang Y, et al. Investigation of scuffing resistance of piston rings run against piston ring grooves. Tribol. Trans. 2008;51:621–626.
[58] Grünling HW, Schneider K, Singheiser L. Mechanical Properties of coated systems. Mater. Sci. Eng. 1987;88:177–189.
[59] Mehran QM, Fazal MA, Bushroa AR, et al. A Critical Review on Physical Vapor Deposition Coatings Applied on Different Engine Components. Crit. Rev. Solid State Mater. Sci. [Internet]. 2018;43:158–175. Available from: https://doi.org/10.1080/10408436.2017.1320648.
[60] Guo Y, Lu X, Li W, et al. Interfacial stress and failure analysis for piston ring coatings under dry running condition. Tribol. Trans. 2013;56:1027–1034.
[61] Mishra PC, Bhattacharya S, Pandey P. Finite element analysis for coating strength of a piston compression ring in contact with cylinder liner: A tribodynamic analysis. Tribol. Ind. 2015;37:42–54.
[62] Posmyk A, Bakowski H. Wear Mechanism of Cast Iron Piston Ring/Aluminum Matrix Composite Cylinder Liner. Tribol. Trans. 2013;56:806–815.
[63] Kaźmierczak A. Study and the implementation of the new technology of piston rings production. Ind. Lubr. Tribol. 2006;58:140–144.
[64] Gopi E, Saleem M, Chandan S, et al. Thermal and Static analysis of Engine Piston rings. Int. J. Ambient Energy [Internet]. 2019;0:1–8. Available from: https://doi.org/01430750.2019.1636875.
[65] Baranowska J. Surface quality of grey cast irons in the context of nitriding and oxygen-sulphur nitriding. Surf. Coatings Technol. [Internet]. 1998;100–101:271–275. Available from: http://linkinghub.elsevier.com/retrieve/pii/S0257897297006312.
[66] Aizawa T, Kuwahara H. Plasma Nitriding as an Environmentally Benign Surface Structuring Process. Mater. Trans. [Internet]. 2003;44:1303–1310. Available from: http://joi.jlc.jst.go.jp/JST.JSTAGE/matertrans/44.1303?from=CrossRef.
[67] Michalski J, Wach P, Tacikowski J, et al. Contemporary industrial application of nitriding and its modifications. Mater. Manuf. Process. 2009;24:855–858.
[68] Röhrle MD. Pistons for Internal Combustion Engines: Fundamentals of Piston Technology. Germany; 1995.
[69] Affenzeller J, Gläser H. Lagerung und Schmierung von Verbrennungsmotoren (Vol.8). Springer-Verlag; 2013.
[70] Kalpeshkumar P. A Review on Surface Treatment on Piston Ring and Cylinder Linear. Int. J. Eng. Dev. Res. 2014;2:1323–1326.
[71] Lima LGDBS, Nunes LCS, Souza RM, et al. Numerical analysis of the influence of film thickness and properties on the stress state of thin film-coated piston rings under contact loads. Surf. Coatings Technol. [Internet]. 2013;215:327–333. Available from: http://dx.doi.org/10.1016/j.surfcoat.2012.04.102.
[72] International A. Introduction to Thermal Spray Processing. Handb. Therm. Spray Technol. 2004. p. 54–76.

[73] Lille H, Kõo J, Kulu P, et al. Residual stresses in different thermal spray coatings. 2002;162–173.
[74] Araujo P, Chicot D, Staia M, et al. Residual stresses and adhesion of thermal spray coatings. 2005;21:35–41.
[75] Vuoristo P. Thermal Spray Coating Processes [Internet]. Compr. Mater. Process. Elsevier; 2014. Available from: http://dx.doi.org/10.1016/B978-0-08-096532-1.00407-6.
[76] Verdian MM. Finishing and Post-Treatment of Thermal Spray Coatings. Compr. Mater. Finish. [Internet]. Elsevier Ltd.; 2017. p. 191–206. Available from: http://dx.doi.org/10.1016/B978-0-12-803581-8.09200-6.
[77] Davis D, Anandhan V, Singh S. Oxidation-induced crack healing and erosion life assessment of Ni–Mo–Al–Cr 7 C 3 –Al 2 O 3 composite coating. Int. J. Appl. Ceram. Technol. 2019;16:1012–1021.
[78] Bobzin K, Öte M, Königstein T, et al. Development of novel Fe-based coating systems for internal combustion engines. Proc. Int. Therm. Spray Conf. 2017;1:228–234.
[79] Böttcher R, Winkler HJ, Dienwiebel M, et al. Tribology of wire arc spray coatings under the influence of regenerative fuels. Lubricants. 2018;6:1–9.
[80] Bouzana A, Guermat A, Belarifi F. Experimental results of a hydrodynamic friction behaviour of a linear contact at low sliding velocity. Mater. Sci. Eng. 2018;
[81] Liu Y, Kim D, Westerfield Z, et al. A comprehensive study of the effects of honing patterns on twin-land oil control rings friction using both a numerical model and a floating liner engine. Proc. Inst. Mech. Eng. Part J J. Eng. Tribol. 2019;233:229–255.
[82] Lyubimov V V., Voevodin AA, Yerokhin AL, et al. Development and testing of multilayer physically vapour deposited coatings for piston rings. Surf. Coatings Technol. 1992;52:145–151.
[83] Friedrich C, Berg G, Broszeit E, et al. PVD CrxN coatings for tribological application on piston rings. Surf. Coatings Technol. 1997;97:661–668.
[84] Broszeit E, Friedrich C, Berg G. Deposition , properties and applications of PVD Cr N coatings. Surf. Coatings Technol. 1999;115:9–16.
[85] Lorenzo Martin C, Ajayi O, Torrel S, et al. Effect of coating thickness on tribological performance of CrN in dry sliding contact. 2012;10–12.
[86] Ali M, Hamzah E, Qazi IA, et al. Effect of cathodic arc PVD parameters on roughness of TiN coating on steel substrate. Curr. Appl. Phys. [Internet]. 2010;10:471–474. Available from: http://dx.doi.org/10.1016/j.cap.2009.07.007.
[87] Ferrarese A, Martínez D, Keuerleber M. Steel ring pack for high speed large bore applications. 2012;1–7.
[88] Lorenzo-Martin C, Ajayi O, Erdemir A, et al. Effect of microstructure and thickness on the friction and wear behavior of CrN coatings. Wear [Internet]. 2013;302:963–971. Available from: http://dx.doi.org/10.1016/j.wear.2013.02.005.
[89] Araujo JA, Araujo GM, Souza RM, et al. Effect of periodicity on hardness and scratch resistance of CrN/NbN nanoscale multilayer coating deposited by cathodic arc technique. Wear [Internet]. 2015;330–331:469–477. Available from: http://dx.doi.org/10.1016/j.wear.2015.01.051.
[90] Singh SK, Chattopadhyaya S, Pramanik A, et al. Wear behavior of chromium nitride coating in dry condition at lower sliding velocity and load. Int. J. Adv. Manuf. Technol. 2017;1–11.
[91] Zhuo S, Peijun Z, Leheng Z, et al. Multi-layer compound coating on cast iron piston ring by multi-arc and magnetron sputtering ion compound plating technique. Surf. Coatings Technol. 2000;131:422–427.

[92] Wopelka T, Cihak-bayr U, Lenauer C, et al. Wear of different material pairings for the cylinder liner – piston ring contact. Ind. Lubr. Tribol. 2018;70:687–699.
[93] Lifshitz Y. Diamond-like carbon — present status. Diam. Relat. Mater. [Internet]. 1999;8:1659–1676. Available from: http://linkinghub.elsevier.com/retrieve/pii/S0925963599000874.
[94] Robertson J. Diamond-like amorphous carbon. Mater. Sci. Eng. R Reports. 2002;37:129–281.
[95] Bewilogua K, Hofmann D. History of diamond-like carbon films - From first experiments to worldwide applications. Surf. Coatings Technol. [Internet]. 2014;242:214–225. Available from: http://dx.doi.org/10.1016/j.surfcoat.2014.01.031.
[96] Tietema R. Large-Scale Industrial Coating Applications and Systems. Compr. Mater. Process. Elsevier; 2014.
[97] Vetter J. 60years of DLC coatings: Historical highlights and technical review of cathodic arc processes to synthesize various DLC types, and their evolution for industrial applications. Surf. Coatings Technol. [Internet]. 2014;257:213–240. Available from: http://dx.doi.org/10.1016/j.surfcoat.2014.08.017.
[98] Gangopadhyay A, Zdrodowski RJ, Simko SJ. Interactions of Diamond-Like Carbon Coatings with Fully Formulated Engine Oils. Tribol. Trans. 2014;57:503–514.
[99] Vinoth IS, Detwal S, Umasankar V, et al. Tribological studies of automotive piston ring by diamond-like carbon coating. Tribol. - Mater. Surfaces Interfaces [Internet]. 2019;13:31–38. Available from: https://doi.org/10.1080/17515831.2019.1569852.
[100] Acunaş Karagöz ZB, Demirtaş S, Kaleli H, et al. Review of tribological behavior of graphene coatings on piston rings in engines. Ind. Lubr. Tribol. 2019;
[101] Tahir NAM, Abdollah MF Bin, Tamaldin N, et al. A brief review on the wear mechanisms and interfaces of carbon based materials. Compos. Interfaces [Internet]. 2018;25:491–513. Available from: http://doi.org/10.1080/09276440.2018.1380472.
[102] Martinella R. Selection and application of wear-resistant materials to increase service life of components. Ceram. Int. 1993;19:375–389.
[103] Donnet C, Erdemir A. Tribology of Diamond-Like Carbon Films [Internet]. Tribol. Diamond-Like Carbon Film. Fundam. Appl. 2008. Available from: http://www.springerlink.com/index/10.1007/978-0-387-49891-1.
[104] Dorner-Reisel A, Lieberwirth R, Svoboda S, et al. Wear behaviour of hydrogen free diamond-like carbon thin films in diesel fuel at different temperatures. Diam. Relat. Mater. 2014;44:78–87.
[105] Lubwama M, Corcoran B, Sayers K. DLC films deposited on rubber substrates: A review. Surf. Eng. 2015;31:1–10.
[106] Tung SC, Gao H. Tribological investigation of piston ring coatings operating in an alternative fuel and engine oil blend. Tribol. Trans. 2002;45:381–389.
[107] Beake BD, Liskiewicz TW, Vishnyakov VM, et al. Development of DLC coating architectures for demanding functional surface applications through nano- and micro-mechanical testing. Surf. Coatings Technol. [Internet]. 2015;284:334–343. Available from: http://dx.doi.org/10.1016/j.surfcoat.2015.05.050.
[108] Smart RF, Moore JC. Materials selection for wear resistance. Wear [Internet]. 1979;56:55–67. Available from: http://www.sciencedirect.com/science/article/pii/0043164879900061.
[109] Kano M. Diamond-Like Carbon Coating Applied to Automotive Engine Components. Tribol. Online [Internet]. 2014;9:135–142. Available from: http://jlc.jst.go.jp/DN/JST.JSTAGE/trol/9.135?lang=en&from=CrossRef&type=abstract.

[110] Tas MO, Banerji A, Lou M, et al. Roles of mirror-like surface finish and DLC coated piston rings on increasing scuffing resistance of cast iron cylinder liners. Wear [Internet]. 2017;376–377:1558–1569. Available from: http://dx.doi.org/10.1016/j.wear.2017.01.110.
[111] Wan S, Li D, Zhang G, et al. Comparison of the scuffing behaviour and wear resistance of candidate engineered coatings for automotive piston rings. Tribol. Int. [Internet]. 2017;106:10–22. Available from: http://dx.doi.org/10.1016/j.triboint.2016.10.026.
[112] Okubo H, Watanabe S, Tadokoro C, et al. Ultralow Friction of a Tetrahedral Amorphous Carbon Film Lubricated with an Environmentally Friendly Ester-Based Oil. Tribol. Online [Internet]. 2016;11:102–113. Available from: https://www.jstage.jst.go.jp/article/trol/11/2/11_102/_article.
[113] Higuchi T, Mabuchi Y, Ichihara H, et al. Development of Hydrogen-Free Diamond-Like Carbon Coating for Piston Rings. Tribol. Online [Internet]. 2017;12:117–122. Available from: https://www.jstage.jst.go.jp/article/trol/12/3/12_117/_article.
[114] Mabuchi Y, Higuchi T, Inagaki Y, et al. Wear analysis of hydrogen-free diamond-like carbon coatings under a lubricated condition. Wear [Internet]. 2013;298–299:48–56. Available from: http://dx.doi.org/10.1016/j.wear.2012.11.046.
[115] Wu Y, Zhao J, Li Y. Thickness of Transition Layer Effect on Bonding Strength in DLC Film. 2017;486–491.
[116] Gåhlin R, Larsson M, Hedenqvist P. ME-C:H coatings in motor vehicles. Wear. 2001;249:302–309.
[117] Guo CQ, Pei ZL, Fan D, et al. Microstructure and tribomechanical properties of (Cr, N)-DLC/DLC multilayer films deposited by a combination of filtered and direct cathodic vacuum arcs. Diam. Relat. Mater. [Internet]. 2015;60:66–74. Available from: http://dx.doi.org/10.1016/j.diamond.2015.10.019.
[118] Zhang Y, Zhai Y, Li F, et al. Effect of microstructure and mechanical properties difference between sub-layers on the performance of alternate hard and soft diamond-like carbon multilayer films. Surf. Coatings Technol. [Internet]. 2013;232:575–581. Available from: http://dx.doi.org/10.1016/j.surfcoat.2013.06.030.
[119] Kilman L, Jaoul C, Colas M, et al. Friction and wear performance of multilayered a-C:H:Al coatings. Surf. Coatings Technol. [Internet]. 2015;284:159–165. Available from: http://dx.doi.org/10.1016/j.surfcoat.2015.07.079.
[120] Zhang W, Tanaka A, Xu BS, et al. Study on the diamond-like carbon multilayer films for tribological application. Diam. Relat. Mater. 2005;14:1361–1367.
[121] Mutyala KC, Singh H, Evans RD, et al. Effect of Diamond-Like Carbon Coatings on Ball Bearing Performance in Normal, Oil-Starved, and Debris-Damaged Conditions. Tribol. Trans. [Internet]. 2016;59:1039–1047. Available from: http://dx.doi.org/10.1080/10402004.2015.1131349.
[122] Kot M, Major, Lackner JM, et al. Mechanical and Tribological Properties of Carbon-Based Graded Coatings. J. Nanomater. 2016;2016.
[123] Lin J, Wei R, Bitsis DC, et al. Development and evaluation of low friction TiSiCN nanocomposite coatings for piston ring applications. Surf. Coatings Technol. [Internet]. 2016;298:121–131. Available from: http://dx.doi.org/10.1016/j.surfcoat.2016.04.061.
[124] Zhang C, Liu L, Xu H, et al. Role of Mo on tribological properties of atmospheric plasma-sprayed Mo-NiCrBSi composite coatings under dry and oil-lubricated conditions. J. Alloys Compd. [Internet]. 2017;727:841–850. Available from: https://doi.org/10.1016/j.jallcom.2017.08.195.

[125] Linsler D, Kümmel D, Nold E, et al. Analysis of the running-in of thermal spray coatings by time-dependent stribeck maps. Wear [Internet]. 2017;376–377:1467–1474. Available from: http://dx.doi.org/10.1016/j.wear.2017.02.026.
[126] Hovsepian PE, Mandal P, Ehiasarian AP, et al. Friction and wear behaviour of Mo-W doped carbon-based coating during boundary lubricated sliding. Appl. Surf. Sci. [Internet]. 2016;366:260–274. Available from: http://dx.doi.org/10.1016/j.apsusc.2016.01.007.
[127] Müller IC, Sharp J, Rainforth WM, et al. Tribological response and characterization of Mo–W doped DLC coating. Wear [Internet]. 2017;376–377:1622–1629. Available from: http://dx.doi.org/10.1016/j.wear.2016.11.036.
[128] Hovsepian PE, Lewis DB, Müunz WD, et al. Chromium nitride/niobium nitride superlattice coatings deposited by combined cathodic-arc/unbalanced magnetron technique. Surf. Coatings Technol. 1999;116–119:727–734.
[129] Münz W-D, Lewis DB, Hovsepian PE, et al. Industrial scale manufactured superlattice hard PVD coatings. Surf. Eng. [Internet]. 2001;17:15–27. Available from: http://www.ingentaconnect.com/content/maney/se/2001/00000017/00000001/art00001%5Cnhttp://www.ingentaselect.com/rpsv/cgi-bin/cgi?ini=xref&body=linker&reqdoi=10.1179/026708401101517557.
[130] Ehiasarian AP, Hovsepian PE, Hultman L, et al. Comparison of microstructure and mechanical properties of chromium nitride-based coatings deposited by high power impulse magnetron sputtering and by the combined steered cathodic arc/unbalanced magnetron technique. Thin Solid Films. 2004;457:270–277.
[131] Purandare YP, Ehiasarian AP, Hovsepian PE. Deposition of a nanoscale multilayer CrN/nBn physical vapor deposition coatings by high power impulse magnetron sputtering. J. Vac. Sci. Technol. A Vacuum, Surfaces, Film. 2008;26:288–296.
[132] Cameron DC, Aimo R, Wang ZH, et al. Structural variations in CrN/NbN superlattices. Surf. Coatings Technol. 2001;142:567–572.
[133] Bemporad E, Pecchio C, De Rossi S, et al. Characterisation and wear properties of industrially produced nanoscaled CrN/NbN multilayer coating. Surf. Coatings Technol. 2004;188–189:319–330.
[134] Cansever N. Properties of niobium nitride coatings deposited by cathodic arc physical vapor deposition. Thin Solid Films. 2007;515:3670–3674.
[135] Venkateswara Babu P, Syed I, Beera S Ben. Influence of positive texturing on friction and wear properties of piston ring-cylinder liner tribo pair under lubricated conditions. Ind. Lubr. Tribol. 2019;71:515–524.
[136] Vlădescu SC, Ciniero A, Tufail K, et al. Optimization of Pocket Geometry for Friction Reduction in Piston–Liner Contacts. Tribol. Trans. 2018;61:522–531.
[137] Senatore A, Aleksendric D. Engine piston rings improvement through effective materials, advanced manufacturing methods and novel design shape. Ind. Lubr. Tribol. 2014;66:298–305.
[138] Koszela W, Pawlus P, Galda L. The effect of oil pockets size and distribution on wear in lubricated sliding. Wear. 2007;263:1585–1592.
[139] Wos S, Koszela W, Pawlus P. Determination of oil demand for textured surfaces under conformal contact conditions. Tribol. Int. [Internet]. 2016;93:602–613. Available from: http://dx.doi.org/10.1016/j.triboint.2015.05.016.
[140] Li X, Olofsson U. A study on friction and wear reduction due to porosity in powder metallurgic gear materials. Tribol. Int. [Internet]. 2017;110:86–95. Available from: http://dx.doi.org/10.1016/j.triboint.2017.02.008.

[141] Schubert A, Neugebauer R, Sylla D, et al. Manufacturing of surface microstructures for improved tribological efficiency of powertrain components and forming tools. CIRP J. Manuf. Sci. Technol. [Internet]. 2011;4:200–207. Available from: http://dx.doi.org/10.1016/j.cirpj.2011.01.010.
[142] Braun D, Greiner C, Schneider J, et al. Efficiency of laser surface texturing in the reduction of friction under mixed lubrication. Tribol. Int. [Internet]. 2014;77:142–147. Available from: http://dx.doi.org/10.1016/j.triboint.2014.04.012.
[143] Abdul Rahman H, A. Ghani J, Wan Mahmood WMF, et al. Computational fluid dynamic study on the tribological performance of dimple-textured surface fabricated using the turning process. Ind. Lubr. Tribol. 2019;71:594–602.
[144] Grützmacher PG, Rosenkranz A, Szurdak A, et al. Multi-scale surface patterning – an approach to control friction and lubricant migration in lubricated systems. Ind. Lubr. Tribol. 2019;
[145] Burstein L. Surfaces with size different pores: hydrodynamic lubrication quality. Ind. Lubr. Tribol. 2018;70:1234–1242.
[146] Ji J, Fu Y, Bi Q. The influence of partially textured slider with orientation ellipse dimples on the behavior of hydrodynamic lubrication. Ind. Lubr. Tribol. 2014;66:161–167.
[147] Ronen A, Etsion I, Kligerman Y. Friction-reducing surface-texturing in reciprocating automotive components. Tribol. Trans. 2001;44:359–366.
[148] Wang H, Zhu H, Zhou Y, et al. Experimental Study on the Friction Characteristics of Textured Steel Surface with Ring-Shaped Pits under Lubricated Sliding Conditions. Tribol. Trans. 2015;58:712–717.
[149] Wang S, Yan F, Chen A. Tribological effects of laser surface texturing and residual stress. Ind. Lubr. Tribol. 2016;
[150] Zhang Y, Zhang X, Wu T, et al. Effects of surface texturing on the tribological behavior of piston rings under lubricated conditions. Ind. Lubr. Tribol. 2016;68:158–169.
[151] Bruzzone AAG, Costa HL, Lonardo PM, et al. Advances in engineered surfaces for functional performance. CIRP Ann. - Manuf. Technol. 2008;57:750–769.
[152] Martz LS. Preliminary report of developments in interrupted surface finishes. Proc. Inst. Mech. Eng. 1949;16:1–9.
[153] Grabon W, Koszela W, Pawlus P, et al. Improving tribological behaviour of piston ring-cylinder liner frictional pair by liner surface texturing. Tribol. Int. [Internet]. 2013;61:102–108. Available from: http://dx.doi.org/10.1016/j.triboint.2012.11.027.
[154] Tomanik E. Friction and wear bench tests of different engine liner surface finishes. Tribol. Int. 2008;41:1032–1038.
[155] Vlădescu SC, Olver A V., Pegg IG, et al. Combined friction and wear reduction in a reciprocating contact through laser surface texturing. Wear. 2016;358–359:51–61.
[156] Vlədescu SC, Medina S, Olver A V., et al. Lubricant film thickness and friction force measurements in a laser surface textured reciprocating line contact simulating the piston ring-liner pairing. Tribol. Int. [Internet]. 2016;98:317–329. Available from: http://dx.doi.org/10.1016/j.triboint.2016.02.026.
[157] Vlădescu SC, Ciniero A, Tufail K, et al. Looking into a laser textured piston ring-liner contact. Tribol. Int. 2017;115:140–153.
[158] Hua X, Sun J, Zhang P, et al. Research on discriminating partition laser surface micro-texturing technology of engine cylinder. Tribol. Int. 2016;98:190–196.

[159] Vladescu SC, Olver A V., Pegg IG, et al. The effects of surface texture in reciprocating contacts - An experimental study. Tribol. Int. [Internet]. 2015;82:28–42. Available from: http://dx.doi.org/10.1016/j.triboint.2014.09.015.
[160] Profito FJ, Vlădescu SC, Reddyhoff T, et al. Transient experimental and modelling studies of laser-textured micro-grooved surfaces with a focus on piston-ring cylinder liner contacts. Tribol. Int. 2017;113:125–136.
[161] Biboulet N, Lubrecht AA. Analytical solution for textured piston ring - Cylinder liner contacts (1D analysis). Tribol. Int. [Internet]. 2016;96:269–278. Available from: http://dx.doi.org/10.1016/j.triboint.2015.12.042.
[162] Zavos A, Nikolakopoulos P. Effects of surface irregularities on piston ring-cylinder tribo pair of a two stroke motor engine in hydrodynamic lubrication. Tribol. Ind. 2015;37:1–12.
[163] Usman A, Park CW. Optimizing the tribological performance of textured piston ring-liner contact for reduced frictional losses in SI engine: Warm operating conditions. Tribol. Int. [Internet]. 2016;99:224–236. Available from: http://dx.doi.org/10.1016/j.triboint.2016.03.030.
[164] Tomanik E. Modelling the hydrodynamic support of cylinder bore and piston rings with laser textured surfaces. Tribol. Int. [Internet]. 2013;59:90–96. Available from: http://dx.doi.org/10.1016/j.triboint.2012.01.016.
[165] Gu C, Meng X, Xie Y, et al. Effects of surface texturing on ring/liner friction under starved lubrication. Tribol. Int. [Internet]. 2016;94:591–605. Available from: http://dx.doi.org/10.1016/j.triboint.2015.10.024.
[166] Zavos AB, Nikolakopoulos PG. Simulation of piston ring tribology with surface texturing for internal combustion engines. Lubr. Sci. 2015;27:151–176.
[167] Ryk G, Etsion I. Testing piston rings with partial laser surface texturing for friction reduction. Wear. 2006;261:792–796.
[168] Ryk G, Kligerman Y, Etsion I, et al. Experimental investigation of partial laser surface texturing for piston-ring friction reduction. Tribol. Trans. 2005;48:583–588.
[169] Etsion I, Sher E. Improving fuel efficiency with laser surface textured piston rings. Tribol. Int. 2009;42:542–547.
[170] Shen C, Khonsari MM. The effect of laser machined pockets on the lubrication of piston ring prototypes. Tribol. Int. [Internet]. 2016;101:273–283. Available from: http://dx.doi.org/10.1016/j.triboint.2016.04.009.
[171] Zavedeev E V., Zilova OS, Barinov AD, et al. Femtosecond laser microstructuring of diamond-like nanocomposite films. Diam. Relat. Mater. 2017;74:45–52.
[172] Al-Azizi AA, Eryilmaz O, Erdemir A, et al. Nano-texture for a wear-resistant and near-frictionless diamond-like carbon. Carbon N. Y. 2014;73:403–412.
[173] Mishra P, Ramkumar P. Effect of additives on a surface textured piston ring–cylinder liner system. Tribol. - Mater. Surfaces Interfaces [Internet]. 2019;13:67–75. Available from: https://doi.org/10.1080/17515831.2019.1588554.
[174] Cai AH, Xiong X, Liu Y, et al. Consolidation of Cu based amorphous powder by hot pressing method. Powder Metall. 2011;55:22–28.
[175] M. Girish B, B. B, M. Satish B, et al. Electrical Resistivity and Mechanical Properties of Tungsten Carbide Reinforced Copper Alloy Composites. Int. J. Compos. Mater. 2012;2:37–43.
[176] Vignesh Babu R, Verma KA, Charan M, et al. Tweaking the diameter and concentration of carbon nanotubes and sintering duration in Copper based composites for heat transfer applications. Adv. Powder Technol. [Internet]. 2018;29:2356–2367. Available from: https://doi.org/10.1016/j.apt.2018.06.015.

[177] Zhang J, Zhang S, Wang L, et al. Copper and copper alloy powder technology and market developments in China. Powder Metall. 2014;57:314–315.
[178] Mosher WGE, Kipouros GJ, Caley WF, et al. On hot deformation of aluminium–silicon powder metallurgy alloys. Powder Metall. 2011;54:366–375.
[179] Konstanty J. Production parameters and materials selection of powder metallurgy diamond tools. Powder Metall. 2006;49:299–306.
[180] Konstanty J. Sintered diamond tools: trends, challenges and prospects. Powder Metall. 2013;56:184–188.
[181] Saba F, Zhang F, Liu S, et al. Reinforcement size dependence of mechanical properties and strengthening mechanisms in diamond reinforced titanium metal matrix composites. Compos. Part B Eng. [Internet]. 2019;167:7–19. Available from: https://linkinghub.elsevier.com/retrieve/pii/S1359836818325009.
[182] Zhou L, Xiong J, Guo Z, et al. Design and preparation of gradient graphite/cermets self-lubricating composites. J. Mater. Sci. Technol. [Internet]. 2018;34:1378–1386. Available from: https://doi.org/10.1016/j.jmst.2017.09.018.
[183] Garcia J, Ferreira AR, Silva FS, et al. Production and tribological characterization of a textured diamond-reinforced copper-beryllium alloy. Tribol. Int. [Internet]. 2019;140:105843. Available from: https://linkinghub.elsevier.com/retrieve/pii/S0301679X19303500.
[184] Littmann W, Storck H, Wallaschek J. Sliding friction in the presence of ultrasonic oscillations: Superposition of longitudinal oscillations. Arch. Appl. Mech. 2001;71:549–554.
[185] Kumar VC, Hutchings IM. Reduction of the sliding friction of metals by the application of longitudinal or transverse ultrasonic vibration. Tribol. Int. 2004;37:833–840.
[186] Gutowski P, Leus M. Computational model for friction force estimation in sliding motion at transverse tangential vibrations of elastic contact support. Tribol. Int. 2015;90:455–462.
[187] Storck H, Littmann W, Wallaschek J, et al. The effect of friction reduction in presence of ultrasonic vibrations and its relevance to travelling wave ultrasonic motors. Ultrasonics. 2002;40:379–383.
[188] Chowdhury MA, Helali M. The effect of amplitude of vibration on the coefficient of friction for different materials. Tribol. Int. 2008;41:307–314.
[189] Wang P, Ni H, Wang R, et al. Experimental investigation of the effect of in-plane vibrations on friction for different materials. Tribol. Int. [Internet]. 2016;99:237–247. Available from: http://dx.doi.org/10.1016/j.triboint.2016.03.021.
[190] Yoo SS, Kim DE. Effects of vibration frequency and amplitude on friction reduction and wear characteristics of silicon. Tribol. Int. 2016;94:198–205.
[191] Whittaker D. PM structural parts move to higher density and performance. Powder Metall. 2007;50:99–105.
[192] Bains PS, Sidhu SS, Payal HS. Fabrication and Machining of Metal Matrix Composites: A Review. Mater. Manuf. Process. [Internet]. 2016;31:553–573. Available from: http://dx.doi.org/10.1080/10426914.2015.1025976.
[193] Zheng L, Gao Y, Zhong Y, et al. The size effect of hexagonal texture on tribological properties under mixed lubrication. Ind. Lubr. Tribol. 2018;70:1798–1805.
[194] Rao X, Sheng C, Guo Z, et al. Influence of Surface Groove Width on Tribological Performance for Cylinder Liner–Piston Ring Components. Tribol. Trans. [Internet]. 2019;62:239–248. Available from: https://doi.org/10.1080/10402004.2018.1539201.
[195] Zhan J, Yang M. Investigation on Dimples Distribution Angle in Laser Texturing of Cylinder-Piston Ring System. Tribol. Trans. 2012;55:693–697.

[196] Montes JM, Cuevas FG, Cintas J, et al. Densification rate of metal powders during hot uniaxial compaction. Powder Metall. 2011;55:388–394.
[197] Mamedov V. Spark plasma sintering as advanced PM sintering method. Powder Metall. [Internet]. 2002;45:322–328. Available from: http://www.tandfonline.com/doi/full/10.1179/003258902225007041.
[198] Capus JM. PowderMet2009: prospects improving after automotive debacle. Powder Metall. 2009;52:274–277.
[199] Chang SH, Liang C, Huang JR, et al. Cr50Cu50 alloys produced from submicrometre structured powders through hot pressing at different pressures. Powder Metall. 2016;59:142–147.
[200] Mitra R. Intermetallic Matrix Composites - Properties and Applications. Jones G, editor. Matthew Deans; 2018.
[201] Zou Q-H, Zhao HM, Zhang D-Y, et al. Thermophysics characteristics and densification of powder metallurgy composites. Powder Metall. 2006;49:183–188.
[202] Babu M V, Kumar RK, Prabhakar O, et al. Simultaneous optimization of flame spraying process parameters for high quality molybdenum coatings using Taguchi methods. Surf. Coat. Technol. 1996;79:276–288.
[203] Tung SC, Gao H. Tribological characteristics and surface interaction between piston ring coatings and a blend of energy-conserving oils and ethanol fuels. Wear. 2003;255:1276–1285.
[204] Karamiş MB, Yildizli K, Çakirer H. An evaluation of surface properties and frictional forces generated from Al-Mo-Ni coating on piston ring. Appl. Surf. Sci. 2004;230:191–200.
[205] Karamiş MB, Yildizli K, Çakirer H. Wear behaviour of Al-Mo-Ni composite coating at elevated temperature. Wear. 2005;258:744–751.
[206] Houdková Š, Kašparová M, Zahálka F. The friction properties of the HVOF sprayed coatings suitable for combustion engines, measured in compliance with ASTM G-99. WIT Trans. Eng. Sci. 2010;66:129–139.
[207] Biberger J, Füßer HJ. Development of a test method for a realistic, single parameter-dependent analysis of piston ring versus cylinder liner contacts with a rotational tribometer. Tribol. Int. [Internet]. 2017;113:111–124. Available from: http://dx.doi.org/10.1016/j.triboint.2016.10.043.
[208] Liu L, Xu H, Xiao J, et al. Effect of heat treatment on structure and property evolutions of atmospheric plasma sprayed NiCrBSi coatings. Surf. Coatings Technol. [Internet]. 2017;325:548–554. Available from: http://dx.doi.org/10.1016/j.surfcoat.2017.07.011.

# CHAPTER 3.

## A new tribometer for the automotive industry: development and experimental validation

Published in Experimental Mechanics, 2022, 62: 483-492
R. Ferreira [a,c,d,*], Ó. Carvalho [a], J. Pires [a], L. Sobral [c], S. Carvalho [d], F. Silva [a]

[a] Centre for Micro-Electro Mechanical Systems (MEMS) University of Minho, Campus de Azurém, 4800-058 Guimarães, Portugal
[b] Mechanical Engineering Department, Universidade do Minho, 4800-058 Guimarães, Portugal
[c] MAHLE - Componentes de Motores S.A., Núcleo Industrial Murtede, 3060-372 Cantanhede, Portugal
[d] GRF-CFUM, Department of Physics, University of Minho, Campus de Azurém, 4800-058 Guimarães, Portugal

## Abstract

Background: In automotive engineering, the piston ring-cylinder liner pair is among the most studied contacts. From the three piston rings of a conventional internal combustion engine, the top compression ring has a crucial role. The main challenge is to prevent that during the engine lifecycle, the degradation of the piston ring surface might limit the engine's durability. Objective: However, a reliable evaluation of the piston rings tribological response requires a steady method. To test and study the tribological performance of the ring-liner pair, the development of a customized test rig is presented in this work. Methods: The new oscillating tribometer will test and study the performance of new and commercial piston rings and cylinder liner solutions. According to the foreseen engine operation, four conditions were appointed to perform the control tests, and a testing protocol was established. The selected stainless-steel piston rings were coated with a diamond-like carbon layer, and the cylinder liner parts had the typical plateau honed texture in the contact surface. The friction force measures were recorded. It was also investigated the influence of distinct parameters (such as temperature and contact pressure) in the friction coefficient of this pair. Results: According to the exploratory tests, the major COF was registered for the testing condition with a lower load. In contrast, the lower COF values were recorded for those conditions with superior normal loads and temperatures. Conclusions: The functionality of the developed test rig was verified to evaluate the ring's performance and the liner contact.

Keywords: *automotive, mechanical development, piston ring, cylinder liner, friction sliding.*

## 3.1 Introduction

The enhancement of the engine's performance urges as one of the most relevant topics in the research and development of internal combustion engines. The competitiveness of electric cars has been pressing the conventional automotive industry [1, 2]. New and optimized solutions for mechanical and materials engineering issues are needed to compete with those new products. In balance, engine manufacturers have a priority concern, the ecological consequences of the engine's mechanical limitations, such as the high emission of atmospheric pollutants [3].

The piston ring–cylinder liner contact is one of the most representative pairs of the tribological concerns associated with the internal combustion engine. The lack of efficiency in the top compression piston ring role has as a primary consequence the ineffective sealing of the combustion chamber. When in operation, the sealing of the combustion chamber prevents lubrication oil contamination within the combustion mixture. This contamination occurs due to excessive consumption of fuel moved towards the crankcase.

As one of the most representative systems of the engine, piston ring assembly has been widely studied [4–10]. Comfort [11] associated the piston ring assembly with 45-50 % of the mechanical losses of a heavy-duty diesel engine. The remaining is from the valve train, engine

bearings, and other auxiliary systems. Different aspects influence the piston ring performance. Some are related to the piston ring's cross-sectional geometry, dimensional tolerances, and surface material properties. Others are associated with the surrounding elements, like the piston ring groove or the cylinder liner surface properties.

The research and development of innovative solutions to improve piston ring performance might include a new material or different surface characteristics. New surface properties and features of the piston ring will result in new operating conditions. That unknown response will have an impact on the performance of each ring-liner pair. The final validation of those new solutions demands the proper test resources as close as possible of the last use domain. For that purpose, the primary need is to develop specific and reliable tools and methods to investigate the frictional losses of the piston ring-cylinder liner contact.

Several studies related to the piston ring assembly were published in the last years, including modeling, experimental studies, and full-scale engine tests. The purpose of the research included analyzing different lubricants, the measurement of the oil film thickness, the coefficient of friction, and the wear resistance of the ring-liner system. About the latter, most of the published works encompassed tests in lower-speed test rigs or conventional methods, like ball-on-disc or pin-on-plate. Two of the most common testing devices used for this purpose are the Cameron Plint [12–15] high-frequency test rig and the SRV4 [16–18] from Optimol Instruments. Table 3.1 are presented some parameters of the experimental conditions of six of those research works using the previously mentioned commercial models.

Table 3.1 Published works using commercial friction testers and some experimental conditions.

| Test rig model | Ref. | Load (N) | Temperature (°C) | Frequency x 2 Stroke (m/s) | Stroke (mm) |
|---|---|---|---|---|---|
| Plint – Cameron | [15] | 80 | 20 | 0.27 | 4.5 |
| TE77 | [14] | 330 | 60 | 0.30 | 10.8 |
| | [13] | 100 | 90 | 0.16 | 82 |
| SRV4 (Optimol | [16] | 200 | 120 | 0.15 | 1.5 |
| Instruments) | [18] | 300 | 170 | 0.12 | 2 |
| | [17] | 35 | 40 | 0.10 | 5 |

In general, the mentioned studies were performed to evaluate a coating system or study a specific material pair. Those investigations were restricted to the characteristics of the commercial apparatus. However, in demand for more flexibility, adaptability to different sample geometries,

and broader ranges for the testing parameters, the development of customized test rigs needs to be considered.

In the last years appeared a few works proposing customized test rigs for large bore engines. Andersson [19] presented the development of a new test rig with subsequent functional tests, using a temperature of 110 °C, 500 N of load, and up to 20 Hz of test frequency. Later, Johansson et al. [5] presented the model and the simultaneous experimental validation study using an optimized tribometer from an automotive manufacturer. They highlighted the use of real parts in those tribological studies, referring to the advantage of test with the authentic surface geometry and morphology, coating thickness, and material composition. Most recently, Syed and Wani [20] and Fayaz and Wani [21] used a customized test rig to evaluate the scuffing failure of the piston ring under dry sliding. In both studies, the adapted test rig tested piston rings from a heavy-duty engine under lubricant starvation conditions.

In the present work, the purpose was to develop and verify a methodology able to effectively reproduce diverse engine operation conditions, as at the boundary and mixed lubrication regimes. The diverse engine operation conditions were related to the possibility of varying the speed, the normal load, and the lubrication of the contact (the type of oil, the oil temperature, and the presence or absence of contaminant). The developed tool would be useful for further analysis of the frictional losses and wear.

A significant achievement using this test rig would be to test new proposed solutions intended to decrease the coefficient of friction of this pair or even the engine power losses due to the frictional ring dynamics. Advanced solutions include enhanced coatings, either using the conventional PVD (physical vapour deposition) or using other technologies (such as powder metallurgy) [9]. In this approach, exploratory tests were performed to investigate the effect of different running conditions on friction results. The functionality of the test rig and the repeatability of the results were also considered for this work.

## 3.2 Materials and methods

### 3.2.1 Testing device development – a proposed approach

In this work is presented the design and development of a new test rig. The customized test rig can test new commercial piston ring and cylinder liner solutions from heavy-duty diesel engines

using a linear reciprocating system. Either piston ring and cylinder liner parts of large-bore engines or components from smaller engines may be used.

Commonly, the COF measurement of the ring-liner contact is more complex to obtain when using a floating liner or a full-scale engine tester. The surrounding parts would influence the physical contact between the ring and the liner. This test rig will not represent an issue since the piston ring holder is suspended and stationary. It does not only have contact with the cylinder liner, neither influence by secondary ring motion [22]. It is possible to isolate the ring-liner pair and evaluate this contact without external disruptions with this latter condition.

When assembled into the cylinder, the top compression ring has a pre-compression to fit geometrically into the bore. Still, the lack of circularity in the external geometry of the piston ring allows the presence of clearances between ring gaps and around the ring-liner contact [23]. This characteristic is schematically represented in Figure 3.1.

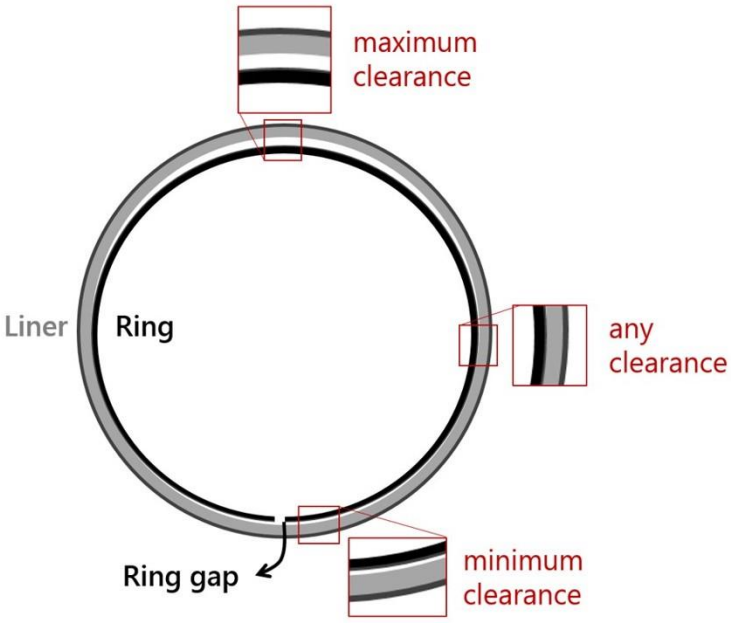


Figure 3.1 Schematic representation of the avoidance or presence of variable clearances between the piston ring and cylinder liner when the piston ring is assembled.

. Several approaches were possible to reproduce the ring-liner contact in the test rig structure. Smith et al. [14] used the piston ring to the in-cylinder designed radius in a compression state. In the developed equipment, the piston ring radius is modeled to the cylinder radius through the effect of the normal load.

Following a general classification about the test rig dynamics, testing devices can be of the low-speed or high-speed test rigs. Usually, the low-speed test rigs are used to investigate the operational performance close to the reversal zones, although the influence on friction power loss is negligible. The friction power loss depends on oil viscosity, tangential load (not quantified in the present work), and speed.

Power loss studies and measurements related to fuel and oil consumption use high-speed test rig. Soderfjall [24] et al. proposed using a high-speed test rig to evaluate the friction benefits that can affect fuel consumption. They refer to the test rig developed by Akalin and Newaz [25] as one with the faster-operating conditions, achieving 750 rpm with a stroke length of 84 mm. For some studies, high-speed test rigs generated large dynamic forces, which creates more significant vibrations.

To favor the high adaptability of the testing parameters, the available speed range of the developed test rig should be as comprehensive as possible. Lower speed values would be useful for future studies close to the reversal zones, while high speeds would be helpful for power loss studies.

Regarding its prompt application, the new test rig intends to investigate different rings and liners, distinct running conditions, and the resulted tribological behavior of a new pair of materials. Besides friction and wear investigations, several testing conditions can be varied to study different surface topographies and materials.

The tribometer arrangement is mainly over a structural table, except the motion system located under the basis platform connected with the upper structure through a driving shaft. This section comprehends the test rig design description, and a schematic view is presented in Figure 3.2.

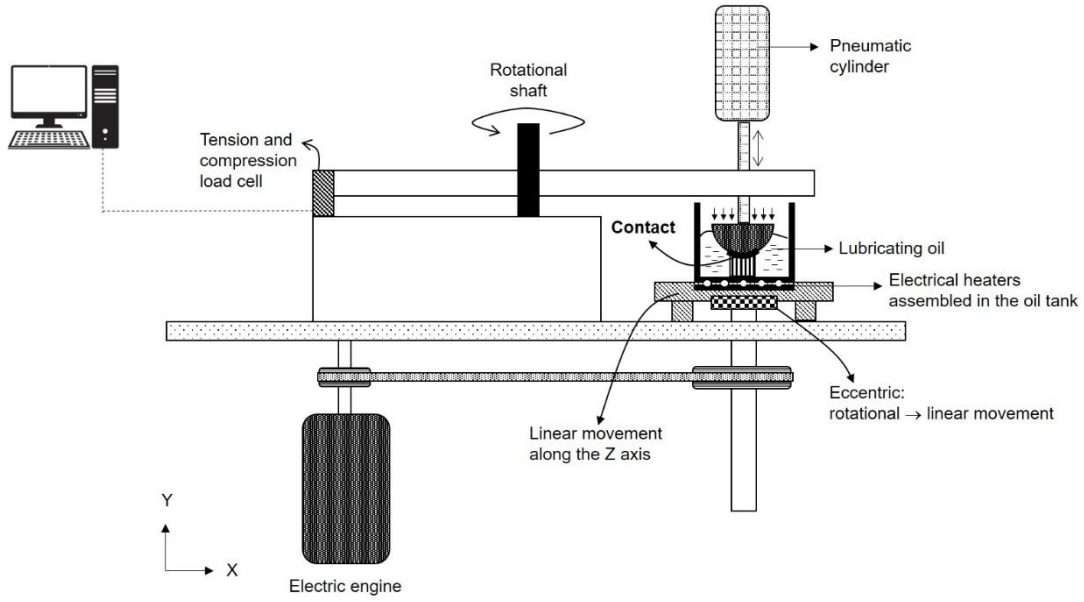


Figure 3.2 Schematic representation of the central systems of the new ring-liner test rig.

The structure of the developed testing device comprises five different subsystems:

*A. Loading system*

Under operation, the piston ring is continuously pressed against the cylinder liner due to its elastic spring force and, during compression and combustion strokes, the gas pressure acting on its inner surface. It is used as a pneumatic system to reproduce that resultant load acting on the back surface of the piston ring against the cylinder liner. When using the compressed air network, a stem allows the variation of the loading profile during the test. It will create a loading profile to simulate the loading changes during the combustion process and the real ring gap effect.

The load ranges from 10 N up to 400 N. The lowest limit, which corresponds to the inherent elastic spring force of the piston ring, represents a contact pressure of around 0.4 MPa. The maximum operational value (400 N) corresponds to 16 MPa, a value far superior to the real operating pressures. Those values were calculated considering the surface area of the ring-liner contact.

According to Tamminen et al. [26], considering a 4-stroke diesel engine, the maximum pressure behind the first compression ring rounds 4 MPa in the compression stroke. It reaches a value close to 12 MPa in the expansion stroke. In the intake and exhaust strokes, the pressure is lower than 0.4 MPa. Thus, the developed test ring can test, evaluate, and define the functional limits for a new pair of materials.

### *B. Ring-liner contact holding system*

The rig was designed to fit standard ring-liner pairs from heavy-duty diesel engines, but it can be adapted for samples with diameters in the range of 80-200 mm.

The upper structure includes a piston ring holder clamped in the extremity of a shaft, which can be moved in height (through a bearing) but is static in the reciprocating movement plane. The ring holder (located in the upper position of the contact) is presented in Figure 3.3a). It was designed to ensure that the measured ring-liner friction has any influence from other contact friction sources.

The cylinder liner sample, presented in Figure 3.3b) is in the lower position of the contact. It is fixed inside of the oil tank over the reciprocating plate. The contact area between the ring and the liner samples is noticeable due to a wear track visible in the liner surface.

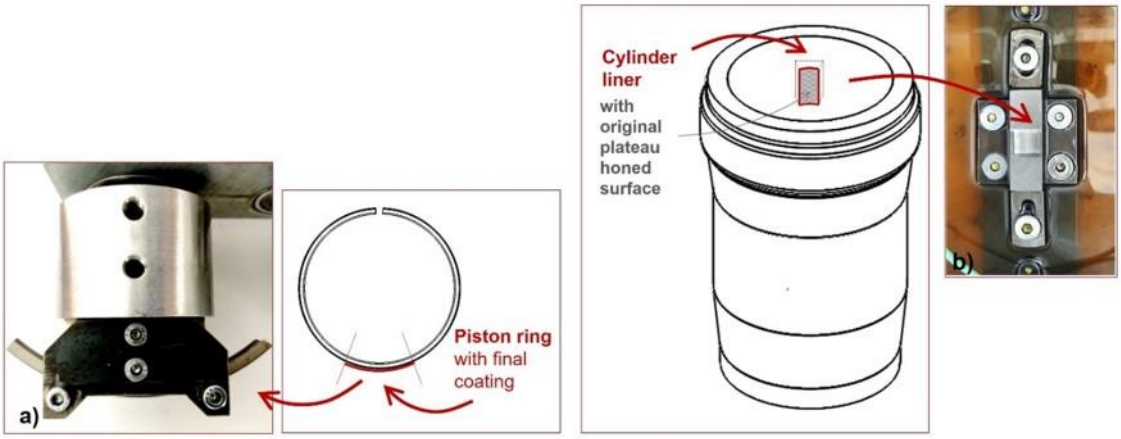


Figure 3.3 Detailed view of the piston ring a) and cylinder liner b) holding structures after a tribological assessment.

### *C. Lubrication and heating system*

The heating system is installed in the oil tank. Five electrical heaters of 120 W each are used to raise the temperature of the oil tank, where are the lubrication oil and the ring-liner contact. A thermocouple placed close to the ring-liner contact measures the temperature of the oil submerged into the oil tank. Additionally, a temperature micro-controller enables to regulate the electrical heaters.

Different lubrication regimes may be simulated using this apparatus. If the interface of the piston ring and the cylinder liner is within the lubrication oil bath, it replicates a fully flooded lubrication. Besides fully flooded also boundary lubrication and dry tests are possible to perform. It is possible to simulate a boundary lubrication environment controlling the input of the oil volume in the ring-liner contact. The boundary lubrication condition is implemented by using a syringe to control the oil volume introduced initially in the contact. A thin film will be formed and disseminated throughout the test. The mixed lubrication is considered when the oil is filled to a lower level than the contact surfaces. With the reciprocating movement, the oil will be conveyed to the piston ring-cylinder liner proximity. Dry tests may be suitable to simulate extreme operational conditions or even to test new coating materials as solid lubricants.

Concerning the testing temperature range, the maximum temperature value of 160 °C is close to the real maximum values of the top ring groove. Some authors defend that the average oil film temperature in a cycle would be lower than 100-130 °C [26, 27]. However, others referred that there is a significant difference between the temperature in the region of the ring gap and a point diametrically opposite the gap [28]. Different works proclaim a temperature superior to 200 °C in the top piston ring groove [29, 30], but a further increase of the temperature may be restricted by the flashpoint of the used engine oil (by the demand to set up a ventilation system).

### *D. Acquiring data system*

A measuring system for friction force has an integrated solution from LCM Systems Lda. It consists of a tension-compression load cell with a rated load of 100N and a resolution of 0.1N (model DCE-100N); a digital conditioner USB module for signal conditioning of the load cell, and data acquisition (model DSC USB); data acquisition software for offline processing. The friction force is sampled at up to 200 Hz rate and recorded at 100ms intervals.

Additionally, the controller of the oil temperature uses a closed-loop consisting of a thermocouple type K with the hermetically sealed tip for electric isolation from the medium and cold-junction compensation (sensor); cartridge heating resistance of 120W of rated power with ceramic insulation (actuator); PID temperature controller with auto-tuning and relay output (model Love 4C-3) (controller).

### *E. Motion and driving system*

The test rig has an electric motor of 2000 RPM. Its rotational movement is transmitted to a drive shaft through a tire coupling, then connected to the reciprocating parts. An eccentric converts the shaft rotation into a reciprocating sliding of the moving plate (the support table in Figure 3.4) over the parallel guides. The eccentric position can be altered to vary the sliding amplitude, and consequently, the stroke length.

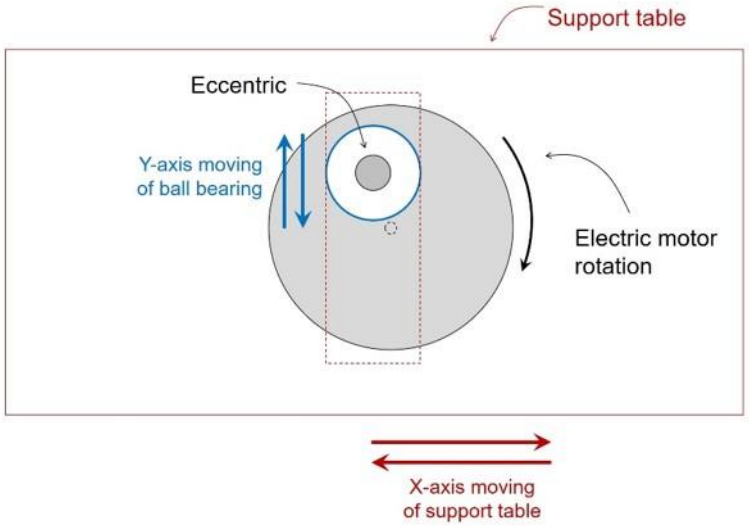


Figure 3.4 The system used to convert the rotary motion from the electric motor into the linear movement of the support table.

The testing speed creates dynamic forces and the presence of vibrations in the test rig. Those are kept low as little as possible, and to mitigate their effects, are used rubber plates in the metallic screwing connections. Additionally, the test rig fixation represents an active vibration absorption.

One complete rotation of the driven gear corresponds to one stroke (for a displacement of 10 mm, one stroke represents 20 mm). The number of strokes per second defines the frequency.

The maximum mean testing speed is 0.35 m/s. This value was found multiplying the double of the stroke (correspondent to a cycle) for the maximum test frequency value, around 15.9 Hz. A gear ratio of 3:1 allows a further increase of the drive shaft speed, and consequently, the reciprocating sliding rate.

The available displacement range, already tested and validated, is between 5 and 15 mm. The stroke is not altered during the experiment. It is necessary to disassemble the reciprocating table and change the position of the eccentric using the leadscrew for stroke variation. Figure 3.5 is given a realistic view of the final testing device.

Figure 3.5 Overview of the developed piston ring tribometer.

The use of sections of the original parts, not the whole element, makes the variation of the testing parameters more intuitive to extreme boundary conditions.

The developed test rig will measure the coefficient of friction and determine the wear resistance of coated rings in dry, boundary, and full lubricated conditions. According to the system configuration, the static piston ring segment is the upper part, and the reciprocating lower part is a liner sample cut from the bulk cylinder. Figure 3.6 demonstrates how physical contact occurs between a piston ring segment and a section of a cylinder liner.

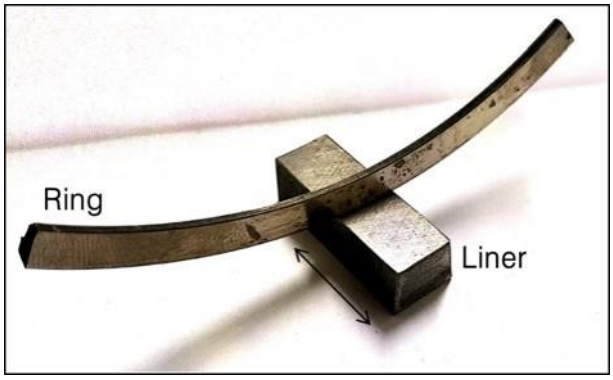


Figure 3.6 Physical contact between the piston ring and the cylinder liner parts.

Using the presented layout, the main drawback is the alignment between the piston ring and the cylinder circularities. Before each test, a pre-evaluation of the linear alignment using a test sample can prevent that problem. Optionally, using the cylinder liner fixing elements in a semi-free state, the circularities of both parts aligned autonomously during the running-in period. This second method must set the screws at the end of the running-in period to fix the cylinder liner in the aligned position.

To validate the reproducibility of the developed tribometer it was required to perform more than one exploratory test. The goal of those studies was to evaluate the frictional response under different operating conditions, with interest in the study of the piston ring component.

### 3.2.2 Definition of the exploratory tests

Following the development of the tribometer a batch of tests was performed to evaluate the functionality of the test rig. For that purpose, the definition of the testing conditions followed an empirical method based on the operating range of the developed test rig. Figure 3.7 is presented the expected variation for each control variable. The compression piston ring thermodynamics can be qualitatively predicted based on a four-stroke diesel engine [11, 31–33]. The prediction of the lubrication oil film behavior was defined based on the results obtained by Rakopoulos and Giakoumis [34]. The upper and lower limits for each variable range were restrained based on the tribometer operational limits.

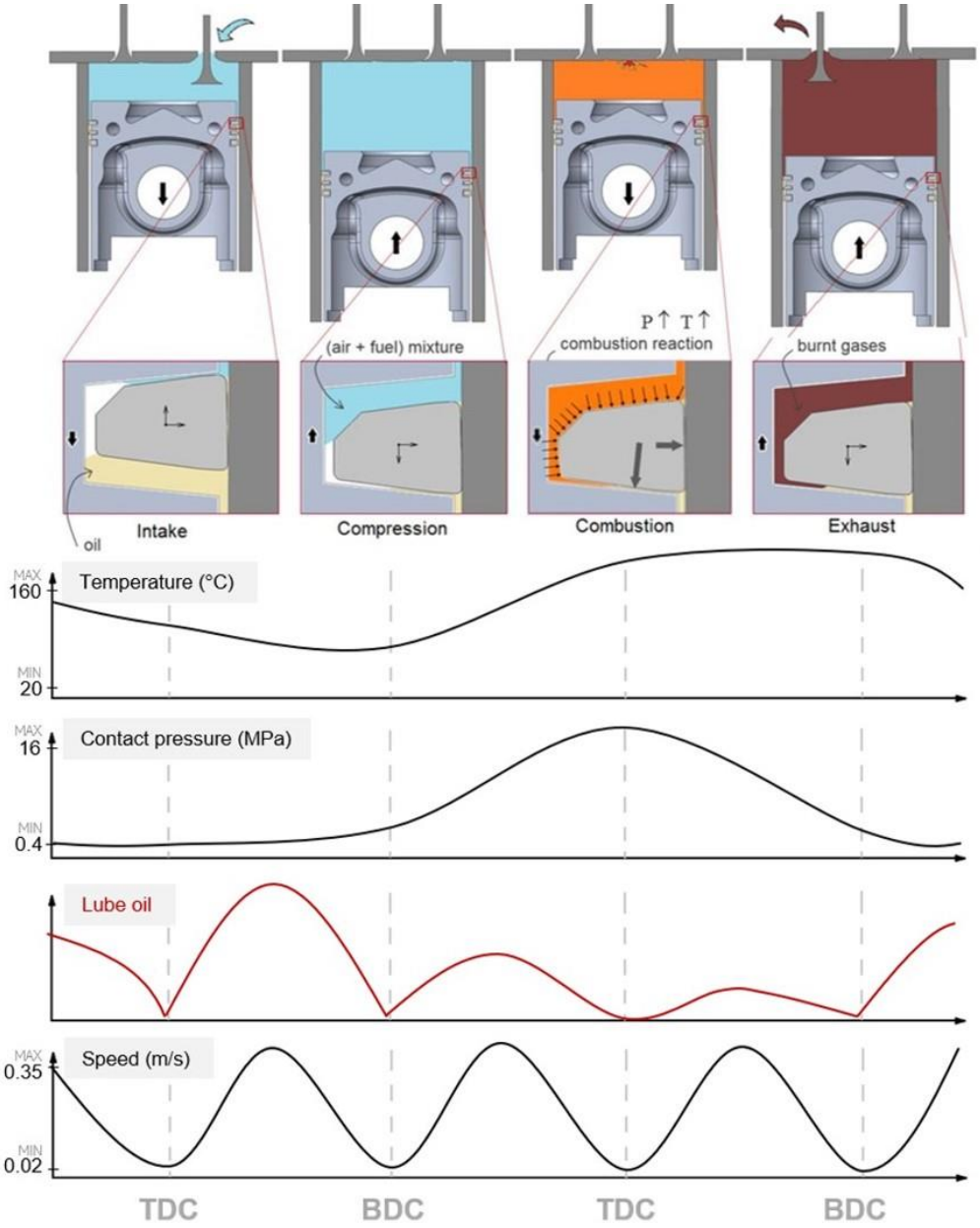


Figure 3.7 Expected operational profile for the controlled variables of a four-stroke diesel engine, considering the functional limits of the developed tribometer.

Those will be the studied conditions in this work regarding the four dead center positions of a piston in a four-stroke diesel engine as the most detrimental zones for the top compression ring service life. In the dead centers, the piston inverts the movement direction, which means that speed decreases to zero, and consequently, the lubrication oil film achieves its minimum. The presence of a higher normal load from the gases acting on the back of the piston ring and the increase of the temperature (which decreases the oil film viscosity) contribute to an even greater ring-liner approach, particularly before the start of the compression and combustion strokes.

Based on the operational range and the predicted behavior of each variable, the defined testing conditions are presented in Table 3.2.

Table 3.2 Testing conditions for friction measurements based on the predicted functioning of a four-stroke diesel engine.

| | TDC 1 | BDC 1 | TDC 2 | BDC 2 |
|---|---|---|---|---|
| Temperature (°C) | 100 | 80 | 160 | 160 |
| Normal load (N) / Contact pressure | 10 / 0.4 | 100 / 4 | 400 / 16 | 100 / 4 |
| Lubrication | *boundary* | *boundary* | *boundary* | *boundary* |
| Speed (m/s) | 0.04 | 0.04 | 0.04 | 0.04 |

The maximum temperature represents the top compression ring temperature in the real engine to reproduce those testing conditions. The lubrication oil was heated up to each of those temperatures and maintained until it reached the steady-state condition. That was the necessary period to achieve that temperature in the cylinder liner sample (and consequently, in the ring-liner contact) by the heat conduction effect.

In similarity to the real operating conditions, the minor normal load value represents the inherent spring force. In contrast, the maximum value represents the maximum contact pressure resultant from the combustion gases effect.

As previously described, the developed tests can be performed according to three different lubrication regimes: a fully lubricated contact with the contact submersed in the lubricating oil bath, a boundary lubrication regime using a thin oil film, and a dry contact, with any lubricant. In those trials, to achieve boundary lubrication conditions, before each run, a dosage of 0.0258 ml of oil was dispensed into the contacting area using a syringe.

Relatively to the reciprocating movement reproduced by the tribometer, the speed value is the result of multiplying the test frequency by double of the stroke.

To ensure the same surface conditions at the beginning of all tests, each test used a different cylinder liner sample and a new piston ring sample. The samples holder was designed to improve the adjustability and flexibility in the piece reassembling. The flexibility of the test rig allows the variation of the loading profiles and the reproduction of a test under multiple conditions.

### 3.2.3 Testing protocol

As previously mentioned, the testing samples consist of a piston ring and cylinder liner fragments from a heavy-duty diesel engine. The used stainless-steel top compression rings have a physical vapor deposited DLC (Diamond-Like Carbon) coating deposited at the MAHLE, Componentes de Motores, S.A. The coating on the piston ring surface is structurally amorphous with $sp^2$ and $sp^3$-bonded carbon atoms, with hardness values above 1000 HV. The cast-iron cylinder liner samples have a typical plateau honed texture in the inner surface, which consists of a surface texture that improves oil storage capacity and the distribution of lubricating oil in the cylinder liner [35]. The grey cast iron is naturally softer with a microstructure of graphite in transformed austenite and cementite matrix. Its typical hardness values are around 240 HV.

Regarding the selected surface materials for the contact between ring and liner bodies, low COF values (below 0.2) can result from the DLC layer [36, 37]. In the present work, this low value can be related to graphitic zones in the cylinder liner surface or the DLC metallographic structure. The latter may reveal lubricious-like properties (when $sp^2$ hybridizations are dominant among the atoms), reducing friction against a metallic surface.

A minimum of three repetitions of the same testing conditions is necessary to find accuracy and repeatability. As previously referred, the central challenge in this equipment is the geometrical alignment among the cylinder liner and piston ring circularity. In those evaluations, the adjustment of the line contact between the piston ring and cylinder liner segment was performed through a dynamic auto-alignment.

Some tribological experiments comprise a running-in period at the beginning of each test to avoid the influence of the surface's topography. The current approach considers the all range of the test results because the initial surface roughness can be a decisive parameter in the tribological performance of piston rings [38], especially those with PVD coatings. During the trial, the friction coefficients and sliding time were recorded automatically (as described in the Acquiring data system description). The coefficient of friction represents the mean value obtained for each condition.

The fully synthetic motor oil applied was an SAE 5W30, with the viscosity and density values presented in Table 3.3.

Table 3.3 Lubricant oil (SAE 5W30) viscosity and density values at different temperatures.

| | |
|---|---|
| Density @ **15 °C** (kg/m3) | 850 |
| Kinematic viscosity @ **40 °C** (cSt) | 54 |
| Kinematic viscosity @ **100 °C** (cSt) | 9.6 |
| Viscosity Index | 166 |
| Flash Point (°C) | 185 |
| Ash, Sulphated (% wt) | 0.49 |

The test stroke was 10 mm, and the COF value was recorded using a data logging of 10 measures per second during 600 cycles.

## 3.3 Results and Discussion

The present section will be exposed and discussed the coefficient of friction results for each tested condition. The COF value is presented in Figure 3.8 as a function of the number of cycles run for each testing condition reproducing the dead-centers functioning.

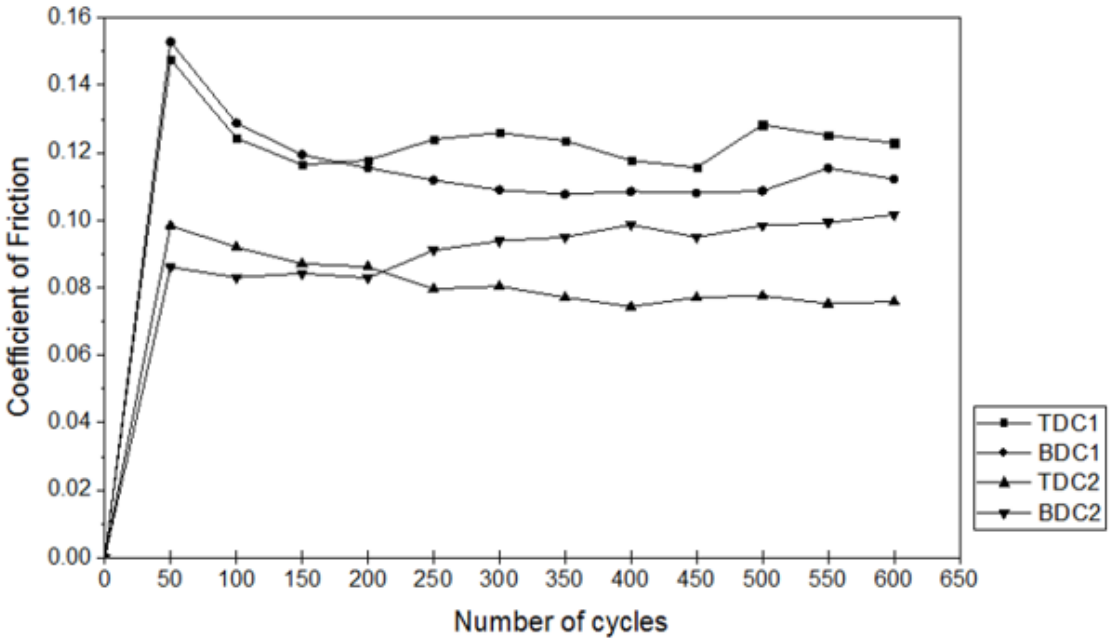


Figure 3.8 COF values resulted from the dead-centers testing conditions as a function of the number of cycles.

Regarding that, all samples have the same initial topographic, structural, and chemical properties. The analysis of those results will concern the variation of the testing conditions and its impact on the tribological and physical contact of the sliding surfaces. The lower COF values are registered for those conditions reproducing the second top dead center and the second bottom

dead center, namely, combustion and exhaust. Since speed and lubrication oil types were constant for every experiment, load and temperature will play a decisive role in the tribological behavior.

The measured values are in the range of the conventional tribological performance of DLC films against stainless steel [39]. However, the major COF was registered for the testing condition with a lower load. A fluctuating profile is verified by analyzing the evolution of the coefficient of friction value with the increase of the number of cycles. Those variations may be caused by vibrations in the test rig, which may have more influence on the ring-liner contact when using lower normal loads. In another point of view, when reproducing the test conditions of the first top dead center, the use of a low load led to a real contact established only by the DLC coating and the grey cast iron asperities. Regarding the divergence on the material's hardness, the asperities of the DLC coating could have an abrasive effect on the cylinder liner surface.

Along with the progression of the test, the COF values of the TDC1, BDC1, and BDC2 tend for a similar coefficient of friction value. As an exception, the testing conditions simulating the second top-dead-center, using a superior normal load and temperature, presented the lower COF value. In the TDC2, the rise of the normal load and the contact temperature would cause a decrease in the oil film thickness existing in the contact. The increased possibility of an interaction between ring and liner surfaces, associated with the lowest COF value, demanded a more detailed analysis of the surface contact.

To understand the interaction between both surfaces, the morphology of each part is shown in Figure 3.9. Figure 3.9a) has a reference to the arithmetic average roughness of the piston ring DLC layer, and Figure 3.9b) has a reference to the cross-hatched texture of the cylinder bore surface used to prevent seizure under hot engine running conditions. The coating surface roughness was evaluated using the Mitutoyo Surftest SJ-210 portable surface roughness tester.

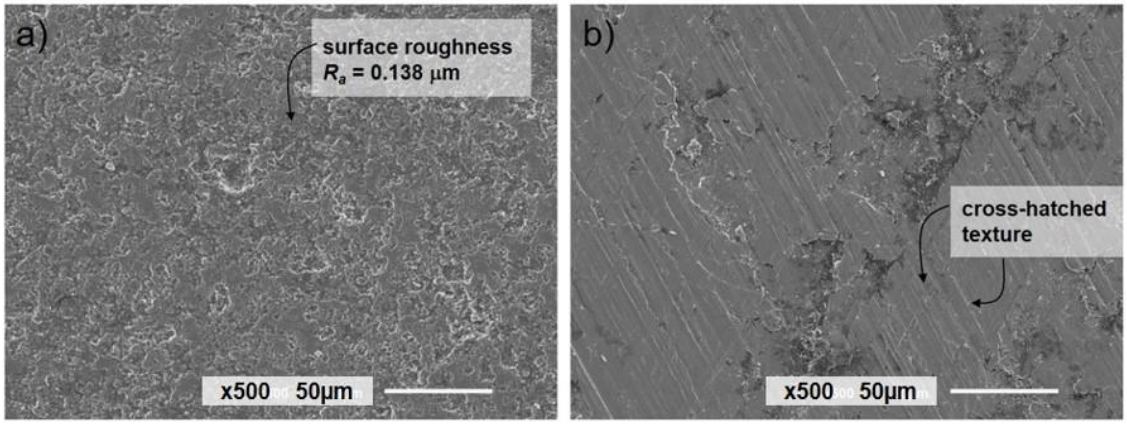


Figure 3.9 Original surface morphology of the a) piston ring DLC film and b) cylinder liner bore.

Besides the lower hardness of the cylinder liner, the sulfur content of the grey cast iron chemical composition favors graphite flakes. During the friction measurements, those graphite flakes might help to retain the restricted quantity of lubricant.

With an increase of the normal load, the stress was concentrated in the flakes of graphite of the grey cast iron leading to low toughness and consequently to the transference of material. As shown in Figure 3.10, the adhesion of the cylinder liner to the asperities of the piston ring surface, generating low friction from the contact between the cast iron of the cylinder liner and the cast iron attached to the DLC surface.

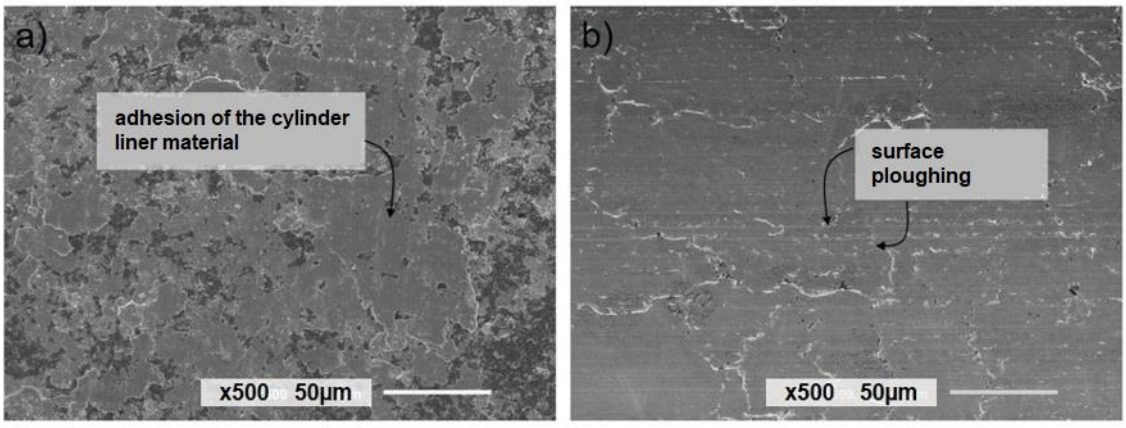


Figure 3.10 Surface morphology of the a) piston ring and b) cylinder liner bore after the friction test using the test conditions reproducing the second top dead center.

Figure 3.10a) can verify the mask of the DLC coating with the material resulting from the adhesion to the cylinder liner sample. Consequently, in Figure 3.10b), the cross-hatched texture was entirely removed. Ploughed channels appeared in the cylinder liner due to the plastic deformation of its soft surface caused by the DLC hard contact.

In those experiments, the increase of the normal load and the contact temperature promotes the softer material (cast iron) transference to the contact interface and its adhesion to the piston ring coating, covering the harder surface. Consequently, the COF value decreases due to the prevalence of the cast iron-cast-iron contact in a dynamic and lubricated contact. A similar phenomenon is observed in the SEM analysis of the second bottom dead center surface presented in Figure 3.11. Comparatively to TDC2, a lower quantity of material was transferred to the piston ring surface due to a decrease in the applied normal load.

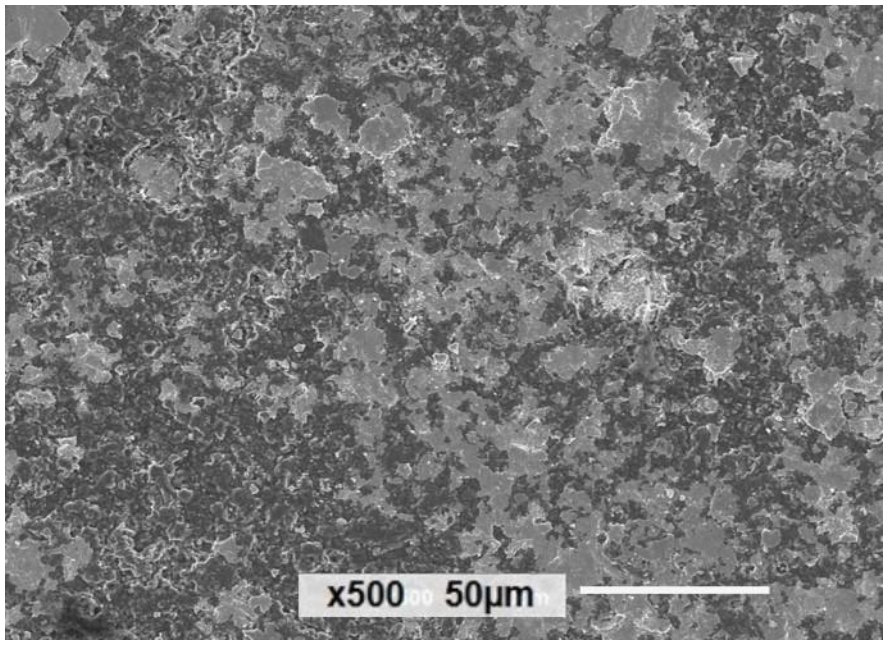


Figure 3.11 Surface morphology of the piston ring surface after the friction test using the test conditions reproducing the second bottom dead center.

Depending on the operating conditions, the presence of a hard layer (such as the DLC film) in the piston ring surface may cause excessive wear and an abrasive effect in the counter-body. An efficient contact and a durable tribological pair (with a long lifetime) depend on the tribological resistance of both surfaces.

The development of the presented testing device allowed the tribological analysis of the piston ring-cylinder liner contact. This equipment will be used for further improvements and future investigations.

## 3.4 Conclusions

A new piston ring-cylinder liner testing equipment was developed, and the present work described its central constituent systems. As a predefined requirement, the test rig enables to use of standard commercial components. The advantage of using real components instead of simplified parts is to test using the coating's original surface morphology and reliable material properties.

The use of different testing parameters to study their effects on the coefficient of friction was demanded to explore the functionality and repeatability of the developed test rig. It was possible to reproduce different engine operating conditions according to the functional limits of the developed tribometer. Regarding the 4-stroke diesel engine cycle, dead-center positions were selected to investigate the variation of the COF values.

The performance of this tribological pair was not only influenced by the nature and the structure of both materials but principally by the testing parameters, such as load and temperature. For this purpose, further research can be performed in the future, including extended wear tests for each test condition. This device aims to represent a relevant tool to study the piston ring tribological performance and evaluate potential new solutions.

## Acknowledgements

This work was supported by FCT (Fundação para a Ciência e Tecnologia) and MAHLE, Componentes de Motores, S.A. through the grant SFRH/BDE/110654/2015, by FCT (Fundação para a Ciência e Tecnologia) with the reference project UID/EEA/04436/2019 and by the project POCI-01-0145-FEDER-006941 and the project with reference NORTE-01- 0145-FEDER-000018-HAMaBICo.

## References

[1] Assanis D, Delagrammatikas G, Fellini R, et al (1999) Optimization Approach to Hybrid Electric Propulsion System Design. Mech Struct Mach 27:393–421. https://doi.org/10.1080/08905459908915705
[2] Barbosa TP, da Silva LAR, Pujatti FJP, Gutiérrez JCH (2020) Hydraulic hybrid passenger vehicle: Fuel savings possibilities. Mech Based Des Struct Mach 0:1–19. https://doi.org/10.1080/15397734.2020.1714447

[3] Eckert JJ, Santiciolli FM, Bertoti E, et al (2018) Gear shifting multi-objective optimization to improve vehicle performance, fuel consumption, and engine emissions. Mech Based Des Struct Mach 46:238–253. https://doi.org/10.1080/15397734.2017.1330156
[4] Shuster M, Mahler F, Macy D, et al (2010) Piston Ring Microwelding Phenomenon and Methods of Prevention. SAE Tech Pap Ser 1:. https://doi.org/10.4271/960745
[5] Johansson S, Nilsson PH, Ohlsson R, Rosén B (2011) Experimental friction evaluation of cylinder liner / piston ring contact. 271:625–633. https://doi.org/10.1016/j.wear.2010.08.028
[6] Zhan J, Yang M (2012) Investigation on Dimples Distribution Angle in Laser Texturing of Cylinder-Piston Ring System. Tribol Trans 55:693–697. https://doi.org/10.1080/10402004.2012.694581
[7] Chaudhari T, Sutaria B (2016) Investigation of friction characteristics in segmented piston ring liner assembly of IC engine. Perspect Sci 8:599–602. https://doi.org/10.1016/j.pisc.2016.06.032
[8] Li T, Lu X, Ma X, et al (2019) Numerical and Experimental Analysis of the Honing Texture on the Lubrication Performance of Piston Ring–Cylinder Liner Tribosystem. Tribol Trans 62:991–1006. https://doi.org/10.1080/10402004.2019.1640330
[9] Ferreira R, Martins J, Carvalho Ó, et al (2020) Tribological solutions for engine piston ring surfaces : an overview on the materials and manufacturing and manufacturing. Mater Manuf Process 35:498–520. https://doi.org/10.1080/10426914.2019.1692352
[10] Liang X, Wang X, Liu Y, et al (2020) Simulation and Experimental Investigation on Friction Reduction by Partial Laser Surface Texturing on Piston Ring. Tribol Trans 0:000. https://doi.org/10.1080/10402004.2019.1696433
[11] Comfort A (2003) An Introduction to Heavy-Duty Diesel Engine Frictional Losses And Lubricant Properties Affecting Fuel Economy - Part I. SAE Tech Pap 2003-01-3225. https://doi.org/10.4271/2003-01-3225
[12] Truhan JJ, Qu J, Blau PJ (2005) A rig test to measure friction and wear of heavy duty diesel engine piston rings and cylinder liners using realistic lubricants. Tribol Int 38:211–218. https://doi.org/10.1016/j.triboint.2004.08.003
[13] Tamura K, Kasai M (2014) Impact of Boundary Lubrication Performance of Engine Oils on Friction at Piston Ring-Cylinder Liner Interface Yukinobu Nakamura and Tomoyuki Enomoto. 875–881. https://doi.org/10.4271/2014-01-2787
[14] Smith OM, Michlberger A, Jayne D, et al (2014) Advanced Power-Cylinder Tribology Using A Dynamically Loaded Piston Ring on Cylinder Bore Tribometer. SAE Tech Pap. https://doi.org/10.4271/2014-01-2783.Copyright
[15] Bouzana A, Guermat A, Belarifi F (2018) Experimental results of a hydrodynamic friction behaviour of a linear contact at low sliding velocity. Mater Sci Eng
[16] Lenauer C, Tomastik C, Wopelka T, Jech M (2015) Piston ring wear and cylinder liner tribofilm in tribotests with lubricants artificially altered with ethanol combustion products. Tribol Int 82:415–422. https://doi.org/10.1016/j.triboint.2014.04.034
[17] Cousseau T, Sebastian J, Acero R, Sinatora A (2015) Tribology International Tribological response of fresh and used engine oils : The effect of surface texturing , roughness and fuel type. Tribiology Int 1–10. https://doi.org/10.1016/j.triboint.2015.11.016
[18] Wan S, Li D, Zhang G, et al (2017) Comparison of the scuffing behaviour and wear resistance of candidate engineered coatings for automotive piston rings. Tribol Int 106:10–22. https://doi.org/10.1016/j.triboint.2016.10.026
[19] Andersson P (2003) A new tribometer for piston ring friction measurements. Tribol Res Des Eng Syst 501–510

[20] Syed D, Wani MF (2019) Tribological behavior of chrome-deposited SAE9254 grade steel top compression piston ring under lubrication starvation and mild extreme pressure lubrication. Int J Engine Res. https://doi.org/10.1177/1468087419890995
[21] Fayaz SD, Wani MF (2020) Evaluating scuffing failure in dry sliding conditions of monolayer chromium piston ring/bulk grey cast iron liner interface. Tribol Online 15:9–17. https://doi.org/10.2474/trol.15.9
[22] Zhang W, Becker E, Wang Y, et al (2008) Investigation of scuffing resistance of piston rings run against piston ring grooves. Tribol Trans 51:621–626. https://doi.org/10.1080/10402000802044316
[23] Dunaevsky V, Alexandrov S (2005) Three-dimensional engineering approach to conformability analysis of piston rings. Tribol Trans 48:108–118. https://doi.org/10.1080/05698190590903105
[24] Söderfjäll M, Almqvist A, Larsson R (2016) Component test for simulation of piston ring – Cylinder liner friction at realistic speeds. Tribol Int 104:57–63. https://doi.org/10.1016/j.triboint.2016.08.021
[25]. Akalin O, Newaz GM (2001) Piston Ring-Cylinder Bore Friction Modeling in Mixed Lubrication Regime: Part I—Analytical Results. J Tribol 123:211. https://doi.org/10.1115/1.1286337
[26] Tamminen J, Sandström CE, Andersson P (2006) Influence of load on the tribological conditions in piston ring and cylinder liner contacts in a medium-speed diesel engine. Tribol Int 39:1643–1652. https://doi.org/10.1016/j.triboint.2006.04.003
[27] Harigaya Y, Suzuki M, Takiguchi M (2003) Analysis of Oil Film Thickness on a Piston Ring of Diesel Engine: Effect of Oil Film Temperature. J Eng Gas Turbines Power 125:596. https://doi.org/10.1115/1.1501078
[28] Ruddy BL, Dowson D, Economou PN (1981) Prediction of Gas Pressures Within the Ring Packs of Large Bore Diesel Engines. J Mech Eng Sci 23:295–304. https://doi.org/10.1243/JMES_JOUR_1981_023_054_02
[29] Furuhama S, Suzuki H (1979) Temperature Distribution of Piston Rings and Piston in High Speed Diesel Engine. Japan Soc Mech Eng 22:
[30] MAHLE GmbH (2012) Pistons and engine testing, 1st ed. Vieweg+Teubner Verlag, Stuttgard
[31] Tian T (1997) Modeling the performance of the piston ring-pack. Massachusetts Institute of Technology
[32] Andersson P, Tamminen J, Sandstrom C-E (2002) Piston ring tribology - A literature survey. Espoo
[33] Lakshminarayanan PA, Nayak NS (2011) Critical component wear in heavy duty engines. John Wiley & Sons
[34] Rakopoulos CD, Giakoumis EG (2007) Prediction of friction development during transient diesel engine operation using a detailed model. Int J Veh Des 44:143–166. https://doi.org/10.1504/IJVD.2007.013223
[35] Rao X, Sheng C, Guo Z, Yuan C (2019) Influence of Surface Groove Width on Tribological Performance for Cylinder Liner–Piston Ring Components. Tribol Trans 62:239–248. https://doi.org/10.1080/10402004.2018.1539201
[36] Neuville S, Matthews A (2007) A perspective on the optimisation of hard carbon and related coatings for engineering applications. Thin Solid Films 515:6619–6653. https://doi.org/10.1016/j.tsf.2007.02.011

[37] Bewilogua K, Hofmann D (2014) History of diamond-like carbon films - From first experiments to worldwide applications. Surf Coatings Technol 242:214–225. https://doi.org/10.1016/j.surfcoat.2014.01.031
[38] He Z, Zhang J, Ma W, et al (2014) A Concurrent Reynolds BC Algorithm for Piston Ring Cavitation Lubrication Problems with Surface Roughness. Tribol Trans 57:353–365. https://doi.org/10.1080/10402004.2013.871376
[39] Mobarak HM, Niza Mohamad E, Masjuki HH, et al (2015) Friction and wear characteristics of hydrogenated and hydrogen-free DLC coatings when lubricated with biodegradable vegetal oil. Key Eng Mater 642:50–54. https://doi.org/10.4028/www.scientific.net/KEM.642.50

# CHAPTER 4.

## Influence of morphology and microstructure on the tribological behavior of arc deposited CrN coatings for the automotive industry

Published in Surface and Coatings Technology, 2020, 397: 126047
R. Ferreira [a,c,d,*], Ó. Carvalho [a], L. Sobral [c], S. Carvalho [d], F. Silva [a]

[a] Centre for Micro-Electro Mechanical Systems (MEMS) University of Minho, Campus de Azurém, 4800-058 Guimarães, Portugal
[b] Mechanical Engineering Department, Universidade do Minho, 4800-058 Guimarães, Portugal
[c] MAHLE - Componentes de Motores S.A., Núcleo Industrial Murtede, 3060-372 Cantanhede, Portugal
[d] GRF-CFUM, Department of Physics, University of Minho, Campus de Azurém, 4800-058 Guimarães, Portugal

## Abstract

PVD coatings are widely used in the automotive industry for tribological purposes. In heavy-duty diesel engines, piston rings represent a challenging component concerning its tribological performance. Top piston rings were designed as an additional part with a supporting role in the sealing or prevention of gas leakages from the combustion chamber. Several studies have been published proposing metal nitride coatings for the piston ring's functional surface. CrN coatings are among those most frequently proposed, but regularly using magnetron sputtering as the predefined deposition method. In a large-scale production framework, different deposition methods with improved deposition rates must be adopted. Cathodic arc deposition is currently widely implemented in several industries, such as in the automotive one. Although this technique is consolidated in the industrial environment, the deposition process and parameters are continuously under optimization.

In the present study, two different CrN coatings deposited on the piston ring's functional surface are studied. Using other deposition conditions, two distinct morphologies are achieved in the coating layer: a denser structure (CrN-A) and a columnar structure (CrN-B). Those coatings were tested using a locally developed test rig, adapted to test the piston rings under conditions close to the real engine operation. The microstructure and mechanical properties of the CrN-A and CrN-B coatings were evaluated using X-ray diffraction and micro-indentation. The surface morphology and wear mechanism were characterized using SEM and EDS techniques before and after to perform the wear and friction tests.

Keywords: *piston ring; cathodic arc; chromium nitride; tribology; automotive industry.*

## 4.1 Introduction

Physically Vapour Deposited (PVD) coatings are widely used in the automotive industry for tribological purposes. They were introduced to replace the electroplating coating process and its related environmental problems. The increased wear resistance of PVD coatings allowed the lowering of the coating thickness and thin hard coatings to become widely used, mainly to improve the tribological performance of parts with relative sliding movement.

The automotive industry is one of the most relevant contributors to the development of PVD technology, where hard coatings have an efficient tribological function. In heavy-duty diesel engines, piston rings represent a challenging component concerning its tribological performance. Top piston rings were designed as an additional part with a supporting role in the sealing or prevention of gas leakages from the combustion chamber. During operation, the piston ring is exposed to high mechanical loading. However, its reliability over a long lifetime is required. For this reason, the reduction of the wear rate is mandatory for the efficient performance of the engine over a long time.

With regard to the piston ring's functional surface, several studies proposing metal nitride coatings for tribological purposes have been published [1–3]. Compared to other conventional metal nitride coatings, CrN has an excellent corrosion resistance (both at environmental and high temperatures) and a high deposition rate for similar deposition parameters. Nowadays, CrN coatings are still considered for piston rings in which its high wear and scuffing resistance are associated with their competitive lower cost, determinant for large scale production industries.

Regarding CrN coatings development and deposition, the analysis of the influence of the deposition conditions in the final coating properties or the study of the CrN coating tribological response were study aims of some of those investigations [4–9].

Friedrich et al. [4] studied CrxN coatings for tribological applications on piston rings. All coatings deposited with a reactive nitrogen flow showed superior hardness than Cr coatings. Those using 15 $cm^3$/min ($Cr_2N$) and 25 $cm^3$/min (CrN) of nitrogen gas flow presented a hardness value above 30 GPa. From their study, the friction coefficient is slightly decreasing with increasing hardness (due to the reduced plasticity of the contact). Broszeit et al. [5] continued the previous study regarding the development of $Cr_xN$ coatings. In this study, the authors also compared the tribological performance of CrN coatings deposited by PVD and electroplated chromium coatings, and the former reported better results. In other investigations about CrN coatings, Barata et al. [6] studied the influence of magnetron sputtering deposition parameters in the crystal phases, and Bouzid et al. [8] investigated the tribological resistance of a CrN coating deposited by R.F. magnetron sputtering. In the latter, the non-alloyed CrN layer CrN coatings achieved the lowest coefficient of friction.

One of the main disadvantages of magnetron sputtering in comparison with other PVD techniques is its low deposition rates, which does not make it feasible for applicability in large-scale production industries, such as the automotive one. With different attempts made to enhance this condition, among the different variants of the magnetron sputtering deposition technique, the most recent one focuses on the production of highly ionized fluxes of the sputtered material, named High-Power Impulse Magnetron Sputtering (HiPIMS). However, there are other PVD techniques which are employed in obtaining an improved deposition efficiency (regarding the productiveness and the financial feasibility), such as cathodic arc technique [10].

Depending on the final use, large production series demand very high production rates. The cathodic arc technique fulfills this requirement. For this reason, this technique has been widely used for protective and tribological coatings in several industries, such as the automotive one.

A brief overview of this process can be used to describe the coating's deposition in three steps. Initially the vaporization of the solid cathode material through an arc erosion occurs using high current and low voltage conditions. In the second step, the vaporized cathode material is converted into a gaseous plasma, which is considered as a kind of fluid conductor between the electrodes (cathode and anode). The third step is the energetic condensation from plasma ions that arrive at the substrate surface [11]. The plasma density produced was found to be directly proportional to the arc discharge current [12].

The presence of a high energy density in the cathode-spot region induces the cathode material to go through the four phases, from solid to plasma (with possible liquid and vapor intermediate phases). This plasma transformation leads to three resultant types of cathode erosion: ions, neutrals, and macroparticles. The energy of ions can be controlled by the difference in plasma potential and substrate surface potential. The substrate surface potential is determined by the applied bias voltage, which can be used to affect the energy of the condensing plasma. Among those, different deposition parameters can be controlled using a cathodic arc technique, and their variation will influence the final properties of the deposited coating.

On balance, the cathodic arc systems with higher deposition rates (associated with copious amounts of plasma produced) and lower equipment costs operate with continuous, direct current (DC). The principal weakness of this process is the presence of macroparticles into the deposited coating. Macroparticles are growth defects that are produced at cathode spots along with the plasma. Usually, those materials with a low melting point (or of low cohesive energy), provide more and larger macroparticles [13]. Conversely, additional advantages of this technology are the excellent adhesion of the coatings, the relative ease of forming hard layers, and the relatively wide range of usable partial pressure of reactive gas when creating stoichiometric coatings [14].

Chromium nitride (CrN) thin coatings are deposited by reactive vapor deposition. These metal nitride coatings result from the reaction of the working reactive gas, the nitrogen, with the Cr metal atoms from the cathode spot plasma. This interaction depends on several parameters, such as gas pressure or gas type.

Among the published studies about CrN coatings deposited by cathodic arc, Lee et al. [15] presented a mechanical property evaluation of a cathodic arc deposited CrN coating on Fe-Mn-Al-C alloy. For the CrN coating deposition, they used an $N_2$ gas partial pressure of 2.67 Pa, a substrate bias voltage of -150 V, and an arc current of 70 A. The deposition temperature was 275 °C. In this study, a complete characterization of the CrN layer was performed. The high hardness (around

22.7 GPa using 10 gf load), high elastic modulus, and excellent adhesion properties were validated. The wear resistance was evaluated using a pin on disk wear test, and using 10 N, the weight loss of the CrN coated sample (0.3 mg) had better results than the uncoated sample.

Later, Mo and Zhu [16,17] performed a similar study using the filtered cathodic vacuum arc technique. In their first study, they compared the mechanical and tribological properties of two CrN coatings, one deposited using multi-arc ion plating and the other using filtered cathodic vacuum arc technique. Using the fist technique, the deposition parameters were 0.1 Pa of $N_2$ gas partial pressure, a bias voltage of -100 V, and a deposition temperature of 450 °C. With the filtered cathodic vacuum arc, an $N_2$ gas partial pressure of 0.08-0.2 Pa was used, and a bias voltage varying from -50 V up to -200 V and deposition temperature of 300 °C were observed. Using the filtered deposition, the reduction of macroparticles and defects was significantly improved, as well as the anti-spalling and anti-abrasive properties of the CrN coating. An improved hardness was also obtained using the filtered cathodic vacuum arc (of 1923 HV, when compared to 1765 HV of multi-arc ion plating). In the tribological assessment, a reciprocating tribometer with 10 N of load was used. An improved wear resistance for the filtered technique was found.

The effect of the substrate bias voltage on the physical and mechanical properties of a CrN coating deposited by cathodic arc evaporation was evaluated by Warcholinski and Gilewicz [18]. The $N_2$ partial pressure the arc current was 1.8 Pa and 80 A, respectively. The deposition temperature was 300 °C and the bias voltage varied from -10 V up to -300 V. Tribological properties were not evaluated in this study. The resulted hardness changed with the applied bias voltage without any linear relation. The nominal hardness value was 18 GPa for -10 V, and the highest hardness value was of 26.5 GPa, obtained for -150 V.

Regarding the referred published research, it is possible to verify that even using the same technique/equipment, similar substrate materials, or analogous targets, the final properties of the deposited coating are strongly dependent on the chamber conditions. Moreover, the obtained coating structure is directly dependent on the presence or absence of defects, crystallographic orientation, and substrate morphology.

The present study will be used as an industrial case-study with a straight impact in one of the most relevant current industries: automotive. The added value is the use of large-scale equipment and the study of the effect of industrial deposition parameters in the top piston ring as

an end-product. Two different CrN coatings deposited in the piston ring's functional surface will be studied.

Using different deposition conditions, the two coating layers possessed distinct morphologies: a more sense structure (CrN-A) and a columnar structure (CrN-B). Each layer was physically and mechanically characterized, as well as this, its its chemical composition was analyzed. Both coatings were then tribologically evaluated according to the same conditions. Those coatings were tested using a locally developed test rig, adapted to test the piston rings under conditions close to the real engine operation. This study come to show the influence of the microstructure and morphology of deposited coating in the performance of the piston ring-cylinder liner tribological pair.

## 4.2 Materials and methods

### 4.2.1 Coating preparation

The studied coatings were deposited by an industrial cathodic arc plasma equipment (a HAUZER batch machine) on a gas nitrided stainless steel piston rings of heavy-duty diesel engines. The piston rings were assembled in the planetary system, as shown in Figure 4.1.

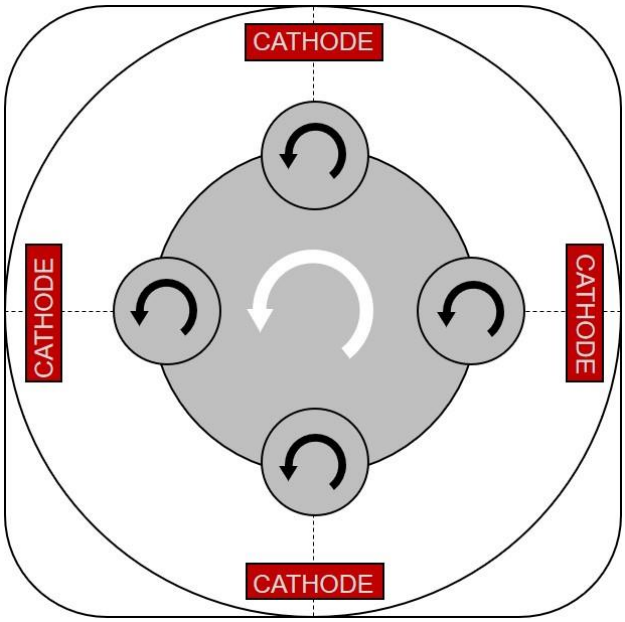


Figure 4.1 Schematic representation of the planetary system into the chamber.

To prepare the surface, steel piston rings were ground before deposition. The piston rings were sequentially immersed in different tanks with an alkaline cleaning solution to remove the surface contaminations. Two dryers and a nitrogen gas flow were used to remove the humidity from the cleaned piston rings.

Before deposition the specimens were cleaned by ion etching and heated in an Ar atmosphere. The preliminary ion etching was used to remove the impurities and oxides from the surface. This operation allowed the adhesion of the coating to be improved. The coatings were produced from pure chromium target and nitrogen atmosphere.

Since those coatings were deposited in an industrial environment, no filter facility was used during the deposition, regarding its negative effect on the reduction of the deposition rate. The use of macroparticles filters causes significant plasma losses, leading to lower deposition rates, hence the loss of economic benefits.

In Table 4.1 the varied deposition parameters to obtain both coatings are listed.

Table 4.1 Deposition parameters to obtain the coatings CrN-A and CrN-B.

| | CrN-A | CrN-B |
|---|---|---|
| $N_2$ flow (sccm) | 1200 ± 50 | 1400 ± 50 |
| $N_2$ pressure (Pa) | 5.1 ± 3 | 9.8 ± 2 |
| Bias Voltage (V) | -25 ± 5 | -10 ± 5 |

The substrate temperature was in the range of 490-510 °C for CrN-A and 470-490 °C for CrN-B. After deposition, additional polishing (using abrasive sandpaper) and lapping (using a diamond paste) stages ensured the control of the coating surface's roughness, to avoid the influence of the macroparticles possibly present on the surface.

### 4.2.2 Morphological, chemical and physical characterization

The morphological analysis was performed by scanning electron microscopy (SEM) ((JSM-6010 LV, JEOL). The thickness of the coatings was obtained through a cross-sectional study also by SEM. The in-depth chemical composition measurements were performed through the cross-sectional profile using SEM and the connected energy dispersive spectroscopy (EDS) (INCAx-Act, PentaFET Precision, Oxford Instruments) equipment.

To study the cross-sectional micrography, the piston rings were fractured (exposing the coating to tensile loads) according to the schematic representation of Figure 4.2.

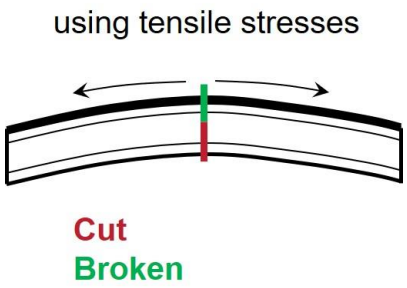


Figure 4.2 Schematic representation of the preparation method of the piston ring samples for the cross-sectional analysis.

Along with the surface morphology, the coating surface's roughness was evaluated using the Mitutoyo Surftest SJ-210 portable surface roughness tester. The measured parameters followed the norm EN ISO 4287.

The surface wettability to the lubricant oil is considered a relevant property of the top compression ring functional surface. The contact angle of the lubricant oil liquid in the CrN-A and CrN-B coatings surface were quantified to evaluate this physical surface feature. The measurements were performed using the sessile drop method using the optical goniometer OCA 15 plus (Datatphysiscs, Germany). Regarding the final application of the deposited coatings, the selected liquid was the commercial Castrol EDGE Professional 5W-30 oil. Before each measurement, the samples were ultrasonically cleaned using the cleaning unit Hielscher UP200St-G, with an isopropyl alcohol bath for 1 min.

In these experiments, four consecutive droplets of this lubrication oil with a volume of 2.5 µL and a dosing rate of 1.0 µL/s were dispensed from a micrometric syringe. The dispensed oil was brought into contact with the surface, and the contact angle was read.

The experiments were conducted at room temperature (19.1 °C), and a minimum of four contact angle readings were taken for each coating, always using dry surfaces.

### 4.2.3 Structural and mechanical characterization

The internal crystalline structure was evaluated using the X-Ray Diffraction (XRD) (Bruker D8 Discover) analysis. A classical $\theta$-$2\theta$ diffractometer with a Bragg-Brentano geometry using CuK$\alpha$ radiation. The step size was 0.04° $2\theta$, with 4 s/step and a $2\theta$ range of 15°-90°. The

preferential orientation and phase composition were analyzed from the diffractograms, while the lattice parameter and grain size were calculated from XRD patterns.

Hardness measurements were performed using a Micro Materials NanoTest indentation system with 1500 mN for CrN-A and 750 mN for CrN-B. The hardness value represents the average of at least five measurements. The indentation depths were up to 10% of the coating thickness to minimize the substrate influence. These measurements also allowed for Young's modulus to be determined.

### 4.2.4 Functional assessment of the deposited coatings

A portion of each CrN coated piston rings were tested against cast iron cylinder liners, as demonstrated in Figure 4.3. The sliding contact had 10 mm of stroke. The liner samples machined from the same commercial cylinder liner had the typical plateau honed surface texture that exists in the cylinder bore, as identified in the micrograph of the cylinder bore represented in Figure 4.3.

The applied normal load was in the range of 350-380 N to simulate the most severe operating conditions. This load amplitude intended to reproduce the continuous radial contact between the piston ring and the cylinder liner (due to the inherent compression ring spring force) and the effect of the combustion gases acting on the back of the ring and forcing it against the liner surface.

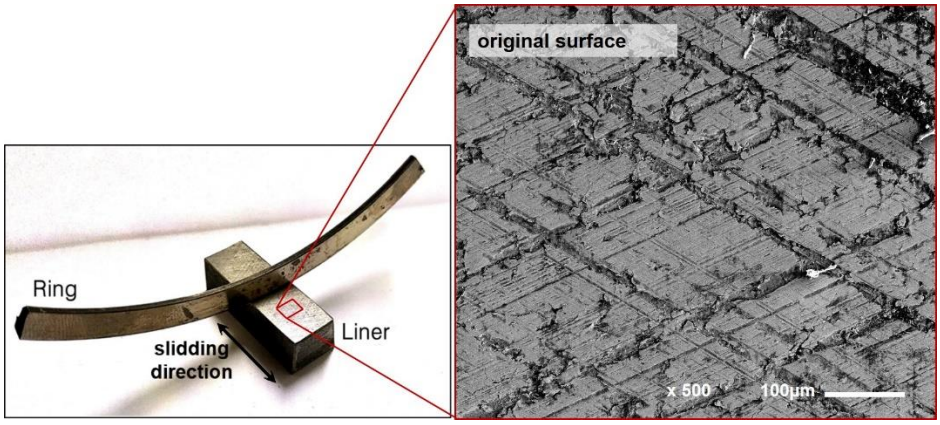


Figure 4.3 Representation of the physical contact between the piston ring and cylinder liner samples indicating the direction of the sliding movement, with an SEM micrograph of the original surface morphology of the cylinder bore.

Each test had a duration of 240 min, corresponding to the number of cycles of 216000. The sliding velocity was fixed on 0.3 m/s during the whole period.

A commercial Castrol EDGE Professional 5W-30 oil was used to lubricate the contact under fully fluid lubrication. Alumina particles in the range of 5 μm were dispersed into the lubricating oil bath. The alumina particles were added to the lubrication oil to accelerate the wear of the sliding surfaces. Otherwise, substantially longer tests would be demanded to observe worn surfaces. The use of a contaminant is widespread in industrial protocols. It is also used to simulate the presence of a third body between the ring and the liner surfaces. Each test used the same amount of alumina, and at the same time, it had to be dispersed in the same quantity of oil, to ensure the same conditions.

Moreover, during the engine functioning, the presence of debris resultant from the fuel contamination or the inefficient combustion of the fuel and air mixture is frequent. The presence of those particles fosters the surface wear due to the third body abrasion in the real conditions. These alumina particles were also representative of that debris.

The lubrication oil temperature was around 135±5 °C. To ensure that the specimens were thermally in a stable condition, the entire setup temperature was at testing temperature one hour before initiating the test, ensuring that the test components were in thermal equilibrium.

The coefficient of friction (COF) was measured before the wear test, for 15 min, using the same testing conditions, except the normal load, which was of 50 N.

The worn specimens and the respective counterpart were ultrasonically cleaned in isopropanol alcohol for 10 min at the end of each test. This cleaning operation is used to remove the lubrication oil and wear debris resulting from the sliding contact. The sample mass was measured before and after the tribological assessment using an analytical balance Kern ABS-N / ABJ-NM with 0.0001-g accuracy. The worn surface of the piston ring and the cylinder liner were analyzed by SEM and EDS. Both piston rings profiles were measured before and after being tested using a contact profilometer.

## 4.3 Results and Discussion

### 4.3.1 Coating's morphology and properties

The properties of the deposited coating are determined by process parameters, fixture configuration, and deposition time. Different parameters may be controlled during the coating deposition. In reactive arc deposition, gas flow control must be established and monitored. The

nitrogen partial pressure must also be accurately regulated. It should be low to minimize the collisions between the atoms detached from the target surface and the energetic ions of the plasma. But, if it decreases excessively, it may not allow the ionic bombardment, which is necessary for plasma maintenance. The application of a bias voltage to the substrate is recognized as an essential tool to control the energy of the ions. Consequently, it influences the adhesion and the microstructure of the coating.

The adhesion of the coating is greatly affected by the chemistry of the coating and substrate, as well as by stress. A critical factor is whether the coating material forms chemical bonds with the substrate material. In this context, a pure Cr interlayer is used to improve the adhesion strength of the deposited CrN coating to the substrate.

In Figure 4.4 the SEM micrographs of the cross-sectional view of both coatings are presented. It is well established that the coating microstructure strongly influences the properties of physical vapor deposition (PVD) coatings. Analyzing the fracture morphology of both top layers, CrN-A coating has a denser structure than the CrN-B.

This distinction can be associated with the different deposition parameters, and consequently, their effect on the energy of ions arriving on the surface. Among those parameters, the substrate bias is related to the energy of the ions. Increasing negative substrate bias voltage increases the mobility of the ions to move the atoms. That high mobility stimulates new nucleation sites into the inter-grain voids creating denser structures (and grain refinement). In the CrN-B coating, a columnar growth microstructure is perceptible. The presence of voids is frequent in those columnar microstructures, as is observed in Figure 4.5.

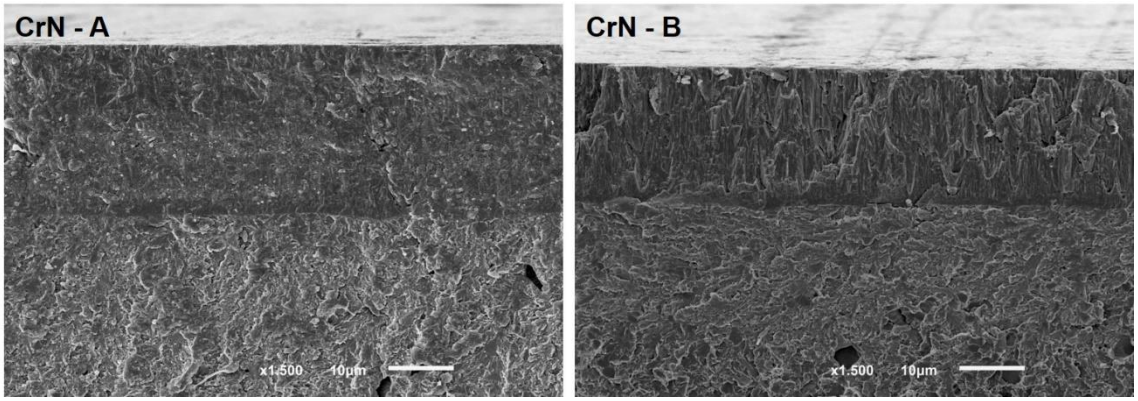


Figure 4.4 SEM micrographs of the cross-sectional fracture of the a) CrN-A and b) CrN-B coatings.

The nitrogen pressure also influences the morphology of the coating. With higher gas pressures, the ions and atoms collisions rate also increases. Consequently, the energy of the ions that arrive at the substrate is lower, leading to a columnar growth microstructure.

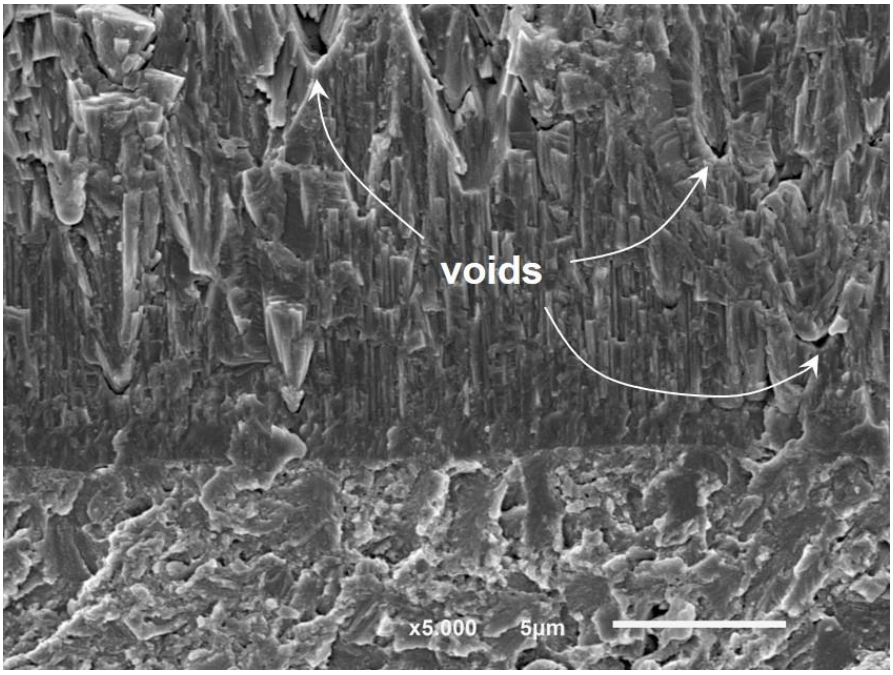


Figure 4.5 SEM micrograph of the CrN-B coating fracture with an indication of the possible presence of voids (common in columnar and less dense microstructures).

The thickness of both layers is similar, as the thickness of CrN-A is slightly higher (with 25±1 µm) than the CrN-B thickness (about 20±1 µm). The in-depth chemical composition of the CrN-A and CrN-B coatings is exposed in Figure 4.6. The chemical analysis was performed using SEM-EDS through the cross-sectional study of the fractured samples.

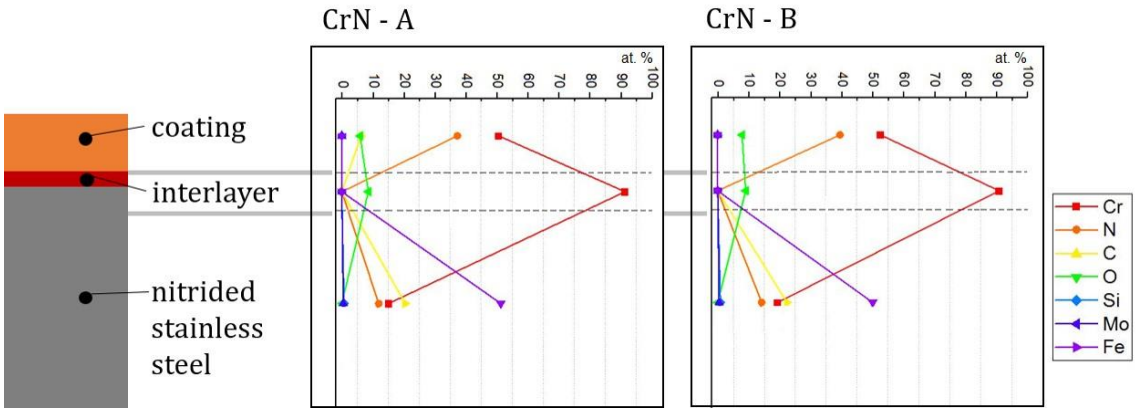


Figure 4.6 Graphical representation of the in-depth chemical composition of CrN-A and CrN-B coatings.

With regard to the in-depth graphical representation, the chemical composition of each coating layer (CrN), the interlayer (Cr), and the substrate (nitrided stainless steel piston ring) were quantified. The different coating layers showed a similar chemical composition, with no significant impact of the deposition parameters on those properties, as expected.

The surface morphology of the bare substrate and the CrN-A and CrN-B coatings is shown in Figure 4.7. Before deposition, the roughness value (Ra) of the substrate was measured as ~0.088 μm.

After coating's depositions, large roughness of the surface could be related to a columnar structure from low negative substrate bias voltages. Conversely, when a high substrate bias voltage is used, it also induces energetic particle bombardment during the material deposition, which influences the surface roughness. In this study, a lapping stage was performed after PVD deposition to control the surface roughness of the piston rings functional surface. In the SEM images of both coatings some polishing marks were visible. A high surface roughness could be achieved in both deposition conditions, but this operation hid the possible effects of the different deposition parameters in the surface morphology. As this process is integrated into the manufacturing line of compression piston rings, it was used in this research. Therefore, the posterior tribological assessment of the as-deposited surfaces would not represent the real conditions.

The presence of some macroparticle droplets or some surface irregularities is inherent to the cathodic arc deposition technique.

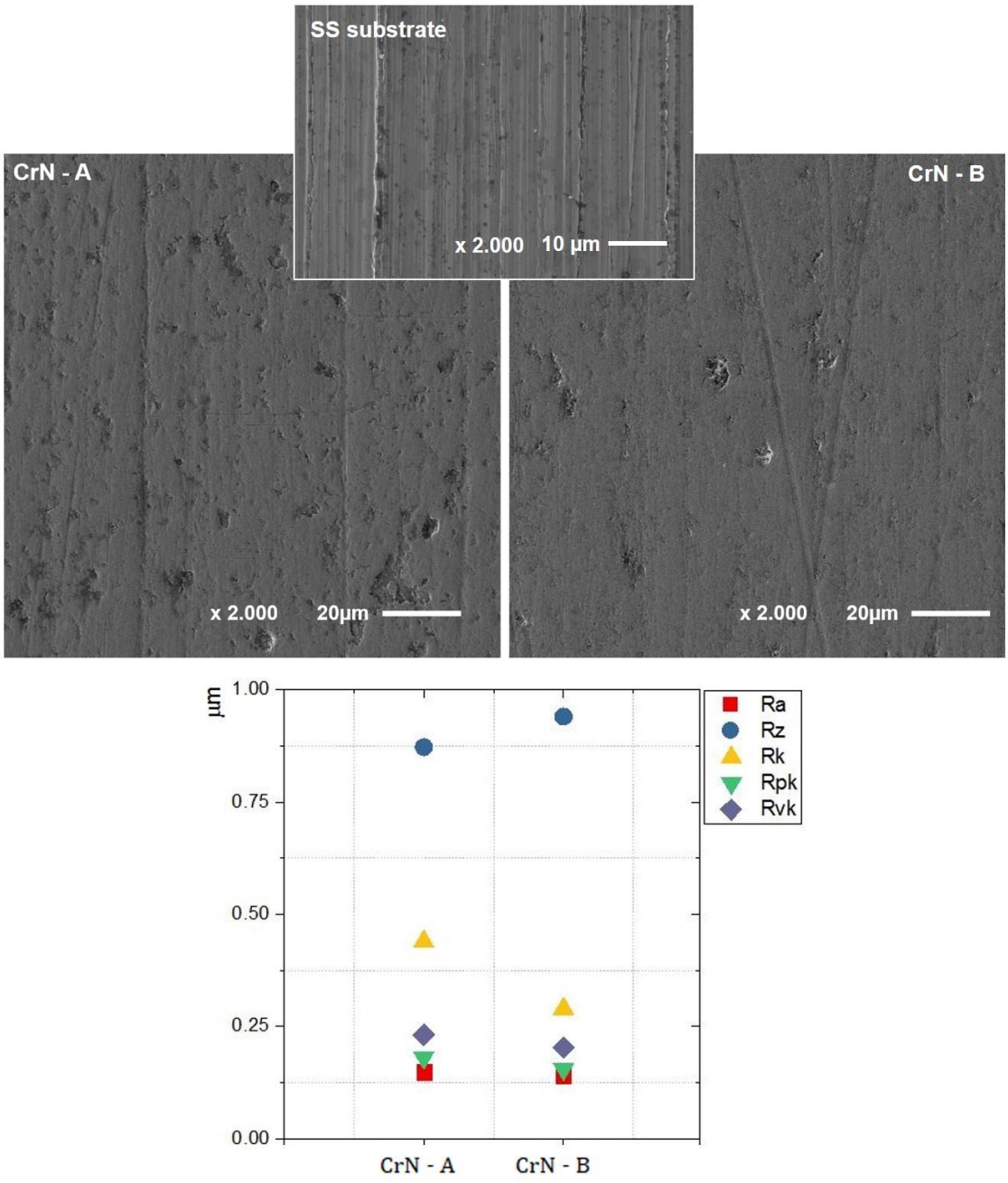


Figure 4.7 Morphology of the substrate, CrN-A, and CrN-B coatings surface and graphical representation of the final measured roughness parameters.

To analyze the surface roughness of the coatings, a more comprehensive analysis was performed. Regarding the surface roughness of both coating surfaces, two amplitude parameters were considered, Ra and Rz. The former, which is similar for both coatings, represents the arithmetic average of the profile heights over the evaluation length. The parameter that quantifies the maximum roughness (Rz) is slightly superior for CrN-B (the one with columnar microstructure). Three functional parameters were also considered: Rk, Rpk, and Rvk. The measured values for those parameters revealed the inverse, higher costs were found for the CrN-A coating surface.

From the operational point of view, Rpk represents those peaks that might be eliminated during function, Rvk those valleys that will retain lubricant or worn-out materials. Finally, Rk describes the central region of the profile, which is neither peaks nor valleys. The superior core roughness depth of the denser coating can be related to its improved mechanical properties (and consequent higher resistance to the surface finishing process).

In this study, the surface wettability was assessed by Oil Contact Angle (OCA). The contact angle is defined as the angle at which a liquid/vapor interface meets a solid surface. Considering the geometry of the compression piston ring, the radius of curvature of the surface under analysis (the top surface of the ring illustrated in Figure 4.2), the contact angles were analyzed at 0s. In Figure 4.8 the mean values of the contact angle measurements for each coating are presented. An image of the shape of a droplet in the moment of contact with the surface is shown.

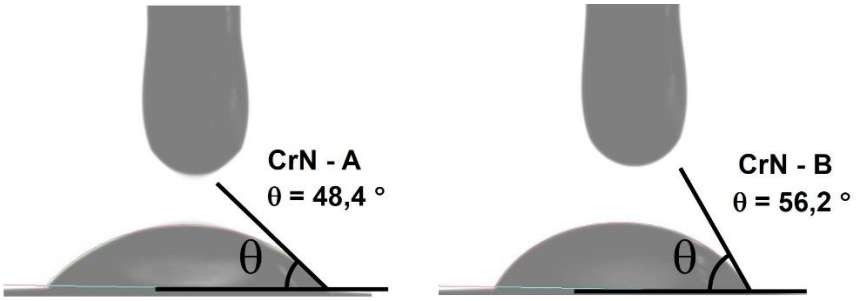


Figure 4.8 Contact angle measures using the 5W30 lubrication oil.

When observing the obtained results, it is visible that both physically-vapor deposited coatings have hydrophilic behavior. They exhibit good surface wettability properties. Although, comparing both results, the denser coating (CrN-A) revealed lower contact angle values, therefore, showing an improved wettability to the lubricating oil. According to Sun et al. [19], lower contact angles are related to higher surface free energies, and the latter can be linked to an increased surface roughness (which is verified for CrN-A, excluding those discrete maximum roughness values, Rk).

### 4.3.2 Phase analysis and mechanical results

Coatings made by energetic deposition tend to grow with a preferred orientation, thereby minimizing the system's energy. The deposition conditions have a direct impact on the ion's mobility and then influence the internal structure of the deposited coating. In this study, the phase

composition of the coatings was characterized by observing the diffraction peaks in the range of 15- 90° using XRD. The XRD patterns of the CrN-A and CrN-B coatings are shown in Figure 4.9. The identification and quantification of phases were carried out using X' Pert High Score software and Joint Committee on Powder Diffraction and Standards (JCPDS) databases. The XRD diffractograms were fitted using a Pseudo-Voigt function to calculate both the full width at half maximum (FWHM) and the peak position (2θ) using Origin software. The obtained values were used to calculate the grain size of the coatings using Scherrer's equation [20].

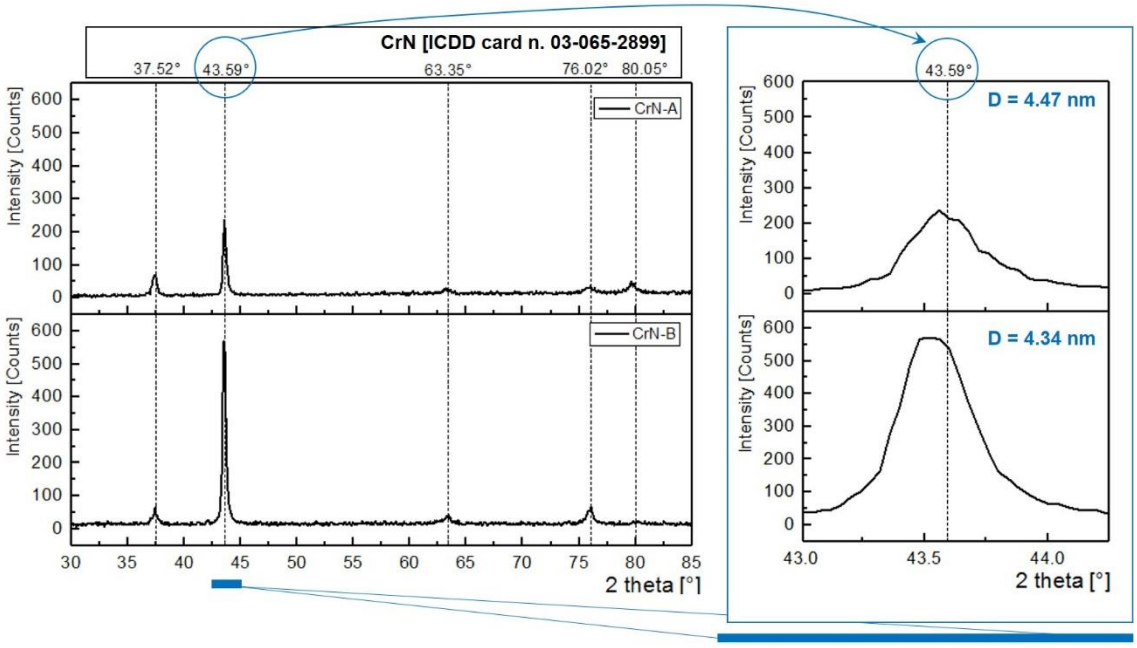


Figure 4.9 XRD patterns of the CrN-A and CrN-B coatings using different deposition conditions.

From the analysis of the diffractograms one can see that it is not necessary for the occurrence of a significant variation of the deposition conditions to notice slight differences in the crystalline arrangement of the deposited coatings, even though both coatings have a similar chemical composition and an identical surface topography.

For both layers, the face-centered cubic CrN phase (ICDD card n.° 03-065-2899) is dominant. In both depositions a reactive regime occurs forming a stoichiometric system (CrN). If one compares the experimental diffraction with those of the database, the correspondence between them may be established. With regard to the presence of different crystallographic planes of this phase, both have (200) preferred orientation. A similar peak broadening occurs for CrN-A and CrN-B diffraction peaks around 43.5°, which resulted in a value of average particle size (D), of 4.47 nm and 4.34, respectively.

All XRD diffraction peaks are shifted to lower angles, which can be explained by a combination of the thermal expansion effect and the presence of compressive residual stresses. In PVD deposited coatings, residual stresses are generally compressive due to coating bombardment. According to the analysis performed using the X' Pert High Score software, the body-centered cubic Cr(N) phase (ICDD card n. 01-088-2323) is potentially present in both coatings.

The presence of tensile stresses in the coating would cause the formation of cracks in the coating with lateral propagation, and the cracked coating could debond from the substrate. The presence of compressive residual stresses suggests a crack-free coating, which provides both an improved wear resistance.

With regard to the mechanical property assessment, hardness represents one of the most critical material properties and can be related to the material tribological features, like its resistance to wear. In Table 4.2 the micro-indentation results of both coatings using the same testing load are presented.

Table 4.2 Micro-hardness measurements of the CrN-A and CrN-B coatings

| | Max. Load (mN) | Max. Depth (μm) | Hardness (GPa) | E (GPa) |
|---|---|---|---|---|
| CrN-A | 1500 | 2.34 ± 0.11 | 16.3 ± 1.8 | 267 ± 12 |
| CrN-B | 750 | 2.01 ± 0.10 | 9.4 ± 1.5 | 247 ± 14 |

It would be expected that with the nitrogen flow increase, the hardness of the coatings would also increase [6]. However, the maximum hardness was obtained for the layer produced with lower N2 flow. In this context, the small grain size and the possible presence of the $Cr_2N$ phase may be enhanced factors of the coating hardness. The decrease of the bias voltage and the increase of the nitrogen pressure are also associated with a less dense and more porous coating layer, therefore lower hardness.

### 4.3.3 Tribological performance

The tribological properties of CrN-A and CrN-B coatings were comparatively investigated.

The main advantage of using original surface topographies from the piston ring and cylinder liner is the possibility of reproducing the behavior of original engine parts. Besides the use of original engine parts, similar realist environment conditions should also be provided to establish a close relation between engine testing and laboratory environment testing.

Figure 4.10 presents the weight loss of the tested piston ring and the respective counterpart, the cylinder liner sample. The coefficient of friction for each sliding pair is also displayed.

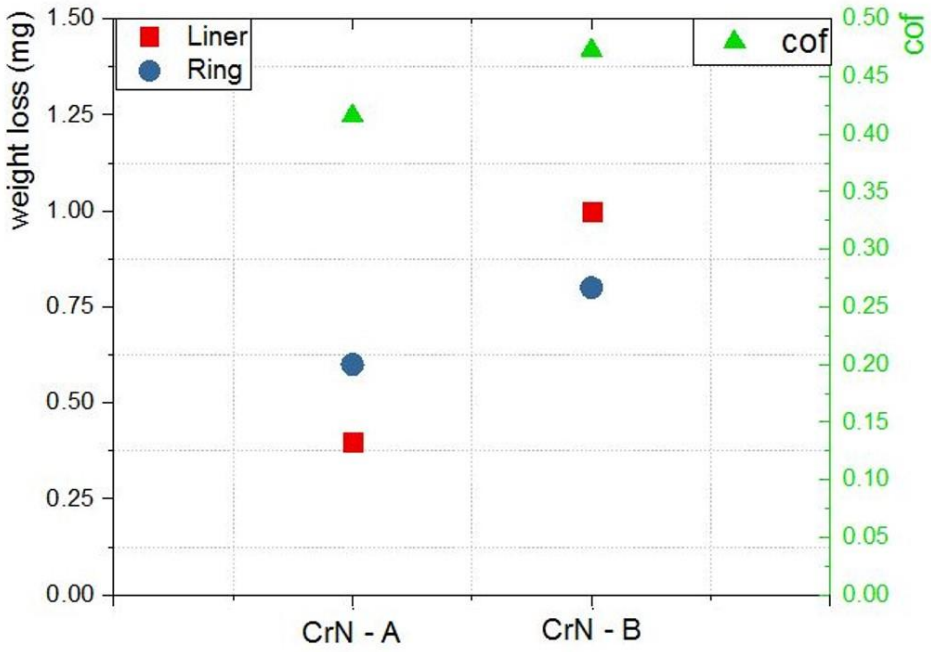


Figure 4.10 Weight loss of piston ring and cylinder liner counterpart and coefficient of friction measurements for each tribological pair.

In general, the weight loss is residual, considering the performance of CrN coating tested under the conditions established in the previously defined protocol. In both pairs, either the piston ring or the respective cylinder liner specimen exhibited weight loss. The harder layer is the one with better wear resistance when comparing the weight lost by CrN-A and CrN-B. In contrast, the hardness of the coatings is not related to the effect on the counterpart result. Further conclusions can be drawn through the COF values and by analysis of the surface morphology before and after the tribological tests.

Regarding the coefficient of friction, the presented results are in correspondence with the values registered in some published studies [8,16,21], although the experimental condition is not the same. The tribological pair, including CrN-A coating, resulted in a lower coefficient of friction. Based on the results of the surface roughness measurements presented in the graphical representation of Figure 4.7, the Rvk parameter was slightly higher for CrN- A coating. As previously referred, this functional parameter represents the valleys that will retain lubricant or worn-out materials, which could have influenced the lower coefficient of friction of this coating. Besides Rvk

measurement, CrN-B coating is also the one that presents a higher Rz value (which quantifies the maximum roughness), due to its columnar structure. The higher COF result for CrN-B (around 0.47) is related to the more significant impact on the respective counterpart, and the consequent higher weight loss.

In Figure 4.11 the wear track border of the CrN-A and CrN-B and the respective cylinder liner worn surfaces are presented, together with the difference in the piston rings' profile caused by the wear test.

According to the SEM micrographs of the piston ring wear tracks, it is possible to verify that a higher depth was achieved in the CrN-B coating because the surface cavities were empty. Wear debris possibly held into the cavities were removed because of the surface wear. In contrast, the accumulation of debris is visible in the CrN-A surface. These findings are consistent with the resultant weight loss of both coatings.

When comparing the respective counterparts, on both surfaces, the presence of the original cross-hatched texture created in the inner cylinder surface to prevent seizure under hot engine running conditions is perceptible. In the worn surface of the CrN-A counterpart, the detached material, and the wear debris resultant of the sliding contact are accommodated into the cross-hatched textures. The higher ductility of the grey cast iron cylinder liner in comparison with the deposited chromium nitride coating favored the detachment of the counterpart material. This phenomenon was validated through the analysis of the chemical composition of the material adhered to the liner texture. The presence of an attached material is observed in Figure 4.12.

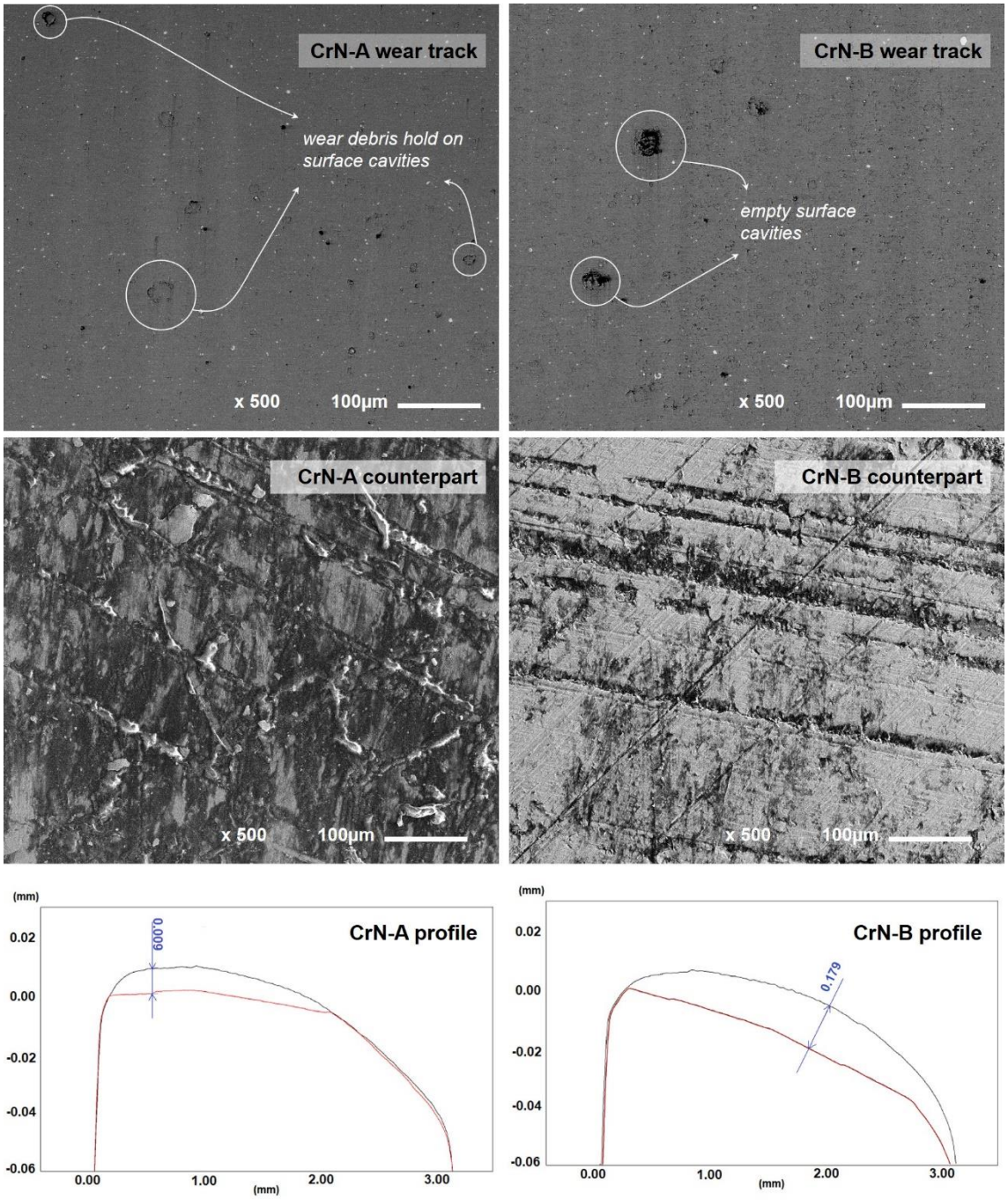


Figure 4.11 SEM micrographs of the wear track in the piston ring and cylinder liner surfaces and schematic representation of the dimensional differences in the piston ring profile before and after wear tests.

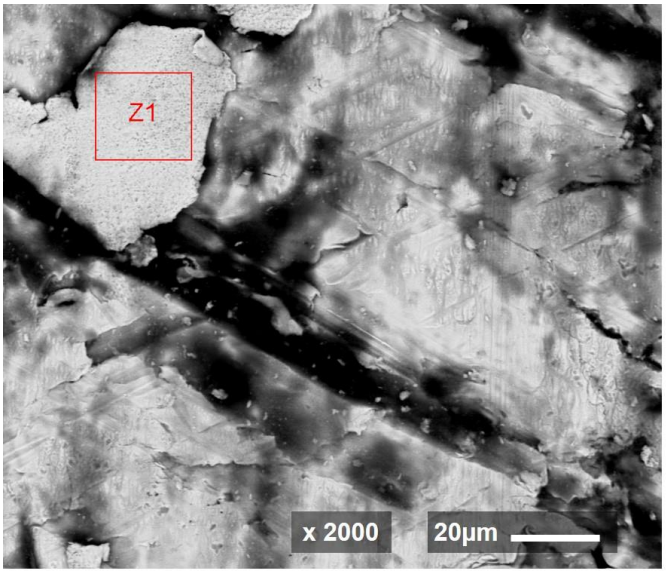


Z1

| Elem | At % |
|---|---|
| C K | 24.28 |
| O K | 9.97 |
| Al K | 1.91 |
| Si K | 3.23 |
| Mn K | 0.55 |
| Fe K | 60.05 |
| **Total** | **100.00** |

Figure 4.12 SEM micrograph of the CrN-A coating using a higher magnification and EDS analysis of the adhered material resultant from the ring-liner sliding contact.

According to the chemical composition analysis, the adhered material was removed from the cylinder liner surface. The presence of grey cast iron flakes in the ring-liner contact can also influence the friction and wear behavior by the formation of a graphite surface layer. The lower coefficient of friction achieved by the CrN-A coating and the respective counterpart could be associated with the graphitization of the grey cast iron flake like debris.

Observing the CrN-B counterpart surface, the liner material hauling along the sliding direction is perceptible. However, the presence of wear debris was not verified for this contact. The analysis of the surface morphology of the worn surfaces of each cylinder liner is also coherent with the results of Figure 4.9. The low weight loss of the cylinder liner specimen tested against the CrN-A coating (when compared with the remaining parts) could be influenced by the presence of the detached wear debris into the cross-hatched textures.

In general, the absence of deep wear scars and the presence of relatively smooth coating surface morphology indicated the possibility that an adhesion wear mechanism had occured. The relative sliding between the asperities of the contacting surfaces may cause the bonding between them and posterior rupture, transferring the detached material to the contact. As expected, the separation occurred in the material with lower shear strength, the grey cast iron. Evaluating the piston ring coatings surface, no delamination or spalling of the CrN-A and CrN-B deposited coatings were observed.

## 4.4 Concluding Remarks

The main results of this study can be summarized according to the following statements:

1. The morphology of the different coating layers analyzed through the SEM micrographs of the cross-section is visibly different. The coating deposited using lower nitrogen flow and higher substrate bias voltage, CrN-A, is denser than the CrN-B. The latter presented a columnar growth structure.

2. In the top view analysis, no substantial differences were found because of the surface finishing process after coating deposition. When comparing both coatings, CrN-A revealed slightly superior surface roughness values, except for the discrete maximum roughness values controlled by the Rk parameter. This characteristic can be associated with the lower contact angle of the CrN-A surface, and therefore, its improved wettability.

3. XRD data also showed slight differences, but both presented a dominant face-centered cubic CrN phase, with similar peak positioning and peak broadening. The peak shift to lower angles revealed the presence of compressive residual stresses.

4. As expected, in the denser coating layer, a higher micro-hardness, close of 20 GPa, was measured. The coating possessing a columnar structure did not achieve 10 GPa.

5. The tribological experiments revealed that the best wear resistance is achieved by the coating with superior hardness. In the CrN-A coating a lower weight loss of the ring was verified, and at the same time, the lower weight loss of the respective liner was also attested to (the former, probably due to the accumulation of wear debris into the cross-hatched textures). Yet the coefficient of friction of this pair was revealed to be lower due to the presence of grey cast iron flake like debris. In general, both showed excellent wear resistance under severe tribological conditions such as high temperature, applied pressure, and speed.

## Acknowledgements

This work was supported by FCT (Fundação para a Ciência e Tecnologia) and MAHLE, Componentes de Motores, S.A. through the grant SFRH/BDE/110654/2015, by FCT (Fundação para a Ciência e Tecnologia) with the reference project UID/EEA/04436/2019 and by the project POCI-01-0145-FEDER-006941 and the project with reference NORTE-01- 0145-FEDER-000018-HAMaBICo. The authors would like to acknowledge the financial support from the projects: ATRITO-0 [co-financed via FEDER (PT2020) POCI-01-0145-FEDER-030446 and FCT (PIDDAC)].

## References

[1] K.O. Legg, M. Graham, P. Chang, F. Rastagar, A. Gonzales, B. Sartwell, The replacement of electroplating, Surf. Coatings Technol. 81 (1996) 99–105. https://doi.org/10.1016/0257-8972(95)02653-3.
[2] C. Öner, H. Hazar, M. Nursoy, Surface properties of CrN coated engine cylinders, Mater. Des. 30 (2009) 914–920. https://doi.org/10.1016/j.matdes.2008.05.018.
[3] S. Wan, J. Pu, D. Li, G. Zhang, B. Zhang, A.K. Tieu, Tribological performance of CrN and CrN/GLC coated components for automotive engine applications, J. Alloys Compd. 695 (2017) 433–442. https://doi.org/10.1016/j.jallcom.2016.11.118.
[4] C. Friedrich, G. Berg, E. Broszeit, F. Rick, J. Holland, PVD CrxN coatings for tribological application on piston rings, Surf. Coatings Technol. 97 (1997) 661–668. https://doi.org/10.1016/S0257-8972(97)00335-6.
[5] E. Broszeit, C. Friedrich, G. Berg, Deposition , properties and applications of PVD Cr N coatings, Surf. Coatings Technol. 115 (1999) 9–16. https://doi.org/10.1016/S0257-8972(99)00021-3.
[6] A. Barata, L. Cunha, C. Moura, Characterisation of chromium nitride films produced by PVD techniques, Thin Solid Films. 398–399 (2001) 501–506.
[7] J. Lin, N. Zhang, W.D. Sproul, J.J. Moore, A comparison of the oxidation behavior of CrN films deposited using continuous dc, pulsed dc and modulated pulsed power magnetron sputtering, Surf. Coatings Technol. 206 (2012) 3283–3290. https://doi.org/10.1016/j.surfcoat.2012.01.033.
[8] K. Bouzid, N.E. Beliardouh, C. Nouveau, Wear and Corrosion Resistance of CrN-based Coatings Deposited by R . F Magnetron Sputtering, Tribol. Ind. 37 (2015) 60–65.
[9] F. Ferreira, J.C. Oliveira, A. Cavaleiro, CrN thin films deposited by HiPIMS in DOMS mode, Surf. Coatings Technol. 291 (2016) 365–375. https://doi.org/10.1016/j.surfcoat.2016.02.064.
[10] A. Anders, A review comparing cathodic arcs and high power impulse magnetron sputtering (HiPIMS), Surf. Coatings Technol. 257 (2014) 308–325. https://doi.org/10.1016/j.surfcoat.2014.08.043.
[11] D. Mattox, Handbook of Physical Vapor Deposition (PVD), 1998.
[12] B. Juettner, Characterization of the Cathode Spot., (1986) 90–98.
[13] A. Anders, Cathodic Arcs. From Fractal Spots to Energetic Condensation, Springer Science, 2008. https://doi.org/10.1007/978-0-387-79108-1.
[14] A. Anders, Unfiltered and filtered cathodic arc deposition, in: Handb. Depos. Technol. Film. Coatings, 2010: pp. 466–531.
[15] J.W. Lee, J.G. Duh, J.H. Wang, Mechanical property evaluation of cathodic arc plasma-deposited CrN thin films on Fe-Mn-Al-C alloys, Surf. Coatings Technol. 168 (2003) 223–230. https://doi.org/10.1016/S0257-8972(03)00222-6.
[16] J.L. Mo, M.H. Zhu, Tribological characterization of chromium nitride coating deposited by filtered cathodic vacuum arc, Appl. Surf. Sci. 255 (2009) 7627–7634. https://doi.org/10.1016/j.apsusc.2009.04.040.

[17] J.L. Mo, M.H. Zhu, A. Leyland, A. Matthews, Impact wear and abrasion resistance of CrN, AlCrN and AlTiN PVD coatings, Surf. Coatings Technol. 215 (2013) 170–177. https://doi.org/10.1016/j.surfcoat.2012.08.077.
[18] B. Warcholinski, A. Gilewicz, Effect of substrate bias voltage on the properties of CrCN and CrN coatings deposited by cathodic arc evaporation, Vacuum. 90 (2013) 145–150. https://doi.org/10.1016/j.vacuum.2012.04.039.
[19] C.C. Sun, S.C. Lee, W.C. Hwang, J.S. Hwang, I.T. Tang, Y.S. Fu, Surface free energy of alloy nitride coatings deposited using closed field unbalanced magnetron sputter ion plating, Mater. Trans. 47 (2006) 2533–2539. https://doi.org/10.2320/matertrans.47.2533.
[20] P. Scherrer, Bestimmung der Grobe und der inneren Struktur von Kolloidteilchen mittels Rontgenstrahlen, Nachrichten Gesellschaft Wiss. Gottingen. 2 (1918) 98–100.
[21] E. Bemporad, C. Pecchio, S. De Rossi, F. Carassiti, Characterisation and wear properties of industrially produced nanoscaled CrN/NbN multilayer coating, Surf. Coatings Technol. 188–189 (2004) 319–330. https://doi.org/10.1016/j.surfcoat.2004.08.069.

# CHAPTER 5.

## Influence of a DLC coating topography in the piston ring/cylinder liner tribological performance

Published in Journal of Manufacturing Processes, 2021, 66: 483-493
R. Ferreira [a,c,d,*], R. Almeida [a], Ó. Carvalho [a], L. Sobral [c], S. Carvalho [d], F. Silva [a]

[a] Centre for Micro-Electro Mechanical Systems (MEMS) University of Minho, Campus de Azurém, 4800-058 Guimarães, Portugal
[b] Mechanical Engineering Department, Universidade do Minho, 4800-058 Guimarães, Portugal
[c] MAHLE - Componentes de Motores S.A., Núcleo Industrial Murtede, 3060-372 Cantanhede, Portugal
[d] GRF-CFUM, Department of Physics, University of Minho, Campus de Azurém, 4800-058 Guimarães, Portugal

## Abstract

In the piston ring-cylinder system, the surface topography is crucial to their tribological performance, emphasizing the relevance of the surface finishing processes. The present work studied the influence of different finishing processes in the surface roughness parameters of the coated compression piston rings. Three distinct surfaces' finishing processes were used in the first approach: Option A, B, and C. Options D comprised the variation of different processing parameters. The piston rings with different surface topographies were tribologically evaluated using a tribometer developed explicitly for this industrial evaluation. Regarding the tribological performance, it was concluded that the use of the surface finishing processes fostered a decrease in the coefficient of friction. The surface finishing had also impacted the wear of the piston ring and in the counterbody. An increase in the piston rings' surface roughness led to a rise in the surface's weight loss.

Keywords: *piston ring; surface topography; tribological performance.*

## 5.1. Introduction

The automotive industry has made efforts to overcome its most known limitations, pollutant emissions. Pollutant emission legislation and the rise of the fuel price, emphasize the concern about the piston ring's tribological research and liner contact [1]. Engine manufacturers have a priority concern: fuel consumption optimization. Fuel economy is one of the most relevant modern engine goals, which must be achieved without sacrifice engine durability. Turbocharging and direct injection fueling systems are recent trends in the automotive industry. With those trends, cylinder pressures have increased, and as a consequence, the operating environment requires an upgraded performance of the engine parts.

Those widespread concerns appear because of the low performance of different systems in the engine. Piston ring-cylinder liner contact is one of the main contributors to mechanical friction losses in internal combustion engines [2]. Regarding its role, the top ring is responsible for the sealing of the combustion chamber, avoiding the air and fuel mixture to go down (and preventing blow-by), and the lubrication oil to go up and infect the combustion mixture, as illustrated in Figure 5.1 [3].

Acting as one of the main contributors to the internal combustion engine's mechanical friction losses, piston ring-cylinder liner contact is one of the most studied tribological pairs. A decrease in the piston ring friction would reduce the mechanical losses of the internal combustion engine [4]. To minimize friction of the piston ring cylinder liner contact, it demands a better understanding of how the different parameters are related.

Also, the wear of functional parts represents one of the main concerns of the automotive industry [5]. Worn surfaces have as main consequence the modification of the surface dimensions and geometry. This consequence, directly impacts the top piston ring role since its main function is the combustion chamber sealing [6]. Once changed, its surface will not fit properly against the cylinder liner, and for that reason, the sealing of the combustion chamber will not be effective. In this way, lower pressures will be achieved into the combustion chamber, consequently reducing the engine power.

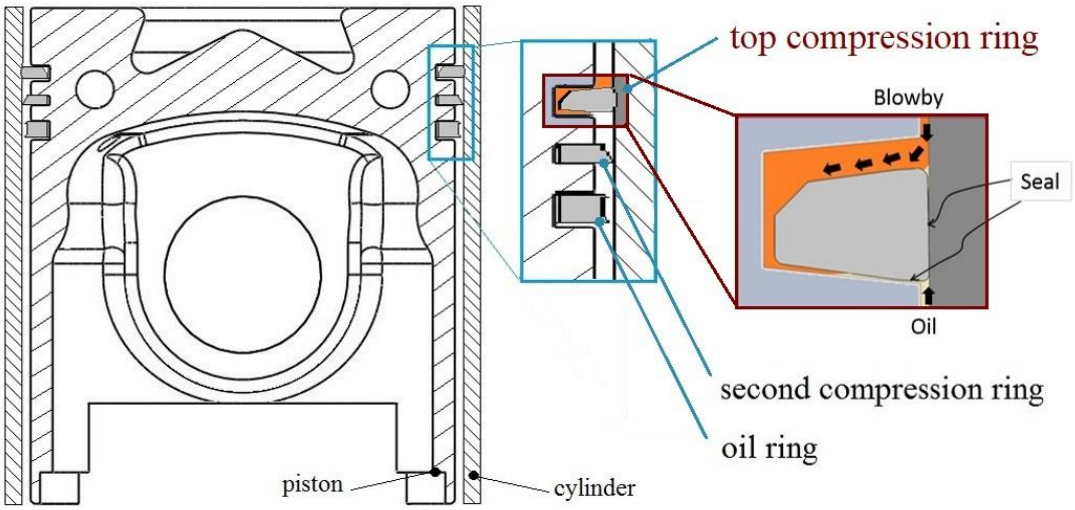


Figure 5.1 Simplified representation of the compression piston ring role.

Nowadays, several coating materials have been studied to improve the wear resistance of the top compression ring. Ferreira et. al [7] presented the state-of-the-art of hard coatings applied to the compression piston ring surfaces. Conventional solutions used chromium-based coatings, but the achieved results compromise their use in the most recent engines, where high powers and enhanced performances are expected [8].

The Diamond-Like Carbon (DLC) coating was proposed for the piston ring's surface with these goals. DLC coatings represent one of the most advantageous carbon-based material solutions. Its amorphous structure has graphite (providing superlubricity) and diamond (offering a high hardness), necessary for low surface wear [9]. Compared with the conventional CrN coatings, its superior tribological resistance will increase the service life and contribute to improving the piston ring's performance. Moreover, DLC coatings can simultaneously offer high hardness and superlubricity conditions, competing with conventional solutions [10]. These characteristics result

of the diamond-like carbon amorphous structure composed of graphite (the softest) and diamond (the hardest) properties, corresponding respectively to the $sp^2$ and $sp^3$-bonds, resulting in the $sp^2/sp^3$ ratio. The increase or decrease of the $sp^2/sp^3$ rate is related to a more lubricious behavior or a harder and more resistant surface, respectively [11].

The graphitization rules the tribological performance of DLC coatings. This mechanism consists of the transference of particles of the counterbody surface, forming a transfer layer. The formation of a transfer layer rich in carbon present on the sliding contact surfaces contributes to an extended friction reduction [12]. This layer will protect the softer counterbody surface against the harder coating. This wear mechanism in the real engine piston ring also depends on their surface characteristics.

The dimensional and topographical characteristics of the deposited coating layer is controlled by the substrate roughness and the deposition process. In such massive industrial sectors, large-scale fabrication imposes several constraints. Most of them have economical and quality (including reproducibility and reliability) arguments. In a large-scale fabrication, either the coating deposition or the surface finishing processes need to be implemented using profitable and cost-effective technologies.

Among the different physical vapor deposition (PVD) techniques, cathodic arc evaporation is the one most applied [13]. Its use is associated with its very high deposition rates (compared with the standards of physical vapor deposition), necessary to optimize the manufacturing outputs. Using this arc-evaporation technique, several physical, mechanical, and chemical properties can be controlled during the deposition process. In addition to coating thickness, most of the coating properties are limited by the deposition process. For instance, the coating morphology is affected by the number of particles deposited on the coating surface controlled by some process parameters, namely the substrate bias voltage and the nitrogen pressure [14]. The influence of manufacturing and processing conditions in the surface topography is explored in a few works, such as in those performed by Wei [15], Morris et al. [6], Gu et al. [16] and Meng et al [17].

The surface topography is a crucial parameter in the ring/liner contact [18], impacting the mechanical and tribological performance [19]. Michail and Barber [20] proposed a new model to evaluate the effect of roughness on the hydrodynamic lubrication of a single-piston ring. In this new theoretical approach, not only Gaussian surfaces were considered, but any distribution of asperities heights was took into account. Michail and Barber [21] also studied the cylinder wall surface and

the oil film's thickness interaction. This later study concluded the oil film thickness is thicker for a transversely-oriented crosshatch in the cylinder liner surface.

The presence of the surface asperities will affect tribological performance mainly under some lubrication conditions [22]: a) in the hydrodynamic lubrication regime, the properties of the lubricant are the dominant features in the ring-liner contact; b) in a mixed/boundary lubrication regime, which occurs with lower speeds, the surface characteristics are determinant [23]. When the oil film in the contact is insufficient, both surfaces' asperities have a continuous interaction because of the high degree of mechanical interlocking occurring between rough surfaces [24].

When DLC coatings are deposited by unfiltered arc-PVD, its surface roughness is relatively high, typically due to microparticles and droplet deposition ejected from the carbon targets [25]. In these cases, under severe operating conditions (high pressures, high temperatures, and high variation loads), the increased roughness of the DLC coated part induce the local fracture of the coating due to the stress concentration. However, its surface finishing represents a challenge for manufacturers due to its superior hardness.

However, polished surfaces (ring and liner) to improve tribological performance are not a consensual approach in this context. Galligan et al., in their both studies [26] and [27], evaluated the influence of surface finish on scuffing resistance of the piston ring-cylinder liner contact. The resultant surface roughness were assessed at the end of the scuffing tests. The piston ring's surface finish had a minor change, but the surface finish of the liner became smoother. A decrease in the liner roughness was related to the increase of friction and consequent polishing effect on the liner surface.

Most of the referred studies focused on the influence of surface roughness on the tribological performance, reported several numerical simulation approaches using the regular analytical models [6,17,23]. The Greenwood - Tripp model is one of the most used numerical models, applied by He et al. [28] and Checo et al. [29]. In this work, practical experiments focused on this topic will be followed using original engine parts, about which there is a lack of studies.

Different piston rings coated by the cathodic arc deposition technique with a DLC layer were submitted to different surface finishing conditions. These piston rings were then tested against a cast iron cylinder liner surface using a home-made oscillating tribometer. Several surface roughness parameters were measured and correlated with tribological performance and mainly

the final weight loss. The present work's main goal was to understand the influence of the coating surface topography on the final tribological performance of the piston ring-cylinder liner pair.

## 5.2 Experimental procedures

### 5.2.1 Surface coating deposition

Before coating deposition, several surface grinding stages were applied to the stainless-steel piston rings profile to remove material and provide the final cross-sectional geometry.

The piston ring samples were coated using an industrial cathodic arc plasma equipment. The piston rings were assembled in the planetary system, as shown in Figure 5.2. An initial ion etching to improve coating adhesion enabled the removal of a thin surface oxide layer and triggered the surface temperature increase.

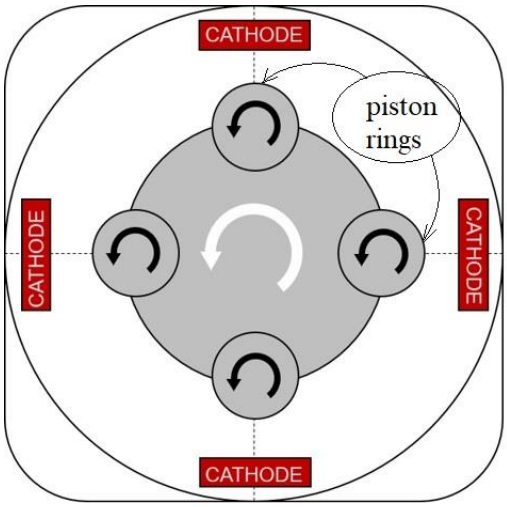


Figure 5.2 Schematic representation of the planetary system into the chamber.

The coatings were produced from a pure carbon target and argon atmosphere. Before the DLC deposition, a pure Cr interlayer was used to improve the coating adhesion to the substrate. The pulsed cathodic graphite arc was used to prepare the DLC films. The carbon layer of around 25-30 μm was deposited at a graphite-target current of 75±5 A and a substrate bias of - 30±10 V. The deposition was carried out at the gas pressures 2.5 to 250 Pa. No pulse of the filter facility was used during the deposition.

### 5.2.2 Surface finishing methodology

During the PVD deposition, the surface roughness increased associated with macroparticles deposited during the coating growth (a common characteristic of the unfiltered cathodic arc deposition). Figure 5.3 exposes the four different strategies (Option A-D) used after PVD deposition covering two separate studies: Study on Surface Finishing Processes and Study on Surface Finishing Parameters. Three different approaches were used concerning the coating's surface finishing processes to study the influence of varying surface topographies in the DLC coated piston rings' tribological performance.

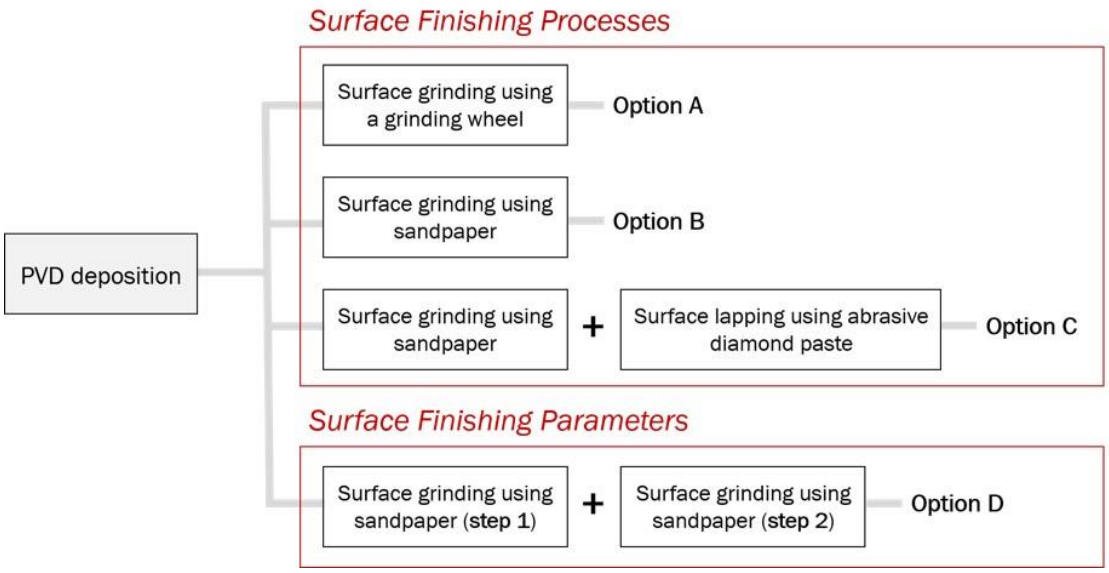


Figure 5.3 Four different strategies were used in the coated piston rings' post-treatment to modify the surface roughness of the DLC coating.

The Option A used a grinding wheel composed of an abrasive compound. Usually, this compound consists of a composite material with a particle aggregate (dimensions) in a cementing matrix. Option B is similar, but instead of a compound tool, it used a rubber roll enveloped in sandpaper (with abrasives in the granulometry range of 30-40 μm). The pressure was applied against the piston ring sample's surface, and the rubber roll favored the full contact between the pieces and the sandpaper due to its pliability. In Option C lapping process was added to Option B. This additional step intended a further decrease in the surface roughness using an abrasive fluid compound (a dispersion of abrasive particles) under continuous movement between the piston

rings outer surface and the inner surface of a lapping cylinder. The grain size range of the abrasive particles was about 1.5 – 3 μm.

In option D, the same process was consecutively repeated. They were differentiated by varying the operational parameters. Table 1 lists the parameters of the surface grinding process changed, including the first and second steps of option D.

Table 5.1 Variation of some operational parameters of the second surface grinding using sandpaper

| **Step 2** | **Abrasive particles size (μm)** | **Duration (s)** | **Pressure (bar)** | **Speed (rpm)** |
|---|---|---|---|---|
| Cond**1** | 20 | 200 | 1,5 | 285 |
| Cond**2** | 30 | 200 | 1,5 | 285 |
| Cond**3** | 20 | 600 | 1,5 | 285 |
| Cond**4** | 20 | 200 | 3,0 | 285 |
| Cond**5** | 20 | 200 | 3,0 | 400 |
| Cond**6** | 20 | 900 | 1,5 | 285 |

The parameters varied were the abrasive particle size, the duration of the surface finish process, the pressure applied by the rubber roll against the piston ring samples, and the rubber roll's rotation speed enveloped in the sandpaper. In this strategy, the main objective was to understand each operational parameter's influence on the final topography of the DLC coating.

### 5.2.3 Characterization methods

The morphology and cross-sectional microstructures of the DLC coatings were analyzed using a scanning electron microscope (SEM) coupled with energy dispersive spectroscopy (EDS) (INCAx-Act, PentaFET Precision, Oxford Instruments) equipment for chemical composition measurements.

The hardness and elastic modulus of the films were measured using the NanoTest instrument from the Micro Materials company with a Berkovich indenter. The indentation load was 5 N.

For evaluating the coating surface roughness, the measuring methods can operate in a tactile or non-contact mode. The first methods use a conventional profilometer, which works like a phonograph. In the non-contact mode, a white light interferometer or a confocal microscope is used. The measurement effectiveness using the last two methods depends on the light incidence's

surface response, which is not feasible for the dark DLC coating appearance. The typical characterization method combines several surface roughness parameters: amplitude and functional. The coating surface roughness were evaluated using the Mitutoyo Surftest SJ-210 portable surface roughness tester. A diamond tip with 2 μm of diameter and 60° of angle was used to measure the surface roughness parameters. A total length of 4.8 mm was used for a measurement length of 4.0 mm and a cut-off of 0.8 mm. Each condition was evaluated twice. The measurement speed was 0.5 mm/s, and it was applied a gauss filter.

Generally, the surface roughness represents the measure of thinner random irregularities of a surface, and it is correlated with the surface macroparticle density. In the present work, the considered roughness amplitude parameters include Ra (the arithmetic average of the profile heights over the evaluation length) and Rz (the average of the successive absolute vertical distances between the maximum profile peak height and the maximum profile valley depth over the evaluation length). Also, functional parameters were studied to perform a complete overview of the surface roughness: Rk, Rpk, and Rvk. These functional parameters followed the ISO standards of Table 2. Among the functional parameters, the core roughness depth is defined by Rk, where Rpk represents those peaks that might be eliminated during function and Rvk those valleys that will retain lubricant or worn-out materials. The representation of the surface roughness parameters is illustrated in Figure 5.4.

Table 5.2 Roughness parameters measured according to ISO standards

| **Parameter** | **Standard** |
|---|---|
| Ra<br>Rz | EN ISO 4287 |
| Rk<br>Rpk<br>Rvk | EN ISO 13565-2 |

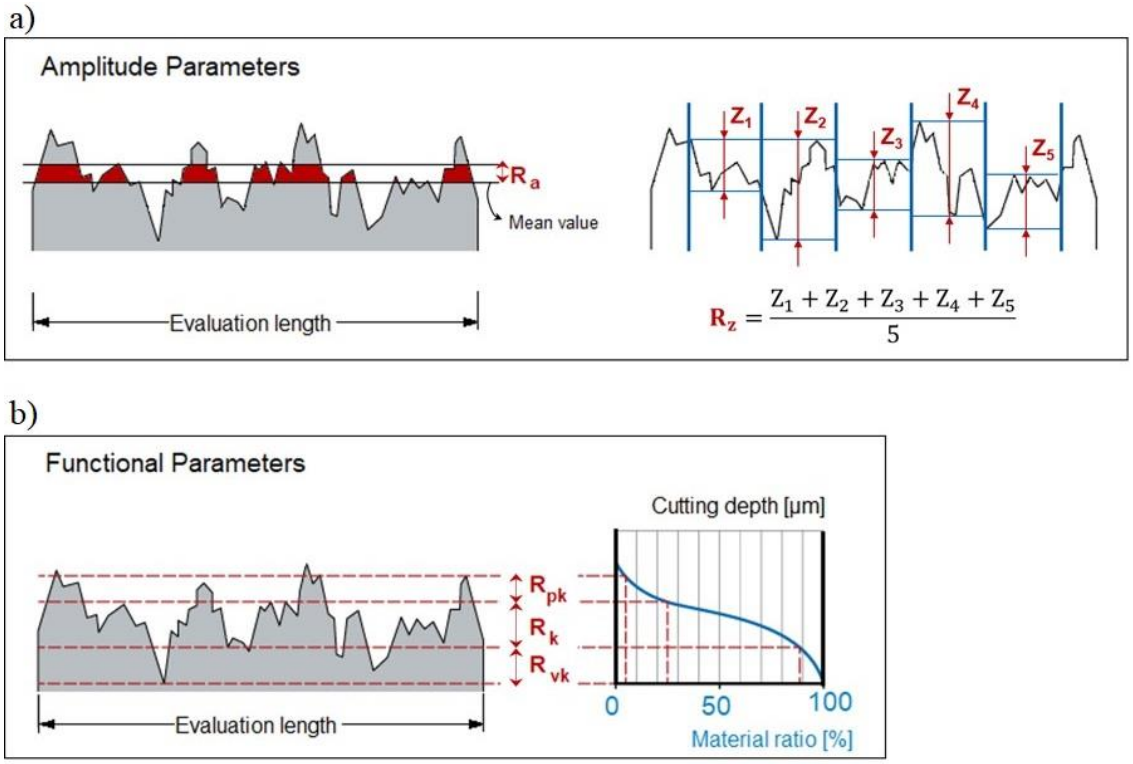


Figure 5.4 Schematic representation of the surface roughness parameters measured in the present work: a) Amplitude Parameters and b) Functional Parameters.

The baseline surface used to compare the surface finishing processes' effect is the surface roughness of the DLC coating after deposition. The measured parameters, Ra, Rz, Rk, Rpk, and Rvk, were measured in the longitudinal direction, according to Figure 5.5.

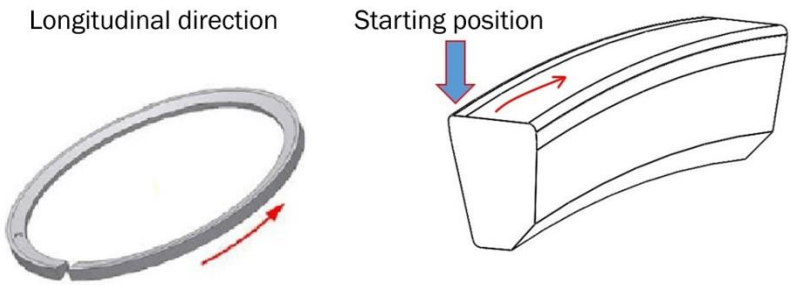


Figure 5.5 The direction of the surface roughness measurement in the piston ring samples.

### 5.2.4 Tribological assessment

The frictional response of the PVD coatings is strongly influenced by a range of extrinsic factors (testing conditions) and intrinsic factors (coating properties). Some outside factors include

the ambient temperature, contact pressure, sliding velocity, type of sliding motion, the presence or absence of a liquid, and solid lubricant on sliding surfaces. The most important intrinsic factors are film composition, structural nature (including nanolayers and nanophases), thickness, surface roughness, and a range of mechanical properties, including hardness and elastic modulus.

In this research, the tribological performance was evaluated in a home-made tribometer using testing conditions to mimic the engine operation. The main advantage of using a locally developed test rig is the possibility of defining the most important variables/systems to be controlled and the respective operational limits. Furthermore, the use of original engine parts and similar conditions to the realist environment creates a close relation between laboratory environment testing and real engine testing.

The structure of the developed testing device comprises five different subsystems: (A) a loading system used to press the piston ring sample against the cylinder liner sample; (B) a ring-liner contact holding system which was designed to fit samples from standard ring-liner pairs of heavy-duty diesel engines; (C) a lubrication and heating system that includes the oil tank; (D) an acquiring data system used to acquire friction force measurements and control the oil temperature and (E) a motion and driving system to generate the rotational movement and convert it into a reciprocating sliding motion. Figure 5.6 presents a scheme of the test rig structure.

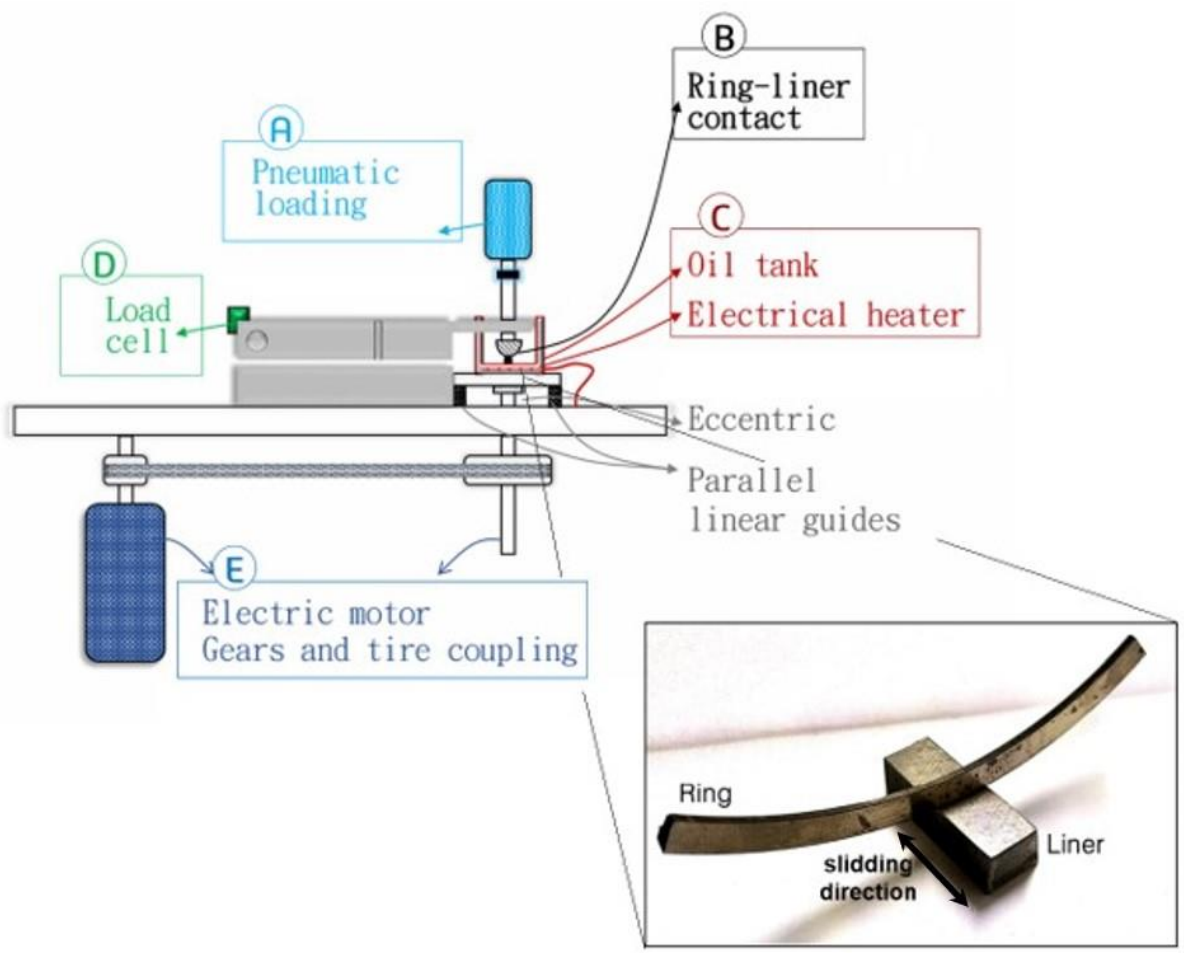


Figure 5.6 Schematic representation of the developed test rig identifying the constituent systems and focusing the piston ring-cylinder liner samples contact.

The piston rings are tested against cylinder liner specimens produced from a commercial cylinder liner of a heavy-duty diesel. The roughness of the cylinder liner consists of a crosshatch pattern. The purpose of relatively deep valleys is to capture small wear debris and retain reservoirs of lubricant oil. The surface roughness of the cylinder bore surface was characterized by a Ra mean value of 0.256 μm and an Rz mean value of 2.544 μm.

The testing conditions for the wear evaluation are presented in Table 3. The test rig is presented in Figure 5.7.

Figure 5.7 Test rig developed for the piston ring tribological assessment.

Friction measurements were performed using a lower load range of 45-60 N. At the end of the test, the worn specimens and the respective counterpart were ultrasonically cleaned in isopropanol alcohol for 10 min to remove the lubrication oil and wear debris resulted from the sliding contact.

Table 5.3 Tribological testing conditions for the DLC coatings evaluation

| **Variable** | **Value** |
|---|---|
| Load | 350-380 N |
| Speed | 0.3 m/s |
| Temperature | 135±5 °C |
| Lubrication oil | 5W30 |
| Duration | 240 min |
| Alumina particles size | 5 µm |

Before and after the tribological assessment, the sample mass was measured using an analytical balance Kern ABS-N / ABJ-NM with 0.0001-g accuracy. SEM and EDS analyzed the worn surface of the piston ring and the cylinder liner.

## 5.3 Results and Discussion

### 5.3.1 Characterization of the DLC coating

The cross-sectional morphology of the DLC coating at the end of the Option C (Figure 5.3) is also observed in Figure 5.8, together with the chemical composition and coating thickness. The selected deposition parameters provided a relatively dense columnar microstructure.

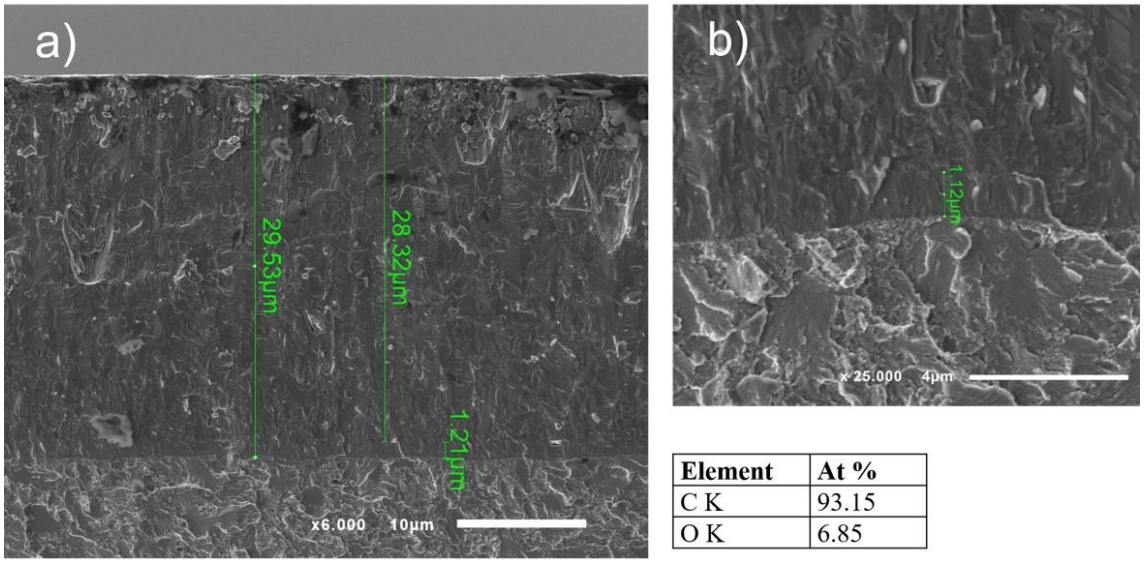


| Element | At % |
|---|---|
| C K | 93.15 |
| O K | 6.85 |

Figure 5.8 Scanning electron micrograph of the DLC coating cross-section with a) a view of the total coating in-depth and b) magnification of the Cr interlayer and the chemical composition of the deposited DLC film.

The thickness of the Cr interlayer varies from 1 to 1.5 µm. The residual oxygen presence can be originated by the residual atmosphere in the deposition chamber or from the porous graphite target contamination.

### 5.3.2 Mechanical properties

The hardness measurements of the DLC deposited layer were measured by microindentation. The hardness of the DLC film depends on the structure and binding energy of

carbon atoms. The values obtained for 5 N of the load were 15.5 GPa, and the respective maximum depth was of 4.55 μm. Due to surface roughness variations, it was exceeded the limit of 10% of the coating depth.

In the surface contact, the property which limits the elastic behavior is the hardness over elasticity modulus (H/E ratio). The measured elasticity modulus followed the same profile presented by the hardness results. The resultant H/E ratio was 0.071.

### 5.3.3 Impact of the surface finishing methodologies in the surface roughness

*Options A, B, and C*

In Figure 5.9 are presented the surface roughness parameters obtained for the as-deposited surface and the DLC coated piston ring prepared using the Option A (the surface grinding using a grinding wheel), the Option B (the surface grinding using sandpaper), and Option C (the surface grinding using sandpaper followed by the surface lapping using abrasive diamond paste).

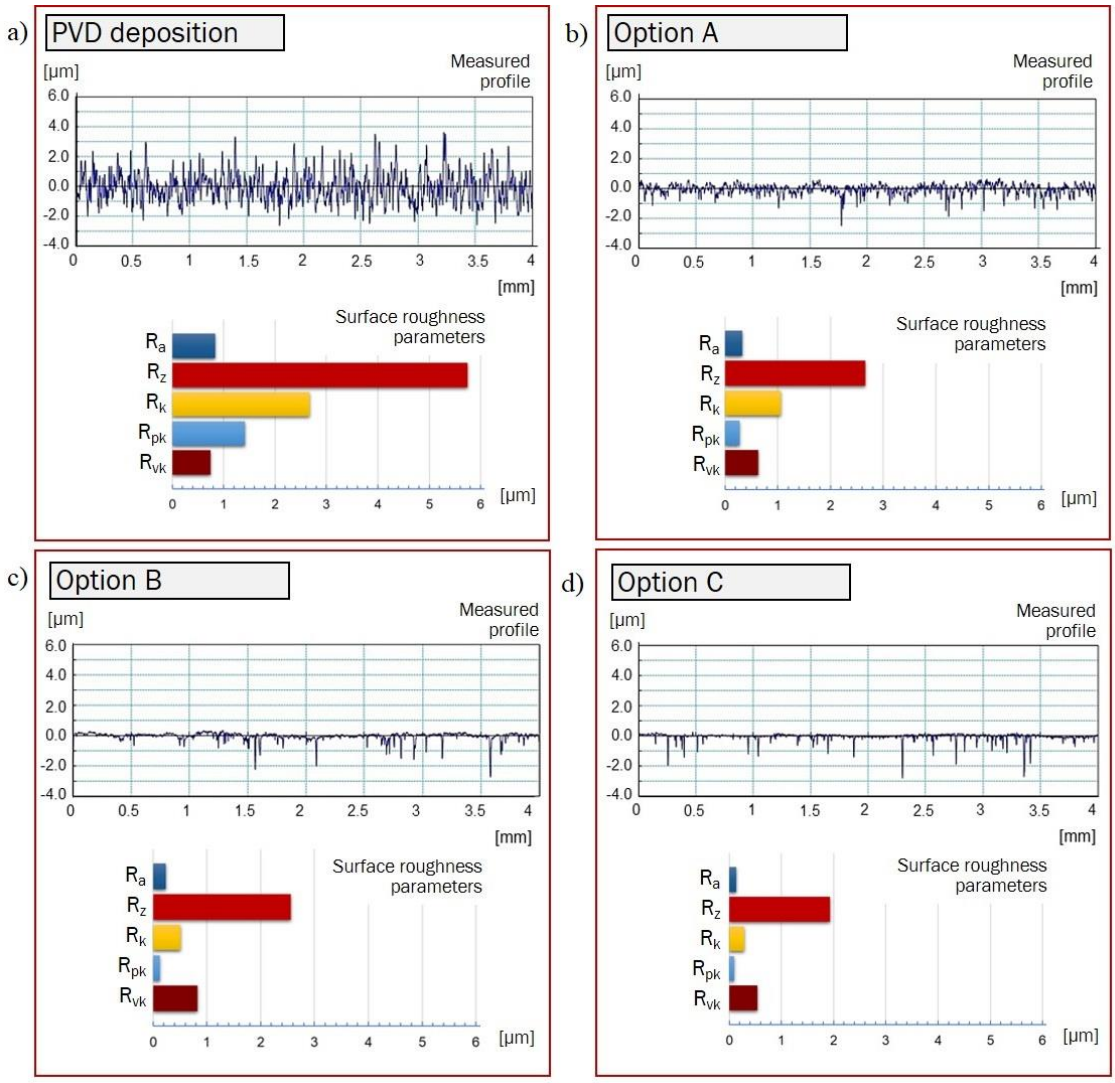


Figure 5.9 Surface roughness parameters measured for the DLC samples to compare the surface finish of the a) as-deposited surface with those resulted from b) Option A, c) Option B, and d) Option C.

According to the measured profile of each condition, it is perceptible the smoothing of the surface roughness comparing the as-deposited surface with Option A. The same trend is seen comparing Option A with the Option B or with Option C.

Comparing Option B, with Option C (the latter including an additional step using abrasive diamond paste), no significant variations are perceptible in the measured profile. However, by the measurement of the surface roughness parameters, all of them were reduced in Option C. This enhancement can influence the functional response of the DLC coating, and consequently, the piston ring performance.

*Option D*

The surface roughness parameters measured for the different testing conditions proposed in Option D are presented in Figure 5.10.

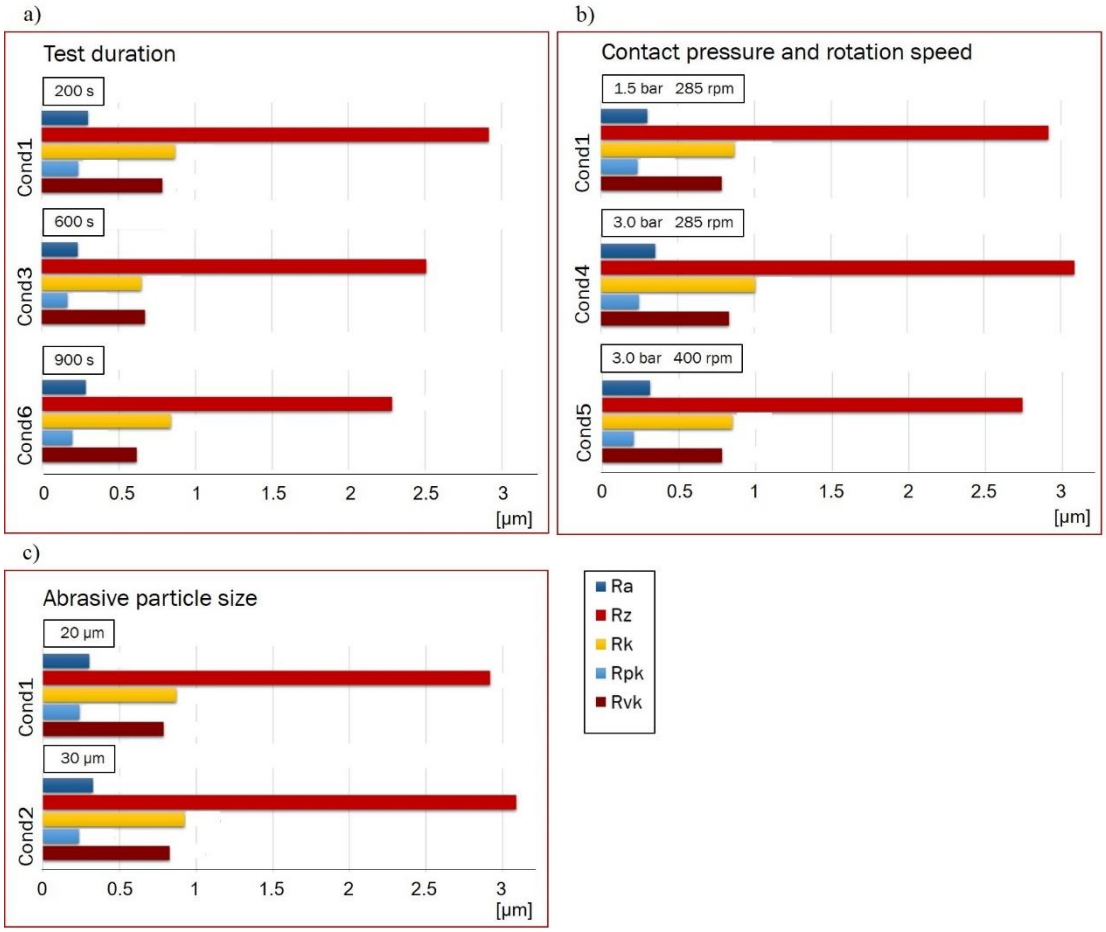


Figure 5.10 Surface roughness parameters measured for Option D, considering a) the analysis of different test durations, b) different contact pressures, and rotation speeds, and c) different abrasive particles size.

In the analysis of those results, the measurements were grouped in three different approaches to analyze the impact of the variation of a) the test duration, b) the contact pressure and rotation speed, and c) the abrasive particle size. As previously mentioned, those variables were changed in the second grinding step using sandpaper, and in the first stage, are kept constant in the same conditions for every trial.

Considering the variation of the second stage period, it is not perceptible a gradual variation of the surface roughness parameters with a time increase from 200 s up to 900 s. The second stage length increase up to 600 s was beneficial for the surface finishing, decreasing every measured parameter. However, the same trend is not verified for a further rise in the second stage, up to 900 s, except for Rz, defined as the average of the maximum profile peak heights. In this

way, and regarding those conditions, it was proved that the continuous increase of the second surface grinding stage is not a worthwhile industrial investment for the piston ring manufacturers.

The second group considered the first iteration with an increase of the pressure applied by the rubber roll against the piston ring samples from 1.5 bar up to 3.0 bar. The increase of the contact pressure itself (Cond4) had no positive effect on the resultant surface finishing. The second iteration used the higher contact pressure value, but increased the rotation speed of the rubber roll enveloped in the sandpaper from 285 rpm up to 400 rpm, which promoted an improved finishing surface.

The increase of the abrasive particle size from 20 μm up to 30 μm was addressed in the third group. Larger abrasive particles are less effective in the coating surface finishing, which means that minor particles provided a smoother surface. This conclusion is by the basic knowledge of the surface finishing technique.

### 5.3.4 Influence of the surface roughness on the wear resistance of the DLC coating

*Options A, B, and C*

The piston ring and cylinder liner weight loss, together with the coefficient of friction of each tribological pair, are presented in Figure 5.11.

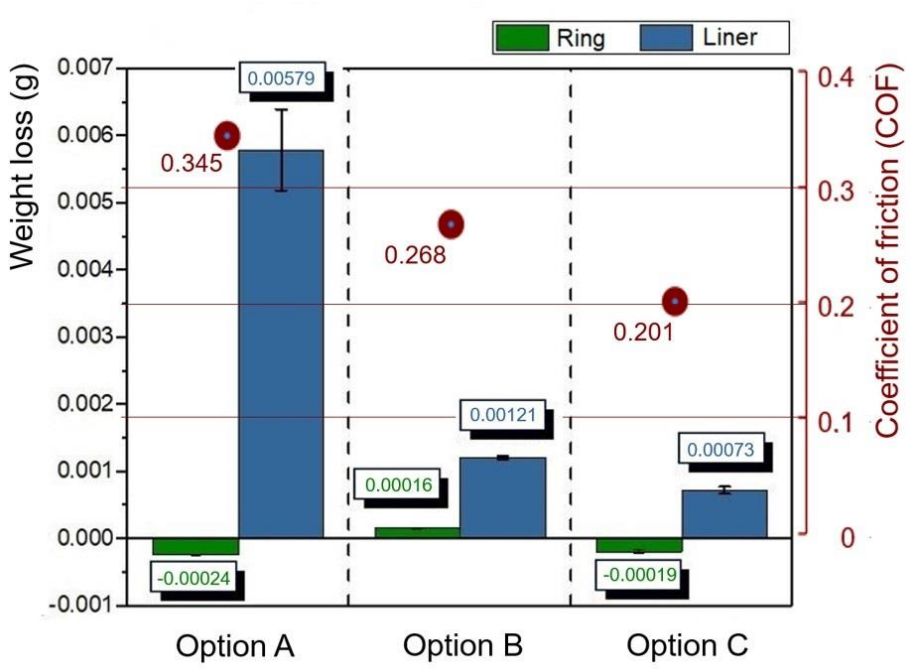


Figure 5.11 Weight loss and coefficient of friction values resultant from the tribological tests performed with the piston rings prepared according to the processes defined in Option A, B, and C.

As expected, the lower the surface roughness values of the piston ring surface, the better the tribological results obtained. The coefficient of friction resultant of each surface finishing condition presented a decrease from the Option A (finished using a grinding wheel) up to the Option C (ground using sandpaper and an additional surface lapping using abrasive diamond paste). The best tribological results are found in the Option C. As previously mentioned, a DLC coating is characterized by its amorphous structure with $sp^2$ and $sp^3$-bonded carbon atoms. When more $sp^2$-bonded carbon atoms are present, the coating acquires a graphite-like response, and as a consequence, low COF values.

In all experiments occurs a weight loss of the respective counterbody. Regarding the hardness of the deposited DLC coating around 15 GPa (compared with the conventional grey cast iron, which is naturally softer), a rougher DLC surface removed more material in the liner surface. The piston ring specimen of Option B had an insignificant weight loss. The specimens of Option A and Option B presented a slight weight gain. In Figure 5.12 are shown the SEM micrographs of the piston ring sample's surface after wear tests.

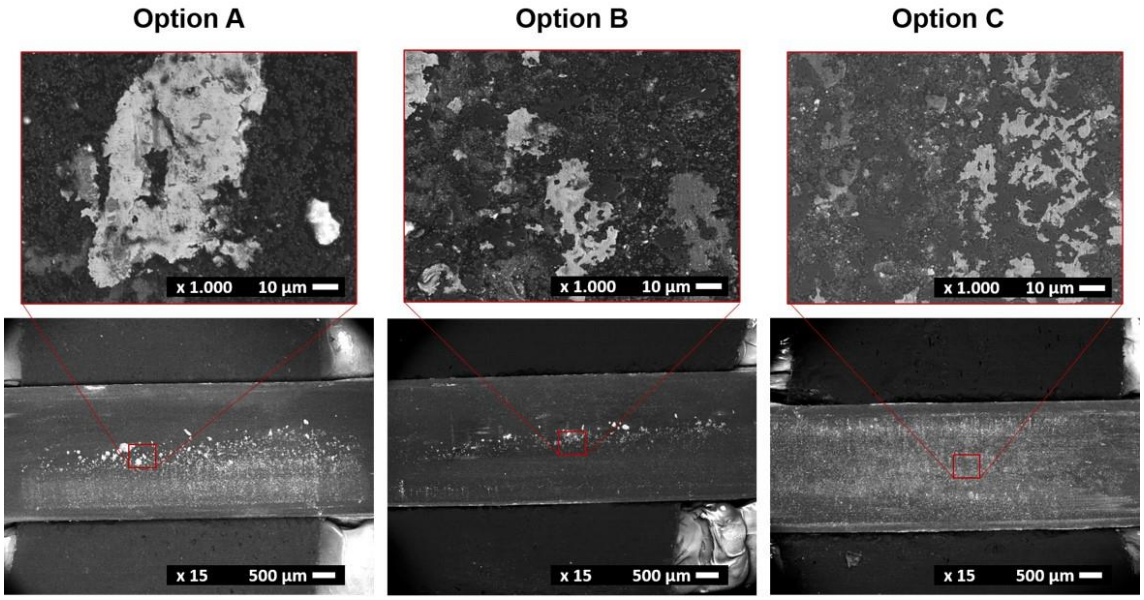


Figure 5.12 SEM micrographs of the piston ring specimen's resultant from the wear experiments performed for the Option A, B, and C.

According to the analysis of each surface, it is possible to see different results for the piston ring specimens of Option A, Option B, and Option C, however on all surfaces is perceptible the entrapment of external particles. Those particles can be the wear debris of the material detached from the liner surface or alumina agglomerates (added in the tribological experiments).

According to the surface images, the piston ring of Option B is the one with fewer particles entrapped on its surface. In the final balance of its weight, the piston ring specimen lost more material than accumulated, considering its total weight loss and external particle entrapment. This result is validated by the Option B surface's image, which is seen as the one with less entrapped particles.

*Option D*

The tribological evaluation results obtained for Option D are presented in Figure 5.13.

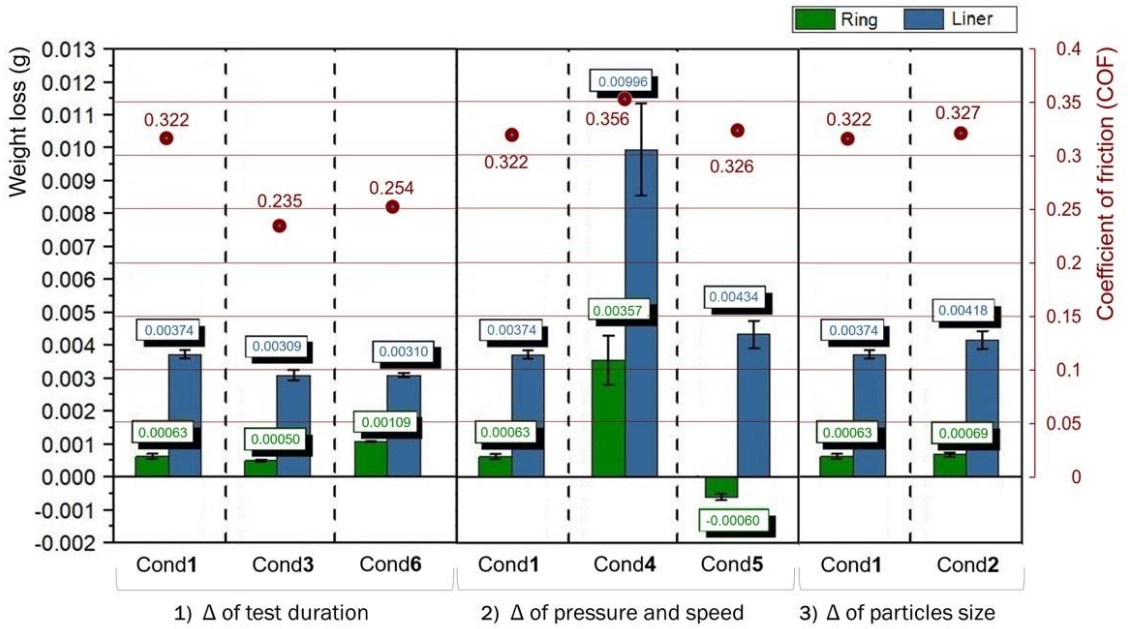


Figure 5.13 Weight loss and coefficient of friction values resultant from the tribological tests performed with the piston rings prepared according to the processes defined in Option D.

As with the surface roughness outcomes, the results of the tribological tests performed for Option D were also gathered in the same three groups according to the test duration, the contact pressure, rotation speed, and the abrasive particle size.

The weight loss of the piston ring and cylinder liner samples was quantified to analyze the impact of the piston ring surface roughness on its performance and the consequent effect on the counterbody surface. According to the purpose of the research, different outcomes can be the target of this investigation. From the materials research point of view, the best tribological pair should be considered the piston ring with the lowest wear (considered the one with the lowest weight loss), but with the highest weight loss of the counterbody. But, regarding the study of their functional performance, the piston ring and the cylinder liner roles are affected by the presence of worn surfaces. In this way, the best tribological pair with the lowest weight loss, either of the ring or the liner.

In the first group, the best result is from the Cond3, achieving the lowest weight loss for the piston ring sample and the respective cylinder liner. The second group highlighted the worst outcome of all experiments, with the highest weight loss values. It should also be pointed out that those samples produced using the Cond4 had the roughest surfaces. The most relevant effect of increasing the contact pressure and the rotation speed (comparing the Cond1 and the Cond5) is

the significant reduction of the piston ring weight loss. Those samples had a similar effect (entrapment of wear particles) as those obtained in Option A and Option C, as shown in Figure 5.14.

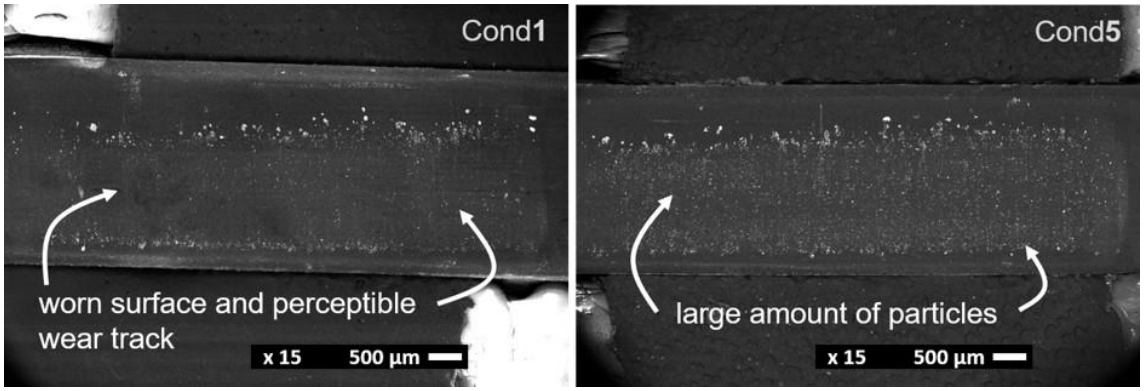


Figure 5.14 SEM micrograph of the piston rings produced using the Cond1 and the Cond 5 after the tribological assessment.

The SEM micrograph of the piston ring surfaces from Cond1 and Cond5 validated the weight loss measurements. In the former, it is perceptible the wear track where the sliding contact occurred, while in the latter can be observed the entrapment of a large number of particles.

The increase of the abrasive particle size studied in the third group did not enhance the tribological performance of the piston ring-cylinder liner pair. With a higher surface roughness, it increased the weight loss caused in the cylinder liner sample and contributed to a higher weight loss of the piston ring.

The COF measurements for those samples using different test durations followed the same trend of the surface roughness results. The lowest value of 0.235 resulted from a second step period of 600 s, which was the most effective for the DLC surface finishing. The worst result from this group (0.356) is from Cond4, following the tendency verified for the surface roughness parameters for different pressure and rotation speed values. On the other hand, the increase of the abrasive particle size had a minor influence on the coefficient of friction values.

## 5.4 Concluding remarks

Compression piston rings used in heavy-duty diesel engines were tribologically evaluated using a developed tribometer. About the impact of the surface finishing conditions in the piston ring roughness parameters it was concluded that:

• the use of an additional surface lapping step with abrasive diamond paste is useful in reducing the surface roughness parameters.

• the continuous increment in the length of the surface finishing process may not have implicit an enhancement of the surface roughness parameters.

• an increase of the rubber roll's rotation speed enveloped in the sandpaper can be more effective in reducing the surface roughness parameters than the rise of the contact pressure applied by the rubber roll against the piston ring samples.

• the use of larger abrasive particle size was not efficient for a surface roughness decrease.

About the influence of the surface roughness parameters in the tribological performance of the piston ring – cylinder liner pair it can be concluded:

• the wear resistance and the frictional response of the piston ring-cylinder liner pair vary according to the surface roughness of the DLC coating.

• the increase of the surface roughness parameters (rougher surfaces) led to higher COF values and greater weight loss (either of the piston ring or the counterpart).

• the presence of rough surfaces may instigate wear debris entrapment due to the high coating hardness, and the consequent superior wear resistance of the DLC surface, compared with the grey cast iron from the cylinder.

Further studies comprising longer tribological tests are necessary to evaluate the durability of the DLC coating.

## Acknowledgements

This work was supported by FCT (Fundação para a Ciência e Tecnologia) and MAHLE, Componentes de Motores, S.A. through the grant SFRH/BDE/110654/2015, by FCT (Fundação para a Ciência e Tecnologia) with the reference project UID/EEA/04436/2019 and by the project POCI-01-0145-FEDER-006941 and the project with reference NORTE-01- 0145-FEDER-000018-HAMaBICo, and ATRITO-0 (co-financed via FEDER (PT2020) POCI-01-0145-FEDER-030446.

## References

[1] Holmberg K, Andersson P, Nylund NO, Mäkelä K, Erdemir A. Global energy consumption due to friction in trucks and buses. Tribol Int 2014;78:94–114. doi:10.1016/j.triboint.2014.05.004.
[2] Tung SC, McMillan ML. Automotive tribology overview of current advances and challenges for the future. Tribol Int 2004;37:517–36. doi:10.1016/j.triboint.2004.01.013.
[3] Tian T. Modeling the performance of the piston ring-pack 1997:194.
[4] Mishra PC. A review of piston compression ring tribology. Tribol Ind 2014;36:269–80.
[5] Andersson P, Tamminen J, Sandstrom C-E. Piston ring tribology - A literature survey 2002:105.
[6] Morris N, Rahmani R, Rahnejat H, King PD. The influence of piston ring geometry and topography on friction 2012;227:141–53. doi:10.1177/1350650112463534.
[7] Ferreira R, Martins J, Carvalho Ó, Sobral L, Carvalho S, Ferreira R, et al. Tribological solutions for engine piston ring surfaces : an overview on the materials and manufacturing and manufacturing. Mater Manuf Process 2020;35:498–520. doi:10.1080/10426914.2019.1692352.
[8] Friedrich C, Berg G, Broszeit E, Rick F, Holland J. PVD CrxN coatings for tribological application on piston rings. Surf Coatings Technol 1997;97:661–8. doi:10.1016/S0257-8972(97)00335-6.
[9] Robertson J. Diamond-like amorphous carbon. Mater Sci Eng R Reports 2002;37:129–281. doi:10.1016/S0927-796X(02)00005-0.
[10] Bewilogua K, Hofmann D. History of diamond-like carbon films - From first experiments to worldwide applications. Surf Coatings Technol 2014;242:214–25. doi:10.1016/j.surfcoat.2014.01.031.
[11] Lifshitz Y. Diamond-like carbon — present status. Diam Relat Mater 1999;8:1659–76. doi:10.1016/S0925-9635(99)00087-4.
[12] Donnet C, Erdemir A. Tribology of Diamond-Like Carbon Films. 2008. doi:10.1007/978-0-387-49891-1.
[13] Singh SK, Chattopadhyaya S, Pramanik A, Kumar S. Wear behavior of chromium nitride coating in dry condition at lower sliding velocity and load. Int J Adv Manuf Technol 2017:1–11. doi:10.1007/s00170-017-0796-x.
[14] Anders A. Cathodic arc plasma deposition. Vac Technol Coat 2002;3:1–26. doi:10.1016/0040-6090(88)90494-4.
[15] Wei H. Study on the tribology of the cylinder and piston ring of the vehicle diesel with surface roughness and lubrication oil. Adv. Mater. Res., vol. 268–270, 2011, p. 322–5. doi:10.4028/www.scientific.net/AMR.268-270.322.
[16] Gu C, Meng X, Xie Y, Zhang D. Mixed lubrication problems in the presence of textures: An efficient solution to the cavitation problem with consideration of roughness effects. Tribol Int 2016;103:516–28. doi:10.1016/j.triboint.2016.08.005.
[17] Meng X, Gu C, Zhang D. Modeling the wear process of the ring/liner conjunction considering the evaluation of asperity height distribution. Tribol Int 2017;112:20–32. doi:10.1016/j.triboint.2017.03.025.
[18] Whitehouse DJ. Surface metrology. Meas Sci Technol 1997;8:955–72. doi:10.1088/0957-0233/8/9/002.

[19] Hashimoto F, Chaudhari RG, Melkote SN. Characteristics and Performance of Surfaces Created by Various Finishing Methods ( Invited Paper ). Procedia CIRP 2016;45:1–6. doi:10.1016/j.procir.2016.02.052.
[20] Michail SK, Barber GC. The effects of roughness on piston ring lubrication part I: Model development. Tribol Trans 1995;38:19–26. doi:10.1080/10402009508983375.
[21] Michail SK, Barber GC. The effects of roughness on piston ring lubrication— part II: The relationship between cylinder wall surface topography and oil film thickness. Tribol Trans 1995;38:173–7. doi:10.1080/10402009508983394.
[22] Wolff A. Influence of sliding surface roughness and oil temperature on piston ring pack operation of an automotive IC engine. IOP Conf. Ser. Mater. Sci. Eng., vol. 148, 2016. doi:10.1088/1757-899X/148/1/012090.
[23] Ligier J, Ragot P. Mixed Lubrication and Roughness Surface Effects Application to Piston Rings. CI SI Power Cylind Syst 2007;01.
[24] Shuster M, Mahler F, Macy D, Frame R, Deis M. Piston Ring Microwelding Phenomenon and Methods of Prevention. SAE Tech Pap Ser 2010;1. doi:10.4271/960745.
[25] Anders A. Unfiltered and filtered cathodic arc deposition. Handb. Depos. Technol. Film. Coatings, 2010, p. 466–531.
[26] Galligan J, Torrance AA, Liraut G. A scuffing test for piston ringrbore combinations Part I. Stearic acid lubrication. Wear 1999;236:199–209. doi:10.1016/S0043-1648(99)00277-X.
[27] Galligan J, Torrance AA, Liraut G. A scuffing test for piston ringrbore combinations: Pt. II. Formulated motor lubrication. Wear 1999;236:210–20.
[28] He Z, Zhang J, Ma W, Xie W, Zhang G, He Z, et al. A Concurrent Reynolds BC Algorithm for Piston Ring Cavitation Lubrication Problems with Surface Roughness. Tribol Trans 2014;57:353–65. doi:10.1080/10402004.2013.871376.
[29] Checo HM, Jaramillo A, Ausas RF, Jai M, Buscaglia GC. Down to the roughness scale assessment of piston-ring/liner contacts. IOP Conf. Ser. Mater. Sci. Eng., vol. 174, 2017. doi:10.1088/1757-899X/174/1/012035.

# CHAPTER 6.

## Surface engineering for optimized compression piston ring tribological performance

Revision submitted to *Friction* on: 21th of September, 2022
R. Ferreira [a,b,c,*], Ó. Carvalho [a,b], L. Sobral [c], S. Carvalho [d], F. Silva [a,b]

[a] Centre for Micro-Electro Mechanical Systems (MEMS) University of Minho, Campus de Azurém, 4800-058 Guimarães, Portugal
[b] LABBELS –Associate Laboratory, Braga, Guimarães, Portugal
[c] MAHLE - Componentes de Motores S.A., Núcleo Industrial Murtede, 3060-372 Cantanhede, Portugal
[d] CEMMPRE – Center for Mechanical Engineering, Materials and Processes, University of Coimbra, 3030-788 Coimbra, Portugal

## Abstract

The radial surface coating layer of compression piston rings is used to improve their wear resistance during the internal combustion engine operation. However, at top dead centers, the friction coefficient of the piston ring-cylinder liner pair is detrimental to the engine's tribological performance. In this work, dimples with different texture dimensions and densities were tested in a home-developed tribometer. The friction coefficient was measured for all samples, and for those with the best results, their wear resistance was assessed. The texture with an aspect ratio of 0.25 and a density area of 15% reported the best tribological results.

Keywords: *piston ring, surface texture, friction, wear.*

## 6.1 Introduction

A reciprocating sliding movement between the engine piston and its respective cylinder liner occurs during internal combustion engine operation. Assembled to the piston, the compression piston ring act as a combustion chamber sealing with a continuous contact against the inner liner. The piston assembly, where the piston ring-cylinder contact, represents most of the internal combustion engine frictional losses, between 45% and 55% [1].

Lubricating oils minimize those mechanical losses and the consequent influence on the vehicle's performance [2]. However, the presence and the characteristics of a lubricant layer between the piston ring radial surface and the inner cylinder surface depends on the current engine stroke [3,4]. Distinct lubricant regimes occur during the four strokes, from starved to boundary and hydrodynamic. Top dead-centers, particularly the combustion stroke, gather the most detrimental conditions for the compression piston ring: the maximum gas temperature, the maximum gas pressure, and an almost null sliding speed. As a result, severe scuffing wear of the compression piston ring results in significant frictional losses associated with this tribological pair.

In the compression piston ring component, the characteristics of its radial surface will have a determinant influence on the piston ring-cylinder liner contact [5]. For a tribological purpose, the laser surface treatment of the top ring radial surface has been extensively studied in the academic literature through experimental [6,7] and numerical studies [8–11]. Engineered and textured surfaces developed with a functional purpose are already recognized as available methods to confer desirable surface properties through a specific pattern topography [12,13]. Laser surface texturing represents a potential tool for friction reduction applications with feasible implementation in large-scale production. If properly distributed, the resultant surface textures will allow the entrapment of

wear debris in the texture pockets and act as secondary lubricant reservoirs. On the surface of the piston ring, surface texturing may represent a way to avoid scuffing/spalling issues.

The main functional arguments used for surface texture implementation are the lubricant supply in cases of starved lubrication (acting as micro-reservoirs) and the effect of micro-hydrodynamic bearings during a hydrodynamic lubrication regime, and the entrapment of wear debris.

In cooperation with different researchers, Izhak Etsion produced several studies embracing laser surface texturing and their application in the piston ring-cylinder liner tribological pair [6,14–19]. The use of partial texturing, instead of a total textured surface area, is suggested by Etsion's research group for parallel and flat surfaces, such as the contact of mechanical seals [18,19]. Etsion and Sher [6] investigated the influence of partial laser surface texturing of the top piston rings on fuel consumption and reduced it up to 4%.

Lu and Wood [20] published a review paper focused on the surface texturing process applied to mechanical systems. One of their conclusions was the detrimental effect of deep dimples, and that optimal depth value is dependent on the working conditions. Braun [21] studied the efficiency of laser surface texturing in reducing friction under mixed lubrication. They concluded that an optimum texture is found only for specific operation conditions, even considering the oil temperature and oil viscosity.

One of the most common conclusions found in the published research papers is the reliance on surface texturing effectiveness on several intrinsic and extrinsic parameters. The type of contact, functional conditions, texture dimensions, and geometries represent determinant variables [22–24], together with the component's material and the lubricating oil properties.

Although textures in the piston ring's surface do not yet represent a commercial solution, the surface texturing of the cylinder liner bore is already implemented. Cross-hatched geometries are produced into the cylinder bore to create a plateau-honing surface finishing to foster oil circulation [25–28]. Even in the cylinder liner, the surface texturing is performed where the piston inverts its sliding movement, which is associated with an increase in friction coefficient. Grabon et al. [27,29] studied the tribological response of the honing texture and, more specifically, the honing angles in the cylinder liner's inner surface.

Rao et al. [30] studied the effect of simultaneous surface texture in a diesel engine's cylinder liner inner surface and piston ring radial surface. They used different groove widths in the cylinder

liner surface and dimples of 1 mm in the piston ring surface. In conclusion, the cylinder liner with a larger groove texture (3 mm) associated with a non-textured piston ring can reduce exhaust gas emissions. Miao et al. [31] also evaluated the tribological behavior of the co-textured cylinder liner-piston ring during the running-in of a marine diesel engine. Dimple textures on the piston ring surface are more effective as a mobile oil reservoir than the groove texture on the cylinder liner.

Several authors investigate the combination of surface texturing and thin coating films. Some published studies performed a preliminary surface texturing of the substrate [32–34]. Other works produced micropatterns in the coating layer with a tribological purpose [24,35]. Sedlacek et al. [24] confirmed the beneficial effect of combining coating deposition and texturing (according to this sequence) to decrease the friction coefficient further.

In the present study, a laser surface treatment is applied to a commercial compression piston ring used in heavy-duty diesel engines to produce micro dimples along the radial ring surface. The piston ring possesses an NbN/CrN coating layer, which is used to improve its wear resistance. The influence of the micro dimples in the piston ring tribological response is evaluated using a home-developed tribometer. The coefficient of friction and the wear mass loss of textured and untextured samples were analyzed and compared.

## 6.2 Experimental procedure

### 6.2.1 Piston-ring characterization

The compression piston rings have an NbN/CrN layer deposited by an industrial cathodic arc plasma equipment. The coatings were produced from pure chromium and niobium targets and a nitrogen atmosphere. The substrate was gas nitrided martensitic stainless steel piston rings [36]. A Cr bonding layer was deposited to improve the adhesion between the stainless steel substrate and the deposited coating.

Before the surface texturing treatment, the piston ring and the coating layer were characterized. The surface and cross-sectional analysis of the coatings' morphology was performed by scanning electron microscopy (SEM) (JSM-6010 LV, JEOL). The thickness of the layers was obtained through a cross-sectional study also by SEM. The in-depth chemical composition measurements were performed throughout its profile, using SEM and the connected energy dispersive spectroscopy (EDS) (INCAx-Act, PentaFET Precision, Oxford Instruments) equipment.

Additional qualitative and semi-quantitative chemical composition assessments were performed using the same equipment.

The resultant piston ring surface textures were also dimensionally characterized using the SEM micrographs and an image processing software (ImageJ).

The analysis by X-Ray Diffraction (XRD) (Bruker D8 Discover) was selected to study the coating's internal crystalline structure. This analysis comprised a classical $\theta$-$2\theta$ diffractometer with a Bragg-Brentano geometry using CuK$\alpha$ radiation. The step size was 0.04° $2\theta$, with 4 s/step and a $2\theta$ range of 15°-90°.

Hardness measurements were performed using a Micro Materials NanoTest indentation system with 750 mN. The hardness value represents the average of at least ten measurements. To minimize the substrate influence, the indentation depths were up to 10% of the coating thickness. These measurements also allowed us to determine Young's modulus.

### 6.2.2 Surface texturing process

The functional surface of commercial compression piston rings was modified for the present study. The round dimples were produced using a microsecond pulsed laser (Model: XM-30D Fiber Laser Marking Machine) with a wavelength of 1064 nm and a maximum power of 30W (frequency up to 100 kHz). The spacing between the micro dimple patterns varies according to the laser frequency. In the present work, the laser beam scanning speed was moved with a velocity ranging from 7500 to 15000 mm/s.

After surface texturing, the piston rings underwent an additional lapping stage. The post-texturing lapping is a determinant of removing possible remelting material and consequent bulges around the rim and controlling de coating's surface roughness.

### 6.2.3 Testing method and test conditions

The present work uses a home-developed tribometer designed to fit standard ring-liner pair of heavy-duty diesel engines [37]. The baseline and textured ring samples were tested against cast iron cylinder liner pieces. A schematic view of the test rig is presented in Figure 6.1.

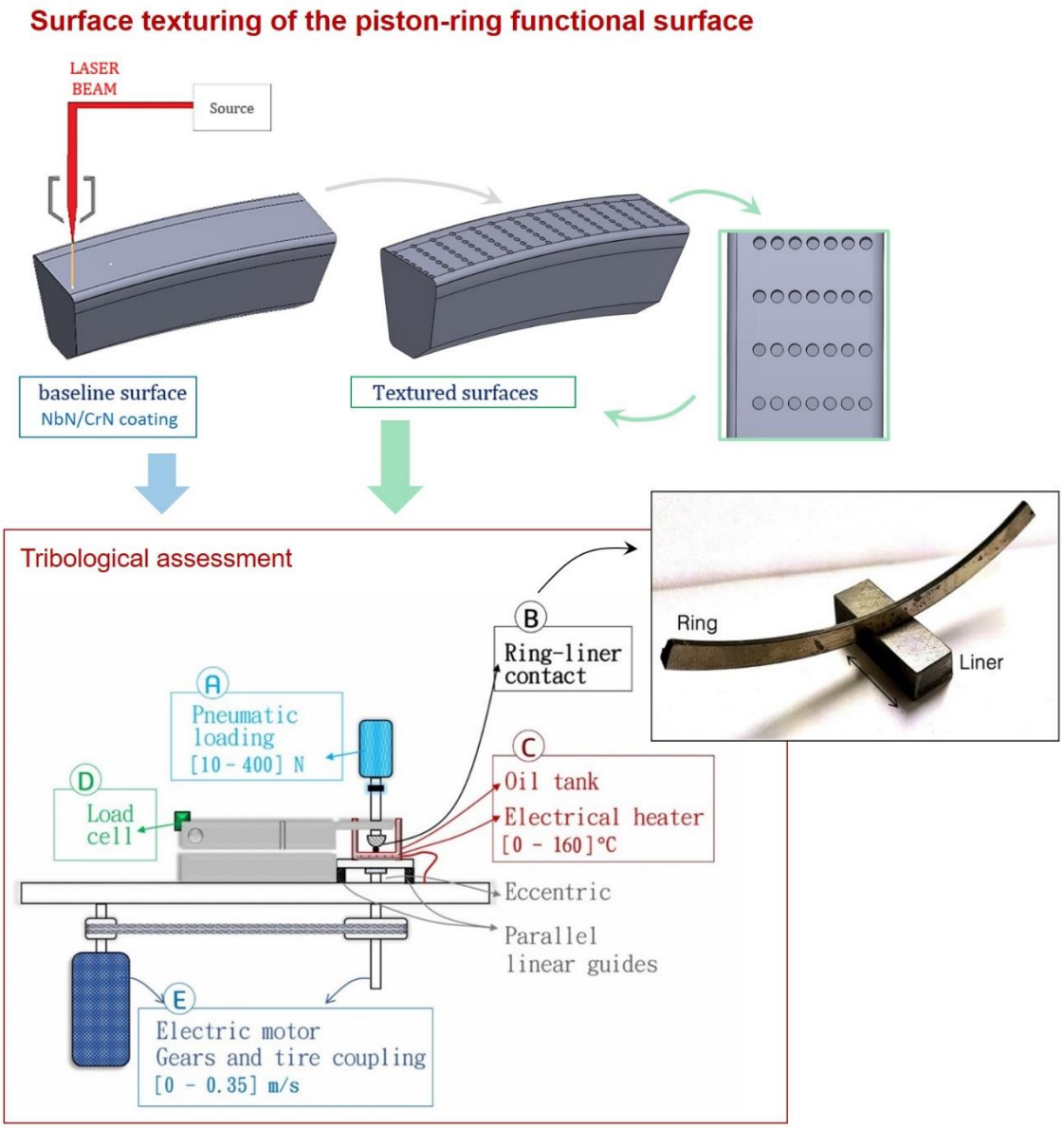


Figure 6.1 Schematic representation of the surface texturing and tribological characterization of the piston-ring functional surface.

The rig consists of five subsystems identified in Figure 6.1 from A to E. The sliding contact had 10 mm of stroke. The liner samples have the typical plateau-honed surface texture existing in the cylinder bore.

The coefficient of friction and wear resistance were analyzed according to different parameters, exhibited in Table 6.1. Based on the four-stroke diesel engine, the frictional response was evaluated by reproducing the top dead center conditions, as indicated in Figure 6.2. With the piston's inversion of movement, the sliding speed decreases to zero, and the effect of the radial

force reduces the oil film, creating a starved lubrication condition. The lubrication regime was created using a syringe with a 0.0258 ml of oil dosage dispensed into the contacting area. The association of the lower sliding speed and the boundary lubrication regime reproduced a starved lubrication condition, characteristic of TDC stroke. The coefficient of friction and the sliding time were continuously recorded.

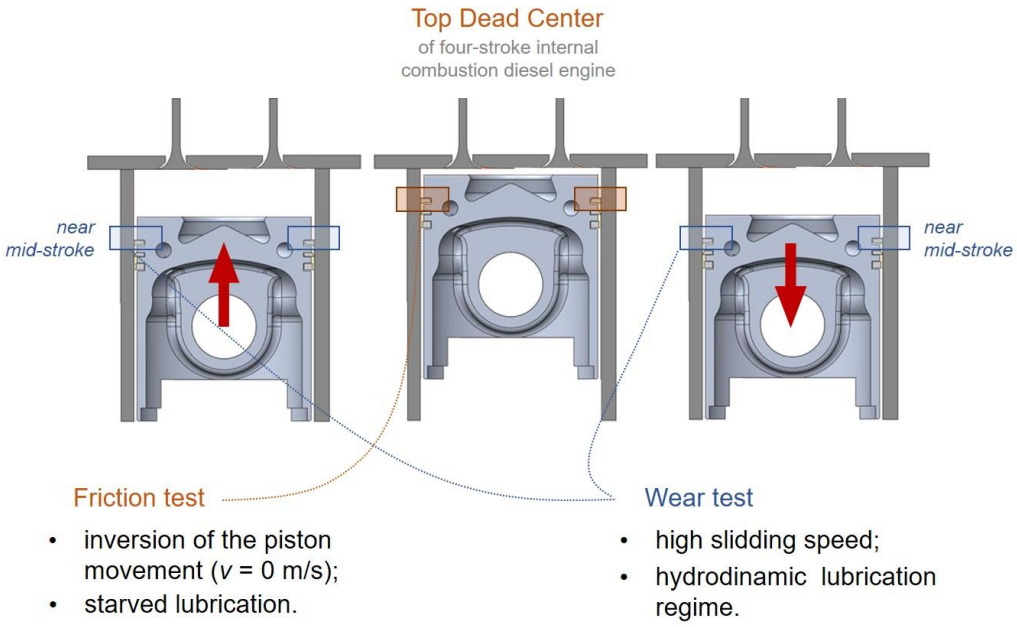


Figure 6.2 Friction and wear test approach.

The wear test protocol reproduced the overall performance of the piston ring during the four-stroke cycle. The high sliding speed achieved by the piston near the mid-stroke into the liner is associated with the hydrodynamic lubrication regime. To foster the ring and liner surface's wear and consequently allow the quantification of their mass loss, 3.5 g of alumina particles were dispersed per 700 ml of lubrication oil. An oil contaminant is widespread in industrial protocols. Otherwise, substantially longer tests would be demanded to observe worn surfaces.

Table 6.1 Specific friction and wear testing conditions used in the tribological assessment.

| **Parameters** | **Friction test** | **Wear test** |
|---|---|---|
| Sliding speed | 0.026 m/s | 0.3 m/s |
| Normal load | 10-11 N | 350-380 N |
| Lubricating oil | 0W20 | 0W20 |
| Lubrication | boundary | fully flooded |
| Oil temperature | 20 ± 3 °C | 135 ± 5 °C |
| Oil contaminant | - | $Al_2O_3$ (5 µm) |

Before the sample's analysis, a cleaning operation is used to remove the lubrication oil and wear debris from the sliding contact. The sample mass was measured before and after the tribological assessment using an analytical balance Kern ABS-N / ABJ-NM with 0.0001-g accuracy. The worn surface morphology of the piston ring and the cylinder liner was characterized through SEM and EDS techniques.

## 6.3 Results and Discussion

### 6.3.1 Morphological, crystallographic, and mechanical characterization

The transition metal nitride coating deposited on the SS substrate and the respective Cr interlayer are exhibited in Figure 6.3. The CrN/NbN layer varies from 24 and 28 μm in thickness and presents a dense columnar microstructure. The chromium bonding layer possesses an average thickness of 1 μm and a columnar structure.

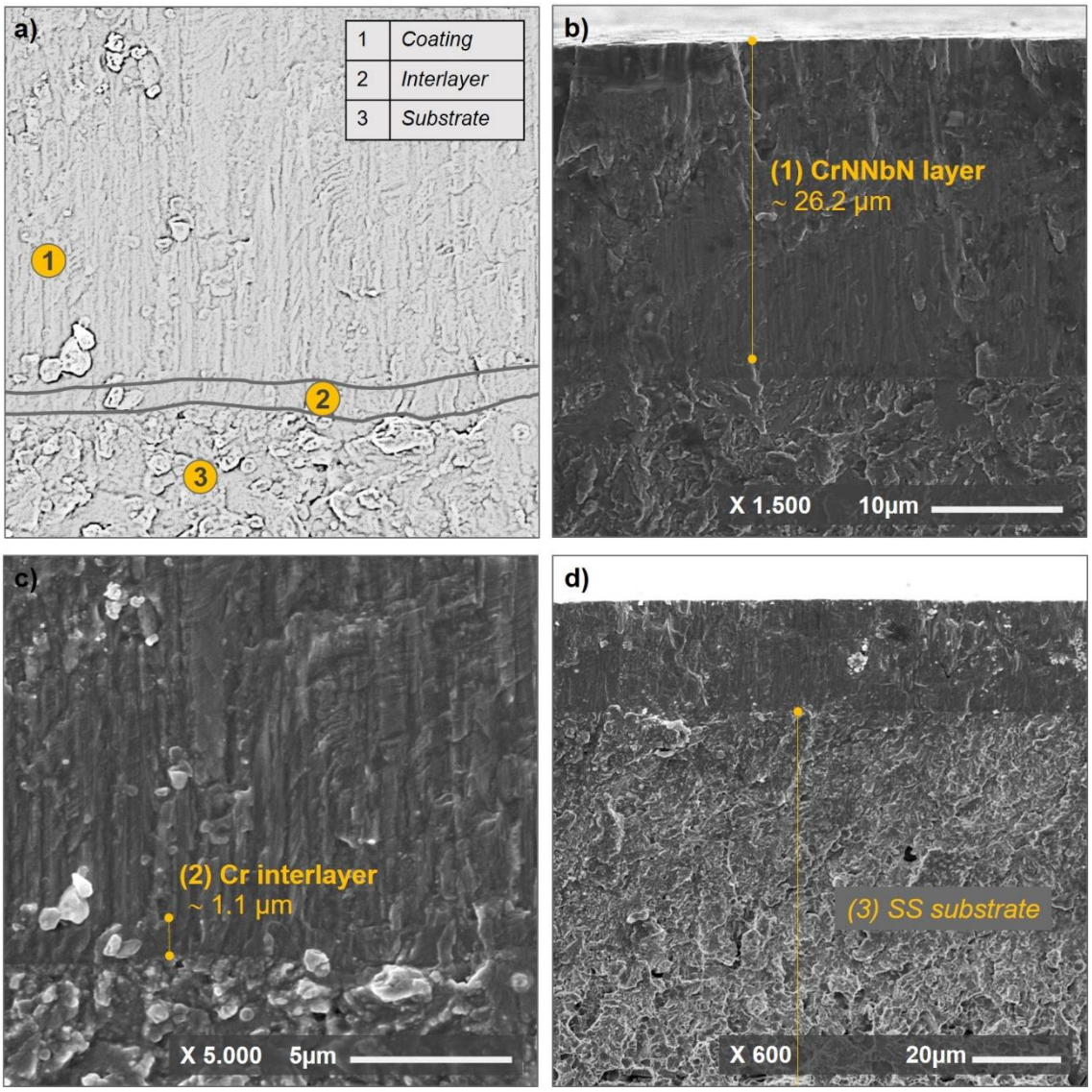


Figure 6.3 SEM analysis of the piston ring cross-section with a) a schematic representation of the piston ring's layers and the detailed micrographs of b) the CrN/NbN coating, c) the Cr interlayer, and d) the SS substrate.

Figure 6.4 displays the in-depth chemical composition of the coating layer. The cross-sectional study of the fractured samples detected the presence of C, with a periodic increase in its content. At the end of the Cr bonding layer, Fe and C elements substantially increased because of the stainless steel chemical composition.

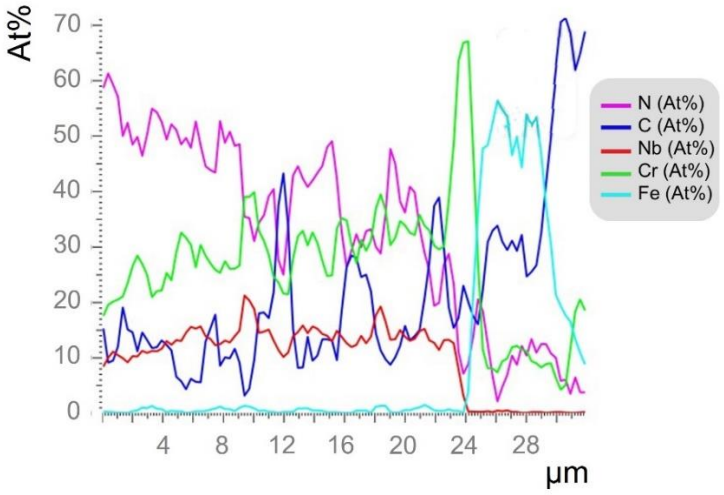


Figure 6.4 In-depth chemical composition of the CrN/NbN coating layer quantified by SEM-EDS.

The phase composition of the coatings was characterized by observing the diffraction peaks in the range of 15-90 using XRD. Figure 6.5 shows the θ-2θ X-Ray diffraction patterns.

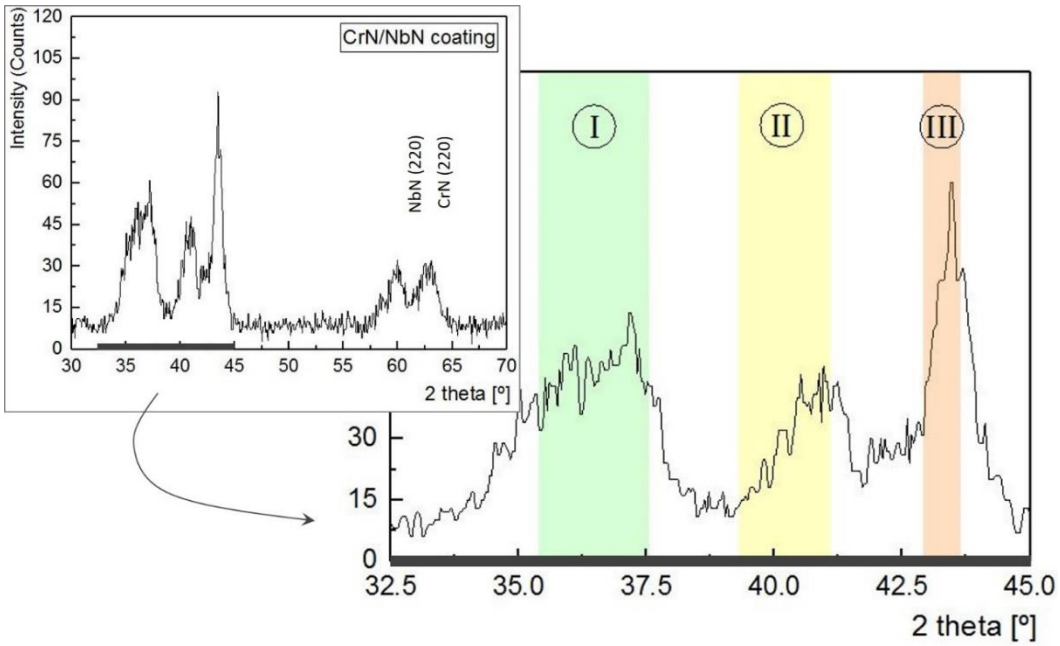


| Zone | Phase | Orientation | 2θ (°) |
|---|---|---|---|
| I | NbN<br>CrN | (111)<br>(111) | 35,4<br>37,5 |
| II | NbN | (200) | 41,0 |
| III | CrN | (200) | 43,6 |

Figure 6.5 X-Ray Diffraction patterns for CrN/NbN coating layer with three peak zones (I, II, and III).

A broader range analysis, between 30° and 70°, identified two distinct peak concentration ranges. The most intense peaks related to NbN and CrN, ICDD #38-1155 and ICDD #11-65 cards, are in the magnified graph (2θ angle: 32.5° to 45°). The coating's mechanical properties were obtained through nanoindentation measurements. The mean hardness value resultant from ten measurements was 24.5 GPa (with a standard deviation of 3.02 GPa). The Young modulus value was 364 GPa, achieving a maximum indentation depth of around 1,4 μm.

### 6.3.2 Characterization of surface textures

Different dimensional characteristics resulted from the laser power and laser scanning speed variation. Table 6.2 presents the dimensional characterization of the textured dimples using 15 W of laser power, constituting group 1 (G1), and 30 W, of group 2 (G2) and different laser speeds. Dimple's aspect ratio was defined as the ratio of the micro-dimple depth to the micro-dimple diameter. The density area represents the ratio of the micro-dimple area over a micro-dimple array. The surface dimples prepared in the present study are exhibited in Figure 6.6.

Table 6.2 Dimensional characterization of piston-ring dimples produced by laser surface texturing.

| | Laser speed (mm/s) | **Dimples dimensional** characterization | | | | |
|---|---|---|---|---|---|---|
| | | Ø $_{aver}$ (μm) | Depth (μm) | Aspect ratio, λ | Pitch (μm) | Density area |
| **G1** | | | Power: 15 W | | | |
| *T1* | 7500 | **132** | 21 | 0.16 | 205 | **22%** |
| *T3* | 10000 | **136** | 19 | 0.14 | 295 | **14%** |
| *T5* | 12500 | **131** | 16 | 0.12 | 385 | **11%** |
| *T7* | 15000 | **128** | 13 | 0.10 | 440 | **9%** |
| **G2** | | | Power: 30 W | | | |
| *T2* | 7500 | **157** | 94 | 0.60 | 190 | **35%** |
| *T4* | 10000 | **170** | 77 | 0.45 | 280 | **27%** |
| *T6* | 12500 | **159** | 55 | 0.35 | 350 | **17%** |
| *T8* | 15000 | **158** | 40 | 0.25 | 450 | **15%** |

The textures obtained using the lower laser power value present nearly the same dimple's diameter, around 130 μm. The variation of the laser speed influenced the dimple's density area. A higher laser texturing speed resulted in spaced laser spots and, thus, an increased distance between consecutive dimples along the machining axis. The dimple's depth range between 13 μm (T7) and 21 μm (T1), with an aspect ratio of 0.1 and 0.16, respectively. The dimple's pitch in the piston ring radial direction was constant for each group: 300 μm for G1 and 280 μm for G2. In

the perpendicular direction, the dimple's pitch increased and, consequently, the density area decreased.

The increase of power (for 30 W) fostered a higher laser energy density of the laser beam discharge. Deeper dimples and larger diameters lead to higher aspect ratio values and increase the obtained density area for the same laser speed.

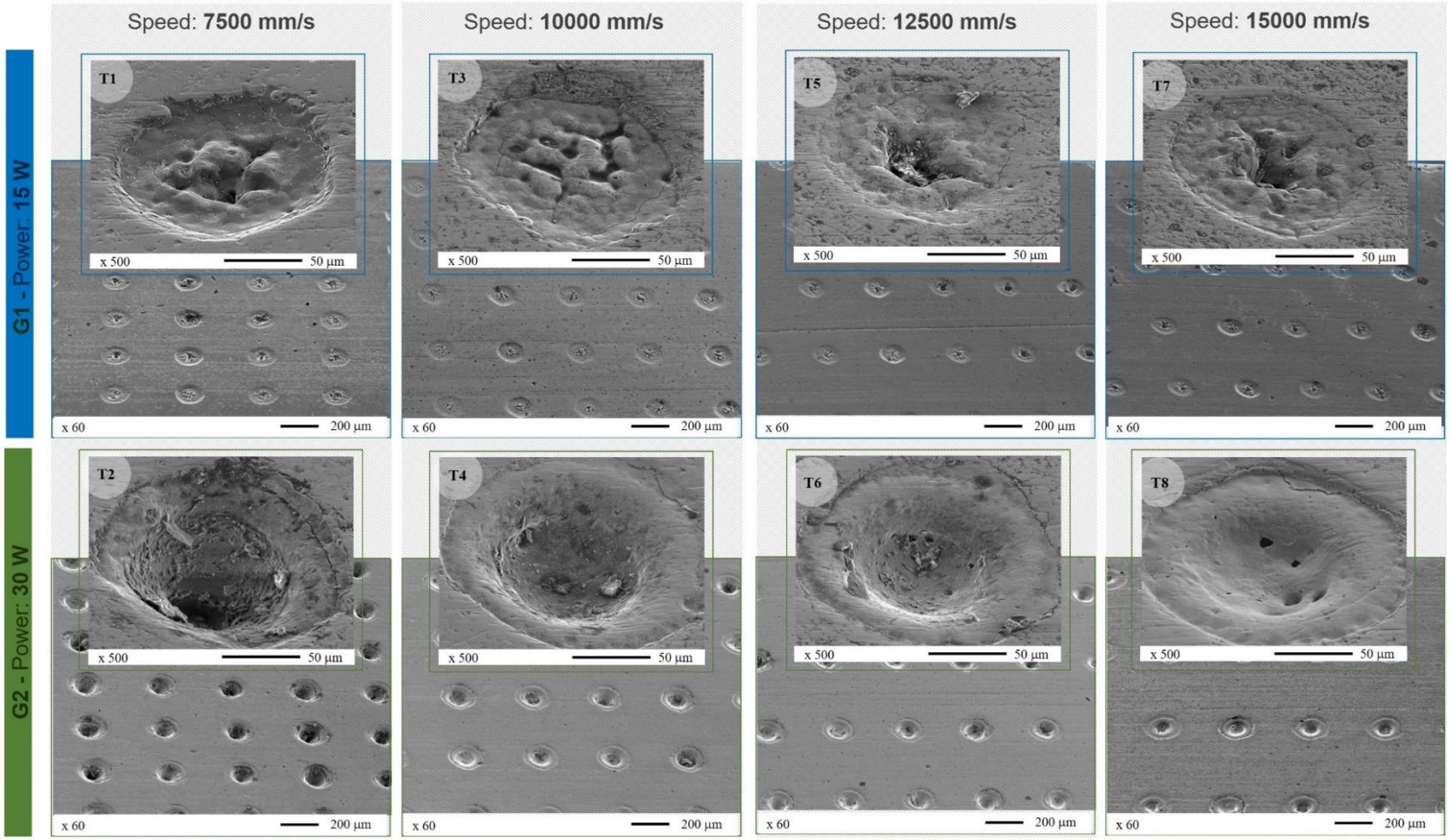


Figure 6.6 SEM micrography of piston-ring dimples produced by laser surface texturing.

### 6.3.3 Tribological results

The friction coefficient testing parameters replicate the most unfavorable conditions, similar to those during start-up under starved and mixed lubrication. COF values were recorded continuously during 5000 cycles, and the average COF results (after the running in period) of non-texture and textured samples are exhibited in Figure 6.7 for different time frames.

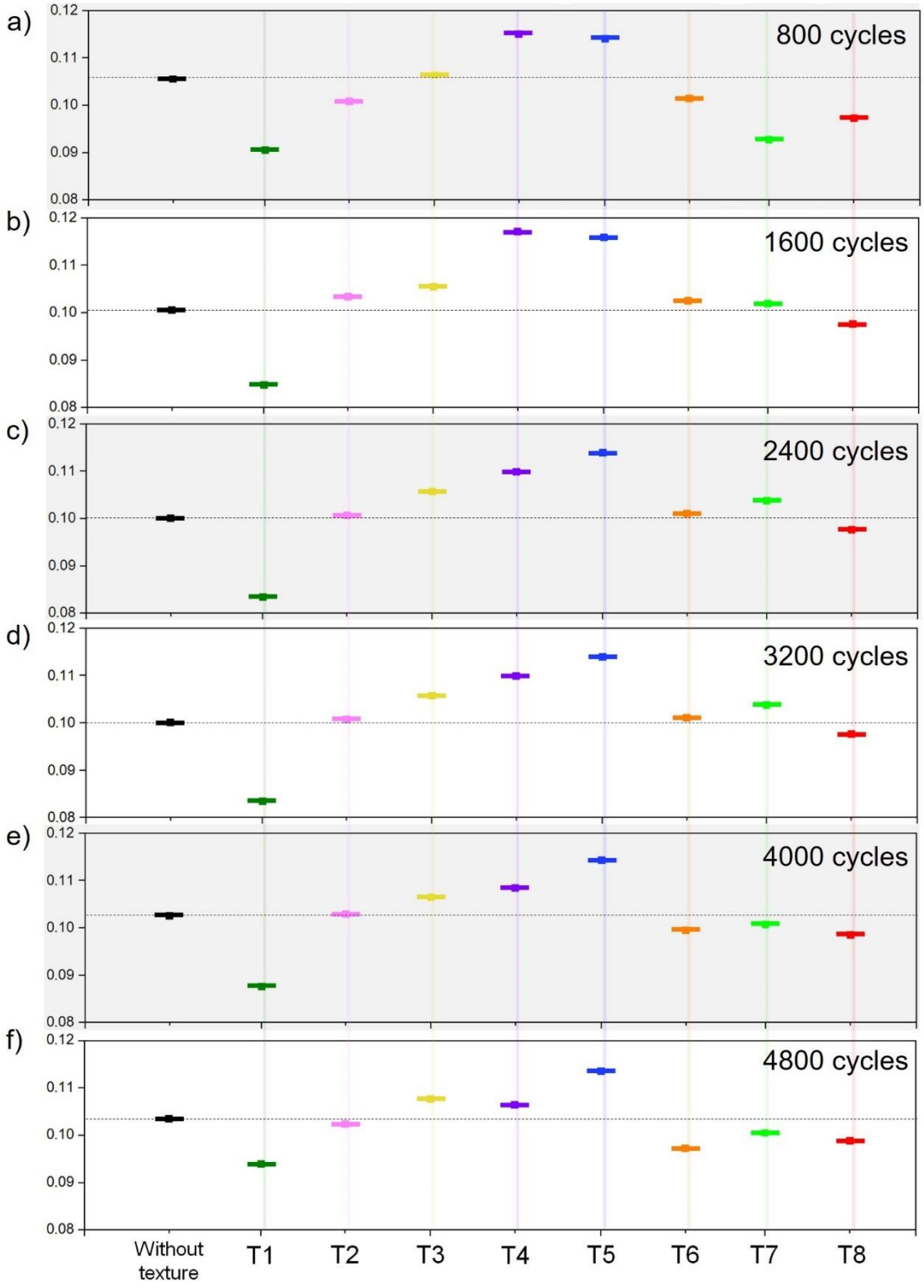


Figure 6.7 Average friction coefficient values of the non-textured and textured samples registered over six distinct time frames: a) 800 cycles; b) 1600 cycles; c) 2400 cycles; d) 3200 cycles; e) 4000 cycles and f) 4800 cycles.

The baseline value was considered for the non-textured piston ring. T3, T4, and T5 textures revealed higher COF than non-textured samples during the entire trial. T2 and T6 textures

presented a behavior similar to the baseline piston ring without significantly improving the frictional response. T1 and T8 improved the frictional performance, with a COF reduction of 14% and 4%, respectively, when compared with the non-textured surface. T7 evidenced an oscillatory response through the experiment, with a higher COF value up to 3200 cycles, followed by a substantial reduction. The average result revealed a COF decrease of 2% for T7 texture.

Gachot et al. [38] presented a summary of surface texturing parameters depending on texture geometry and lubrication conditions. They concluded that a circular pocket is an effective texture geometry for diverse lubrication. Yet, the texture dimensions influence the entire tribological performance. In the absence of a clear trend of the texture's frictional behavior neither for G1 nor for G2, dimensional parameters presented in Table 6.2 were correlated with the tribological results. Figure 6.8 shows the average friction coefficient against dimple's density area, average diameter, and aspect ratio.

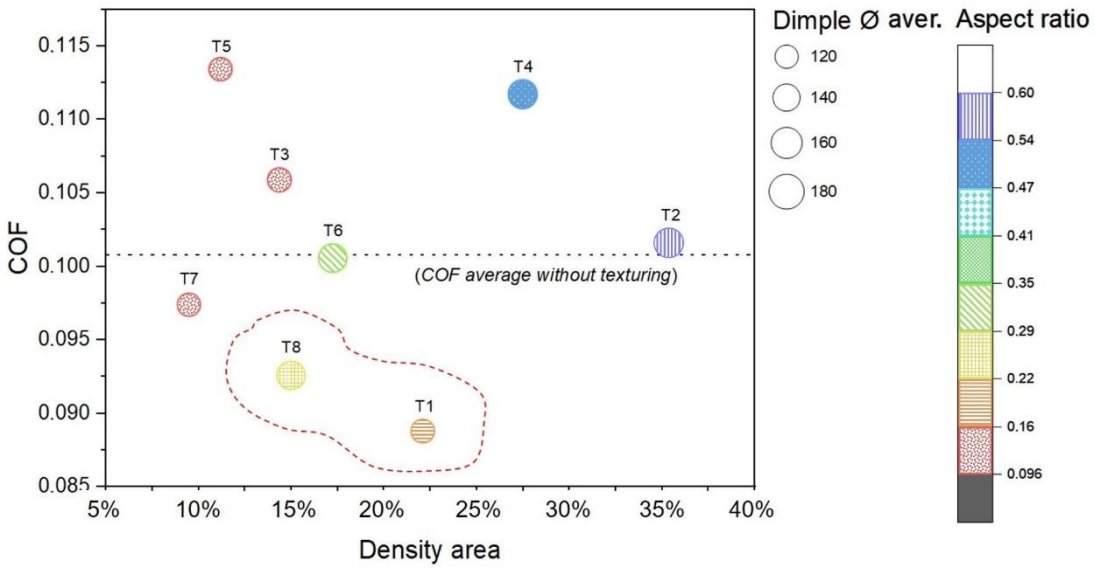


Figure 6.8 Effect of texture's geometric parameters on the friction coefficient results.

A minor variation in the average dimple's diameter of samples from both G1 and G2, of 132 μm and 161 μm. Wu [13] studied the influence of the surface texture parameters under starved lubrication. According to the simulation using TDC conditions, they concluded that distribution density was the parameter with a more significant influence on the friction coefficient reduction.

The dimple's depth was the second most influential parameter, and the dimple's diameter influence was minor.

The best results were obtained for samples with a texture density of 0.15 and 0.22 and an aspect ratio in the range [0.16-0.28]. Zavos and Nikolakopoulos referenced similar values for an optimum aspect ratio [39]. However, using either a different lubrication regime or the texturing of different contact geometries will define new optimum geometric and dimensional parameters. Schubert et al. [40] tested micro dimples on a flat ring-on-disc test rig under a fully-flooded regime and indicated 10% for the pattern density with the best friction coefficient. Wos et al. [41] evaluated the frictional response of dimpled textures, and those with 17% of area density achieved the best results under various lubrication regimes.

Those textures with the best COF results, T1 and T8, were submitted to a wear test to compare their wear resistance and effect on the cylinder liner counterpart with the non-textured samples. In Figure 6.9 are samples' friction coefficient and the weight loss, either of the piston ring samples or the cylinder liner counterpart.

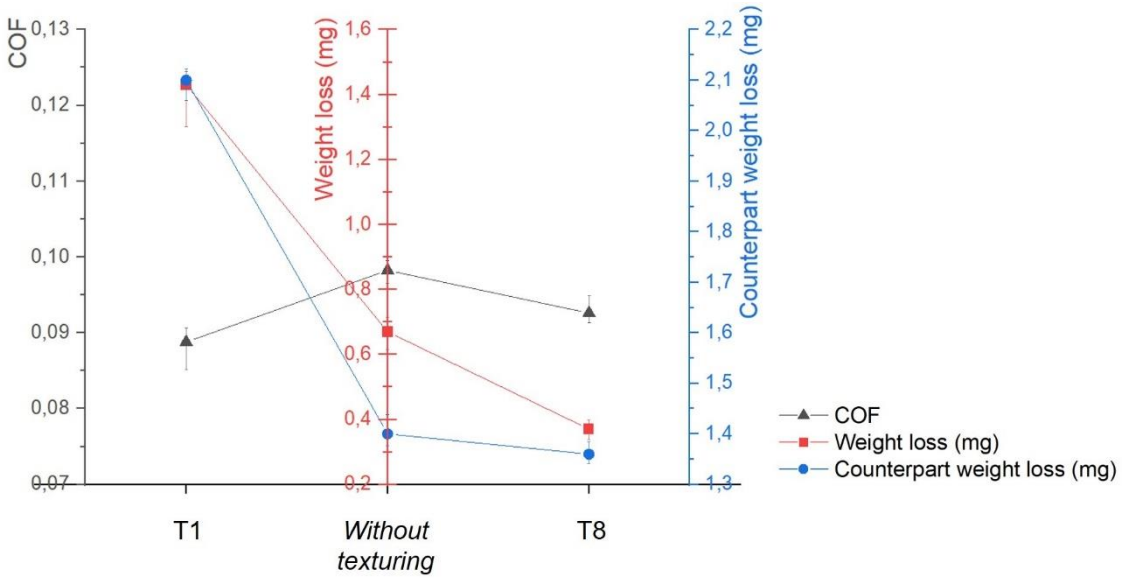


Figure 6.9 Wear test results comprising piston ring and cylinder liner weight loss.

Piston rings already had the previously deposited coating layer to improve their wear resistance. However, surface textures were expected to have an essential role in surface wear resistance. Arslam et el. [23] studied the tribological performance of a pre-textured surface with subsequent deposition of a diamond-like carbon coating. The group with 20% area density got the

best friction coefficient results and a lower wear rate than the untextured sample. Figure 10 exhibits the SEM images of the sample without texture and the T1 and T8 textures, before and after wear tests.

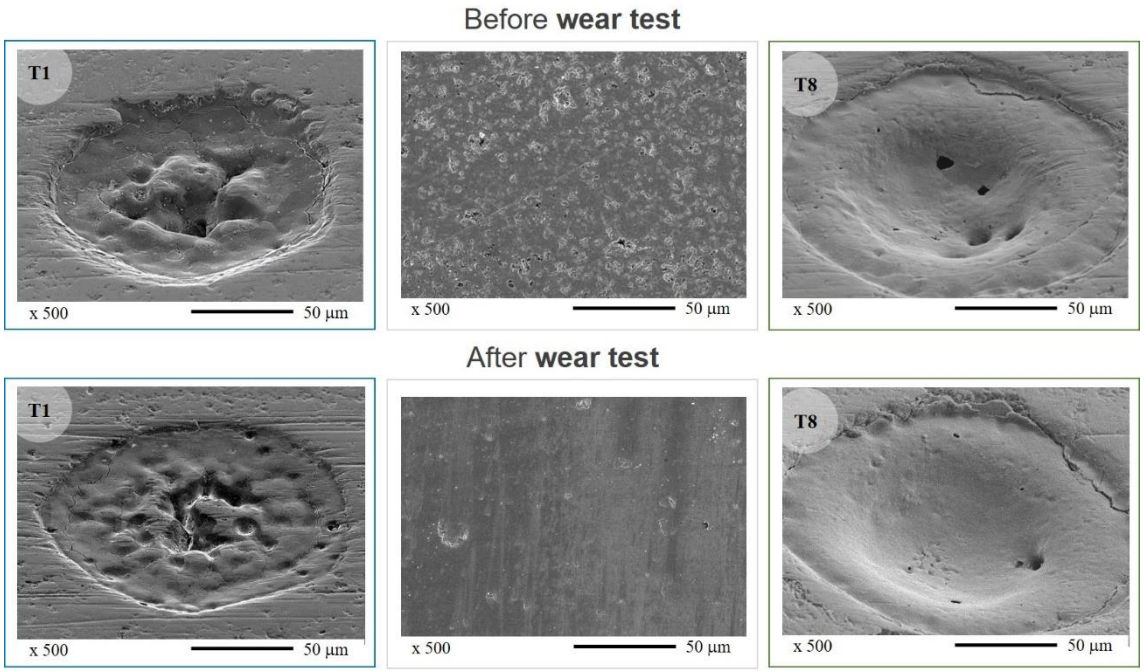


Figure 6.10 SEM micrography of non-textured samples and T1 and T8 piston-ring dimples before and after wear tests.

T1 was the texture with higher COF reduction but the worst performance in the wear test. The piston ring weight loss was superior to the untextured ring, and it produced an increased weight loss on the counterpart. After the wear test assessment, the entrapment of abrasive particles was noticed within some micro dimples. The shallower texture, T1, offered a lower volume for oil reservoirs and wear debris entrapment.

Conversely, deeper dimples of T8 created hydrodynamic pressure pockets. Under high sliding speed, the lubricant film thickness increased, and the contact occurred in a full fluid film lubricant regime.

The internal combustion engine operates in a complete duty cycle in different frictional regimes. T8 possessed the optimized dimple texture parameters, with a simultaneous improvement of the friction coefficient under a boundary lubrication regime and an enhanced wear resistance under a fully flooded film.

## 6.4 Concluding remarks

Friction and wear have a significant influence on the engine's energy consumption. NbN/CrN coated piston rings used in heavy-duty diesel engines were textured and tribologically evaluated using a home-developed tribometer. Several texture dimensions and densities were tested in the compression ring functional surface. According to specified and optimized texturing parameters, micro dimples have the potential to reduce friction-induced wear.

The reported friction coefficient results show that aspect ratio and density area were decisive variables. The wear resistance of textured samples with an enhanced friction coefficient was also compared with the untextured piston ring. T8 presented an overall improvement in the tribological performance with a lower weight loss and a minimized effect on the cylinder liner surface simultaneously. The alternative to a single texture with a global optimized performance could be to apply different textures for distinct purposes.

Further studies are expected about the influence of the secondary movement of the piston ring into the ring groove on the optimum texture parameters.

## Acknowledgments

This work was supported by FCT (Fundação para a Ciência e Tecnologia) and MAHLE, Componentes de Motores, S.A. through the grant SFRH/BDE/110654/2015 and by the project Add-Additive with the reference POCI-01-0247-FEDER-024533.

## References

[1] K. Holmberg, P. Andersson, N.O. Nylund, K. Mäkelä, A. Erdemir, Global energy consumption due to friction in trucks and buses, Tribol. Int. 78 (2014) 94–114. https://doi.org/10.1016/j.triboint.2014.05.004.
[2] K. Tamura, M. Kasai, Impact of Boundary Lubrication Performance of Engine Oils on Friction at Piston Ring-Cylinder Liner Interface Yukinobu Nakamura and Tomoyuki Enomoto, (2014) 875–881. https://doi.org/10.4271/2014-01-2787.
[3] A. Oliva, S. Held, Numerical multiphase simulation and validation of the fl ow in the piston ring pack of an internal combustion engine, Tribiology Int. 101 (2016) 98–109. https://doi.org/10.1016/j.triboint.2016.04.003.
[4] G.G. Fatjo, E.H. Smith, Piston-ring film thickness : Theory and experiment compared, 0 (2017) 1–18. https://doi.org/10.1177/1350650117722257.

[5] R. Ferreira, J. Martins, Ó. Carvalho, L. Sobral, S. Carvalho, F. Silva, Tribological solutions for engine piston ring surfaces: an overview on the materials and manufacturing, Mater. Manuf. Process. 35 (2020). https://doi.org/10.1080/10426914.2019.1692352.
[6] I. Etsion, E. Sher, Improving fuel efficiency with laser surface textured piston rings, Tribol. Int. 42 (2009) 542–547. https://doi.org/10.1016/j.triboint.2008.02.015.
[7] C. Shen, M.M. Khonsari, The effect of laser machined pockets on the lubrication of piston ring prototypes, Tribol. Int. 101 (2016) 273–283. https://doi.org/10.1016/j.triboint.2016.04.009.
[8] M.B. Dobrica, M. Fillon, M.D. Pascovici, T. Cicone, Optimizing surface texture for hydrodynamic lubricated contacts using a mass-conserving numerical approach, Proc. Inst. Mech. Eng. Part J J. Eng. Tribol. 224 (2010) 737–750. https://doi.org/10.1243/13506501JET673.
[9] E. Tomanik, Modelling the hydrodynamic support of cylinder bore and piston rings with laser textured surfaces, Tribol. Int. 59 (2013) 90–96. https://doi.org/10.1016/j.triboint.2012.01.016.
[10] A. Usman, C.W. Park, Optimizing the tribological performance of textured piston ring-liner contact for reduced frictional losses in SI engine: Warm operating conditions, Tribol. Int. 99 (2016) 224–236. https://doi.org/10.1016/j.triboint.2016.03.030.
[11] C. Gu, X. Meng, Y. Xie, Y. Yang, Effects of surface texturing on ring/liner friction under starved lubrication, Tribol. Int. 94 (2016) 591–605. https://doi.org/10.1016/j.triboint.2015.10.024.
[12] H.L. Costa, I.M. Hutchings, Some innovative surface texturing techniques for tribological purposes, Proc. Inst. Mech. Eng. Part J J. Eng. Tribol. 229 (2015) 429–448. https://doi.org/10.1177/1350650114539936.
[13] S. Wu, P. Zhang, H. Wei, L. Chen, Influence of Surface Texture Parameters on Friction Characteristics under Starved Lubrication, Polish Marit. Res. 27 (2020) 96–106. https://doi.org/10.2478/pomr-2020-0031.
[14] A. Ronen, I. Etsion, Y. Kligerman, Friction-reducing surface-texturing in reciprocating automotive components, Tribol. Trans. 44 (2001) 359–366. https://doi.org/10.1080/10402000108982468.
[15] A. Ronen, Y. Kligerman, I. Etsion, Different approaches for analysis of friction in surface textured reciprocating components, Proc. 2nd World .... 2 (2001) 2–5. http://techunix.technion.ac.il/~mermdyk/M-44-03-368-RONEN.pdf.
[16] I. Etsion, State of the art in laser surface texturing, J. Tribol. 127 (2005) 248–253. https://doi.org/10.1115/1.1828070.
[17] A. Kovalchenko, O. Ajayi, A. Erdemir, G. Fenske, I. Etsion, The effect of laser surface texturing on transitions in lubrication regimes during unidirectional sliding contact, Tribol. Int. 38 (2005) 219–225. https://doi.org/10.1016/j.triboint.2004.08.004.
[18] G. Ryk, Y. Kligerman, I. Etsion, A. Shinkarenko, Experimental investigation of partial laser surface texturing for piston-ring friction reduction, Tribol. Trans. 48 (2005) 583–588. https://doi.org/10.1080/05698190500313544.
[19] G. Ryk, I. Etsion, Testing piston rings with partial laser surface texturing for friction reduction, Wear. 261 (2006) 792–796. https://doi.org/10.1016/j.wear.2006.01.031.
[20] P. Lu, R.J.K. Wood, Tribological performance of surface texturing in mechanical applications-a review, Surf. Topogr. Metrol. Prop. 8 (2020). https://doi.org/10.1088/2051-672X/abb6d0.

[21] D. Braun, C. Greiner, J. Schneider, P. Gumbsch, Efficiency of laser surface texturing in the reduction of friction under mixed lubrication, Tribol. Int. 77 (2014) 142–147. https://doi.org/10.1016/j.triboint.2014.04.012.
[22] H.L. Costa, I.M. Hutchings, Hydrodynamic lubrication of textured steel surfaces under reciprocating sliding conditions, Tribol. Int. 40 (2007) 1227–1238. https://doi.org/10.1016/j.triboint.2007.01.014.
[23] A. Arslan, H.H. Masjuki, M.A. Kalam, M. Varman, M.H. Mosarof, R.A. Mufti, M.M. Quazi, L.S. Khuong, M. Liaqat, M. Jamshaid, A. Alabdulkarem, M. Khurram, Investigation of laser texture density and diameter on the tribological behavior of hydrogenated DLC coating with line contact configuration, Surf. Coatings Technol. 322 (2017) 31–37. https://doi.org/10.1016/j.surfcoat.2017.05.037.
[24] M. Sedlaček, B. Podgornik, A. Ramalho, D. Česnik, Influence of geometry and the sequence of surface texturing process on tribological properties, Tribol. Int. 115 (2017) 268–273. https://doi.org/10.1016/j.triboint.2017.06.001.
[25] E. Tomanik, Friction and wear bench tests of different engine liner surface finishes, Tribol. Int. 41 (2008) 1032–1038. https://doi.org/10.1016/j.triboint.2007.11.019.
[26] S. Mezghani, I. Demirci, H. Zahouani, M. El Mansori, The effect of groove texture patterns on piston-ring pack friction, Precis. Eng. 36 (2012) 210–217. https://doi.org/10.1016/j.precisioneng.2011.09.008.
[27] W. Grabon, P. Pawlus, S. Wos, W. Koszela, M. Wieczorowski, Effects of cylinder liner surface topography on friction and wear of liner-ring system at low temperature, Tribol. Int. 121 (2018) 148–160. https://doi.org/10.1016/j.triboint.2018.01.050.
[28] X. Rao, C. Sheng, Z. Guo, C. Yuan, Influence of Surface Groove Width on Tribological Performance for Cylinder Liner–Piston Ring Components, Tribol. Trans. 62 (2019) 239–248. https://doi.org/10.1080/10402004.2018.1539201.
[29] W. Grabon, P. Pawlus, S. Wos, W. Koszela, M. Wieczorowski, Effects of honed cylinder liner surface texture on tribological properties of piston ring-liner assembly in short time tests, Tribol. Int. 113 (2017) 137–148. https://doi.org/10.1016/j.triboint.2016.11.025.
[30] X. Rao, C. Sheng, Z. Guo, X. Zhang, H. Yin, C. Xu, C. Yuan, Effects of textured cylinder liner piston ring on performances of diesel engine under hot engine tests, Renew. Sustain. Energy Rev. 146 (2021) 111193. https://doi.org/10.1016/j.rser.2021.111193.
[31] C. Miao, Z. Guo, C. Yuan, Tribological behavior of co-textured cylinder liner-piston ring during running-in, Friction. (2021). https://doi.org/10.1007/s40544-021-0499-z.
[32] U. Pettersson, S. Jacobson, Influence of surface texture on boundary lubricated sliding contacts, Tribol. Int. 36 (2003) 857–864. https://doi.org/10.1016/S0301-679X(03)00104-X.
[33] A.A. Al-Azizi, O. Eryilmaz, A. Erdemir, S.H. Kim, Nano-texture for a wear-resistant and near-frictionless diamond-like carbon, Carbon N. Y. 73 (2014) 403–412. https://doi.org/10.1016/j.carbon.2014.03.003.
[34] D. He, S. Zheng, J. Pu, G. Zhang, L. Hu, Improving tribological properties of titanium alloys by combining laser surface texturing and diamond-like carbon film, Tribol. Int. 82 (2015) 20–27. https://doi.org/10.1016/j.triboint.2014.09.017.
[35] E. V. Zavedeev, O.S. Zilova, A.D. Barinov, M.L. Shupegin, N.R. Arutyunyan, B. Jaeggi, B. Neuenschwander, S.M. Pimenov, Femtosecond laser microstructuring of diamond-like nanocomposite films, Diam. Relat. Mater. 74 (2017) 45–52. https://doi.org/10.1016/j.diamond.2017.02.003.

[36] J.A. Araujo, R.M. Souza, N.B. De Lima, A.P. Tschiptschin, Thick CrN/NbN multilayer coating deposited by cathodic arc technique, Mater. Res. 20 (2017) 200–209. https://doi.org/10.1590/1980-5373-MR-2016-0293.
[37] R. Ferreira, Carvalho, J. Pires, L. Sobral, S. Carvalho, F. Silva, A New Tribometer for the Automotive Industry: Development and Experimental Validation, Exp. Mech. 62 (2022) 483–492. https://doi.org/10.1007/s11340-021-00805-7.
[38] C. Gachot, A. Rosenkranz, S.M. Hsu, H.L. Costa, A critical assessment of surface texturing for friction and wear improvement, Wear. 372–373 (2017) 21–41. https://doi.org/10.1016/j.wear.2016.11.020.
[39] A.B. Zavos, P.G. Nikolakopoulos, Simulation of piston ring tribology with surface texturing for internal combustion engines, Lubr. Sci. 27 (2015) 151–176. https://doi.org/10.1002/ls.1261.
[40] A. Schubert, R. Neugebauer, D. Sylla, M. Avila, M. Hackert, Manufacturing of surface microstructures for improved tribological efficiency of powertrain components and forming tools, CIRP J. Manuf. Sci. Technol. 4 (2011) 200–207. https://doi.org/10.1016/j.cirpj.2011.01.010.
[41] S. Wos, W. Koszela, P. Pawlus, Determination of oil demand for textured surfaces under conformal contact conditions, Tribol. Int. 93 (2016) 602–613. https://doi.org/10.1016/j.triboint.2015.05.016.

# CHAPTER 7.

## Design, manufacturing, and testing of a laser textured piston ring surface reinforced with a CuCoBe-diamond composite by hot-pressing.

Submitted to *Journal of Powder Technology* on: 21th of September, 2022
R. Ferreira [a,b,c,*], Â. Cunha [a,b], Ó. Carvalho [a,b], B. Trindade [d], L. Sobral [c], S. Carvalho [d,e], F. Silva [a,b]

[a] Centre for Micro-Electro Mechanical Systems (MEMS) University of Minho, Campus de Azurém, 4800-058 Guimarães, Portugal
[b] LABBELS –Associate Laboratory, Braga, Guimarães, Portugal
[c] MAHLE - Componentes de Motores S.A., Núcleo Industrial Murtede, 3060-372 Cantanhede, Portugal
[d] CEMMPRE – Center for Mechanical Engineering, Materials and Processes, University of Coimbra, 3030-788 Coimbra, Portugal
[e] Laboratory for Wear, Testing & Materials, Instituto Pedro Nunes, Rua Pedro Nunes, 3030 -199 Coimbra, Portugal

## Abstract

A CuCoBe – diamond composite was used to reinforce a laser textured 410 stainless steel piston ring by hot-pressing. Different hot pressing parameters were used for the optimization of the sintering process of the CuCoBe particles (P = 25 and 50 MPa, T = 820 and 980 C, and t = 15 and 30 min). The results showed an increase in the hardness of the hot-pressed samples (50.5 % and 48.5% for P= 25 and 50 MPa, respectively). Three textures with different track widths and distances between them were produced by laser on the compression piston rings' surface. The composite powders were used for the reinforcement of the textures by hot pressing at the optizimed sintering parameters (T = 980 °C, P = 25 and 50 MPa, and t = 15 min). The tribological results revealed that larger texture dimensions led to an enhanced tribological performance.

Keywords: *metal matrix composite; hot pressing; diamond; surface textures; tribology.*

## 7.1 Introduction

In the automotive industry, the constant enhancement of the final performance is related to the use of top-of-the-line materials. The better the material's response, the greater the improvement in the final part's performance. Thus, automotive and other demanding industries have researched to develop in situ metal matrix composites (MMCs) [1]. MMCs are widely used in automotive parts due to the variety of its properties [2,3]. The artificial introduction of rigid particles (or fibers) in a ductile metal or alloy matrix can improve the final material's properties. In addition, powder metallurgy shows remarkable advantages in production parts and components from economic and as well as environmental point of view. The reduced granulometry of the reinforcement particles makes these materials (named discontinuous reinforced materials) more cost-effective and valuable in production [4].

The tribological, thermal, and mechanical properties are critical when the material's end-use is in the internal combustion engine. The current target of the compression piston ring investigation is improving those properties. Due to its primary role (the combustion chamber sealing), the compression ring functional surface is continuously under hard tribological and thermal conditions. The conventional solution comprises a ceramic coating layer of a wear-resistant chemical compound deposited through a physical vapor deposition technique. However, the surface wear is not uniform along the whole surface and other relevant characteristics, such as thermal conductivity, are unsuitable for transferring the heat from the combustion chamber. According to the demanding performance, the most recent approach is to develop a multifunctional surface,

through the incorporation on the radial surface cavities of different composite materials, such as using a wear protective material in a confined surface area [5].

Several MMCs under development allow the simultaneous improvement of the tribological and thermal performances. Copper-based composites have been selected due to their high thermal conductivity, good ductility, high wear resistance, and low cost [6]. Copper is used as a metal matrix in composites applied in plane bearings for automobiles, drive shafts and roller bearings, spherical bushings for automotive transmissions, and overhead railways for dams and flood gates.

An advantage of producing new ceramic reinforced - metal matrix composites is combining the good mechanical properties of the metals (such as ductility and toughness) with the high strength and modulus of the ceramic reinforcement. The most common reinforcement materials for those applications are graphite particles, hBN, TiC, SiC, and diamond [7–9]. Diamond offers a group of characteristics: excellent thermal conductivity, great hardness, high wear resistance associated with a low coefficient of friction (COF), and good chemical stability [10]. Micro and nanodiamond particles are embedded in matrix support in wear protection or abrasive applications. The diamond-reinforced copper matrix composite forms a powder composite of a ductile metal shell with a wear-resistant core. The excellent thermal stability represents a fundamental property of diamond particles. However, carbon tends to degrade at high temperatures, with its conversion into a more thermodynamically stable phase (graphite) [8,11–14]. Some authors reported the surface graphitization of diamond particles in vacuum for temperatures is in the range 700°C-1400°C [15–17]. Most recently, Qian et al. [13] investigated the graphitization of diamond powders with sizes from 5 nm to 40 μm, at high pressure and temperature conditions and concluded that it strongly depends on diamond particle size. This effect occurs due to the large surface-to-volume ratio and high thermal conductivity of nanodiamonds. The onset temperature for nanodiamond graphitization was reported to be 666 °C (both in an inert gas at atmospheric pressure), while bulk diamond begins to graphitize above 1526 °C [18].

The manufacturing technology and processing techniques are limited to preserving these effective characteristics of the diamond particles. This constraint defines the upper limit to be implemented during manufacturing to avoid modifying the crystalline diamond structure. Moreover, an effective wetting of the dispersed reinforcement to the matrix prevents the failure of the composite. Conversely, particle clusters may generate high stress in those regions.

Hot-pressing has been shown as an effective and accurate sintering method [19–23], allowing the production of near-net-shaped parts from powders. The hot-pressing is related to high compression rates at high pressures. The mixed powder is simultaneously heated and pressed, producing a final part with enhanced physical properties. The sintering process occurs at 66-75% of the matrix melting point. The area of contact surface increases in proportion to the pressure applied. The applied external force increases the contact area and changes the shape of particles. The consequence of growth in the contact surface is raising the product's strength. The cohesion of particles in a powder pressing is caused by mechanical contact and interlocking among the surface ridges and irregularities of the particles. The temperature increases decrease the amount of pressure necessary for compacting the powder.

The main advantages of hot-pressing are to produce a material with a density up to 95% of the theoretical density and to reach properties close to the solid materials. Greater density is achieved with slower pressing resulting in enhanced final properties.

Few studies use exclusively diamond-reinforced Cu matrix composites without including a third element [24–27]. Some researchers reported poor interfacial bonding between Cu and diamond particles [28–33]. Some strategies to overcome this constraint have been proposed such as the coating the diamond particles or alloying of the metal matrix material. In both approaches the main purpose is the introduction of a carbide forming element (Ti [30,34,35], Cr [31,36–38] or Mo [28,39]). The result is the formation of an interfacial carbide layer at the surface of the diamond particles, physically separating the particles from the metal matrix material. However, in applications where the thermal resistance is determinant, the presence of an interlayer and the interlayer's properties will influence the results. In this case, the metal matrix alloying could be more effective.

To achieve an enhanced thermal conductivity, several authors studied the alloying of the Cu matrix using boron as the third element [32]. However, the interfacial bonding for alloyed metal matrix composites is not fully understood, and the interlayer's characterization is lacking.

From the standpoint of the leading project, the main goal was to develop, through powder metallurgy technology, a multi-material surface, as illustrated in Figure 7.1. In an earlier proposal [5] illustrated in Figure 7.1a), the composite material (for tribological purposes) would be applied in a confined and isolated bore. In the most recent design represented in Figure 7.1b), the

composite material is introduced in the textured cavities. The multi-material surface comprehends multiple regions strategically distributed along the piston ring surface, with the introduced material surrounding rectangular pillars.

Cunha et al. [40,41] explored the combination of a diamond-reinforced Cu-based alloy and a textured SS substrate with a similar distribution for tribological purposes. These authors were focused on the composite performance using different diamond particle sizes with distinct sintering techniques.

The aim of this study was to improve the surface properties of a 410 stainless steel (from now on referred to as 410 SS) piston ring by a CuCoBe-diamond composite.

In the first stage of this work, different hot-pressing parameters were used for composite optimization (mainly physical and metallurgical properties). Then, based on the results obtained, a bi-material (multifunctional surface) piston ring was produced by hot-pressing, consisting of a partial reinforcement of a previously laser-textured 410 SS by the CuCoBe-diamond composites. Different texturing densities (surface ratios between the 410 SS and the composite) and arrangements were produced and analyzed. The friction results and the wear resistance of the developed samples are assessed and discussed.

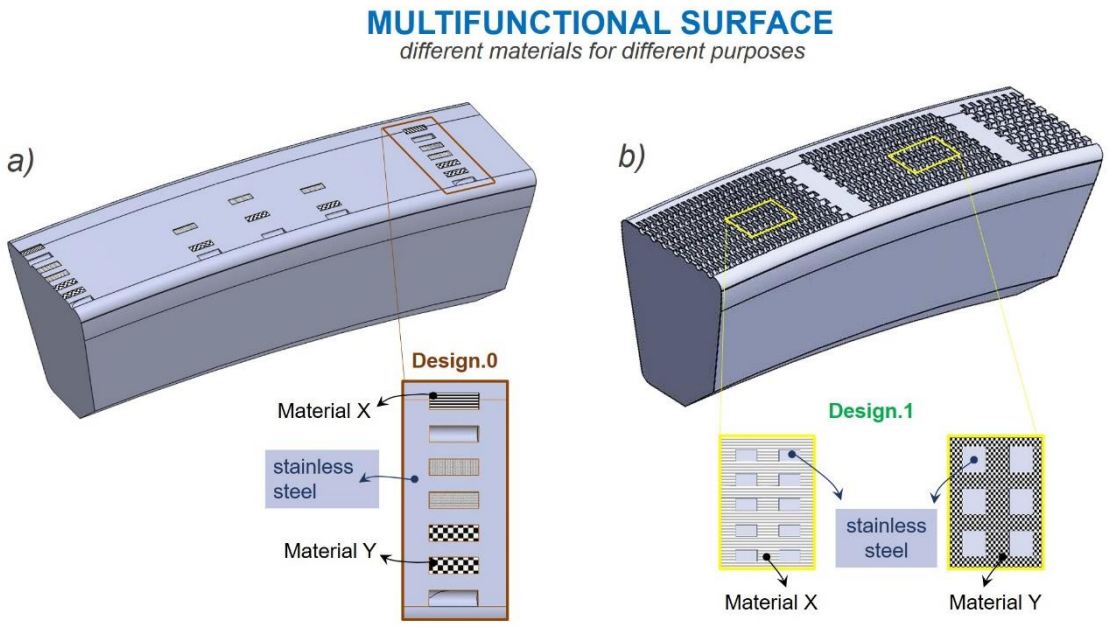


Figure 7.1 Illustration of two different approaches for the production of piston ring multifunctional surfaces: a) early design with the proposal of the piston ring surface reinforcement and b) adapted design to the hot-pressing manufacturing technique (adapted from [5]).

The m is to develop different materials for distinct purposes, such as heat conduction or friction reduction, by the same methodology.

## 7.2 Experimental procedure

### 7.2.1 Powder characterization

Commercial CuCoBe (1.5 wt.% Co and 0.5 wt.% Be) alloyed powders from Testbourne Ltd, England, with 99.9% purity, and diamond particles supplied by PlasmaChem GmbH, Germany, were used for the composites fabrication. The powders' morphology was characterized using an ultra-high-resolution field-emission scanning electron microscope (SEM) (Nova NanoSEM 200 microscope, FEI). The SEM micrographs of the CoCuBe powder and the diamond particles are presented in Figure 7.2a) and Figure 7.2b), respectively.

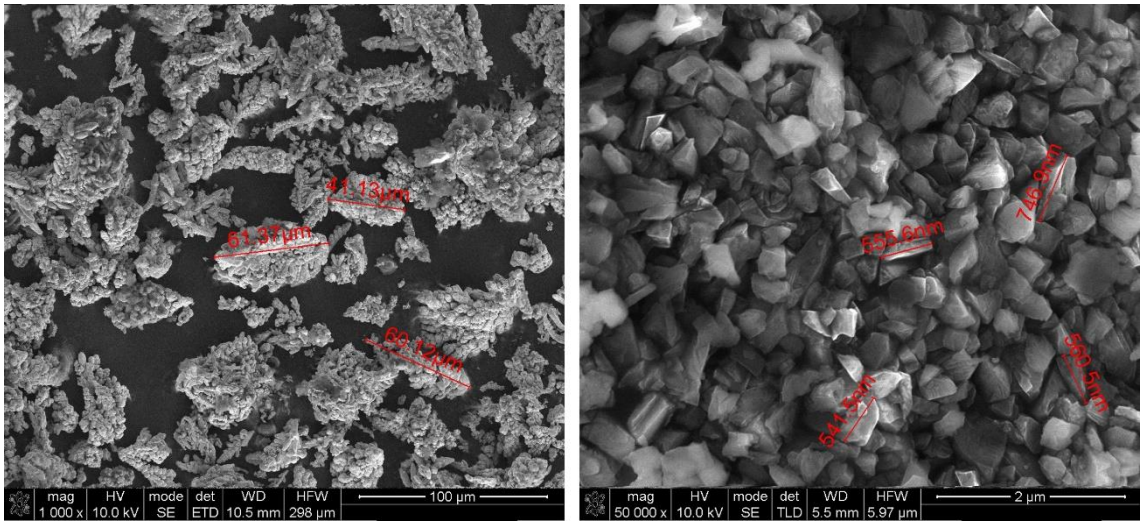


Figure 7.2 SEM micrographs of the a) CoCuBe alloy and b) diamond particles.

The CoCuBe powders present a dendritic morphology with a size of a few tens of micrometers. The diamond powders are sub-micrometers with relatively regular crystal form.

The CoCuBe particles were submitted to thermal analysis for a more effective manufacturing process control and an accurate definition of the hot-pressing conditions. Differential scanning calorimetry (DSC) measurements were performed using a SDT 2960 equipment (TA Instruments).

The samples (with 40-60 mg) were placed in sealed alumina pans under argon purge at a flow rate of 100 ml/min. The samples were heated from 25 °C to 1140°C, at an average heating rate of 15 °C/min.

Figure 7.3 presents the DSC results obtained. The melting temperature of the CoCuBe alloy was determined as 1084 °C.

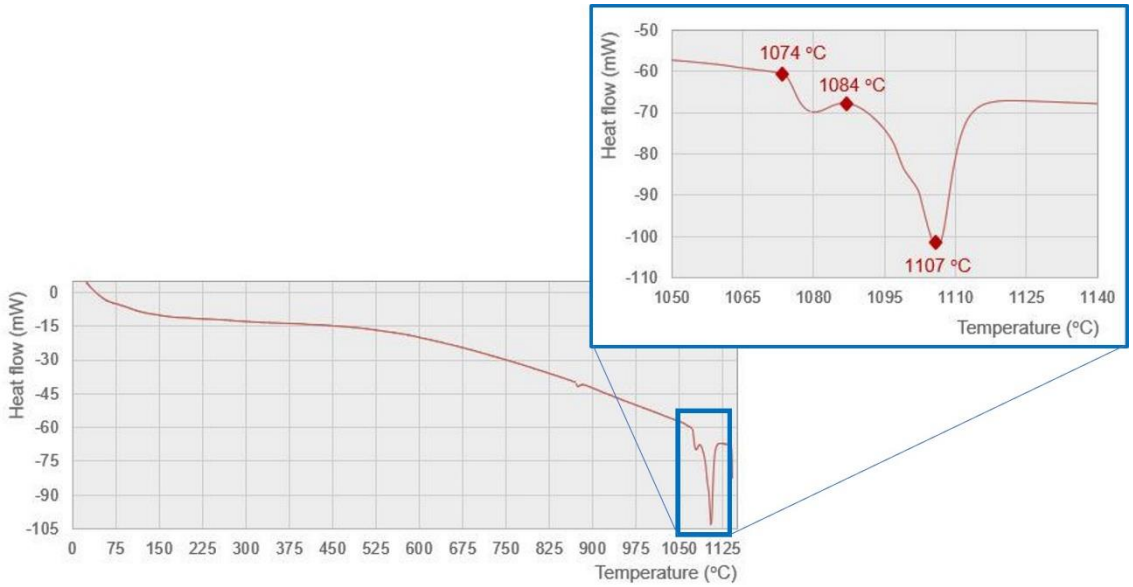


Figure 7.3 Differential scanning calorimetry (DSC) curve of the CoCuBe particles.

### 7.2.2 Manufacturing process

The methodology used for the fabrication of the samples is represented in Figure 7.4. In the first stage of this work, the particles of CoCuBe and diamond were blended in an ultrasonic processor, using 5 wt.% of diamond particles. The powder mixture was then placed inside the graphite mold (diameter of 14 mm) and hot-pressed with different parameters (applied pressure, temperature, and time) in order to optimize the hot-pressing procedure.

After this preliminary stage, a 410 SS piston ring was laser textured and reinforced with the CuCoBe-diamond composite by hot-pressing, in order to obtain a functionalized piston ring.

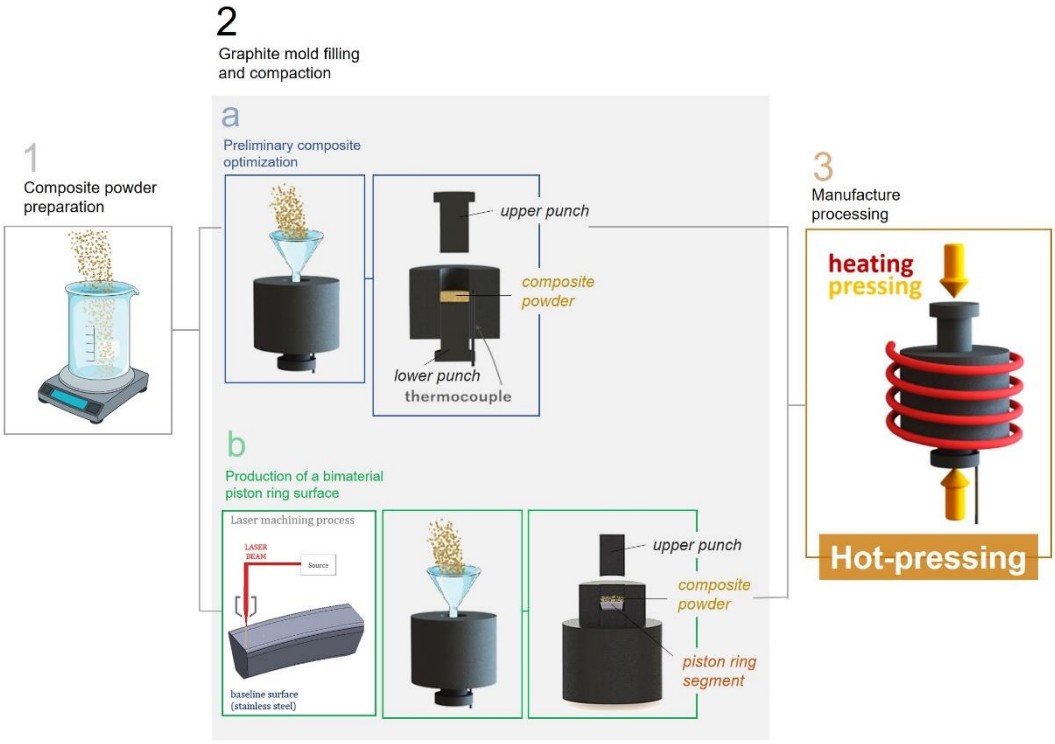


Figure 7.4 Experimental protocol applied in the hot-pressing manufacturing process.

## Stage I: Optimization of the hot-pressing process and production of the CuCoBe-diamond composite

The CoCuBe particles were placed inside a graphite mold (diameter of 14 mm) and hot-pressed with different parameters (Table 7.1). Two sintering temperatures (820 and 980 °C, corresponding to 75% and 90% of the melting temperature of the copper alloy, respectively), pressures (25 and 50 MPa), and dwell times (15 and 30 min) were studied. The higher pressure value was limited by the permission compressive strength of graphite mold. The surface of the graphite die cavity was painted with $ZrO_2$ to prevent carbon contamination of the samples from the mold. A thermocouple fitted in the graphite die controlled the temperature. The pressure-assisted sintering process was performed in a high-frequency induction furnace in a vacuum ($10^{-2}$ mBar) atmosphere. Hot-pressing was performed with a heating rate was 3 °C/sec, in a vacuum. The samples were cooled down up to room temperature inside the die.

After optimization of the hot pressing process, a mixture of CuCoBe with 5 wt.% of diamond particles was blended in an ultrasonic processor, with 5 wt.% of diamond particles. The powder mixture was then hot-pressed at 980 °C, with applied pressures of 25 MPa (T980_P25(C)_t15) and 50 MPa (T980_P50(C)_t15) for 15 min. The objective was to achieve the desired properties at the shorter sintering time possible at the maximum sintering temperature [42].

Table 7.1 Hot-pressing process parameters.

| Designation | Temperature, °C | Pressure, MPa | Time at temperature, min |
|---|---|---|---|
| T820_P25_t15 | 820 | 25 | 15 |
| T820_P25_t30 | | | 30 |
| T820_P50_t15 | | 50 | 15 |
| T820_P50_t30 | | | 30 |
| T980_P25_t15 | 980 | 25 | 15 |
| T980_P25_t30 | | | 30 |
| T980_P50_t15 | | | 15 |
| T980_P50_t30 | | | 30 |

**Stage II: Fabrication of a functionalized piston ring**

The radial surface of commercial 410 SS piston rings were textured through an Nd: YAG laser (Sisma Laser) with a wavelength of 1064 nm, laser power of 5 W, scan speed of 1000 mm/s, number of passes of 32 and frequency of 50 kHz. The geometry of the surface textures was designed to create channels for the composite material. The texture arrangement determined the density area and distribution of the composite material. The textured rings were filled with the CoCuBe-diamond particles. An upper punch with a concave geometry was used to fill the textured cavities. The reinforced samples were than hot pressed with the parameters as the CuCoBe - diamond composites.

### 7.2.3 Characterization of the samples

The morphology and microstructure of all the samples were characterized by SEM. The fracture surface analysis of the hot-pressed CuCoBe alloy was performed through SEM cross-sectional evaluation. Their density was measured by the Archimedes' method. The theoretical density was calculated by the rule of mixtures. The density of copper was considered 8.94 g/cm$^3$

[43] and the density of diamond particles of 3.5 g/cm$^3$ [24]. The relative density of the samples was determined by the measured and the theoretical densities ratio.

X-ray diffraction (XRD) using a Bruker D8 Discover diffractometer was used for phase analysis, with a Bragg-Brentano geometry from 20° to 100° and CuKα radiation. The step size and the acquisition time were 0.04° and 4 s/step, respectively.

All the samples were mechanically characterized through hardness measurements using a EMCO-TEST (DuraScan model) equipment. Five Vickers hardness indentations were made in each sample with an applied load of 30 Kgf and a dwell time of 20 s. The microhardness values were calculated based on optical micrographs and an image processing software (ImageJ).

The tribological performance of the reinforced surfaces was evaluated using a home-developed tribometer [44]. The wear tests were conducted at a sliding speed of 0.3 m/s and an axial load in the range of 350-380 N for 240 min. The lubrication contact was established using a 0W20 fully flooded film at 135 ± 5 °C, containing alumina particles of 5 μm. The coefficient of friction was assessed with a normal load of 10-11 N at a low speed (0.026 m/s) to simulate the top dead center operating conditions. The boundary lubrication regime that occurs in the sliding direction reversal was created using a syringe with a 0.0258 ml of oil dosage dispensed into the contacting area.

All tribological experiments were performed using the samples of a grey cast iron commercial cylinder liner from a heavy-duty diesel engine. The cylinder liner surface represented in Figure 7.5 exhibits a cross-hatched honing texture used to lodge small abrasive particles and to distribute the lubrication oil through the inner wall. The morphology and topography of the produced piston rings and the cylinder counterpart were assessed by SEM before and after tribological testing.

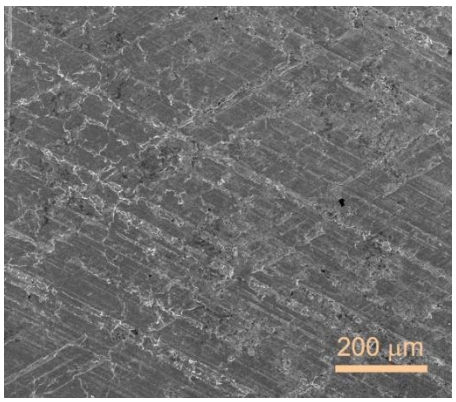


Figure 7.5 The cross-hatched texture of the cylinder liner's inner surface.

## 7.3 Results and Discussion

### 7.3.1 Hot pressing of the CuCoBe powders

Figure 7.6 presents the SEM microstructures of the cross-section fractures of the CuCoBe samples manufactured with different hot-pressing parameters.

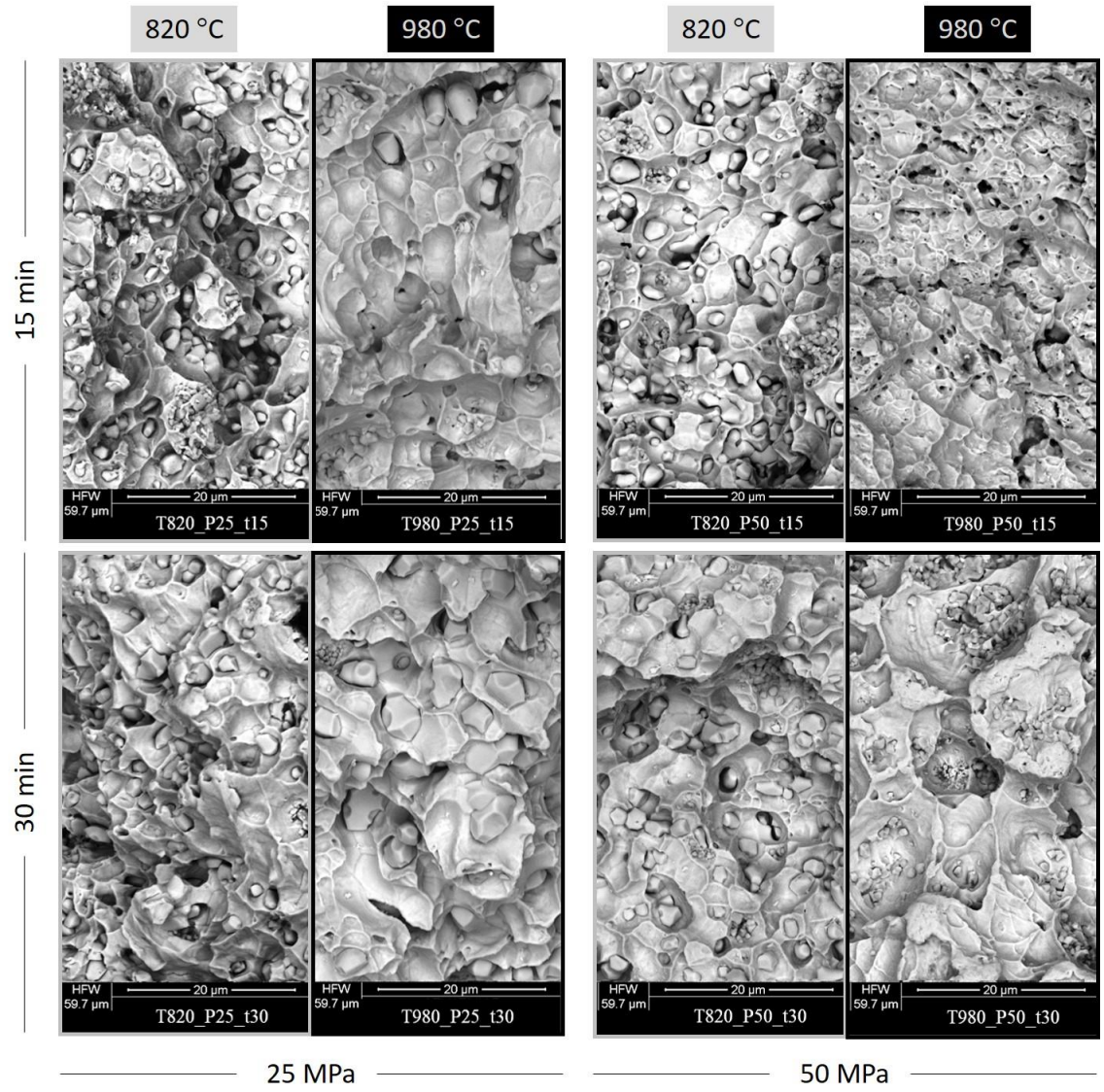


Figure 7.6 SEM micrographs of the cross-sectional fracture of the hot-pressed CuCoBe samples produced at T = 820 and 980 °C, P = 25 and 50 MPa, and t = 15 and 30 min.

For the sintering temperature of 820 °C (temperature below the threshold temperature), the porosity of the samples was relatively high, even for the most elevated applied pressure (50 MPa) and dwell time (30 min.). This means that the sintering process was ineffective, possibly due to the insufficient presence of the liquid phase. The fracture surfaces exhibit many dimples, corresponding to a ductile transgranular failure.

The SEM images of the samples hot-pressed at 980°C (T980_P25_t15 and T980_P50_t15) show a decrease in the number and depth of dimples, corresponding to a more brittle failure. Moreover, compared to the samples processed at 820°C, a grain size increase was observed.

The hardness measurement results are presented in Figure 7.7.

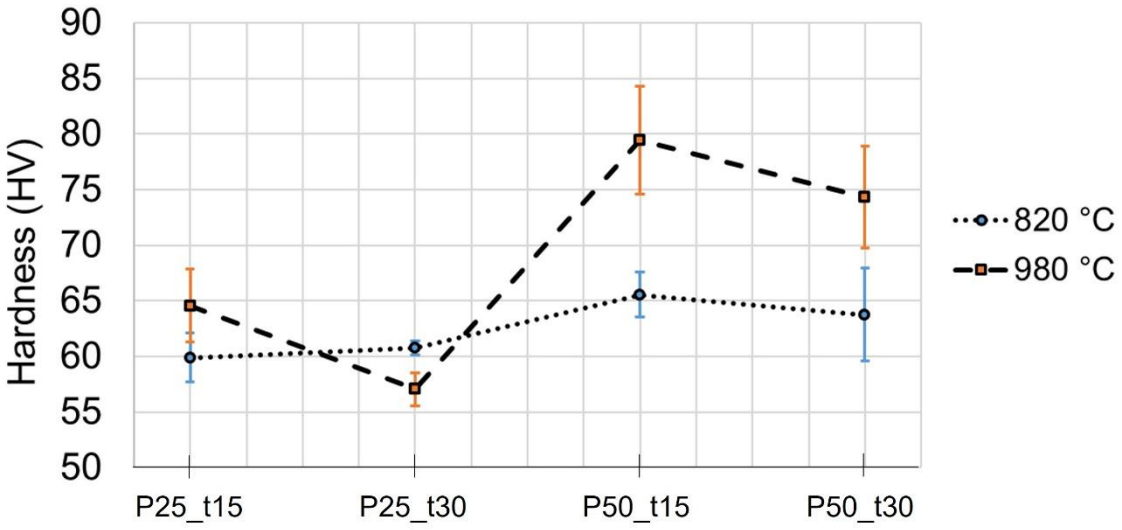


Figure 7.7 Hardness measurement results of the composite samples produced at sintering temperatures of 820 and 980°C.

The hardness results are consistent with the literature. Values of 71.05 HV [43] and 65 HV [42] are reported in the literature for pure copper produced by hot pressing. The applied pressure and dwell time had a negligible influence on the hardness of the samples processed at 820°C. Conversely, a lower grain size was observed for 980 °C. The increase of the applied pressure restrained the grain growth during sintering with a corresponding hardness increase. The hardness of the specimen T980_P50_t15 was enhanced by 23% compared with specimen T980_P25_t15. Contrarily, the increase in the dwell time led to a hardness decrease.

### 7.3.2 Hot pressing of the CuCoBe - diamond composite

Figure 7.8 shows SEM images of the polished surface of the sintered samples. An effective reinforcement dispersion into the matrix powder material was achieved for both sintering conditions.

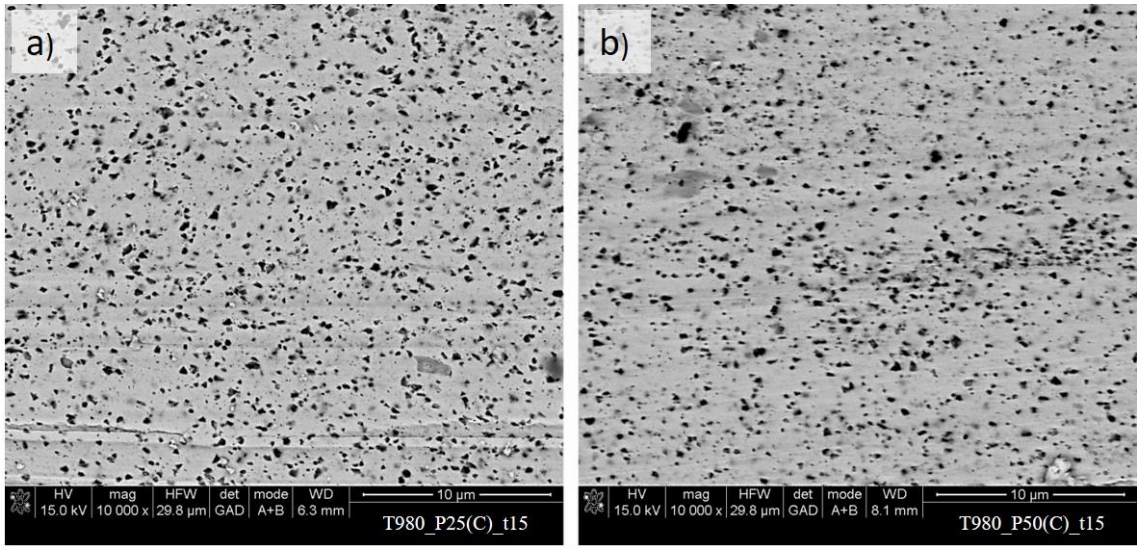


Figure 7.8 SEM micrographs of the CuCoBe – diamond samples processed at 980°C, with pressures of a) 25 and b) 50 MPa and a dwell time of 15 min. (T980_P25(C)_t15 and T980_P50(C)_t15, respectively).

The results of the hardness and density measurements are exhibited in Figure 7.9.

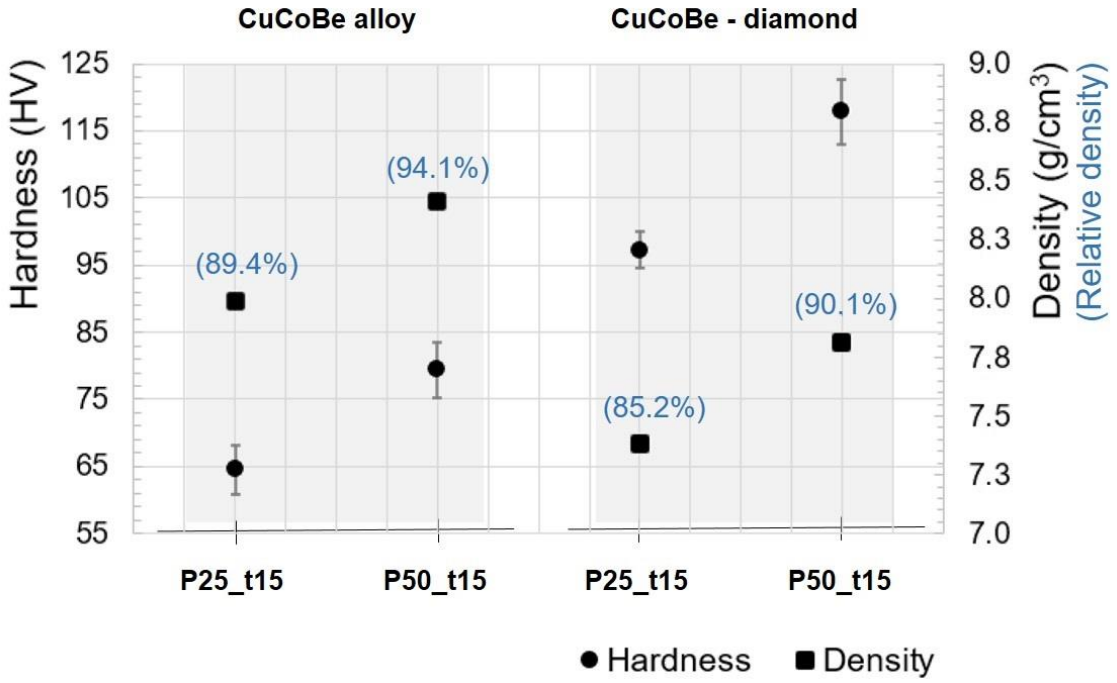


Figure 7.9 Hardness results and measured density of the hot-pressed samples.

The relative density of the non-reinforced samples was improved by increasing the hot-pressing pressure. At 50 MPa, the Cu matrix alloy achieved a relative density of 94,1%, representing an improvement of approximately 5%. Compared to the CuCoBe samples, the diamond-reinforced composite samples processed at 25 and 50 MPa revealed a hardness increase of 50.5 and 48.5%, respectively.

The density of the composite samples decreased compared with the CuCoBe alloy. However, the increase of hot-pressing pressure positively affected the final density. The presence of the diamond particles inhibited the particle rearrangement and, consequently, the coarsening and grain growth during sintering. The fractured morphology of the composite samples is presented in Figure 7.10.

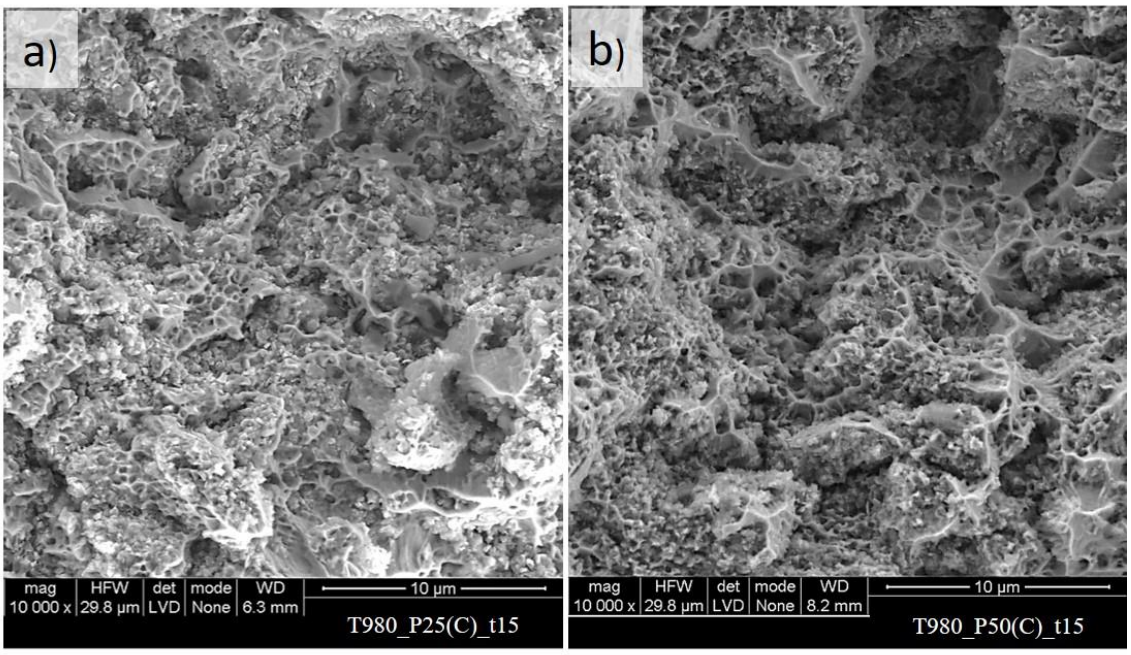


Figure 7.10 SEM micrographs of the cross-sectional fracture of the a) T980_P25(C)_t15 and b) T980_P50(C)_t15 composite samples.

As expected, the diamond particles affected the morphology of the cross-sectional fracture. The fractures of the composite samples present inhomogeneous dimple cavities, with larger grains exhibiting a brittle fracture and small and deep grains of a ductile fracture mechanism. Moreover, they presented a decreased grain size and a denser morphology when compared to the corresponding unreinforced samples. Figure 7.11 shows the XRD patterns of the composite samples.

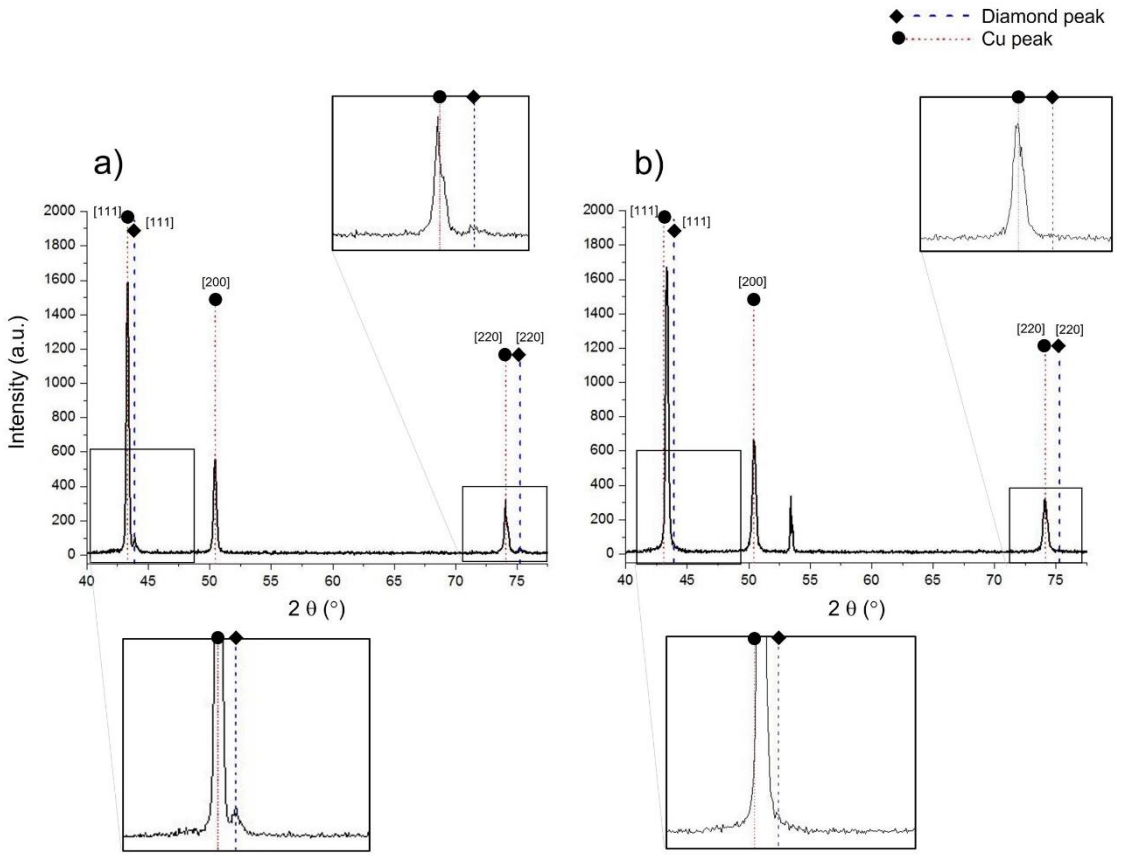


Figure 7.11 XRD patterns of the CuCoBe – diamond samples produced at T = 980°C, and a) P = 25 MPa and b) 50 MPa.

For both hot pressing conditions, the XRD diffractograms show one intense peak located at 2θ ~ 43.32°, and three peaks with relatively lower intensities (50.4°, 74.1°, and 89.8°), corresponding to the FCC copper phase. The main diffraction peak of diamond (111) is detected just for the sample sintered at the lower pressure (P = 25 MPa), suggesting that graphitization occurred only for the maximum applied pressure. This observation is not in agreement with the bibliography data [13] but it might be explained by the diamond particle size. It is established that the pressure and temperature variations result in a more significant effect on the diamond's thermal stability of smaller particles. Particles with 0.5 μm of size have higher surface defects and lower activation energies than bigger ones [45]. In the present work, the increase of the sintering pressure (for the same temperature and holding time conditions) raised the composite powder's contact surface and triggered the diamond to graphite phase transition.

### 7.3.3 Piston rings testing

Figure 7.12 exhibits the three distinct textures, A, B, and C, with different texturing densities and arrangements.

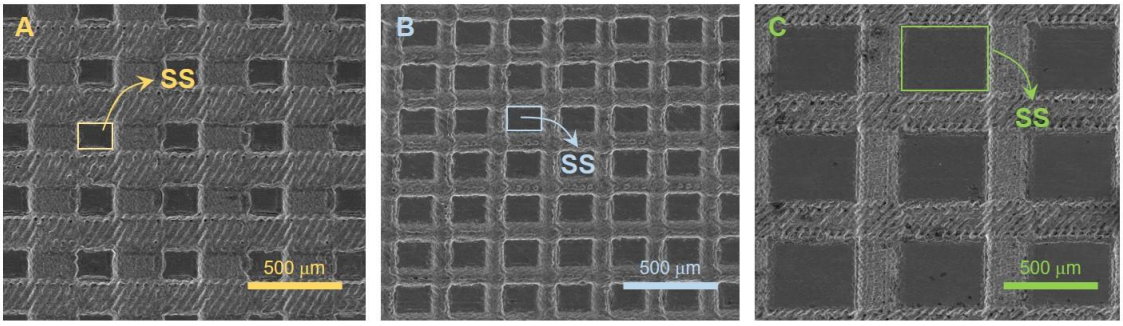


| | |
|---|---|
| Stainless steel | 25 % |
| Cu-based composite | 75 % |

| | |
|---|---|
| Stainless steel | 47 % |
| Cu-based composite | 53 % |

| | |
|---|---|
| Stainless steel | 48 % |
| Cu-based composite | 52 % |

Figure 7.12 Textures A, B, and C machined in the piston ring functional surface through laser surface texturing.

All the textures consisted of rectangular-like elements. Texture A exhibits higher surface textured area (75%) than the other two (B and C). These two have similar texturing densities but different tracks widths and distances between them.

Figure 7.13 shows SEM images of the surfaces of the CuCoBe-diamond reinforced laser textured samples before and after the tribological trials. In the same figure are exhibited the morphology of counterpart worn surfaces.

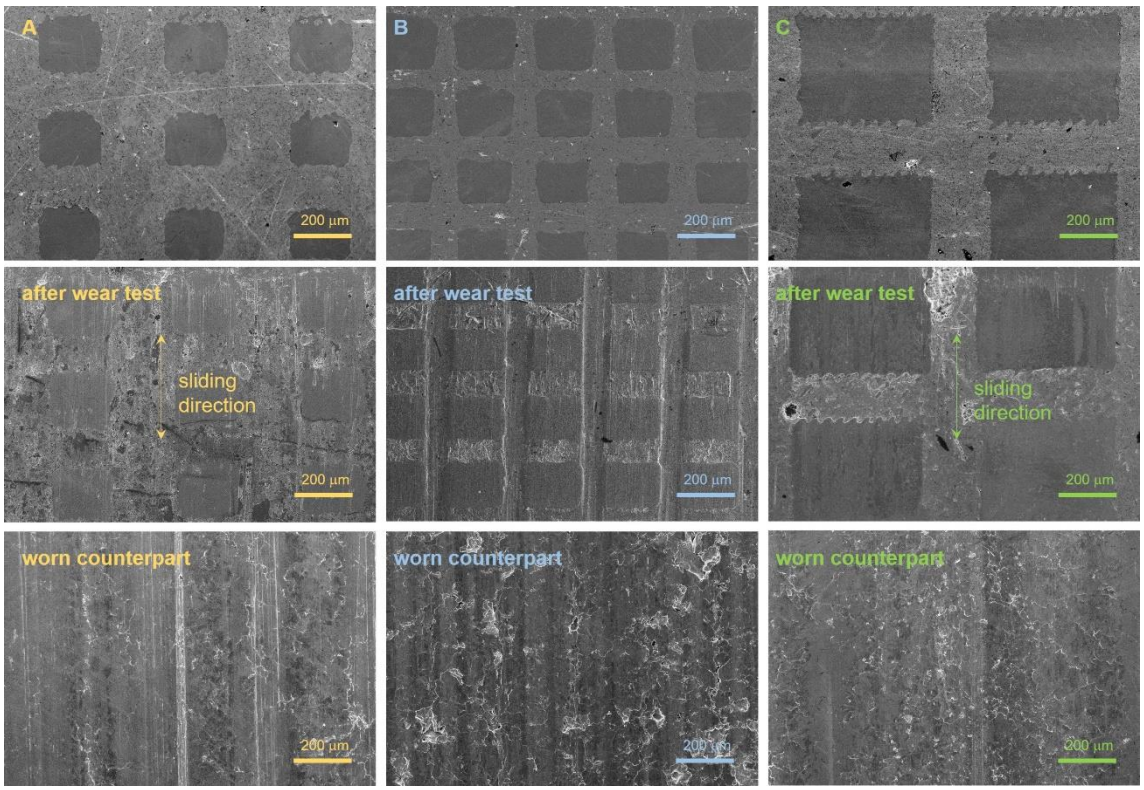


Figure 7.13 SEM images of the reinforced textured surfaces before and after wear tests and the respective worn counterpart.

Figure 7.13 a) to c), show that the hot-pressing process did not alter the surface texture geometry. Wear tracks in the 410 SS material are perceptible along the composite lines, revealing the sliding movement direction. This effect is more noticeable in texture B. The absence of grooves and scratches in the texture C surface indicates its enhanced wear resistance.

In all cases, an abrasive effect on the counterpart surface was detected. Like in the samples rings' surface, this effect is more pronounced for textures A and B.

The wear resistance of the functionalized surfaces was quantified through the weight balance of piston rings and liners samples. Figure 7.14 presents the samples' weight balance and friction coefficient results of a baseline piston ring and functionalized A, B, and C textures. The baseline results for weight balance were obtained by Ferreira et al. [46] using the same wear test protocol but with a 5W30 lubrication oil. The friction coefficient measurement of the conventional piston ring solution (used as a baseline) was performed in the present study, following the test parameters of the remaining samples.

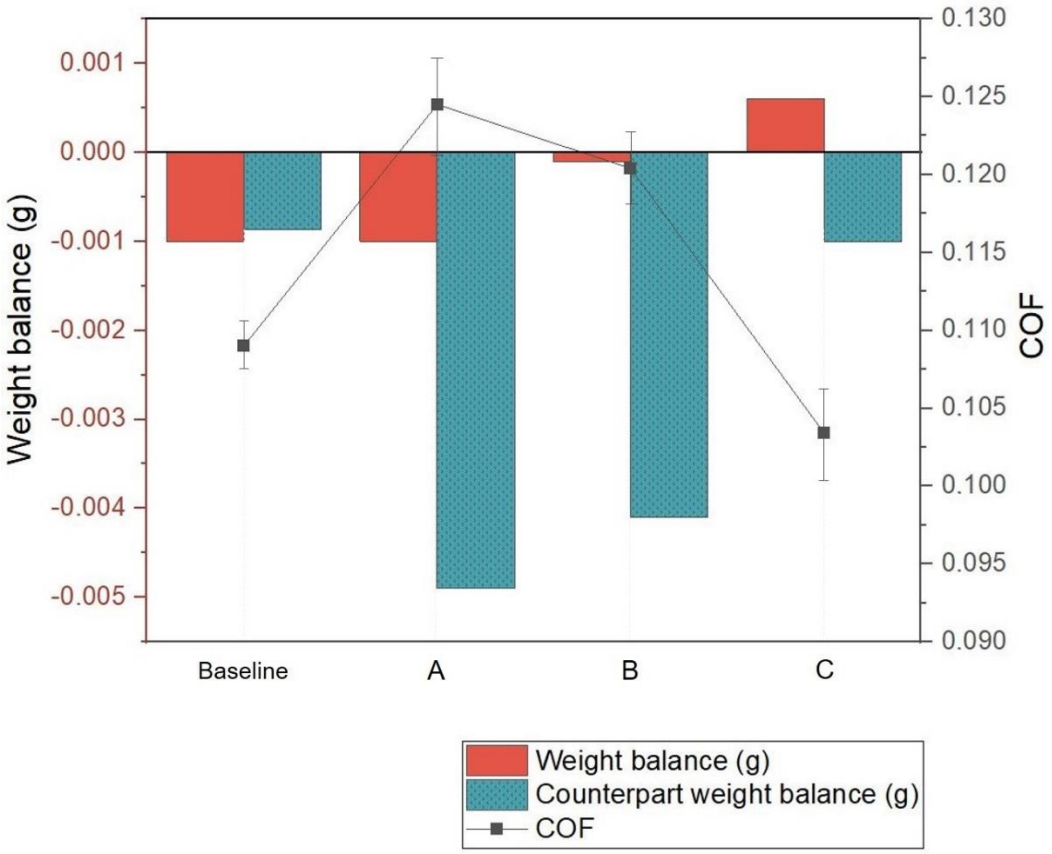


Figure 7.14 Weight balance of piston rings and counterpart samples and friction coefficient results.

Regarding the piston ring samples' weight loss and wear resistance, texture A exhibited a similar result to the baseline piston ring. Textures B and C achieved an almost negligible weight loss (B) or even an increase in the final weight (C). The attachment of wear debris or counterpart material might cause the piston ring weight to increase. This result is consistent with the morphology exhibited in Figure 7.13 for the worn surface of texture C.

The enhanced wear resistance of the functionalized piston rings had an abrasive effect on the cylinder liner, with an increased weight loss of the respective counterpart surface compared with the baseline results. The obtained friction coefficient values are distributed in a narrow range, from 0.103 to 0.125. Textures A and B revealed higher COF values than baseline. However, those are consistent with the literature [44] for top dead-center operating conditions. The texture with larger SS geometries improved 4.5% the COF.

The main goal of the piston ring-cylinder liner pair is enhancing the piston ring surfaces' wear resistance without threatening the counterpart tribological performance. The leading design

corresponding to texture C, with enhanced wear resistance and presented a reduced weight loss of the counterpart.

## 7.4 Concluding remarks

The hot-pressed CuCoBe-diamond composites revealed improved density and hardness properties with increasing sintering temperature and pressure. The reinforced samples processed at 25 and 50 MPa revealed a hardness increase of 50.5 and 48.5%, respectively.

Laser surface texturing and hot-pressing were disclosed as effective manufacturing techniques to produce functionalized piston ring surfaces. The dimensional characteristics of the surface textures were revealed to have a more significant influence on the piston ring tribological performance than the surface area ratio of each material. The texture with larger SS geometries improved the piston ring surface wear resistance (presented lower weight loss) and the reduced 4.5%.

## Acknowledgments

Funding: This work was supported by the Fundação para a Ciência e Tecnologia (FCT) and MAHLE, Componentes de Motores, S.A. [grant number SFRH/BDE/110654/2015]; the FCT via UID/EEA/04436/2019 and UIDB/00285/2020; and LA/P/0112/2020 and by FEDER funds through the COMPETE 2020 – Programa Operacional Competitividade e Internacionalização (POCI) [reference project POCI-01-0145-FEDER-030416].

## References

[1] Tung SC, McMillan ML. Automotive tribology overview of current advances and challenges for the future. Tribol Int 2004;37:517–36. https://doi.org/10.1016/j.triboint.2004.01.013.
[2] Barbezat G. Advanced thermal spray technology and coating for lightweight engine blocks for the automotive industry. Surf Coatings Technol 2005;200:1990–3. https://doi.org/10.1016/j.surfcoat.2005.08.017.
[3] Dahlström M, Larsson M, Giraud Y. High performance PM components heat treated by low pressure carburizing and gas quenching. Int. Powder Metall. Congr. Exhib. Euro PM 2013, 2013, p. 1–7.

[4] Mitra R. Intermetallic Matrix Composites - Properties and Applications. Matthew Deans; 2018.
[5] Ferreira R, Martins J, Carvalho Ó, Sobral L, Carvalho S, Silva F. Tribological solutions for engine piston ring surfaces : an overview on the materials and manufacturing and manufacturing. Mater Manuf Process 2020;35:498–520. https://doi.org/10.1080/10426914.2019.1692352.
[6] Yoshida K, Morigami H. Thermal properties of diamond/copper composite material. Microelectron Reliab 2004;44:303–8. https://doi.org/10.1016/S0026-2714(03)00215-4.
[7] Boland JN, Li XS. Microstructural characterisation and wear behaviour of diamond composite materials. Materials (Basel) 2010;3:1390–419. https://doi.org/10.3390/ma3021390.
[8] Jianxin D, Hui Z, Ze W, Aihua L. Friction and wear behavior of polycrystalline diamond at temperatures up to 700 ??c. Int J Refract Met Hard Mater 2011;29:631–8. https://doi.org/10.1016/j.ijrmhm.2011.04.011.
[9] Tran QP, Chin TS, Kuo YC, Jin CX, Trung T, Tuan C Van, et al. Diamond powder incorporated oxide layers formed on 6061 Al alloy by plasma electrolytic oxidation. J Alloys Compd 2018;751:289–98. https://doi.org/10.1016/j.jallcom.2018.04.089.
[10] Zhang C, Cai Z, Tang Y, Wang R, Peng C, Feng Y. Microstructure and thermal behavior of diamond/Cu composites: Effects of surface modification. Diam Relat Mater 2018;86:98–108. https://doi.org/10.1016/j.diamond.2018.04.020.
[11] Fedoseev D V., Vnukov SP, Bukhovets VL, Anikin BA. Surface graphitization of diamond at high temperatures. Surf Coatings Technol 1986;28:207–14. https://doi.org/10.1016/0257-8972(86)90059-9.
[12] Butenko Y V., Kuznetsov VL, Chuvilin AL, Kolomiichuk VN, Stankus S V., Khairulin RA, et al. Kinetics of the graphitization of dispersed diamonds at “low” temperatures. J Appl Phys 2000;88:4380–8. https://doi.org/10.1063/1.1289791.
[13] Qian J, Pantea C, Huang J, Zerda TW, Zhao Y. Graphitization of diamond powders of different sizes at high pressure-high temperature. Carbon N Y 2004;42:2691–7. https://doi.org/10.1016/j.carbon.2004.06.017.
[14] Westraadt JE, Sigalas I, Neethling JH. Characterisation of thermally degraded polycrystalline diamond. Int J Refract Met Hard Mater 2015;48:286–92. https://doi.org/10.1016/j.ijrmhm.2014.08.008.
[15] Uspenskaya KC, Tormashev UN, Fedoceev DV. Oxidization and graphitization of diamond in condition of low pressure atmosphere. J Phys Chem 1982;56:495–6.
[16] Breusov ON, Drobishev VN, Ivanchihina GE, et al. Effect of high temperature vacuum annealing on properties of detonation synthetic diamond. Proc. Int. Symp. Physico-chemical Prop. Ultra-hard Mater., 1987, p. 48–53.
[17] Fedoseev D V., Buhovets VL, Vnukov SP, et al. Graphitization of diamond at high temperatures, surfacial and thermo-physical properties of diamond. Proc. Int. Symp. Physico-chemical Prop. Ultra-hard Mater., 1985, p. 6–9.
[18] Xu NS, Chen J, Deng SZ. Effect of heat treatment on the properties of nano-diamond under oxygen and argon ambient. Diam Relat Mater 2002;11:249–56. https://doi.org/10.1016/S0925-9635(01)00680-X.
[19] Romanski A. Phase transformation in hot pressed cobalt and cobalt-diamond materials. Powder Metall 2007;50:115–9. https://doi.org/10.1179/174329007X153260.
[20] Ji G, Tan Z, Lu Y, Schryvers D, Li Z, Zhang D. Heterogeneous interfacial chemical nature and bonds in a W-coated diamond/Al composite. Mater Charact 2016;112:129–33. https://doi.org/10.1016/j.matchar.2015.12.013.

[21] Mechnik VA, Bondarenko NA, Dub SN, Kolodnitskyi VM, Nesterenko Y V., Kuzin NO, et al. A study of microstructure of Fe-Cu-Ni-Sn and Fe-Cu-Ni-Sn-VN metal matrix for diamond containing composites. Mater Charact 2018;146:209–16. https://doi.org/10.1016/j.matchar.2018.10.002.
[22] Hou M, Guo S, Yang L, Gao J, Peng J, Hu T, et al. Fabrication of Fe–Cu matrix diamond composite by microwave hot pressing sintering. Powder Technol 2018;338:36–43. https://doi.org/10.1016/j.powtec.2018.06.043.
[23] Hou M, Guo S, Yang L, Ullah E, Gao J, Hu T, et al. Microwave hot press sintering: New attempt for the fabrication of Fe–Cu pre-alloyed matrix in super-hard material. Powder Technol 2019;356:403–13. https://doi.org/10.1016/j.powtec.2019.08.055.
[24] Guillemet T, Geffroy PM, Heintz JM, Chandra N, Lu Y, Silvain JF. An innovative process to fabricate copper/diamond composite films for thermal management applications. Compos Part A Appl Sci Manuf 2012;43:1746–53. https://doi.org/10.1016/j.compositesa.2012.04.015.
[25] Wu Y, Sun Y, Luo J, Cheng P, Wang Y, Wang H, et al. Microstructure of Cu-diamond composites with near-perfect interfaces prepared via electroplating and its thermal properties. Mater Charact 2019;150:199–206. https://doi.org/10.1016/j.matchar.2019.02.018.
[26] Liu D, Tian H, Lin L, Shi W. Microstructure, mechanical and elevated temperature tribological behaviors of the diamond/Cu composites prepared by spark plasma sintering method. Diam Relat Mater 2019;91:138–43. https://doi.org/10.1016/j.diamond.2018.10.022.
[27] Cunha Â, Marques A, Monteiro F, Silva J, Silva M, Trindade B, et al. Tribological behavior of 316l stainless steel reinforced with cucobe + diamond composites by laser sintering and hot pressing: A comparative statistical study. Lect Notes Comput Sci (Including Subser Lect Notes Artif Intell Lect Notes Bioinformatics) 2020;12251 LNCS. https://doi.org/10.1007/978-3-030-58808-3_18.
[28] Kang Q, He X, Ren S, Zhang L, Wu M, Guo C, et al. Effect of molybdenum carbide intermediate layers on thermal properties of copper-diamond composites. J Alloys Compd 2013;576:380–5. https://doi.org/10.1016/j.jallcom.2013.04.121.
[29] Chu K, Jia C, Guo H, Li W. On the thermal conductivity of Cu-Zr/diamond composites. Mater Des 2013;45:36–42. https://doi.org/10.1016/j.matdes.2012.09.006.
[30] Che QL, Zhang JJ, Chen XK, Ji YQ, Li YW, Wang LX, et al. Spark plasma sintering of titanium-coated diamond and copper-titanium powder to enhance thermal conductivity od diaamond/copper composites. Mater Sci Semicond Process 2015;33:67–75.
[31] Cui W, Xu H, Chen J, Ren S, He X, Qu X. Effect of sintering on the relative density of Cr-coated diamond/Cu composites prepared by spark plasma sintering. Int J Miner Metall Mater 2016;23:716.
[32] Bai G, Wang L, Zhang Y, Wang X, Wang J, Kim MJ, et al. Tailoring interface structure and enhancing thermal conductivity of Cu/diamond composites by alloying boron to the Cu matrix. Mater Charact 2019;152:265–75. https://doi.org/10.1016/j.matchar.2019.04.015.
[33] Wei C, Cheng J, Chen P, Wei B, Gao D, Xu D. Facile electroless copper plating on diamond particles without conventional sensitization and activation. Adv Powder Technol 2019;30:2751–8. https://doi.org/10.1016/j.apt.2019.08.022.
[34] Zhang Y, Zhang HL, Wu JH, Wang XT. Enhanced thermal conductivity in copper matrix composites reinforced with titanium-coated diamond particles. Scr Mater 2011;65:1097–100. https://doi.org/10.1016/j.scriptamat.2011.09.028.

[35] Li J, Zhang H, Zhang Y, Che Z, Wang X. Microstructure and thermal conductivity of Cu/diamond composites with Ti-coated diamond particles produced by gas pressure infiltration. J Alloys Compd 2015;647:941–6. https://doi.org/10.1016/j.jallcom.2015.06.062.
[36] Schubert T, Ciupiński, Zieliński W, Michalski A, Weißgärber T, Kieback B. Interfacial characterization of Cu/diamond composites prepared by powder metallurgy for heat sink applications. Scr Mater 2008;58:263–6. https://doi.org/10.1016/j.scriptamat.2007.10.011.
[37] Chu K, Liu Z, Jia C, Chen H, Liang X, Gao W, et al. Thermal conductivity of SPS consolidated Cu/diamond composites with Cr-coated diamond particles. J Alloys Compd 2010;490:453–8.
[38] Grzonka J, Kruszewski MJ, Rosiński M, Ciupiński Ł, Michalski A, Kurzydłowski KJ. Interfacial microstructure of copper/diamond composites fabricated via a powder metallurgical route. Mater Charact 2015;99:188–94. https://doi.org/10.1016/j.matchar.2014.11.032.
[39] Kang Q, He X, Ren S, Zhang L, Wu M, Liu T, et al. Preparation of high thermal conductivity copper-diamond composites using molybdenum carbide-coated diamond particles. J Mater Sci 2013;48:6133–40.
[40] Cunha A, Ferreira R, Trindade B, Silva FS, Carvalho O. Production of a laser textured 316L stainless steel reinforced with CuCoBe + diamond composites by hot pressing: Influence of diamond particle size on the hardness and tribological behaviour. Tribol Int 2020;146:106056. https://doi.org/10.1016/j.triboint.2019.106056.
[41] Cunha A, Ferreira R, Trindade B, Silva FS, Carvalho O. Reinforcement of a laser-textured 316L steel with CuCoBe-diamond composites through laser sintering. Mater Manuf Process 2020;35:1032–9. https://doi.org/10.1080/10426914.2020.1758331.
[42] Upadhyaya GS. Powder Metallurgy Technology. Cambridge Int Sci Publ 2014:1–5. https://doi.org/10.1073/pnas.0703993104.
[43] Fu X, Hu Y, Tao J. Synthesis and tribological properties of copper-alumina nanocomposites prepared by coprecipitation technique. J Wuhan Univ Technol Mater Sci Ed 2016;31:1123–30. https://doi.org/10.1007/s11595-016-1500-y.
[44] Ferreira R, Carvalho, Pires J, Sobral L, Carvalho S, Silva F. A New Tribometer for the Automotive Industry: Development and Experimental Validation. Exp Mech 2022;62:483–92. https://doi.org/10.1007/s11340-021-00805-7.
[45] Chang C, Liao Y, Wang GZ, Ma YR, Fang RC. CVD Diamond Growth. Cryst Growth Technol 2003:93–141.
[46] Ferreira R, Carvalho Ó, Sobral L, Carvalho S, Silva F. Influence of morphology and microstructure on the tribological behavior of arc deposited CrN coatings for the automotive industry. Surf Coatings Technol 2020;397:126047. https://doi.org/10.1016/j.surfcoat.2020.126047.

# CHAPTER 8.

## General discussion and conclusions

## 8.1 General discussion and conclusions

The future of the automotive powertrain solutions cannot be foreseen at present. But, combustion engines will undoubtedly remain in the market with more ecological fuel and its performance will continue to be subject of improvement. The tribological behaviour of the combustion engine contact surfaces compromise the overall engine performance. In the present work was studied the piston ring-cylinder liner tribological pair, and in particular, on the piston ring radial surface solutions.

To ensure the congruity of the developed experimental work, the state-of-the-art piston rings and the solutions developed in the context of this PhD work were tribologically assessed using the same testing device and following the same protocol. The scarcity of a test rig with adaptability to assemble the ring and liner samples, and to reproduce comparable engine operation conditions, encouraged the development of a new tribometer. In chapter 3 was presented the new test rig and described the testing protocol and the central constituent systems. The functionality and the repeatability of the developed device was assessed through preliminary validation tests.

With a functional tool already developed, and previously to the proposal of a new solution, it was necessary to investigate the currently used materials and technologies. Improved tribological results could only be reached with the state-of-the-art solutions already characterized.

In the chapter 4 was studied the influence of the conventional manufacturing technology, the PVD (using the cathodic arc technique), on the final tribological performance. Different deposition parameters resulted on distinct coating's morphology and microstructure, and consequently, on an altered tribological behaviour. The surface roughness parameters and the contact angle were also measured. In this assessment, the denser coating, with superior hardness, revealed an improved wear resistance. The superior surface roughness values of harder coatings revealed that those would require harsh surface finishing techniques. This coating also possessed a lower contact angle, and a consequent improved wettability, which could had contributed for an enhanced tribological result.

The improved tribological result of the harder coating and the predicted influence of the surface roughness conducted to the following study: the assessment of the influence of the

diamond-like carbon coating topography in the tribological performance of the ring-liner contact. In chapter 5 three distinct surface finishing processes were used to investigate their influence on DLC coated compression piston rings. Using a harder coating than CrN, the impact of the surface finishing stage (after the coating deposition) on the surface roughness values was evident. The variation of the surface finishing parameters revealed a direct influence on the wear resistance either of the piston ring or the cylinder liner surfaces. Given the main conclusions that could be drawn, rough surfaces were associated to increased wear debris entrapment and higher COF values.

As overall conclusion of the previous studies, the morphology and topography of contact surfaces demonstrated straight impact on the wear resistance and friction coefficient results. In the Chapter 6 the piston ring radial surface was intentionally modified through a laser ablation technique. This study aimed to research the influence of laser surface textured dimples along the compression piston ring radial surface. In this study the textured dimples were performed over an NbN/CrN coating layer, combining a conventional technology with an innovative manufacturing process. Different designs, comprehending distinct texture dimensions and densities were tested using the developed tribometer. Micro-dimples revealed to be a potential solution to reduce friction-induced wear. Simultaneously, laser surface texturing was disclosed as a flexible and reliable manufacturing technology with potential to produce textures along the piston ring radial surface.

Chapter 7 presented the design, development and testing of an innovative solution. This solution combines two different innovative technologies: laser texturing and powder metallurgy. The main goal of this study was to develop a strategy to manufacture a multifunctional piston ring surface. The laser surface texturing was used to produce channels (cross lines used to embed powder material), which enclose rectangular stainless steel geometries. The powder material used to reinforce the textures obtained its final properties using the hot-pressing. In this study a CuCoBe – diamond reinforced composite powder material was inserted in the textured channels and posteriorly, hot-pressed. The hot-pressing parameters of the composite material were optimized and applied to the functionalized piston ring. Different texture designs were experimented and assessed using the developed testing device. The obtained results were compared with the conventional solution. The texture with larger SS geometries was revealed as a promising design with potentiality to compete with the conventional solution.

## 8.2 Suggestions for Future Works

Based on the findings of this PhD work together with the development of a new piston ring surface solution, some suggestions for future works can be enumerated:

- Study different surface texture parameters for friction reduction purpose: vary dimples distribution and combine distinct texture dimensions;
- Investigate the influence of the dimple surface textures machined over different PVD coatings;
- Evaluate the influence of the powder composite diamond reinforcement weight on the ring and liner wear resistance (weight loss);
- Study the reinforcement of the piston ring surface using more than one composite material disposed along the ring radial surface.

## 8.3 Further Contributions

In addition to the studies developed and described in this thesis, two conferences attendances can also be appointed:

- R. Ferreira, New processing technologies for improved compression piston rings performance. MIT Portugal: 10 years engineering a better future. 30 June 2016, Braga – Portugal.

- R. Ferreira, O. Carvalho, L. Sobral, S. Carvalho, F. Silva. Piston ring/cylinder liner contact: the tribological assessment. 22nd International Conference on Wear of Materials. 14-18 April 2019, Miami, Florida – USA.

**Award:** Peter J. Blau Best Poster Award (2nd place)

- R. Ferreira, A. Cunha, B. Trindade, O. Carvalho, L. Sobral, S. Carvalho, F. Silva. Study of the influence of pressure and temperature processing in the diamond-reinforced composite properties. Euro PM2019 Congress & Exhibition. 13-18 October 2019, Maastricht – The Netherlands. (ISBN: 978-189907251-4)